THE HONG KONG
POLYTECHNIC UNIVERSITY
香港理工大學
Pao Yue-kong Library
包玉剛圖書館

Copyright Undertaking

This thesis is protected by copyright, with all rights reserved.

By reading and using the thesis, the reader understands and agrees to the following terms:

1. The reader will abide by the rules and legal ordinances governing copyright regarding the use of the thesis.

2. The reader will use the thesis for the purpose of research or private study only and not for distribution or further reproduction or any other purpose.

3. The reader agrees to indemnify and hold the University harmless from and against any loss, damage, cost, liability or expenses arising from copyright infringement or unauthorized usage.

Pao Yue-kong Library, The Hong Kong Polytechnic University, Hung Hom, Kowloon, Hong Kong

http://www.lib.polyu.edu.hk

CONCRETE-TO-CONCRETE INTERFACES: BEHAVIOUR AND MODELLING

TAO DING

PhD

The Hong Kong Polytechnic University

This programme is jointly offered by The Hong Kong Polytechnic University and Tongji University

2022

The Hong Kong Polytechnic University

Department of Civil and Environmental Engineering

Tongji University

College of Civil Engineering

Concrete-to-Concrete Interfaces:

Behaviour and Modelling

Tao Ding

A Thesis Submitted in Partial Fulfilment of the Requirements for the Degree of Doctor of Philosophy

November 2021

CERTIFICATE OF ORIGINALITY

I hereby declare that this thesis is my own work and that, to the best of my knowledge and belief, it reproduces no material previously published or written, nor material that has been accepted for the award of any other degree or diploma, except where due acknowledgement has been made in the text.

_____(Signed)

_____DING Tao_____(Name of student)

To My Family

ABSTRACT

Concrete-to-concrete interfaces are widely present in concrete structures. These structures include but are not limited to: i) concrete structures (e.g., concrete beams, slabs and columns) repaired and strengthened through the enlargement of cross-sections, ii) in-situ cast concrete joints between precast concrete components; iii) composite concrete structures comprising multiple components cast at different times. In general, when subjected to tensile or shear stresses, concrete-to-concrete interfaces are the weak links of the structure because the interfacial tensile and shear strengths are normally lower than those of the integrally-cast concrete. However, a thorough understanding of and an accurate model for the behaviour of concrete-to-concrete interfaces are not yet available, making it difficult to fully understand and accurately predict the behaviour of concrete structures in which concrete-to-concrete interfaces play a critical role.

Against the above background, the work presented in this PhD thesis was aimed at advancing the understanding of and developing a sophisticated model for the mechanical behaviour of concrete-to-concrete interfaces through investigations of the following three aspects: (1) Analyse the existing test methods for the interfacial behaviour of concrete-to-concrete interfaces and propose an improved test method that is more robust and accurate; (2) Develop a sophisticated interfacial bond-slip model for concrete-to-concrete interfaces based on a comprehensive experimental study using the improved test method; (3) Conduct numerical simulations, in which the proposed sophisticated interfacial bond-slip model is employed, of the structural performance of concrete structures with concrete-to-concrete interfaces.

The thesis first presents a literature review on and a finite element analysis of the existing shear test methods for concrete-to-concrete interfaces. These investigations revealed the advantages and disadvantages of the existing test methods, based on which an improved test method suitable for studying the interfacial behaviour of concrete-co-

concrete interfaces was proposed. This new test method was validated through a series of trial laboratory tests.

A comprehensive experimental programme using the newly developed test method was conducted to investigate the interfacial behaviour of concrete-to-concrete interfaces by considering factors including the concrete strength, interface roughness and normal stress level. Based on the experimental data, a new bond-slip model for the interface was established. The model describes the complete local interfacial behaviour of concrete-to-concrete interfaces, including damage evolution along the interface.

The developed bond-slip model was then implemented into a finite element framework, which included the appropriate constitutive modelling of both concrete and steel as well as reliable interfacial models for concrete-to-concrete and concrete-to-steel interfaces. This framework was used to simulate the structural behaviour of composite concrete beams, in which the concrete-to-concrete interfaces play a significant role in the mechanical behaviour. The performance of the framework was validated by comparing the predicted results of the flexural behaviour of the beams with the experimental data. Moreover, the framework was used to conduct a parametric study to investigate the influences of the interfacial parameters of the composite beams on the overall behaviour.

The test method, the bond-slip model, and the numerical framework presented in this thesis constitute a major advancement on the understanding and the accurate prediction of the behaviour of concrete-to-concrete interfaces as well as structures containing such interfaces. Future research is needed to improve the current research outcomes to achieve even more accurate predictions of concrete-to-concrete interfaces and to accurately simulate the behaviour of more complicated structures containing such interfaces.

ACKNOWLEDGEMENTS

CONTENTS

LIST OF FIGURES

XX

XXI

LIST OF TABLES

XXII

NOTATION

A_s	area of the steel bars
A_c	area of the concrete-to-concrete interface
b_i	width of bonded interface
b_o	width of old concrete layer
b_n	width of old concrete layer
c	coefficient of cohesion
D	the damage variable
d_a	maximum concrete aggregate size
d_c	compressive damage of concrete
d_t	tensile damage of concrete
e	Euler number
E_c	elastic modulus of the concrete
E_t	strain-softening modulus
E_s'	hardening modulus of steel bars
E_s	elastic modulus of steel bars
f_c	cylinder compressive strength of concrete
f_{cd}	design value of the compressive strength of concrete
f_{ck}	characteristic cylinder compressive strength of concrete
$f_{cu,o}$	cube compressive strength of old concrete
$f_{cu,n}$	cube compressive strength of new concrete
f_t	tensile strength of concrete
$f_{t,o}$	tensile strengths of old concrete
$f_{t,n}$	tensile strengths of new concrete
f_y	yield stress of the reinforcement

f_{yd}	design yield stress of the reinforcement
G_f	interfacial fracture energy
G_n, G_s, and G_t	the work done in the normal, first, and second shear directions
G_I	interfacial fracture energies under tension
G_{II}	interfacial fracture energies under shear
h_c	crack band width
h_o	height of old concrete layer
h_n	height of old concrete layer
k	constant in Eq (2.9)
K_a	shear stiffness of the adhesive layer
K_{nn}, K_{ss} and K_{tt}	values of elastic stiffness in normal and shear directions
L	span of beam
L_e	effective span of beam
L_i	length of bonded interface
n	a parameter that reflects the shear resistance feature of cracked concrete
$P(t)$	shear load of the specimen at time t
P_{max}	peak load
P_r	residual load
R	surface roughness
S	fracture area
s_u	the shear slip corresponding to τ_{max} in Eq. (2.17) and Eq. (2.19)
$s(t)$	slip near the concrete-to-concrete interface at time t
$s_c(t)$	the slip recorded by the clip extensometer at time t
t_n^0, t_s^0 and t_t^0	maximum normal and shear stresses
V	sand volume

V_F	resistance of dowel reinforcement
$V_{F,max}$	maximum force of the dowel action
w_{cr}	maximum crack opening displacement
w_t	crack opening displacement
α	specific parameter in Eq. 6.6
β_w	FRP-concrete width coefficient
γ	flexural resistance coefficient for the dowel reinforcement. in Eq (2.10)
δ_1	slip corresponding to the maximum shear stress
δ_2	slip corresponding to the residual stress
δ_f	ultimate slip
δ_m^0	the effective displacement at initiation of damage
δ_m^f	the effective displacement at complete failure
δ_m^{max}	the maximum effective displacement reached during the history of loading
ε_c	axial strain of concrete
ε_{cr}	concrete cracking strain corresponding to crack opening displacement w_t
$\varepsilon_{cr,u}$	maximum principal concrete cracking strain at crack opening width w_{cr}
ε_n, ε_s and ε_t	the normal and two shear strains
ε_p	corresponding axial strain to σ_p
$\kappa_{2,max}$	interaction coefficient in Eq. 7.2
μ	coefficient of friction
ρ	reinforcing ratio
σ_c	axial stress of concrete

σ_n	Applied compressive stress at the interface
σ_p	peak axial stress
σ_n, σ_s and σ_t	the normal and two shear stresses
$\tau_a(s)$	contribution of adhesion
$\tau_{sf}(s)$	contribution of friction
$\tau_{sr}(s)$	contribution of shear reinforcement crossing the interface
τ_{max}	Maximum shear stress
τ_c	interface-average shear strength
τ_r	residual shear stress

CHAPTER 1

INTRODUCTION

1.1 BACKGROUND

By casting a new piece of concrete onto a previously cast (old) piece of concrete, an interface is generated between the old and new concretes and it is commonly referred to as a concrete-to-concrete interface (Tassios and Vintzēleou, 1987). Concrete-to-concrete interfaces are widely present in concrete structures including but not limited to: *i*) concrete structures (e.g., concrete beams, slabs and columns) repaired and strengthened through the enlargement of cross-sections, *ii*) in-situ cast concrete joints between precast concrete components; or composite concrete structures comprising multiple components cast at different times. Therefore, understanding the mechanical behaviour of concrete-to-concrete interfaces is integral to the understanding of the performance of the relevant structures containing such interfaces.

1.1.1 Concrete-to-Concrete Interfaces in Repaired and Strengthened Concrete Structures

The deterioration and ageing of concrete structures, as well as increased loading on existing structures, have posed a worldwide challenge that calls for cost-effective repair and strengthening methods. Data from the U.S. Federal Highway Administration in 2013 showed that approximately 25% of the 607,000 bridges had structural deficiency (Mabsout *et al*., 2004). A survey of 177 bridges in Okinawa, Japan, showed that the damage rate of bridge decks and reinforced concrete beams had reached more than 90%, and large areas of concrete cracking and considerable reinforcement erosion had occurred (Fujino and Siringoring, 2011). Many concrete structures built in China have undergone different degrees of damage and need to be strengthened (Peng and Stewart,

2016).

The repair and strengthening of concrete structures are often achieved through enlarging the member cross-sections, encasing the concrete with steel tubes, adding external reinforcing components with or without prestress. As one of the cost-effective methods which can maintain the original appearance of the structure, enlarging member cross-sections by adding new concrete to the parent concrete structure is widely employed (Yin *et al.*, 2017). For instance, slabs in reinforced concrete buildings and bridge decks are usually strengthened by adding a layer of concrete to the top or bottom surface of the slabs or decks (Banu and Taranu, 2010); and reinforced concrete jacketing of columns and beams is often adopted to increase their capacities. The mechanical behaviour of the concrete-to-concrete interface has a significant impact on the overall behaviour of repaired or strengthened structures, and their structural integrity and durability rely largely on a strong bond at concrete-to-concrete interfaces.

1.1.2 Concrete-to-Concrete Interfaces in Precast and Design for Deconstruction (DfD) Concrete Structures

Precast concrete structures have been widely used in recent years due to their relatively quick construction, low labour requirement, and superior quality control (Naik 2008; Yee and Eng, 2001; VanGeem, 2006). The material waste for precast concrete construction is lower than that for in situ-cast construction (Jaillon *et al.*, 2009; Lu and Yuan, 2013; Li *et al.*, 2014). Moreover, the standardization and modularization of the concrete components of precast concrete structures can facilitate the reuse of the components after the deconstruction of the structures (Ferdous *et al.*, 2019).

Moreover, in recent years, the reuse of concrete components has been widely investigated in the concrete research domain. Inspired by the design for disassembly in

the mechanical industry, design-for-deconstruction (DfD), as a new concept in civil engineering, corresponds to the further application of precast structures (Addis and Schouten, 2004; Gungor, 2006). In the case of DfD concrete structures, the disassembled concrete components can be reused in new concrete structures to realize a second life.

Considering the concept of DfD structures, the realization of DfD for building structures is expected to reduce the environmental pollution and improve the recycling efficiency in the construction industry (Gorgolewski, 2008). In this manner, the massive construction and demolision waste and the excessive CO_2 emissions associated with construction material production can be reduced, and the amount of new construction material and heavy on-site construction work can be decreased (Tingley and Davison, 2012; Akbarnezhad et $al.$, 2014). Recent studies on DfD concrete structures showed that dry concrete connections (without or with very limited post-cast concrete at the connections) have been widely adopted in beam-to-column joints and shear walls to facilitate easy end-of-life deconstruction as well as recycling or reusing the deconstructed structural components to build new DfD structures (Xiao et $al.$ 2017; Ding et $al.$ 2020). In these dry connections, the multiple prefabricated concrete components are joined with cast-in-place concrete, resulting in a group of concrete-to-concrete interfaces in a connection region. Experimental results demonstrated that the presence of these interfaces has a considerable impact on the failure mode and the overall structural performance (Ong et $al.$ 2013). As a result, to fully understand and accurately predict the structural behaviour of precast concrete structures or DfD concrete structures, the mechanical behaviour of complex multi-interface concrete connections should be thoroughly investigated.

1.2 THE SIGNIFICANCE OF A BOND-SLIP MODEL FOR CONCRETE-TO-CONCRETE INTERFACES

Generally, the compressive strength of concrete-to-concrete interfaces can be considered equal to that of the base concrete material, and the interfaces are only weak parts of the structure when subjected to normal opening (tension) or tangential sliding (shear) actions (Santos and Júlio, 2012). Moreover, concrete is predominantly designed to resist compression-dominated actions so that pure opening actions at concrete-to-concrete interfaces are practically rare. Therefore, the interfacial shear behaviour is by far the more concerning and important one in describing the mechanical behaviour of concrete-to-concrete interfaces.

However, most of the existing studies on the interfacial shear behaviour of concrete-to-concrete interfaces were focused on describing the mechanical behaviour of concrete-to-concrete interfaces using the nominal interfacial shear strength, which is obtained by measuring the shear force causing the interface to debond and divide it by the interfacial area (e.g., Mohamad *et al*., 2015). Such a low-resolution description is based on the assumptions of uniform global interfacial shear stress distribution and linear elastic local bond-slip relationship at the concrete-to-concrete interface. However, both oversimplify the complex interfacial shear behaviour and ignore the intricate interaction between the local bond-slip behaviour and the global shear stress distribution.

To achieve a thorough understanding and the accurate prediction of concrete-to-concrete interfacial behaviour, it is necessary to establish the local bond-slip model and thereby investigate the global stress distribution at the concrete-to-concrete interfaces. Consequently, it remains challenging to accurately predict the response of a concrete-to-concrete interface under various loading conditions and the impact of this response on the overall performance of the concrete structure.

1.3 OBJECTIVES AND SCOPE

The goal of the current thesis is to develop a thorough understanding of the interfacial shear behaviour of concrete-to-concrete interfaces and thereupon explore the structural behaviour of concrete structures containing such interfaces. This goal will be achieved through fulfilling the following experimental-theoretical-numerical trilogy: 1) proposing a new test method that overcomes the deficiencies of the existing shear test methods to investigate the behaviour of concrete-to-concrete interfaces [Chapter 3 & Chapter 4]; 2) establishing the bond-slip model of concrete-to-concrete interfaces through a systematic experimental programme using the proposed test method [Chapter5 & Chapter6]; and 3) exploring the structural behaviour of concrete structures containing concrete-to-concrete interfaces using finite element (FE) models that incorporate the established concrete-to-concrete interfacial bond-slip model [Chapter 7]. A brief overview of each chapter is given below:

Chapter 2 presents a state-of-the-art review of the relevant experimental and theoretical studies on the interfacial shear behaviour at concrete-to-concrete interfaces. The limitations of the existing test methods and the need for developing a more suitable test method are discussed. Chapter 3 describes the evaluation of the existing shear test setups for concrete-to-concrete interfaces using FE analysis. Specifically, the interfacial shear stress distributions in different test setups considering various testing parameters are compared, and thereupon modifications to the existing concrete-to-concrete shear tests are suggested. Chapter 4 describes the newly proposed shear test method that overcomes the deficiencies of the existing shear test methods and can be used to investigate the local shear bond-slip relationship for concrete-to-concrete interfaces. The feasibility and reliability of the proposed test method are verified through example tests.

Chapter 5 presents an experimental programme designed to quantify the interfacial shear bond-slip relationship at concrete-to-concrete interfaces using the test method proposed in Chapter 4. Factors that affect the shear bond performance, including the concrete strength, surface roughness, and applied compressive stress, were all considered in the experimental programme. Chapter 6 explains the proposed interfacial shear bond-slip model based on the test data obtained in Chapter 5. The model describes the local bond-slip behaviour through a linear elastic stage and a damage evolution stage. In the former, the key parameters are the interfacial shear stiffness and maximum shear stress; in the latter, the key parameter is the fracture energy.

Chapter 7 presents the FE analysis of composite concrete beams with the concrete-to-concrete interfaces represented by the developed bond-slip model. The FE predictions of failure mode and load-displacement behaviour of composite concrete beams under bending considering various interfacial conditions are presented and compared with experimental data. Additionally, parametric studies were performed to understanding the key parameters in the design of composite concrete beams, which are critical to repair and strengthening projects involving such beams. Chapter 8 summarizes the conclusions of each chapter and suggests future research regarding concrete-to-concrete interfaces.

1.4 REFERENCES

Addis, W., & Schouten, J. (2004). Principles of design for deconstruction to facilitate reuse and recycling. CIRIA.

Akbarnezhad, A., Ong, K. C. G., & Chandra, L. R. (2014). Economic and environmental assessment of deconstruction strategies using building information modeling. *Automation in Construction*, 37, 131-144.

Banu, D., & Taranu, N. (2010). Traditional solutions for strengthening reinforced concrete slabs. Buletinul Institutului Politehnic din lasi. *Sectia Constructii, Arhitectura*, 56(3), 53.

Ding, T., Xiao, J., Wei, K., & Lu, Y. (2020). Seismic behavior of concrete shear walls with bolted end-plate DfD connections. *Engineering Structures*, 214, 110610.

Ferdous, W., Bai, Y., Ngo, T. D., Manalo, A., & Mendis, P. (2019). New advancements, challenges and opportunities of multi-storey modular buildings–A state-of-the-art review. *Engineering Structures*, 183, 883-893.

Fujino, Y., & Siringoringo, D. M. (2011). Bridge monitoring in Japan: The needs and strategies. *Structure and Infrastructure Engineering*, 7(7-8), 597-611.

Gorgolewski, M. (2008). Designing with reused building components: Some challenges. *Building Research & Information*, 36(2), 175-188.

Güngör, A. (2006). Evaluation of connection types in design for disassembly (DFD) using analytic network process. *Computers & Industrial Engineering*, 50(1-2), 35-54.

Jaillon, L., Poon, C. S., & Chiang, Y. H. (2009). Quantifying the waste reduction potential of using prefabrication in building construction in Hong Kong. *Waste Management*, 29(1), 309-320.

Kirk, R. S., & Mallett, W. (2013). Highway bridge conditions: Issues for Congress. CRS Report prepared for members and committees of congress.

Li, Z., Shen, G.Q. & Alshawi, M., (2014). Measuring the impact of prefabrication on construction waste reduction: An empirical study in China. *Resources, Conservation and Recycling*, 91, 27-39.

Lu, W. & Yuan, H., (2013). Investigating waste reduction potential in the upstream

processes of offshore prefabrication construction. *Renewable and Sustainable Energy Reviews*, 28, 804-811.

Lu, X. Z., Teng, J. G., Ye, L. P., & Jiang, J. J. (2005). Bond–slip models for FRP sheets/plates bonded to concrete. *Engineering Structures*, 27(6), 920-937.

Mohamad, M. E., Ibrahim, I. S., Abdullah, R., Rahman, A. A., Kueh, A. B. H., & Usman, J. (2015). Friction and cohesion coefficients of composite concrete-to-concrete bond. *Cement and Concrete Composites*, 56, 1-14.

Naik, T. R. (2008). Sustainability of concrete construction. *Practice Periodical on Structural Design and Construction*, 13(2), 98-103.

Ong, K. C. G., Lin, Z. S., Chandra, L. R., Tam, C. T., & Dai Pang, S. (2013). Experimental investigation of a DfD moment-resisting beam–column connection. *Engineering Structures*, 56, 1676-1683.

Peng, L., & Stewart, M. G. (2016). Climate change and corrosion damage risks for reinforced concrete infrastructure in China. *Structure and Infrastructure Engineering*, 12(4), 499-516.

Santos, P. M., & Júlio, E. N. (2012). A state-of-the-art review on shear-friction. *Engineering Structures*, 45, 435-448.

Tassios, T. P., & Vintzēleou, E. N. (1987). Concrete-to-concrete friction. *Journal of Structural Engineering*, 113(4), 832-849.

Tingley, D. D., & Davison, B. (2012). Developing an LCA methodology to account for the environmental benefits of design for deconstruction. *Building and Environment*, 57, 387-395.

VanGeem, M. (2006). Achieving sustainability with precast concrete. *PCI Journal*, 51(1), 42-61.

Xiao, J., Ding, T., & Zhang, Q. (2017). Structural behavior of a new moment-resisting DfD concrete connection. *Engineering Structures*, 132, 1-13.

Yee, P. T. L., Adnan, A. B., Mirasa, A. K., & Rahman, A. B. A. (2011). Performance of IBS precast concrete beam-column connections under earthquake effects: A literature review. *American Journal of Engineering and Applied Sciences*, 4(1), 93-101.

Yin, H., Teo, W., & Shirai, K. (2017). Experimental investigation on the behaviour of reinforced concrete slabs strengthened with ultra-high performance concrete. *Construction and Building Materials*, 155, 463-474.

Yu, T., Fernando, D., Teng, J. G., & Zhao, X. L. (2012). Experimental study on CFRP-to-steel bonded interfaces. *Composites Part B: Engineering*, 43(5), 2279-2289.

CHAPTER 2

LITERATURE REVIEW

2.1 INTRODUCTION

This chapter presents a review of existing studies relevant to the interfacial mechanical behaviour of concrete-to-concrete interfaces subjected to shear-dominated loading. The experimental studies employing various test methods to investigate the interfacial shear strength are first reviewed. Then the works studying the effects of fabricating factors on the interfacial mechanical behaviour are reviewed. Subsequently, existing nominal interfacial shear strength models are summarized. Finally, the needs for devising a new shear test method and developing a local bond-slip model for concrete-to-concrete interfaces are discussed.

2.2 EXISTING SHEAR TEST METHODS

Existing test methods aiming at measuring the concrete-to-concrete interfacial shear strength can be generally categorized into the direct shear test (Figure 2.1), where the concrete-to-concrete interface is subjected to shear-dominated stresses, and the slant shear test (Figure 2.2), where the concrete-to-concrete interface is subjected to combined shear and compressive stresses.

2.2.1 Direct Shear Test

The direct shear test is designed to induce shear stresses and minimize normal stresses along the interface to investigate the interfacial shear behaviour. However, normal stresses at the concrete-to-concrete interface cannot be avoided in the direct test method. Hence, the local stress state at a point along the interface is a combination of shear and

normal stresses. The direct shear test can be further divided into the one-interface shear test (commonly referred to as the push-off test, see Figure 2.1 (a)), the L-shaped one-interface shear test (Figure 2.1 (b)), and the two-interface shear test (commonly referred to as the push-out test, see Figure 2.1 (c)).

The one-interface shear test specimen is composed of a new and an old concrete block without dowel reinforcement crossing the interface (Saucier *et al*., 1991). During testing, the specimen is subjected to a pair of forces acting respectively on the two blocks, and an optional compressive force can be applied, as indicated in Figure 2.1 (a) (Clímaco and Regan, 2001). Since the pair of forces is not coplanar with the interface, they generate non-trivial normal stresses, both tensile and compressive, along the interface, which substantially complicate the interfacial shear behaviour (Gohnert, 2003). Moreover, stress concentration occures at the ends of the interface, where local failures may occur, and terminating the loading process prematurely before the complete process of debonding can be measured (Mohamad *et al*., 2015).

The L-shaped one-interface test specimen (Figure 2.1 (b)) is made of two L-shaped halves that are anti-symmetrically placed and connected by cross-interface steel dowel reinforcement (Hofbeck *et al*., 1969). During testing, the specimen is compressed at the ends to produce a shear force for the interface (Mattock, 1976). Although the compressive force is coplanar with the interface, considerable normal stresses along the interface are still generated due to the bending moment induced in the L-shaped halves (Walraven *et al*., 1987). The dowel reinforcement and the concrete-to-concrete interface act together as a parallel system, which prevents sudden fracture at the interface and permits gradual interfacial debonding. Therefore, the complete debonding process embodied in the measured descending branch of the load-displacement relationship can be obtained (Mattock and Hawkins, 1972; Xiao *et al*., 2012). However, due to the

entangled interaction between the interface and the dowel reinforcement, it is difficult to separate their contributions. Hence, the test data are not directly conducive to understanding the mechanical behaviour of concrete-to-concrete interfaces without dowel reinforcement (Júlio *et al.*, 2010; Randl, 2013).

The two-interface shear test specimen (Figure 2.1 (c)) is made by casting a new concrete block between two old concrete blocks without dowel reinforcement. During testing, the middle block is subjected to a push-out force resisted by the reactions applied to the other two blocks (Theodossius and Vintzeleou, 1987). In this approach, local fracture does not immediately terminate the test because of the confinement on both sides (Caliskan *et al.*, 2002; Yang *et al.,* 2014). Normal stresses of a similar level with those in the one-interface shear tests are generated at the interfaces, complicating the interfacial shear stress distribution and strength behaviour (Chen *et al.*, 1995). Table 2.1 summarizes the key characteristics of these test methods.

2.2.2 Slant Shear Test

In the slant shear test shown in Figure 2.2, a concrete specimen containing a concrete-to-concrete interface of a certain orientation (usually defined as the angle between the interface and the longitudinal axis of the specimen) is subjected to compressive forces at the two ends, which induce combined compression and shear stresses at the interface. The first slant shear test was conducted by Tabor (1978), in which the specimen contained an interface with an orientation of 30°. Thereafter, this test method has been widely adopted since the combined compressive and shear actions at the interface are close to the loading conditions of concrete-to-concrete interfaces in practical scenarios (Clark and Gill, 1985; Wall and Shrive, 1988; Santos and Júlio, 2011).

It has been experimentally observed that the interfacial stress distribution, the load-

bearing capacity, and the failure mode of slant test specimens are strongly dependent on the orientation of the interface and the surface roughness (Wall and Shrive, 1988). For instance, in the tests conducted by Austin *et al.* (1999), the interfacial bond failure occurred only in the specimens with an interface orientation of 30°. Moreover, theoretical analyses performed by Austin *et al.* (1999) and Naderi (2009) indicated that for a given interface orientation, the slant test specimen may fail by interfacial debonding if the surface roughness is relatively low, while it may fail by crushing if the surface roughness is high enough.

However, the influences of the interface orientation and surface roughness on the interfacial stress distribution, the specimen load-bearing capacity, and the failure mode have not been well understood due to the complex interaction between the interfacial normal and shear stresses in a slant test specimen (Tabor, 1978; Santos *et al.*, 2007). Consequently, this test method is unlikely to provide critical insights upon which fundamental understandings of the concrete-to-concrete interfacial shear behaviour can be established.

Taken collectively, although in practical scenarios the concrete-to-concrete interfaces are predominantly subjected to combined shear and compressive actions, the slant shear test simulating such loading conditions may not be as conducive as the direct shear test that focuses on establishing a thorough understanding of the shear behaviour without the complications brought about by the compressive action. Nonetheless, the existing direct shear test methods are inadequate in the following aspects in establishing a thorough understanding of the interfacial shear behaviour. They can only measure the nominal interfacial shear strength that is roughly estimated by assuming a uniform distribution of the interfacial shear stress, which is insufficient in understanding the local shear stress-relative slip relationship as well as the actual global interfacial shear

stress distribution. Further, a specimen without dowel reinforcement is subjected to brittle failure that does not allow the measurement of the complete process of debonding, while one with dowel reinforcement does not allow the accurate isolation of the contribution of the interface. Therefore, a new test method suitable for evaluating the interfacial shear behaviour, particularly the local bond-slip response, of concrete-to-concrete interfaces is necessary.

2.3 EXPERIMENTAL STUDIES ON SHEAR TRANSFER BEHAVIOUR OF CONCRETE-TO-CONCRETE INTERFACES

2.3.1 Existing Experimental Studies

This section collects 456 related experimental studies on the bond behaviour of concrete-to-concrete interfaces from the literature, with the aim to evaluate the factors affecting the bond behaviour of concrete-to-concrete interfaces. The following factors were focused:

• Specific test methods

• The strength of old or new concrete (although many studies do not strictly distinguish the strength of new and old concrete)

• Surface roughness of old concrete

• Interfacial reinforcement ratio

• Yield strength of interfacial reinforcement

• External normal stress

There are still many studies that are focused on other special variables that affect the bond behaviour of concrete-to-concrete interfaces. However, those studies, which are excluded from the literature collection since they are beyond the scope of the present study, cover such situations as:

- The interface is between two surfaces of concrete cracks, so it is not a strict interface between two concrete blocks;

- Other test methods, such as the slant shear test, instead of the direct shear test method, are used,

- The direction of the reinforcement passes through the interface;

- The interface is subjected to cyclic loading

Although, in practical scenarios, concrete-to-concrete interfaces are predominantly subjected to combined shear and compressive actions, it is very difficult to directly understand the coupled interfacial behaviour as the compressive action has a considerable impact on the shear behaviour. Instead, the present study is aimed to understand the Mode-II interfacial behaviour with minimal interfacial compressive stresses and Mode-I opening actions. The interfacial behaviour under combined actions can be studied and understood more thoroughly after achieving this. Therefore, the slant shear test inducing combined compressive and shear actions at the interface was beyond the scope of the present study and only briefly reviewed. According to the above considerations, Table 2.2 provides the detailed information for those experimental studies on the bond behaviour of concrete-to-concrete interfaces. In each of the specific study, the total number of specimens may be greater than the number listed in Table 2.2. This is because those studies also focused on some other variables mentioned above,

which are not the focus of this study.

It can be seen from Table 2 that the L-shaped one-interface shear test method was adopted for most of studies on the bond behaviour of concrete-to-concrete interface, accounting for 61.4% of the total. One-interface shear test was followed, accounting for about 32.8%. However, only 5.7% of the test results are obtained based on the two-interface shear test method.

These studies aim at a wide range of concrete strength variations. The cylinder compressive strength of concrete ranges from 18.1 MPa to 100.3 MPa. Nevertheless, about 70% of the cylinder compressive strength of concrete was between 20.0 MPa and 50.0 MPa. That is to say, the research focus is generally concerned with the interfacial bond behaviour casted by normal concrete. In addition, it should be pointed out that there is no strict distinction between the strength of new concrete and old concrete in about 21.4% of the specimens. This actually confuses the results because it is not clear how the strength of the new concrete or the strength of the old concrete affects the results.

The old concrete surface condition is also the focus of research. It can be found that most studies have investigated the influence of smooth interface or rough interface on the bond behaviour of concrete-to-concrete interfaces. In the previous experimental studies, the maximum surface roughness of old concrete has reached to 6.4 mm (Harries *et al.*, 2012).

In engineering applications, steel bars typically cross the concrete-to-concrete interfaces. Therefore, interfacial reinforcement was considered in most studies. In Table 2, the number of specimens with interfacial reinforcement accounted for 61.4% of the total. In approximately 90% of these studies, the yield stress of the steel bar was less

than 525 MPa, indicating that the interface is generally not reinforced with high-strength bars. The reinforcement ratio ranged from 0 to 22×10^{-3}. Generally, the higher the reinforcement ratio, the smaller the contribution of the concrete-to-concrete interface to the overall resistance. In addition, only one study was found (Mohamad *et al.*, 2015) on the influence of external normal stress on the concrete-to-concrete interface. In other words, the research on the influence of external normal stress on the concrete-to-concrete interface is still obviously insufficient.

In general, as shown in Table 2.2, most of trials were conducted after the year of 2000, with the exception of Hanson (1960), who completed a systematic test in 1960. This shows that before the year of 2000, the shear transfer of the interface between two surfaces of concrete cracks was a hot topic. However, after the year of 2000, the focus of research has gradually turned to the bond behaviour of concrete-to-concrete interfaces.

2.3.2 Factors Affecting the Interfacial Bond Strength

According to the existing theoretical and experimental studies, the concrete-to-concrete interfacial bond behaviour is largely dependent on the material properties of the concretes, the surface roughness of the old concrete, and obviously the reinforcement crossing the interface (dowel action), if any. The studies regarding the influence of these factors on the interfacial shear behaviour of concrete-to-concrete interfaces are reviewed.

(1) Material Properties of Concrete

The strength of concrete has a great impact on the bond behaviour of the concrete-to-concrete interface. The tensile strength of the new or old concrete affects the interfacial shear strength because the tensile strength directly affects the development of cracking.

Many tests have proven that as the new or old concrete tensile strength increases, the shear strength of the interface significantly increases (Kahn and Mitchell, 2002; Júlio *et al.*, 2006; Chilwesa *et al.*, 2017). Therefore, the addition of polymers or fibres to newly cast concrete can enhance the bond properties since it increases the tensile strength of the new concrete and reduces drying shrinkage (Atzeni *et al.*, 1993; Chen *et al.*, 1995).

The vicinity of the concrete-to-concrete interface is commonly referred to as the interfacial transition zone (ITZ) as shown in Figure 2.3 (Xie *et al.*, 2002). The material properties of the ITZ significantly influence the interfacial shear behaviour. Li *et al.* (2001) and Xiong *et al.* (2002) examined the microstructure of the ITZ using the scanning electron microscope (SEM), as well as the energy dispersive spectroscopy (EDS). It was found that using different binders for the ITZ resulted in different microstructures and interfacial shear strengths. Similar results were obtained by Xiao *et al.* (2013) through a nanoindentation test studying the properties of the ITZ in recycled aggregate concrete.

(2) Surface Roughness of the Old Concrete

The surface roughness of the old concrete before casting new concrete to form concrete-to-concrete interfaces has a considerable influence on the interfacial behaviour as it has a direct impact on the friction and aggregate interlocking at the interface (Momayez *et al.*, 2005). The surface roughness can be classified as 'very smooth', 'smooth', 'rough' or 'very rough', as described by Santos and Júlio (2013); it is noted that herein 'smooth' is only used as a description related to 'rough' rather than indicating a friction-free condition. In practice, various surface preparation techniques, such as chemical, mechanical, blasting, flame cleaning, and acid etching, are usually adopted to treat the old concrete surface before casting the new concrete on it. In laboratories, the old

concrete surface is usually intentionally roughened.

Studies conducted by Júlio *et al*. (2004) indicated that the interfacial shear strength increases with the increase of the surface roughness, and the results of direct shear tests indicated that increasing the surface roughness considerably increases the interfacial shear strength (Gohnert, 2003; Mohamad *et al*., 2015; Barbosa *et al*. 2017; Chilwesa *et al.,* 2017).

Since it has been realized that the surface roughness of old concrete has a significant influence on the bond properties of concrete-to-concrete interfaces, Santos *et al*. (2011) summarized the methods to quantify the surface roughness of old concrete. Traditional methods for quantitatively evaluating the surface roughness of concrete include sand-pouring method and fractal dimension method. Recently, a series of new methods with higher accuracy have been proposed by combining digital image technology and computer modeling technology (Huyan *et al*., 2020), such as laser scanning method (Santos and Júlio, 2008), three-dimensional surface fractal dimension method (He *et al*., 2017), etc.

(3) Dowel Action

When slip occurs at the concrete-to-concrete interface, the bond between the concrete-to-concrete interface would decrease rapidly, and the dowel action from the interfacial shear reinforcement provides most of the resistance. Therefore, the shear capacity of the concrete-to-concrete interfaces with dowel reinforcement has been extensively investigated (Paulay *et al*., 1974). Rasmussen *et al*. (1962) proposed an empirical model to estimate the shear capacity considering both the concrete compressive strength and the diameter and yield stress of the dowel reinforcement. Another shear capacity model proposed by Vintzeleou and Tassios (1986) considered the same factors and in addition

took into account the non-coaxiality of the shear forces applied to the dowel reinforcement. Randl (2013) proposed a model for the shear load-slip relationship that is currently widely adopted. In this mode, the shear force is related to the diameter and yield stress of the dowel reinforcement, the compressive strength of the concrete, and the relative sliding displacement at the interface. Nonetheless, all these models are still highly empirical and hence not accurate for different dowel reinforcing configurations. More discussions regarding the dowel action is provided in section 2.4.2.

2.3.3 Shear Transfer Mechanism

The "shear-friction theory" was initially proposed by Birkeland & Birkeland (1966). A simple saw-tooth model was employed to explain the shear transfer mechanism of the concrete-to-concrete interface, seen in Figure 2.4 (Santos and Júlio, 2012). The "shear-friction theory" is applicable to the analysis of various concrete-to-concrete interfaces, such as the interface between prefabricated concrete and cast in-situ concrete, the interface between concretes casted at different times, the interface between existing concrete structure and strengthening concrete layers.

According to the shear-friction theory and a large number of existing experimental studies, the shear force can be assumed to be composed of interfacial adhesion, friction and shear reinforcement crossing the interface. As the slip of the interface increases, the variation of contribution from these three parts are shown in Figure 2.5 (Santos and Júlio, 2012).

When the slip of concrete-to-concrete interface is s, the shear stress $\tau(s)$ can be expressed as:

$$\tau(s) = \tau_a(s) + \tau_{sf}(s) + \tau_{sr}(s) \qquad (2.1)$$

where $\tau_a(s)$ refers to the contribution of adhesion, $\tau_{sf}(s)$ refers to the contribution of friction and $\tau_{sr}(s)$ refers to the contribution of shear reinforcement crossing the interface.

The adhesion is first generated by the chemical action between crystal particles, mainly refers to the van der Waals force and cohesion produced by cement hydration reaction. The adhesion reduces rapidly and then transfers to the interlocking of aggregates with the increase interfacial slip.

The friction is related to the normal stress and roughness of the interface. The normal stress is composed of external load and reinforcement force. The latter one refers to the reverse pressure exerted on the interface by the reinforcement due to the interfacial crack opening after the slip occurs.

The contribution of shear reinforcement crossing the interface, also called dowel action, is important for the shear transfer after large slip.

2.3.4 Comments

At present, the research on the bond behaviour of concrete-to-concrete interface is mainly based on experiments, and basically no systematic theoretical study can be found. It is undeniable that, based on the "shear-friction theory", in view of various influencing factors, such as concrete strength, surface roughness, interfacial shear reinforcement ratio, existing tests have been carried out on concrete-to-concrete interfaces, and rich test data have been obtained. Considering the discreteness of concrete materials, those expressions on bond strength obtained by regression analysis are obviously different, which will also be pointed out later.

21

Although several test methods to the bond behaviour of concrete-to-concrete interfaces are available, researchers realized that each test method has its potential defects. The L-shaped one interface shear test method seems to be the most widely used test method at present. However, whether L-shaped one interface shear test is the most reasonable test method or whether the test method can be improved, has not yet been determined.

It can be seen from the factors affecting the bond strength of the concrete-to-concrete interface that the main methods to improve the bond behaviour of the concrete-concrete interface include are: increasing the surface roughness of old concrete, increasing the strength of new or old concrete, using appropriate interface agents, increasing the interfacial shear reinforcement ratio or the yield strength of the steel bar. In particular, when the slip is large, the interfacial shear reinforcement can not only significantly increase the bearing capacity of concrete-to-concrete interfaces, but also transform the brittle failure of the interface into ductile failure. However, in the absence of interfacial shear reinforcement, few studies can be found on the concrete-to-concrete interface.

2.4 EXISTING ANALYTICAL MODELS FOR THE NOMINAL INTERFACIAL SHEAR STRENGTH

To achieve a thorough understanding and the accurate prediction of the concrete-to-concrete interfacial shear behaviour, it is necessary to establish the local bond-slip model, upon which the global shear stress distribution can be obtained. Although no systematic research on the local bond-slip model of the concrete-to-concrete interface has been conducted, many nominal interfacial shear strength models have been proposed; the representative ones are reviewed in this section.

2.4.1 Concrete-to-Concrete Interfaces without Dowel Reinforcement

Since 1960's, several empirical models have been proposed to predict the nominal

interfacial shear strength of concrete-to-concrete interfaces based on the one-interface shear test. The nominal interfacial shear strength was obtained by measuring the maximum shear force withstood by the interface and dividing the force by the area of the interface, implicitly assuming that the interfacial shear stress was evenly distributed.

Gaston and Kriz (1964) performed a series of one-interface shear tests and suggested the following equation to estimate the nominal interfacial shear strength for smooth concrete-to-concrete interfaces:

$$\tau_{\max} = 0.3 + 0.78\sigma_n \qquad (2.2)$$

where $\tau_{\max}$ is the nominal interfacial shear strength that can be withstood by the interface and σ_n is the corresponding normal stress at the interface (positive values indicate compressive stresses). This model relates the interfacial shear strength with the applied normal stress, which has since been adopted by most of the subsequent models. However, it is obvious that this model is empirical and can hardly be accurate for interfaces with various properties.

Tsoukantas and Tassios (1989) proposed a model for the nominal interfacial shear strength for considering different surface roughness conditions of the old concrete as follows:

$$\tau_{\max} = 0.4\sigma_n \quad \text{for smooth surfaces} \qquad (2.3)$$

$$\tau_{\max} = 0.5\sqrt[3]{f_{ck}^2 \sigma_n} \quad \text{for rough surfaces} \qquad (2.4)$$

where f_{ck} is the characteristic cylinder compressive strength of concrete (the strength of new and old concrete is consistent in this study). This model differentiates the interfacial behaviour for different surface roughness conditions, and empirically incorporates the compressive strength of the base concrete for rough surfaces.

Based on the results of 90 shear tests, Gohnert (2003) proposed an empirical model to evaluate the nominal interfacial shear strength:

$$\tau_{\max} = 0.029R + 0.7719 \tag{2.5}$$

where R is a parameter reflecting the surface roughness. This model indicates that it is more accurate in predicting the interfacial shear strength if the surface roughness is directly considered as a key parameter in the model. Santos and Júlio (2014) proposed a model considering both the cohesion and friction effects at the interface:

$$\tau_{\max} = 1.062R^{0.145} f_t \tag{2.6}$$

where R is the surface roughness. f_t is the new or old concrete tensile strength of representing the cohesion effect, since the strength of new and old concrete is almost the same in this study. Subsequently, Mohamad *et al.* (2015) proposed a model considering the friction and cohesion effects, the surface roughness and the applied normal stress as follows:

$$\tau_{\max} = (0.2363e^{0.237R})f_{t,n} + (0.8766R^{0.3978})\sigma_n \tag{2.7}$$

where R is the surface roughness, e is Euler number, and $f_{t,n}$ is the new concrete tensile

strength.

In general, the existing models for the concrete-to-concrete interfacial nominal shear strength are empirical models considering the applied normal stress, both the new and base concrete uniaxial compressive strength and tensile strength, and surface roughness of the base concrete. The accuracy of the models is largely dependent on the test method and the conditions of the concretes.

2.4.2 Concrete-to-Concrete Interfaces with Dowel Reinforcement

For concrete-to-concrete interfaces with dowel reinforcement, the applied shear load is resisted by the interface and the dowel together. Therefore, if the overall shear strength of concrete-to-concrete interfaces has been reached while the dowel reinforcement has not failed, the dowel can provide sufficient resistance to avoid brittle failure. That is, the dowel reinforcement and the interfacial concrete resistance form a parallel system. The following are some representative models for the nominal interfacial shear strength of concrete-to-concrete interfaces with dowel reinforcement.

A linear equation was proposed by Birkeland and Birkeland (1966) to determine the nominal interfacial shear strength of concrete-to-concrete interfaces when considering the dowel reinforcement as follows.

$$\tau_{max} = \mu \rho f_y \qquad (2.8)$$

where ρ is the ratio between the total cross-sectional area of the dowel reinforcement and the area of the interface (i.e., reinforcing ratio), f_y is the yield stress of the reinforcement, and μ is the friction coefficient (taken as 1.4 for artificially roughened surfaces and 0.8–1.0 for the others). This model has not incorporated the effect of

concrete uniaxial compressive strength and is limited to the condition that the reinforcing ratio is smaller than 1.5%.

Loov (1978) explicitly incorporated the concrete uniaxial compressive strength into the model for the nominal interfacial shear strength of dowel-reinforced concrete-to-concrete interfaces. The following expression was proposed:

$$\tau_{max} = kf_c\sqrt{\frac{\rho f_y + \sigma_n}{f_c}} \tag{2.9}$$

where f_c is cylinder compressive strength of concrete, k is a constant coefficient and is suggested to be 0.5. This model was the first to take the contribution of concrete-to-concrete interfaces into account, which was basically ignored by the prior models, probably with the consideration that the contribution of the dowel reinforcement is significantly greater.

The model proposed by Randl (1997) further incorporated the effects of cohesion and friction as follows:

$$\tau_{max} = cf_c^{1/3} + \mu\left(\rho kf_y + \sigma_n\right) + \gamma\rho\sqrt{f_y f_c} \tag{2.10}$$

where c is the coefficient of cohesion, k is the efficiency coefficient for the tensile load transmitted to the dowel reinforcement, and γ is the coefficient for the flexural resistance of the dowel reinforcement.

In order to extend the applicability of the model to high-strength concrete, Kahn and Mitchell (2002) proposed design expressions for high strength concrete interface (f_c <

96.5 MPa), as follows:

$$\tau_{\max} = 0.05 f_c + 1.4 \rho f_y \qquad (2.11)$$

2.4.3 Remarks

The review of the representative models for the interfacial shear behaviour at concrete-to-concrete interfaces indicates that all the models have been developed to predict the nominal interfacial shear strength, which can be multiplied by the area of the interface to obtain the interfacial shear capacity exceeding which interfacial debonding will occur. The premise of this method is the assumption that the interfacial shear stress is uniformly distributed along the bondline. However, this assumption is obviously erroneous based on the experimental observations and numerical simulations (Wall and Shrive, 1988; Austin *et al.*, 1999; Zanotti and Randl, 2019). Therefore, while these models are to some extent useful in evaluating the shear capacities of concrete-to-concrete interfaces, they are not helpful in developing a thorough understanding of the local bond-slip relationship and the global interfacial stress distribution.

Without such thorough understandings, the mechanical behaviour of concrete-to-concrete interfaces in concrete repair and strengthening works, precast and DfD structures cannot be fully understood. Moreover, accurate nonlinear FE simulations require an accurate local bond-slip relationship for concrete-to-concrete interfaces. Therefore, a local bond-slip model describing the local shear stress-slip relationship is necessary.

2.5 EXISTING BOND-SLIP MODELS FOR CONCRETE-TO-CONCRETE INTERFACES

Only one shear bond-slip model for concrete-to-concrete interfaces with smooth or rough concrete surface is available in the literature. Tassios and Tsoukantas (1989) proposed an empirical bond-slip model and this bond-slip model was adopted in the CEB-FIP Model code (1990).

Equations 2.12~2.15 describe the idealized and normalized relationships between shear stress and shear slip in the case of smooth joint interfaces from CEB-FIP Model code (1990). The bond-slip model shown in Figure 2.6 (a) can be described as

$$\tau = \tau_{max} \cdot \frac{s}{s_u} \qquad if \qquad s \le s_u \qquad (2.12)$$

$$\tau = \tau_{max} \qquad if \qquad s > s_u \qquad (2.13)$$

$$\tau_{max} = 0.4\sigma_c \qquad (2.14)$$

$$s_u = 0.15\sqrt{\sigma_c} \qquad (2.15)$$

where σ_c is the average normal compressive stress on the interface due to external actions. s_u is the shear slip corresponding to τ_{max}.

Equations 2.16~2.19 describe the idealized and normalized relationships between shear stress and slip in the case of interfaces with dowel action. The bond-slip model shown in Figure 2.6 (b) can be formulated as

$$\tau_{max} = 0.40 f_{cd}^{2/3} \left(\sigma_c + \rho f_{yd} \right)^{1/3} \qquad (2.16)$$

$$\frac{\tau}{\tau_{max}} = 10 \cdot \frac{s}{s_u} \qquad if \qquad \frac{s}{s_u} \le 0.05 \qquad (2.17)$$

$$1.7\left[\left(\frac{\tau}{\tau_{\max}}\right)^4 -0.5\left(\frac{\tau}{\tau_{\max}}\right)^3\right]+0.05=\frac{s}{s_u} \quad if \quad \frac{s}{s_u} > 0.05 \tag{2.18}$$

$$s_u=2 \ mm \tag{2.19}$$

where f_{cd} is the design value of the compressive strength of concrete, f_{yd} is the design yield stress of the reinforcement which perpendicularly to the interface, s_u is ultimate shear slip.

2.6 CONCLUSIONS

This chapter has presented a review of the existing experimental and theoretical studies on the interfacial shear behaviour of concrete-to-concrete interfaces. The existing test methods include the direct shear test and the slant shear test; the former aims at minimizing interfacial normal stresses to investigate the interfacial shear behaviour, while the latter aims to simulate the practical loading condition wherein the interface is subjected to combined shear and compressive stresses. A direct shear test specimen without dowel reinforcement is subjected to brittle failure that does not allow the measurement of the complete process of debonding; while a direct shear test specimen with dowel reinforcement does not allow the accurate isolation of the contribution of the concrete-to-concrete interface. The slant shear test is inappropriate for investigating the interfacial shear behaviour because the interfacial stress state is complicated by many testing parameters, and therefore it is difficult to establish a fundamental understanding of the interfacial shear behaviour.

The existing studies investigating factors affecting the interfacial shear behaviour have identified that the concrete material properties, surface roughness, and dowel reinforcement are the principal factors governing the shear capacity of concrete-to-concrete interfaces. However, the influences of these factors on the shear capacity have

only been empirically investigated, while a thorough understanding and accurate quantification have not been achieved.

Based on the shear test data and the understanding of the main factors, analytical models have been proposed to predict the nominal interfacial shear strength of concrete-to-concrete interfaces, which can be used to describe the shear capacity of the interface. However, such models are based on the assumption that the interfacial shear stress is uniformly distributed along the interface. However, this assumption deviates from experimental observations and numerical simulations, and the nominal interfacial shear strength alone is far from sufficient for understanding the interfacial shear stress distribution and the accurate analysis of mechanical behaviour of structures containing concrete-to-concrete interfaces.

Given this background, it is necessary to first devise a new test method through which the complete process of concrete-to-concrete interfacial debonding under shear-dominated stresses can be achieved. Thereupon, a local bond-slip model for the concrete-to-concrete interface needs to be developed as the foundation for further investigations of the interfacial behaviour under more complicated conditions.

2.7 REFERENCES

ACI Committee, & International Organization for Standardization. (2008). Building code requirements for structural concrete (ACI 318-08) and commentary. American Concrete Institute.

Atzeni, C., Massidda, L., & Sanna, U. (1993). Dimensional variations, capillary absorption and freeze-thaw resistance of repair mortars admixed with polymers. *Cement and Concrete Research*, 23(2), 301-308.

Austin, S., Robins, P., & Pan, Y. (1999). Shear bond testing of concrete repairs. *Cement and Concrete Research*, 29(7), 1067-1076.

Barbosa, A. R., Trejo, D., & Nielson, D. (2017). Effect of high-strength reinforcement steel on shear friction behavior. *Journal of Bridge Engineering*, 22(8), 04017038.

Birkeland, P. W., & Birkeland, H. W. (1966). Connections in precast concrete construction. *PCI Journal Proceedings*, 63(3), 345-368.

Caliskan, S., Karihaloo, B. L., & Barr, B. I. G. (2002). Study of rock–mortar interfaces. Part I: surface roughness of rock aggregates and microstructural characteristics of interface. *Magazine of Concrete Research*, 54(6), 449-461.

CEB-FIP model code 1990 (1990). Design of Concrete Structures, Paris.

Chen, P. W., Fu, X., & Chung, D. D. L. (1995). Improving the bonding between old and new concrete by adding carbon fibers to the new concrete. *Cement and Concrete Research*, 25(3), 491-496.

Chilwesa, M., Minelli, F., Reggia, A., & Plizzari, G. (2017). Evaluating the shear bond strength between old and new concrete through a new test method. *Magazine of Concrete Research*, 69(9), 425-435.

Clark, L. A., & Gill, B. S. (1985). Shear strength of smooth unreinforced construction joints. *Magazine of Concrete Research*, 37(131), 95-100.

Clímaco, J. D. S., & Regan, P. E. (2001). Evaluation of bond strength between old and new concrete in structural repairs. *Magazine of Concrete Research*, 53(6), 377-390.

Crane, C. K. (2010). Shear and shear friction of ultra-high performance concrete bridge girders. *PhD thesis*, Georgia Institute of Technology.

EN 1998-3 Eurocode 8 (2005). Design of structures for earthquake resistance—Part 3:

Assessment and retrofitting of buildings, CEN.

*f*ib model code for concrete structures 2010 (2013). Berlin, Germany.

Gaston, J. R., & Kriz, L. B. (1964). Connections in precast concrete structures--scarf joints. *PCI Journal*, 9(3), 37–59.

Gohnert, M. (2003). Horizontal shear transfer across a roughened surface. *Cement and Concrete Composites*, 25(3), 379-385.

Hanson, N. W. (1960). Precast-prestressed concrete bridges 2: Horizontal shear connections. *Portland Cement Association, Research and Development Laboratories*, 2 (2): 38-58

He, Y., Zhang, X., Hooton, R. D., & Zhang, X. (2017). Effects of interface roughness and interface adhesion on new-to-old concrete bonding. *Construction and Building Materials*, 151, 582-590.

Hofbeck, J. A., Ibrahim, I. O., & Mattock, A. H. (1969). Shear transfer in reinforced concrete. *ACI Journal*, 66(2), 119-128.

Huyan, J., Li, W., Tighe, S., Sun, Z., & Sun, H. (2020). Quantitative analysis of macrotexture of asphalt concrete pavement surface based on 3D data. *Transportation Research Record*, 2674(8), 732-744.

Julio, E. N., Branco, F. A., & Silva, V. D. (2004). Concrete-to-concrete bond strength. Influence of the roughness of the substrate surface. *Construction and Building Materials*, 18(9), 675-681.

Júlio, E. N., Branco, F. A., Silva, V. D., & Lourenço, J. F. (2006). Influence of added concrete compressive strength on adhesion to an existing concrete substrate. *Building and Environment*, 41(12), 1934-1939.

Júlio, E. N. B. S., Dias-da-Costa, D., Branco, F. A. B., & Alfaiate, J. M. V. (2010). Accuracy of design code expressions for estimating longitudinal shear strength of strengthening concrete overlays. *Engineering Structures*, 32(8), 2387-2393.

Kahn, L. F., & Mitchell, A. D. (2002). Shear friction tests with high-strength concrete. *ACI Structural Journal*, 99(1), 98-103.

Li, G., Xie, H., & Xiong, G. (2001). Transition zone studies of new-to-old concrete with different binders. *Cement and Concrete Composites*, 23(4-5), 381-387.

Loov, R. E. (1978). Design of precast connections. *Paper presented at a seminar organized by Compa International Pt., Ltd*. Singapore.

Loov, R. E., & Patnaik, A. K. (1994). Horizontal shear strength of composite concrete beams. *PCI Journal*, 39(1), 48-69.

Mattock, A. H., & Hawkins, N. M. (1972). Shear transfer in reinforced concrete: Recent research. *PCI Journal*, 17(2), 55-75.

Mattock, A. H. (1976). Shear transfer under monotonic loading, across an interface between concretes cast at different times. *University of Washington report SM*, 76-3.

Mohamad, M. E., Ibrahim, I. S., Abdullah, R., Rahman, A. A., Kueh, A. B. H., & Usman, J. (2015). Friction and cohesion coefficients of composite concrete-to-concrete bond. *Cement and Concrete Composites*, 56, 1-14.

Momayez, A., Ehsani, M. R., Ramezanianpour, A. A., & Rajaie, H. (2005). Comparison of methods for evaluating bond strength between concrete substrate and repair materials. *Cement and Concrete Research*, 35(4), 748-757.

Naderi, M. (2009). Analysis of the slant shear test. *Journal of Adhesion Science and Technology*, 23(2), 229-245.

Paulay, T., Park, R., & Phillips, M. H. (1974). Horizontal construction joints in cast-in-place reinforced concrete. *ACI Special Publication*, 42, 599-616.

Randl, N. (1997) Investigations on transfer of forces between old and new concrete at different joint roughness. *PhD thesis*. Austria: University of Innsbruck.

Randl, N. (2013). Design recommendations for interface shear transfer in fib Model Code 2010. *Structural Concrete*, 14(3), 230-241.

Rasmussen, B. H. (1962). Strength of transversely loaded bolts and dowels cast into concrete. Laboratoriet for Bugningastatik, Denmark Technical University, Meddelelse, 34(2).

Santos, P. M., & Julio, E. N. (2007). Correlation between concrete-to-concrete bond strength and the roughness of the substrate surface. *Construction and Building Materials*, 21(8), 1688-1695.

Santos, P. M., & Júlio, E. N. (2008). Development of a laser roughness analyser to predict in situ the bond strength of concrete-to-concrete interfaces. *Magazine of Concrete Research*, 60(5), 329-337.

Santos, P. M., & Júlio, E. N. (2011). Factors affecting bond between new and old concrete. *ACI Materials Journal*, 108(4), 449.

Santos, P. M., & Júlio, E. N. (2012). A state-of-the-art review on shear-friction. *Engineering Structures*, 45, 435-448.

Santos, P. M., & Júlio, E. N. (2013). A state-of-the-art review on roughness quantification methods for concrete surfaces. *Construction and Building Materials*, 38, 912-923.

Santos, P., & Júlio, E. N. (2014). Interface shear transfer on composite concrete members. *ACI Structural Journal*, 111(1), 113-120.

Saucier, F., Bastien, J., Pigeon, M., & Fafard, M. (1991). A combined shear-compression device to measure concrete-to-concrete bonding. *Experimental Techniques*, 15(5), 50-55.

Scott, J. (2010). Interface shear strength in lightweight concrete bridge girders. *MS thesis*, Virginia Polytechnic Institute, Blacksburg.

Shaw, D. M., & Sneed, L. H. (2014). Interface shear transfer of lightweight-aggregate concretes cast at different times. *PCI Journal*, 59(3), 130-144.

Sneed, L. H., Krc, K., Wermager, S., & Meinheit, D. (2016). Interface shear transfer of lightweight-aggregate concretes with different lightweight aggregates. *PCI Journal*, 61(2), 38-55.

Tabor, L. J. (1978). The evaluation of resin systems for concrete repair. *Magazine of Concrete Research*, 30(105), 221-225.

Tassios, T. P., & Vintzēleou, E. N. (1987). Concrete-to-concrete friction. *Journal of Structural Engineering*, 113(4), 832-849.

Tsoukantas, S. G., & Tassios, T. P. (1989). Shear resistance of connections between reinforced concrete linear precast elements. *ACI Structural Journal*, 86(3), 242-249.

Vintzeleou, E. N., & Tassios, T. P. (1986). Mathematical models for dowel action under monotonic and cyclic conditions. *Magazine of Concrete Research*, 38(134), 13-22.

Wall, J. S., & Shrive, N. G. (1988). Factors affecting bond between new and old concrete. *ACI Materials Journal*, 85(2), 117-125.

Walraven, J. (1987). Influence of concrete strength and load history on the shear friction capacity of concrete members. *PCI Journal*, 32(1), 66-83.

Waseem, S. A., & Singh, B. (2016). Shear transfer strength of normal and high-strength

recycled aggregate concrete–An experimental investigation. *Construction and Building Materials*, 125, 29-40.

Xiao, J., Li, W., Sun, Z., Lange, D. A., & Shah, S. P. (2013). Properties of interfacial transition zones in recycled aggregate concrete tested by nanoindentation. *Cement and Concrete Composites*, 37, 276-292.

Xiao, J., Xie, H., & Yang, Z. (2012). Shear transfer across a crack in recycled aggregate concrete. *Cement and Concrete Research*, 42(5), 700-709.

Xie, H. C., Li, G. Y., & Xiong, G. J. (2002). Microstructure model of the interfacial zone between fresh and old concrete. *Journal of Wuhan University of Technology-Mater. Sci. Ed.*, 17(4), 64-68.

Xiong, G., Liu, J., Li, G., & Xie, H. (2002). A way for improving interfacial transition zone between concrete substrate and repair materials. *Cement and Concrete Research*, 32(12), 1877-1881.

Yang, S., Huang, W., & Liu, Y. (2014). Push-out test to study bond properties of mortar–concrete interface. *Magazine of Concrete Research*, 66(21), 1104-1115.

Zanotti, C., & Randl, N. (2019). Are concrete-concrete bond tests comparable?. *Cement and Concrete Composites*, 99, 80-88.

Table 2.1 A summary of shear test methods for concrete-to-concrete interfaces

Test methods	One-interface shear test (Push-off shear test)	Two-interface shear test (Push-out shear test)	L-shaped one-interface shear test (Push-off shear test with L-shaped blocks)	Slant shear test
First used by	Saucier et al. (1991)	Theodossius and Vintzeleou (1987)	Anderson (1960).	Tabor (1978)
Dowel reinforcement	No	No	Yes	No
Characteristics	i) Non-negligible normal stresses ii) Local fracture terminates the test	i) Local fracture does not immediately terminate the test ii) Non-negligible normal stresses iii) Two concrete-to-concrete interfaces per specimen	i) Can obtain the descending branch of the load-displacement relationship due to the resistance provided by the reinforcement ii) Difficult to separate the contributions provided by the reinforcement and the concrete-to-concrete interface	i) Relatively low level of scatter for specimens with identical parameters ii) Relatively high sensitivity to specimen parameters including geometries and the orientation of the concrete-to-concrete interface iii) The concrete-to-concrete interface is subjected to combined shear and compressive stresses

Table 2.2 A summary of shear test database on concrete-to-concrete interfaces

Authors	Year	Number of specimens	Test method	Old concrete cylinder compressive strength/MPa	New concrete cylinder compressive strength/MPa	Surface roughness	$\rho \times 10^{-3}$	fy/MPa	External normal stress σ
Hanson	1960	46	L-shaped one-interface shear test	28.1 to 41.6	22.3 to 28.6	Smooth & Rough	0 to 8.18	324 to 358	/
Kahn and Mitchell	2002	12	L-shaped one-interface shear test	27.6 to 96.5	27.6 to 96.5	Rough	4 to 15	413.7	/
Gohnert	2003	90	One-interface shear test	18.1-24.8	32.9-44.4	Rough (0.89 to 4.22 mm)	/	/	Roller support
Crane	2010	20	L-shaped one-interface shear test	84.1	84.1	Smooth &Rough	0 to 7.5	506.7	/
Scott	2010	36	L-shaped one-interface shear test	53.64 to 76.5	39.3 to 42.7	Rough	0 to 5	413.7	/
Harries et al.	2012	16	L-shaped one-interface shear test	41.5	29.1	Rough (6.4 mm)	4.0 to 8.1	424 to 965.3	/
Shaw and Sneed	2014	36	L-shaped one-interface shear test	33.5 to 52.5	31.7 to 54.05	Smooth &Rough	13.3	456.5	/
Mohamad et al.	2015	60	One-interface shear test	40.0	25.0	Smooth &Rough (0 to 6.0 mm)	/	/	0 to 1.5 MPa
Sneed et al.	2016	46	L-shaped one-interface shear test	30.1 to 38.4	30.1 to 38.4	Smooth &Rough	9.0 to 22.0	497.8	/
Waseem et al.	2016	48	L-shaped one-interface shear test	30.2 to 38.2	64.4 to 7.3.6	Smooth	0 to 12.8	525	/
Barbosa et al.	2017	20	L-shaped one-interface shear test	28.9 to 31.7	28.9 to 31.7	Rough (3.2 mm)	4.2 to 6.5	466.1 to 641.2	/
Chiwese et al.	2017	26	Two-interface shear test	28.4	32.4 to 100.3	Smooth &Rough (0 to 5.0 mm)	/	/	/
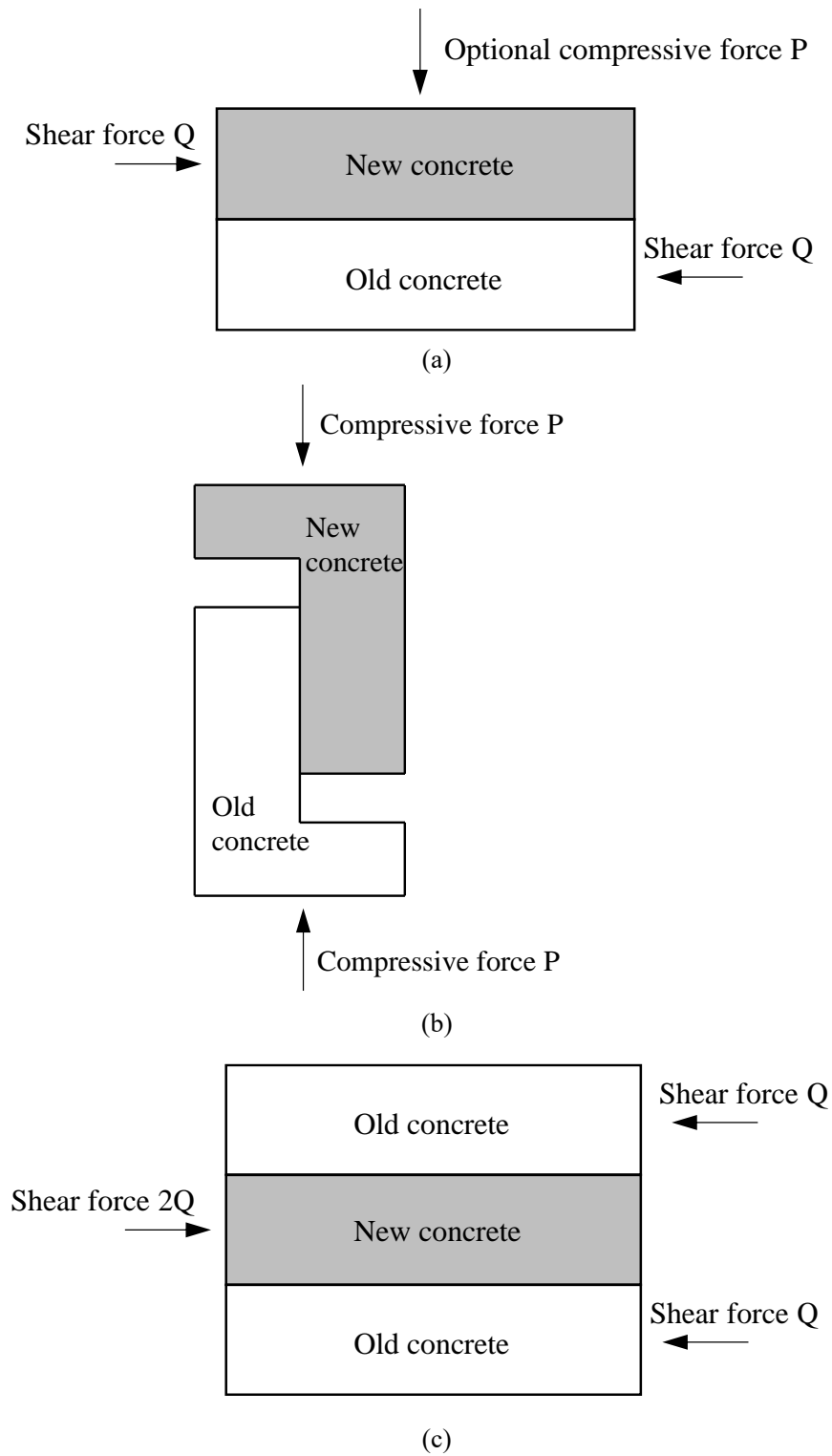
Figure 2.1 Schematics of specimens in: (a) one-interface shear test (b) L-shaped one-interface shear test, (c) two-interface shear test
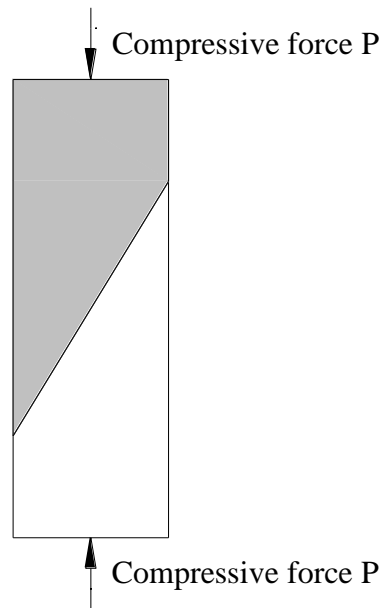
Figure 2.2 Schematic of a specimen in a slant shear test
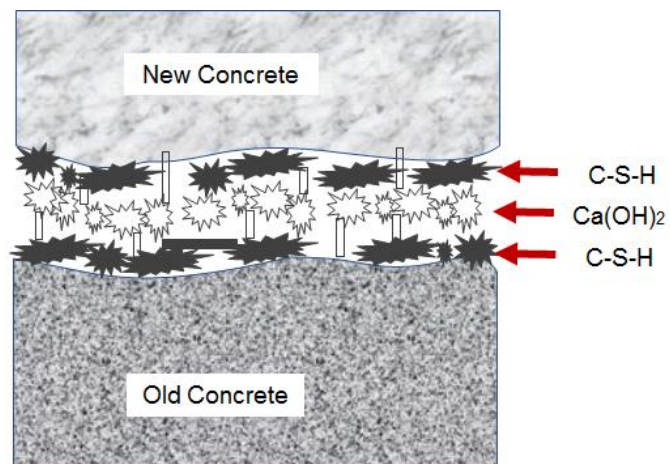
Figure 2.3 Schematic of the interfacial transition zone (ITZ)
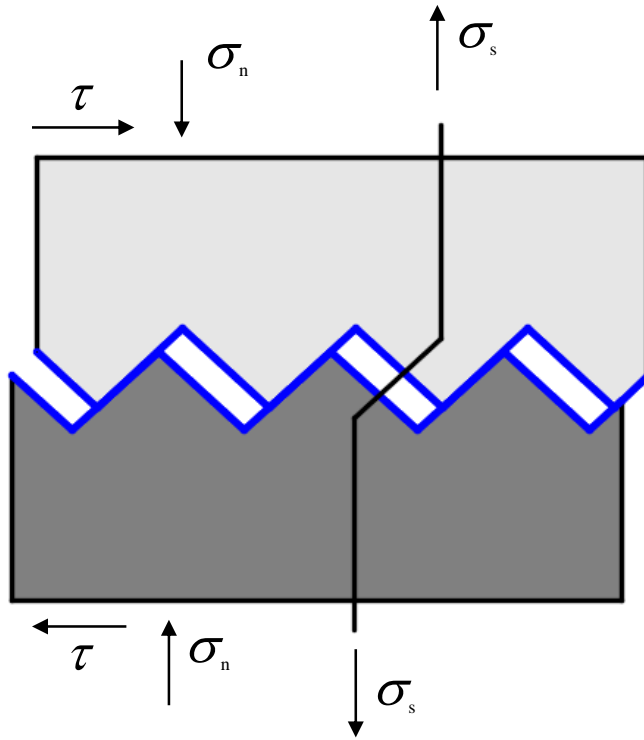
Figure 2.4 Shear-friction theory model (Santos and Júlio, 2012)
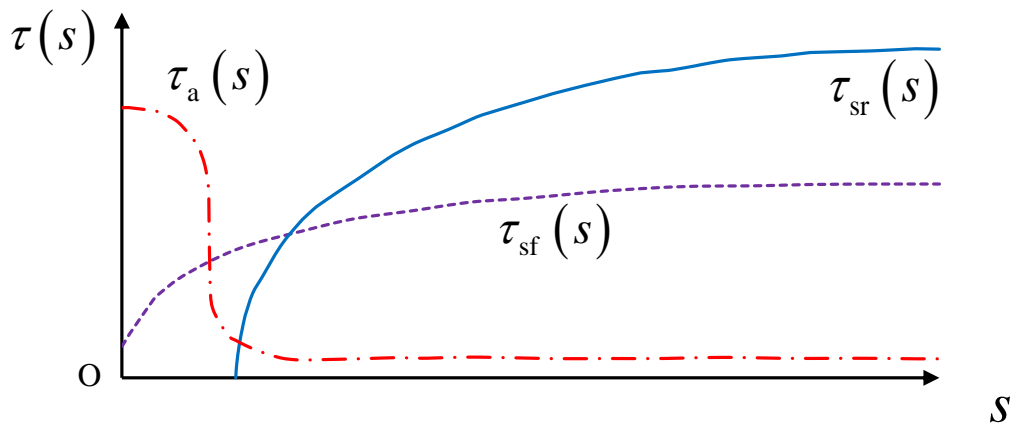
Figure 2.5 Contribution variation of adhesion, friction and dowel action (Santos and Júlio, 2012)

$$\tau_{max}=0.4\sigma_c$$

$$\tau=\tau_{max}\cdot\frac{s}{s_0} \qquad if \qquad s \le s_0$$

(a) Smooth interface

$$1.7\left[\left(\frac{\tau}{\tau_{max}}\right)^4-0.5\left(\frac{\tau}{\tau_{max}}\right)^3\right]+0.05=\frac{s}{s_u} \qquad if \qquad \frac{s}{s_u}>0.05$$

$$\frac{\tau}{\tau_{max}}=10\cdot\frac{s}{s_u} \qquad if \quad \frac{s}{s_u}\le 0.05$$
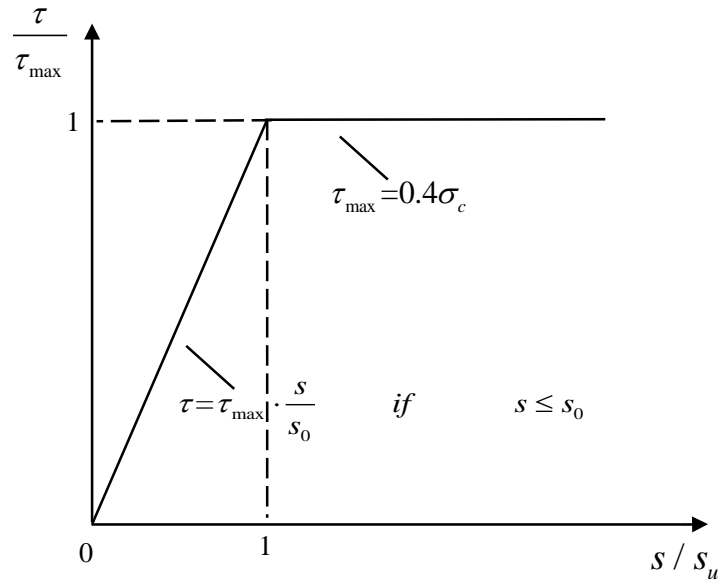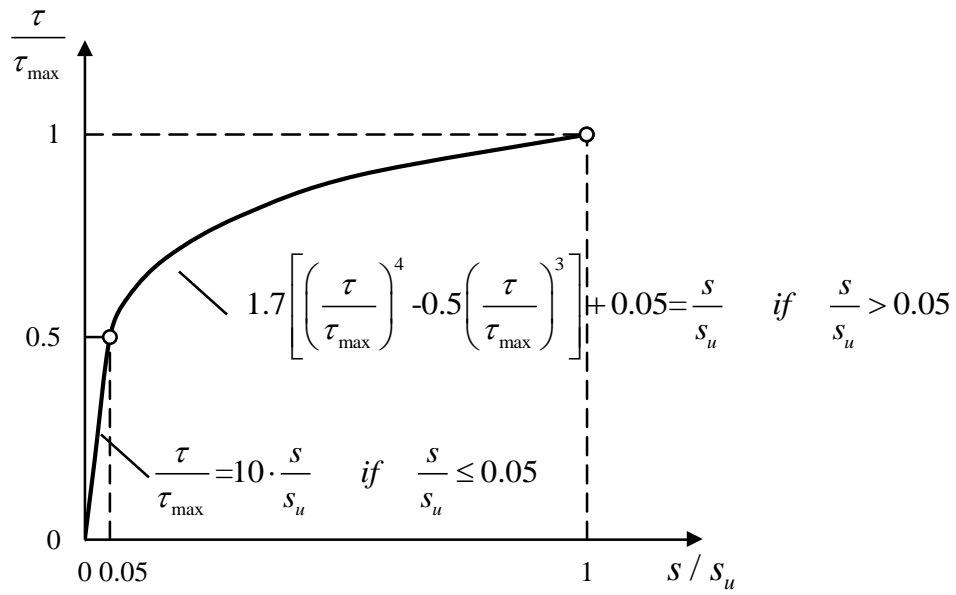
(b) Rough interface

Figure 2.6 Mobilized shear stress- slip relationship suggested by CEB-FIP model code

(1990)

42

CHAPTER 3

FINITE ELEMENT ANALYSIS OF EXISTING SHEAR TESTS FOR CONCRETE-TO-CONCRETE INTERFACES

3.1 INTRODUCTION

Since the 1960s, extensive experimental research has been conducted to investigate the shear behaviour of concrete-to-concrete interfaces (Bissonnette *et al.*, 2011; Santos and Júlio, 2012; Achilllopoulou, 2016). Several test methods have been proposed to quantify the shear strength, and they can be categorised into one-interface shear tests, two-interface shear tests, L-shaped one-interface shear tests, and slant shear tests, as reviewed in detail in Chapter 2. These existing test methods can only measure the global shear resistance and relative slip of the bonded interface, which are simple summations of, but unable to differentiate, the local shear stresses and slips along the interface. Meanwhile, the local shear stress-slip relationship, or more commonly referred to as the bond-slip relationship, of concrete-to-concrete interfaces is an integral component for the numerical analysis of structures containing such interfaces such as repaired or prefabricated concrete structures. However, such an accurate model has not been presented, according to previous studies on the experimental or numerical analysis (Hawileh *et al.*, 2010; Zoubek *et al.*, 2013; Magliulo *et al.*, 2014; Kremmyda *et al.*, 2017), mainly due to the lack of an appropriate test method. Therefore, a new test method suitable for evaluating the local bond-slip relationship is needed.

A proper test method to obtain the bond-slip behaviour should comply with the following requirements: *i*) induces a shear-dominated stress state and minimises the

normal stress at the concrete-to-concrete interface, *ii*) induces a generally uniform shear stress distribution along the interface, and *iii*) enables a stable debonding process after reaching the global peak shear resistance to capture the softening behaviour of the interface.

The slant shear test violates the first requirement since the interface is subjected to combined compressive and shear stresses, as well documented in previous experimental studies (Clark and Gill, 1985; Wall and Shrive, 1988; Clímaco and Reganand, 2001; Júlio *et al*., 2006; Santos *et al*., 2007) and numerical works (Wall and Shrive, 1988; Júlio *et al*., 2006).Therefore, it is inappropriate for investigating the interfacial bond-slip behaviour of concrete-to-concrete interfaces. While the different direct shear tests nominally generate a shear-dominated stress state at the interface, rigorous analyses are needed to examine the normal and shear stress distributions at the interfaces of direct shear test specimens. Therefore, a series of finite element (FE) analyses are presented in this chapter to assess the existing direct shear test methods for concrete-to-concrete interfaces. Based on the numerical results, the characteristics of the stress distribution and the influence of the test parameters are discussed, and thereupon a suitable test method for investigating the bond-slip relationship of concrete-to-concrete interfaces is suggested.

3.2 FINITE ELEMENT MODELLING

FE analyses of three types of direct shear test specimens, including the one-interface, L-shaped one-interface, and two-interface specimens, all without dowel reinforcement, were analysed using the general-purpose FE package ABAQUS 6.8 (2008).

3.2.1 FE Models

Linear elastic FE analyses were performed to explore the stress states of the specimens for different test methods. For clarification, the concrete layer between the new and old concretes is referred to as the 'bondline layer'. According to Zhang and Teng (2010), if the widths of the old concrete block, bondline layer and new concrete block are the same, a two-dimensional (2D) FE model is appropriate. Therefore, a 2D plane stress general FE model was developed to simulate the tests; different direct shear test specimens can be simulated by applying proper boundary conditions.

The geometries of the FE models corresponding to the three shear test setups are shown in Figure 3.1. To compare the shear test setups, the length of the bondline layer was set as 300 mm, and the width of the old and new concrete blocks was set as 100 mm. The depths of the old and new concrete blocks were both 100 mm for the one-interface model, and they were 100 and 200 mm respectively for the two-interface model. A 2 mm thin layer was used to simulate the bondline in all the FE models. Notably, the actual thickness of the bondline layer is very difficult to measure, and the value of 2 mm here is an expedient assumption. Nevertheless, since the objective of the FE analysis is to evaluate interfacial stresses in various kinds of shear tests, the thickness of the bondline layer is of little influence except on the stiffness of this layer. The thickness of the steel loading plate, as shown in Figure 3.1, was assumed to be 50 mm in the FE models, and its effect is further discussed below.

A perfect bond was assumed between the bondline layer and the new and old concretes as well as at the concrete-to-steel interface. The boundary conditions are shown in Figure 3.1. For the base support on the bottom, the Y direction was restrained. For the support on the right side, the X direction was restrained according to the experiment. Practically in the tests, a concentrated force is applied to the specimen using a hinged

steel ball on the steel plate, and thus, the compressive loading on the new concrete block was simulated by applying a concentrated force in the FE models. The value of the concentrated force was equivalent to the application of a uniform compressive stress of 3 MPa on the vertical surface of the new concrete block.

The new concrete, old concrete and bondline layer were set to be linear elastic and isotropic, and meshed with four-node quadrilateral plane stress elements (CPS4). Although inelastic behaviour of the concrete can be expected in reality, for the purpose of comparative study of the interfacial stress distribution for different types of direct shear test setups, the linear elastic assumption is acceptable. The FE analyses of the direct shear tests are mainly focused on evaluating the normal tensile stress concentration at interface ends and the degree of uniformity of the shear stress distribution. If the normal tensile stress exceeds the Mode-I interfacial strength, interfacial debonding is likely to initiate and evolve into complete interfacial debonding. If the shear stress distribution is overly non-uniform, the measured global resistance of the interface cannot be used to accurately represent the local shear resistance. Therefore, both should be avoided for the direct shear test to be successful. With the assumption of linear-elastic behaviour for concrete, the predicted stresses at interface ends may exceed the actual tensile strength of concrete, which indicates the initiation of interfacial cracking. Alternatively, if a more realistic constitutive description considering inelastic behaviour is used for the concrete, the predicted stress level at interface ends will be limited by the peak stress of the constitutive relationship and become zero when debonding has been initiated. Regarding the shear stress distribution, assuming linear-elastic behaviour or inelastic behaviour will likely lead to similar predictions as the influence is expected to be in the vicinities of interface ends. Therefore, both approaches are equally capable of evaluating the appropriateness of direct shear tests, and the linear elastic material assumption is thus selected for its

simplicity. Such an approach has been adopted in previous studies to understand interfacial stresses in concrete members bonded with a thin plate (Teng *et al.*, 2002; Zhang and Teng, 2010) and FRP or steel plate-to-concrete bonded joints (Chen *et al.*, 2001).

The old concrete, new concrete, bondline layer, and steel plate were assigned with elastic moduli of 30.0, 40.0, 15.0 and 200.0 GPa, respectively. Common values of the Poisson's ratio of 0.17 and 0.30 were assumed for the concrete and steel in these FE models, respectively. The geometries and material properties of these components are listed in Table 3.1.

3.2.2 Mesh Convergence Study

The one-interface shear test model shown in Figure 3.1 (a) was used to performe the mesh convergence study. The mesh sensitivity was studied by varying the size of the four-node quadrilateral plane stress elements of the bondline layer. Specifically, the element sizes of 0.01 mm, 0.05 mm, 0.1 mm, 0.2 mm and 0.5 mm were considered, resulting in 200, 40, 20, 10 and 4 elements, respectively, across the thickness (2 mm) of the bondline layer. In the bond length direction, a graded mesh pattern was adopted, as shown in Figure 3.2 for the mesh with an element size of 0.05 mm. The stress distribution along the interface between the new concrete and bondline layer is simplified as the stress along 'NB interface', that along the interface between the old concrete and interface layer as the 'OB interface', and that along the midline of the bondline layer as the 'MB interface', respectively, as indicted in Figure 3.2.

Figures 3.3 (a), (b) and (c) show the normal and shear stress distributions along the NB, OB, and MB interfaces, respectively, for different element sizes. Figure 3.3 (a) indicates that the NB interfacial normal and shear stress distributions are identical for element

sizes ranging from 0.01 to 0.5 mm except at the vicinity of the push end ($x = 0$). Near the push end, both normal and shear stresses increase with the decrease of element size due to the strain/stress singularity at the sharp corner location ($x = 0$) along the NB interface, since the end surfaces of the old concrete, new concrete, and bondline layer were modelled as a flush surface, as discussed by Chen *et al.* (2001) and Teng *et al.* (2002). Therefore, the predicted stresses cannot converge at the NB interface near the push end as the element size decreases. For the present purpose, the FE model is considered to have converged when the impact of mesh refinement is confined within a region of trivial size near the push end. Regarding the stress distribution along the NB interface, it is seen that when the element size is smaller than 0.1 mm, the impact of further mesh refinement is trivial, and the mesh is thus considered to have converged.

Both the normal and shear stresses along the MB interface do not vary considerably with mesh refinement and are influenced only within a small 1 mm region from the push end, as shown in Figure 3.3 (b). The calculated normal and shear stresses at the push end approach zero as the mesh becomes finer, corresponding to the zero shear stress boundary condition of a free surface. The influence of mesh refinement on the normal and shear stress distributions along the OB interface is shown in Figure 3.3 (c). Similar to the stress distributions at the NB and MB interfaces, the effect of mesh refinement is confined in a region of 1 mm from the push end for the OB interface for normal and shear stresses.

Table 3.2 lists the values of normal and shear stresses at the push end, as obtained from the FE analysis results. The normal and shear stresses do not converge for the NB interface. However, for the OB and MB interfaces, the normal stresses do not vary considerably, and the shear stress approaches zero at the push end, while the normal stresses do not vary considerably. Therefore, examining the normal and shear stress

distributions along the MB and the OB interfaces, when the mesh size is smaller than 0.05 mm, the impact of further mesh refinement can hardly be noticed. As a result, the 0.05 mm mesh size is considered to be sufficiently small to achieve converged results for this FE model.

3.2.3 Boundary Conditions for the Direct Shear Tests

In a typical shear test, the pushing force is usually applied using a hinged steel ball, which is then distributed to the surface of the concrete block through a steel plate. However, the impact of the thickness of the steel plate on the stresses in the concrete block has not been investigated in the literature. Thus, using the developed FE model, the stresses in the concrete were predicted by varying the thickness of the steel plate to evaluate its influence. Five thicknesses of the steel loading plate, 10 mm, 25 mm, 50 mm, 75 mm and 100 mm were selected. The resulting stresses in the new concrete block at the loading plane ($x = 0$) are compared in Figure 3.4 (a). With different thicknesses of the steel plate, the resulting normal stresses at the loading surface of the concrete block differ considerably. For thicknesses from 10 mm to 25 mm, highly nonuniform compressive stresses are induced in the concrete block as shown in the figure. For steel plates that are thicker than 50 mm, the induced stresses are rather uniform over the height of the concrete block as shown in the figure. This finding suggests that for such a concrete interface shear test, a steel plate of at least 50 mm thick should be used to realise a uniform compressive stress distribution and prevent unwanted stress concentration. For the steel plate on the support side providing a reaction force, the effect of the thickness of the steel plate is evaluated in Figure 3.4 (b), which indicates that the normal stress distributions are quite uniform in the majority of the region and do not vary with steel plate thickness. Therefore, the thickness of the support steel plate has a very limited effect.

49

In typical one-interface shear tests, roller support is usually placed on top of the new concrete block to prevent any uplifting that may occur during the test. Therefore, various roller support configurations were simulated by adjusting the boundary conditions applied to the top surface of the new concrete. Specifically, the deformations in the *y*-direction on the upper boundary were prevented in four configurations by restraining: *i*) all nodes, *ii*) nodes at a spacing of 10 mm, *iii*) nodes at a spacing of 25 mm, and *iv*) no nodes (i.e., all nodes were free from restraint in the *y*-direction). Figure 3.5 shows the normal and shear stress distributions of MB interface resulting from these configurations. It is seen that the spacing of the restrained nodes does not significantly influence the interfacial stress distributions as long as roller support is used to prevent the uplifting. However, if the upper boundary is free from restraint, the normal stress distribution becomes considerably different. Specifically, normal tensile (peeling) stress appears in a large region (175 mm from the push end) at the MB interface, compared to the normal stress distribution with roller support where normal stress is concentrated in a small region at the interface ends, as shown in Figure 3.5 (a). The widely distributed peeling stress may induce premature splitting at the interface. As a result, roller supports are usually required in such shear tests.

3.3 INTERFACIAL STRESS DISTRIBUTION

3.3.1 Stress Distributions across the Thickness of the Bondline Layer

Through the numerical results of the above-mentioned FE model, important information about the behaviour of the concrete-to-concrete interface for various test specimens can be obtained. Figure 3.6 shows the stress distributions along the thickness of the bondline layer (vertical distance 0.0 mm indicates OB, 1.0 mm indicates MB, and 2.0 mm indicates NB) at various locations near the push end or the support end of the one-interface direct shear test specimen. The horizontal distance from the push end

for each distribution is indicated in the legend.

Figures 3.6 (a) and (b) shows the normal stress distributions at various cross section along the bondline layer thickness. It is seen that, near the push end (x=0.0 ~ 0.4 mm), considerable normal compressive stress appears at the NB interface (y=2.0 mm) while normal tensile stress appears at the OB interface (y=0.0 mm). This indicates that local interfacial splitting may occur at the OB interface in a small region near the push end. Near the support end (x=299.0 ~ 300.0 mm), considerable normal compressive stress appears at the OB interface (y=0.0 mm) while smaller compressive stress appears at the NB interface (y=2.0 mm), indicating no interfacial splitting would occur at the support end. More importantly, the results indicate that except for the small regions around the interface ends, the normal stress distribution along the thickness of the bondline layer is rather uniform, as seen in Figure 3.6 (a) and (b). That is, in the majority of the bondline, the normal stress distribution is identical at the NB, MB, and OB interfaces.

Figures 3.6 (c) and (d) show the shear stress distributions across the thickness of the bondline layer at different locations. In the small region near the push end (x=0.0 ~ 2.0 mm), considerable shear stress appears at the NB interface (y=2.0 mm) while the shear stress is much smaller at the OB and MB interfaces (y = 0 and 1 mm). By contrast, in the small region near the support end (x=299.0 ~ 300.0 mm), considerable shear stress appears at the OB interface (y=0.0 mm) while the shear stress is much smaller at the MB and NB interfaces (y = 1 and 2 mm). More importantly, similar to the distribution of normal stress, the shear stress distribution across the thickness of the bondline layer is rather uniform beyond the small regions near the interface ends. That is, in the majority of the bondline, the shear stress distribution is identical at the NB, MB, and OB interfaces.

Therefore, in general, singular behaviour can be observed at both the OB interface and the NB interface at the interface ends, resulting in high level of normal and shear stresses that may induce local failure at the concrete-to-concrete interface of the specimen. In addition, the normal and shear stress distributions along the thickness are nearly uniform outside of the small region around 2 mm from the push end. Along the mid-plane of the bondline layer, i.e., the MB interface, no obvious singular behaviour is observed.

3.3.2 Comparison of Stress Distributions at the OB, NB and MB Interfaces

Figure 3.7 shows the stress distributions at the NB, MB and OB interfaces within 25 mm from the push end for the one-interface shear test specimen. It can be seen that both normal and shear stress distributions at the NB, MB and OB interfaces are basically identical beyond the small region of 5 mm near the push end. Therefore, only within the small region of 5 mm from the push end the stress distributions at the NB, MB, and OB are different and further discussed.

The FE results clearly show that the NB interface and OB interface exhibit obvious singular behaviour near the push end. The normal stress of the former is compressive stress, while of the latter is tensile stress, as shown in Figure 3.7 (a). However, no obvious singular behaviour can be found at the MB interface. From the shear stress distributions shown in Figure 3.7 (b), it can be seen that the NB interface still exhibits singular behaviour near the push end. However, shear stress approaches zero at the MB and OB interfaces at the push end. The shear stress at these two interfaces reach the maximum values at about 2 mm away from the push end, and then gradually decreases and remains basically the same.

Shear stress plays a key role in the shear failure of concrete-concrete interfaces, which

is also the focus of this study. Therefore, if only the shear stress is considered, it should be ideal to study the stress of both the MB interface and the OB interface. However, this is impractical because stress singularities of OB interface at the push end indicate that the stresses of the OB interface in this area cannot be accurately predicted. Moreover, Teng *et al.* (2002)'s research on concrete beams bonded with a soffit plate showed that the analytical solution of the interface provides the average value of the interface stress, and the predicted results are consistent with the FE result of the stress in the middle part of the adhesive layer. Therefore, it is considered that the interfacial stress at the MB interface represents the average value of the interfacial stress through the thickness of the bondline layer in this study. It is for this reason that the rest of this thesis will only discuss the interfacial stresses of MB interface.

3.3.3 Effect of Bondline Layer Thickness

With other values of the model parameters for the bondline layer fixed, Figure 3.8 presents the interfacial stress distributions at the MB interface near the push end with four different bondline layer thicknesses of 0.5 mm, 1 mm, 2 mm and 4 mm.

It can be seen from Figure 3.8 that when the thickness of the bondline layer is 4 mm, the maximum normal stress near the push end is 2.06 MPa tensile stress, and the maximum shear stress near the push end is 3.43 MPa; when the thickness of the bondline layer is reduced to 0.5 mm, the maximum normal stress near the push end is 9.50 MPa compressive stress, and the maximum shear stress near the push end is 7.74 MPa. This indicates that as the thickness of the bondline layer decreases, the maximum normal stress near the push end turns from tensile stress to a gradually increasing compressive stress; meanwhile, the maximum shear stress near the push end also increases gradually.

In addition, it can be seen that the above-mentioned maximum normal stress and shear stress both appear at a relatively close distance from the push end, about 2 mm. With the decrease of the thickness of the bondline layer, the locations of the maximum normal and shear stresses approach the push end. For example, for the 4 mm bondline layer thickness, the maximum shear stress appears at 3.00 mm from the push end, while for the 0.5 mm bondline layer thickness, the maximum shear stress appears at 0.50 mm from the push end.

In general, for the four different bondline layer thicknesses, the normal and shear stress distributions at the NB, OB, and MB are identical over the majority of the bond length, as shown in Figure 3.8, with differences confined in the vicinity of about 3 mm near the push end. Practically, the thickness of the bondline layer is very difficult to measure, and no specific concensus have been reached on the thickness of the bondline from previous studies. Recent CT scans of the concrete-to-concrete interface in 3D printed concrete showed that the thickness of the bondline layer was between 1.50 mm and 2.24 mm (Sun *et al*., 2020). In another study conducted by Du *et al*., (2013) when focusing on the nonlinear damage and failure behaviour of reinforced concrete members, it was found that the numerical results agreed well with the test results if the bondline layer was simulated with a thickness of 2 mm. Therefore, as a reasonable assumption, a bondline thickness of 2 mm was employed in the simulations conducted in the present study. Moreover, as the focus of this study is to evaluate the interfacial stresses along the entire bond length for various shear test specimens, the assumption of 2 mm thickness of the bondline layer has no significant impact on the main conclusions of this study.

3.3.4 Effect of Bondline Layer Modulus

Figure 3.9 shows the normal stress and shear stress distributions at the MB interface for

different elastic moduli of the bondline layer, with the values of the other parameters fixed. The selection of these elastic moduli is due to the consideration of the elastic modulus range of cement mortar or concrete with normal strength. It is seen from the results that as the elastic modulus of the bondline layer increases, the maximum normal stress and shear stress at the interface increase accordingly. For example, when the elastic modulus of the bondline layer is taken as 7.5 GPa, the maximum normal compressive stress and the maximum shear stress near the push end are 0.48 MPa and 3.83 MPa, respectively; if the elastic modulus of the bondline layer is increased to 40.0 GPa, the maximum normal compressive stress and the maximum shear stress near the pusher are increased accordingly to 2.37 MPa and 5.63 MPa, respectively.

However, unlike the thickness variation of the bondline layer, the location of the maximum normal stress or shear stress does not change significantly with the variation of the bondline layer elastic modulus. For example, for the four different bondline layer elastic moduli, the maximum normal stress occurs at a distance of 0.50 mm from the push end, and the maximum shear stress occurs at a distance of 1.50 mm from the push end. That is, the locations of the maximum normal and shear stresses are nearly independent of the bondline layer elastic modulus, and this behaviour is analogous to the distribution of the interfacial stresses of the reinforced concrete beam bonded with a soffit plate (Teng *et al.* 2002).

In general, the effect of bondline layer elastic modulus is very similar to that of the bondline layer thickness. For both normal stress and shear stress, the stress distribution at the NB, OB, and MB interfaces are identical over the majority of the concrete-to-concrete bond length. Studies have shown that the strength and elastic modulus of the bondline layer were reduced due to the porosity in this region (Du *et al.*, 2013; Xiao *et al.*, 2013). Although no direct measurement of the elastic modulus of the bondline has

been reported in the literature, it is believed that the bondline layer is similar to the interfacial transition zone (ITZ) between the aggregate and mortar in concrete. Xiao *et al.* (2013) performed microscopic tests on the mechanical properties of the ITZ and proved that the elastic modulus of the ITZ was around 15.0 GPa. Therefore, in the present study, the elastic modulus of the bondline layer is taken as 15.0 GPa, which is a reasonable assumption. Moreover, the influence of the elastic modulus of the bondline layer on the prediction of the stress distribution at the concrete-to-concrete interface is insignificant, as shown in Figure 3.9.

3.4 INTERFACIAL SHEAR STRESS DISTRIBUTIONS FOR DIFFERENT TYPES OF SPECIMENS

Based on the above discussions, the FE model for simulating the shear test specimens can be established. The shear stress distribution of concrete-to-concrete interfaces in different types of specimens, as well as the influence of the specimen geometry on the shear stress distribution are examined in detail in this section. The results are then used to assist the design of a shear test specimen that is most appropriate for the investigation of the local bond-slip behaviour at the interface.

3.4.1 Stress Distributions along the Bond Length for Three Types of Direct Shear Test Specimens

The interfacial shear stress distributions of the three representative shear test specimens, including the one-interface shear test, L-shaped one interface shear test, and two-interface shear test are examined in Figure 3.10. Specifically, the interfacial stresses along the MB interface for the specimens of these tests were predicted using the developed FE models.

Figure 3.10 (a) presents a comparison of the normal stress distributions for the three

56

test setups. For the sake of comparison, the interface bond lengths of the three FE models were selected to be 300 mm. Figure 3.10 (a) indicates that although both tensile and compressive stresses appear along the MB interface for the three shear tests, their normal stress distributions are considerably different. In the one-interface shear test, considerable tensile stresses appear at the push end ($x = 0$). Such interfacial tensile stresses will likely induce premature cracking and substantially decrease the interfacial shear strength, and therefore should be avoided. For this test setup, compressive normal stress appears at the support end ($x = l$), where l represents the total bond length. The normal stress distribution of the two-interface shear test exhibits an opposite trend: tensile stresses appear at the support end while compressive stresses appear at the push end. It is obvious that tensile stresses at the support end should also be avoided. For the L-shaped one-interface shear test, tensile stresses appear in the middle part of the interface, while at the support and the push ends, the interfacial normal stresses are compressive. As a result, in order to avoid tensile stresses at the ends of the interface, which are likely to induce premature failure, the L-shaped one-interface shear test is more appropriate than the other two test methods for the investigation of local bond-slip relationship at the interface.

Figure 3.10 (b) compares the interfacial shear stress distributions for the three shear test setups, which are particularly important since, in most of the existing studies employing such test methods, the interfacial shear stress distribution was assumed to be uniformly distributed. However, Figure 3.10 (b) shows clearly that the shear stress distributions for the three test setups are not uniform. Instead, shear stress concentration occurs at the push and support ends, while shear stress is much lower in the intermediate region. Therefore, it is inappropriate to evaluate the interfacial shear behaviour based on the uniform shear stress distribution assumption for all types of tests. Nevertheless, a comparison of the three shear stress distributions indicates that the shear stress

distribution for the one-interface shear test is rather uniform with stress concentrations in the relatively small regions near the interface ends. This implies that with the proper design of the test specimen, a relatively uniformly distributed stress at the interface can still be achieved, and then the uniform shear stress distribution assumption is not entirely unreasonable.

3.4.2 Influence of the Bond Length

The bond length (l) and height of the concrete block (new concrete block thickness h or old concrete block thickness H) are two key parameters that affect the interfacial stress distributions, as also indicated by a previous numerical study of the direct shear test setups (Zanotti and Randl, 2019). Therefore, parametric studies were conducted to further investigate their influences.

Figures 3.11 shows the influence of the bond length on the normal and shear stress distributions for the one-interface shear test. The abscissa indicates the normalised position along the bondline, and the ordinate indicates the value of the normal or shear stress at the MB interface. It is seen that for relatively short bond lengths such as 50 mm and 100 mm, very large tensile and compressive stresses appear near the push end and support end, respectively (Figure 3.11 (a)), and the shear stress distribution is highly non-uniform. In practice, since the tensile strength of concrete is substantially smaller than such stresses predicted from a linear-elastic model, premature interfacial debonding will occur. Meanwhile, the interfacial shear stress also concentrates at the interface ends and distributes highly non-uniformly along the bondline, as indicated in Figure 3.11 (b). As the bond length increases to 200 mm and 300 mm, although the interfacial normal stress becomes much smaller and distributes more uniform, considerable tensile stress still exists at the push end (Figure 3.11 (a)). The shear stress distribution becomes more uniform as well, as shown in Figure 3.11 (b), but the shear

58

stress concentration near the support end. Further increasing the bond length to 500 mm, the normal stress further decreases and the stress concentration at the support end becomes smaller. However, the shear stress becomes more non-uniform and the stress concentration higher at the interface ends than that for a bond length of 200 or 300 mm. In summary, a bond length of 200 to 300 mm for the one-interface shear test specimen produces the most appropriate stress distribution for the investigation of local bond-slip behaviour.

In the case of the two-interface shear test, as shown in Figure 3.12, non-trivial normal tensile stress occurs at the push end when the bond length is as small as 50 mm while it occurs at the support end when the bond length increases. For the shear stress, when the bond length is small, the distribution is relative uniform in half of the bondline from the push end, while concentrates in a large region from the support end. When the bond length is larger than 100 mm, shear stress also concentrates at the push end. As a result, the interfacial stress distribution for the two-interface specimen is not ideal for the bond-slip relationship study.

In the case of the L-shaped one-interface shear test, as shown in Figure 3.13 (a), the normal stress near the push end and support end is compressive and does not lead to tensile failure near the ends. In the middle segment, the tensile stress level is small when the bond length is smaller than 200 mm. For the shear stress, the distribution is more uniform when the bond length is smaller. As the bond length increases, the shear distribution becomes more and more non-uniform; for a bond length of 500 mm, the shear stress is almost zero in the middle while very high at the ends. For a bond length of 50 mm, the interfacial shear stress displays a rather uniform distribution, as indicated in Figure 3.13 (b). Therefore, an L-shaped one-interface specimen with a bond length of 50 mm seems to be suitable for the investigation of local bond-slip behaviour.

3.4.3 Influence of the Concrete Block Height

The height of the concrete block also impacts the distribution and was investigated. The concrete block height ratio was defined as the ratio of the new concrete block height h to the old concrete block height H. In the parametric study, the old concrete block height H was 100 mm, and the bond length l was 300 mm, which remained unchanged in all calculations. Figures 3.14~3.16 show the normal and shear stress distributions for four new concrete block heights (h=50 mm, 75 mm, 100 mm, and 150 mm) for the three test setups, corresponding to concrete block height ratios of 0.5, 0.75, 1.0 and 1.5.

Figure 3.14 shows that for the one-interface shear test, tensile and compressive stresses exist in the left and right half of the specimen along the bondline, respectively. With the increase of the concrete block height ratio from 0.5 to 1.5, the normal stress distribution becomes more non-uniform with the stress concentrations at the ends increasing, while the general trend of the distribution is not changed. For the shear stress distributions, when the concrete block height ratio increases from 0.5 to 1.5, the general stress distribution is not changed considerable, only the stress concentration at the push end increases slightly. It seems that when h/H is 0.75 or 1.0, the shear stress distribution is relatively uniform.

In the case of the two-interface shear test, as shown in Figure 3.15 (a), the normal stress in the left and right half of the bondline are compressive and tensile, respectively, opposite to the distribution of the one-interface specimen. The normal stress distribution changes slightly with the increase of the concrete block height ratio, indicating that the concrete block height ratio does not considerably influence the normal stress distribution of the two-interface shear test. This conclusion also holds for the shear stress distribution, as shown in Figure 3.15 (b). However, it can be seen that the shear stress distribution is the most uneven with a small concrete block height ratio as 0.5.

Finally, for the L-shaped one-interface shear test, as shown in Figure 3.16 (a), for a small concrete block height ratio of 0.5, the interfacial normal tensile stress is as large as 8 MPa near the push end area. When the concrete block height ratio is larger than 0.5, the normal stress distribution at the interface is similar and evenly distributed over the majority of the bondline except for the two ends. Particularly, when the concrete block height ratio is 1.0, the normal stress at the interface is most small and evenly distributed in the middle of the bondline. Also, the interfacial shear stress distribution is highly nonuniform for specimens with concrete block height ratio 0.5, while the stress distributions are similar when the concrete block height ratio is larger than 0.5, as shown in Figure 3.16 (b). This indicates that the concrete block height ratio does not considerably influence the stress distribution for this L-shaped one-interface shear test for a concrete block height ratio of larger than 0.5. In summary, the concrete block height ratio has much smaller impact on the stress distribution than the bond length does. For the one-interface shear test, as well as the L-shaped one-interface shear test, specimens with a concrete block height ratio 1.0 seems to be a better choice.

3.5 SUGGESTIONS FOR A NEW DESIGN OF SHEAR TEST SPECIMEN

The normal stress and shear stress for the three test setups are compared in Figure 3.17. It can be inferred from the normal stress distributions of the three specimens that the interfacial failure of a test specimen may start either from the push end or the support end. For a commonly used test specimen with a bond length and concrete block height ratio of 300 mm and 1.0, respectively, the shear stress near the support end is considerably larger than that at the push end, especially for the one-interface and two-interface shear test specimens, indicating that shear failure is more likely to start from the support end. Moreover, the shear test specimens often failed due to the combination

of shear and tensile stresses. The results in Figure 3.17 show that the failure of a test specimen may also start from the area in which tensile stresses exist, such as the push end of the one-interface shear test specimen, or the support end of the two-interface shear test specimen. Therefore, a favourable shear test set up for the evaluation of concrete-to-concrete interfacial bond-slip behaviour should avoid high interfacial tensile stresses.

Moreover, a uniformly distributed shear stress should be ensured. Based on the analysis in Section 3.4.2, the concrete block height ratio can be set as 1.0; specifically, the new concrete block height should be equal to the old concrete block height. Generally, a uniformly distributed shear stress can be obtained by minimising the bond length, based on the analysis in Section 3.4.1. However, for a commonly used test setup involving a bond length of 300 mm, the shear stress is not quite uniformly distributed, particularly for the L-shaped one-interface shear test.

Based on these considerations, Figure 3.18 shows the major principal stress, normal stress and shear stress distributions of three shear test specimens designed according to the suggested support conditions, concrete block height ratio of 1.0, and a bond length of 50 mm. The results indicate that, with the suggested parameters, the bondline of all three test specimens is dominated by shear stress with relatively small level of normal stress. However, large shear stress still appears at the support end of the one-interface and two-interface specimens. By contrast, the L-shaped one-interface shear test specimen exhibits a nearly uniform shear stress distribution, and a moderate level of normal stress along the bondline without tensile stress at the ends. As a result, the L-shaped one-interface shear test specimen with the suggested parameters is most suitable for the experimental investigation of bond-slip behaviour at the concrete-to-concrete interface, and will be further validated in the next chapter through experiments.

3.6 CONCLUSIONS

Since the slant shear tests are inappropriate for the purpose of understanding the interfacial shear behaviour at the concrete-to-concrete interfaces, the existing direct shear test methods have been studied through a series of FE analyses to understand the characteristics of their interfacial stress distributions and the influence of the test parameters. A 2D plain stress FE model was developed to predict the interfacial stress distributions for the three types of shear test specimens.

Concrete blocks were modelled as linear elastic, and the interface was modelled using a discrete bondline layer. The midplane of the bondline layer is referred to as MB, and the interfaces between the bondline layer and the new and old concrete blocks are referred to as NB and OB. The FE results indicate that the effects of the thickness and elastic modulus of the bondline layer on the interfacial shear stress distribution are confined within a small region about 3 mm near the push end; the effects are trivial in the remaining of the bondline. As a result, a reasonable thickness of 2 mm was selected for the bondline in all the simulations conducted in the present study.

The normal and shear stress distributions across the thickness of the bondline layer are uniform in the majority of the bondline except in a small region (about 2 mm) near the ends. Singular behaviour can be observed at both the OB interface and the NB interface at the interface ends, but no obvious singular behaviour is observed at the MB interface. Moreover, the MB interface basically represents the average stress level across the thickness of the bondline. Therefore, the interfacial stress distribution at the MB interface is taken as the representative interface of the bondline.

The FE model was then used to predict the interfacial stress distributions for the three types of direct shear test specimens. For the interfacial normal stress, the one-interface

shear test induces considerable tensile stress at the push end, while the two-interface shear induces considerable tensile stress at the support end. Both are inappropriate due to the premature cracking caused by the peeling stress. By contrast, the L-shaped one-interface shear test induces tensile stress in the middle part of the interface, which is less likely to induce premature cracking and hence preferred.

For the interfacial shear stress, all specimens exhibit higher shear stress at the push and support ends than that in the intermediate region. Therefore, it is inappropriate to evaluate the interfacial shear behaviour based on the uniform shear stress distribution assumption. Nevertheless, the results imply that the shear stress distribution may be sufficiently uniform if the geometry of the specimen is well designed, and thereupon the uniform shear stress distribution assumption may be applicable to such a specimen.

Accordingly, a parametric study was conducted to investigate the influence of the bond length (l) and height of concrete block (H and h for old and new concretes) on the shear stress distribution. The results show that for the one- and two-interface specimens, either peeling stress concentration or non-uniform shear stress distribution occurs for various bond length and concrete block height combinations. Therefore, for these test methods, the ideal stress distribution cannot be achieved by adjusting the geometry. On the other hand, for the L-shaped one-interface shear test, if the bond length is taken as 50 mm, the interfacial shear stress displays a rather uniform distribution, and the peeling stress is acceptably low, indicating that an L-shaped one-interface specimen with a bond length of 50 mm may be suitable for the investigation of the interfacial shear behaviour, based on the FE analysis. Therefore, this specimen design and its interfacial stress distribution need to be validated experimentally, as discussed in the next chapter.

3.7 REFERENCES

ABAQUS version 6.8. *ABAQUS standard user's manual*. Vol. 1-3, Hibbitt, Karlsson & Sorensen, Pawtucket, 2008.

Achilllopoulou, D. V. (2016). Understanding the basic mechanisms acting on interfaces: Concrete elements, materials and techniques. *Advanced Materials Interfaces*, 205-247.

Bissonnette, B., Courard, L., Fowler, D. W., & Granju, J. L. (Eds.). (2011). Bonded cement-based material overlays for the repair, the lining or the strengthening of slabs or pavements. *State-of-the-art report of the RILEM technical committee 193-RLS (Vol. 3)*. Springer Science & Business Media.

Chen, J. F., Yang, Z. J., & Holt, G. D. (2001). FRP or steel plate-to-concrete bonded joints: Effect of test methods on experimental bond strength. *Steel & Composite Structures*, 1(2), 231-244.

Clark, L. A., & Gill, B. S. (1985). Shear strength of smooth unreinforced construction joints. *Magazine of Concrete Research*, 37(131), 95-100.

Clímaco, J. D. S., & Regan, P. E. (2001). Evaluation of bond strength between old and new concrete in structural repairs. *Magazine of Concrete Research*, 53(6), 377-390.

Du, X., Jin, L., & Ma, G. (2013). A meso-scale analysis method for the simulation of nonlinear damage and failure behavior of reinforced concrete members. *International Journal of Damage Mechanics*, 22(6), 878-904.

Hawileh, R. A., Rahman, A., & Tabatabai, H. (2010). Nonlinear finite element analysis and modeling of a precast hybrid beam–column connection subjected to cyclic loads. *Applied Mathematical Modelling*, 34(9), 2562-2583.

Kremmyda, G. D., Fahjan, Y. M., Psycharis, I. N., & Tsoukantas, S. G. (2017).

Numerical investigation of the resistance of precast RC pinned beam-to-column connections under shear loading. *Earthquake Engineering & Structural Dynamics*, 46(9), 1511-1529.

Júlio, E. N., Branco, F. A., Silva, V. D., & Lourenço, J. F. (2006). Influence of added concrete compressive strength on adhesion to an existing concrete substrate. *Building and Environment*, 41(12), 1934-1939.

Magliulo, G., Ercolino, M., Cimmino, M., Capozzi, V., & Manfredi, G. (2014). FEM analysis of the strength of RC beam-to-column dowel connections under monotonic actions. *Construction and Building Materials*, 69, 271-284.

Santos, P. M., & Julio, E. N. (2007). Correlation between concrete-to-concrete bond strength and the roughness of the substrate surface. *Construction and Building Materials*, 21(8), 1688-1695.

Sun, X. Y., Tang, G., Wang, H. L., Wang, Q., & Zhang, Z. C. (2020). Effect of 3D printing path on mechanical properties of arch concrete bridge. *Journal of Zhejiang University (Engineering Science)*, 54(11), 2085-2091. (in Chinese)

Teng, J. G., Zhang, J. W., & Smith, S. T. (2002). Interfacial stresses in reinforced concrete beams bonded with a soffit plate: a finite element study. *Construction and Building Materials*, 16(1), 1-14.

Xiao, J., Li, W., Corr, D. J., & Shah, S. P. (2013). Effects of interfacial transition zones on the stress–strain behavior of modeled recycled aggregate concrete. *Cement and Concrete Research*, 52, 82-99.

Wall, J. S., & Shrive, N. G. (1988). Factors affecting bond between new and old concrete. *ACI Materials Journal*, 85(2), 117-125.

Zanotti, C., & Randl, N. (2019). Are concrete-concrete bond tests comparable?. *Cement and Concrete Composites*, 99, 80-88.

Zhang, L., & Teng, J. G. (2010). Finite element prediction of interfacial stresses in structural members bonded with a thin plate. *Engineering Structures*, 32(2), 459-471.

Zoubek, B., Isakovic, T., Fahjan, Y., & Fischinger, M. (2013). Cyclic failure analysis of the beam-to-column dowel connections in precast industrial buildings. *Engineering Structures*, 52, 179-191.

Table 3.1 Geometric and material properties

	Depth (mm)	Length (mm)	Young's modulus (GPa)	Poisson's ratio
New concrete	100	300	40.0	0.17
Old concrete	100	300	30.0	0.17
Bondline layer	2	300	15.0	0.17
Steel plate	100	50	200.0	0.30

Table 3.2 Normal and shear stresses of NB, MB and OB at the push end

Min Element Size (mm)	NB interfacial stress (MPa)		MB interfacial stress (MPa)		OB interfacial stress (MPa)	
	Normal	Shear	Normal	Shear	Normal	Shear
0.5	-10.93	7.74	-0.88	1.37	3.27	0.76
0.2	-17.47	10.17	-0.54	0.59	4.07	0.37
0.1	-22.61	12.64	-0.32	0.29	4.49	0.22
0.05	-27.00	15.83	-0.18	0.14	4.78	0.13
0.01	-30.32	25.18	-0.06	0.03	5.15	0.04
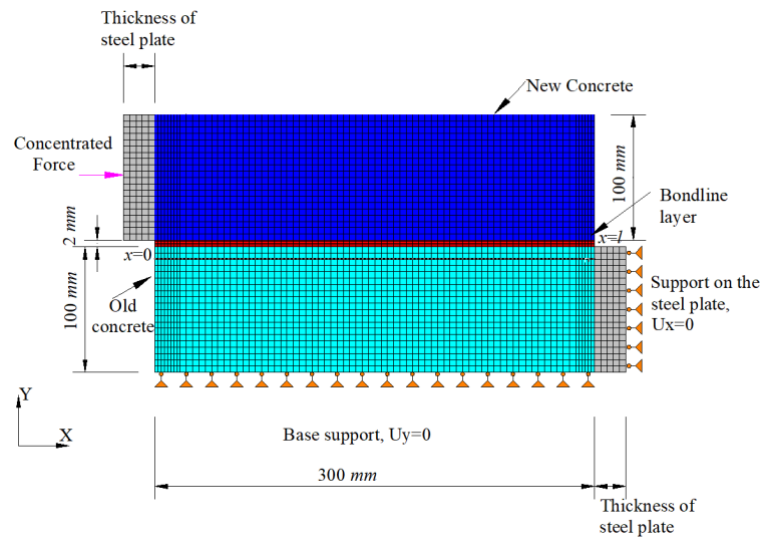
(a) One-interface shear test specimen
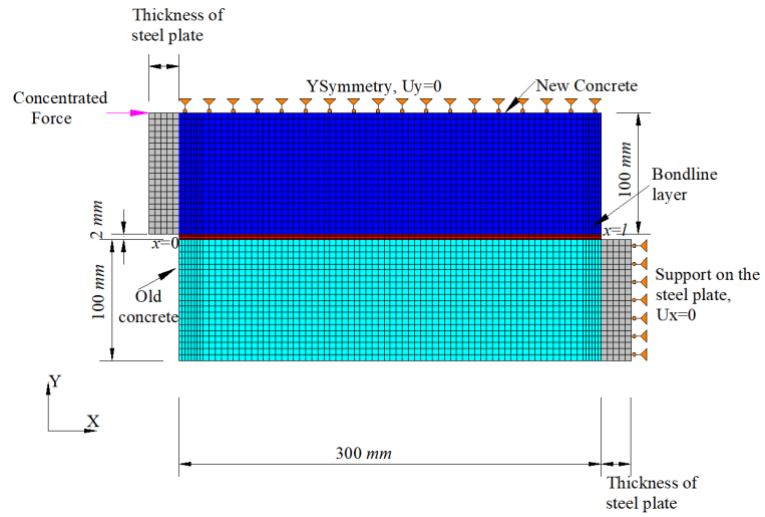
(b) Two-interface shear test specimen
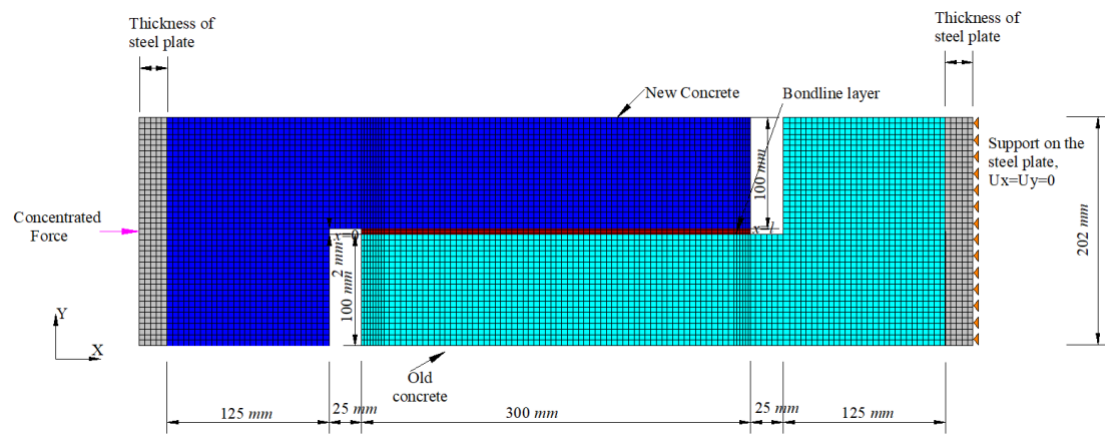
(c) L-shaped one-interface shear test specimen

Figure 3.1 Details of the three test specimens
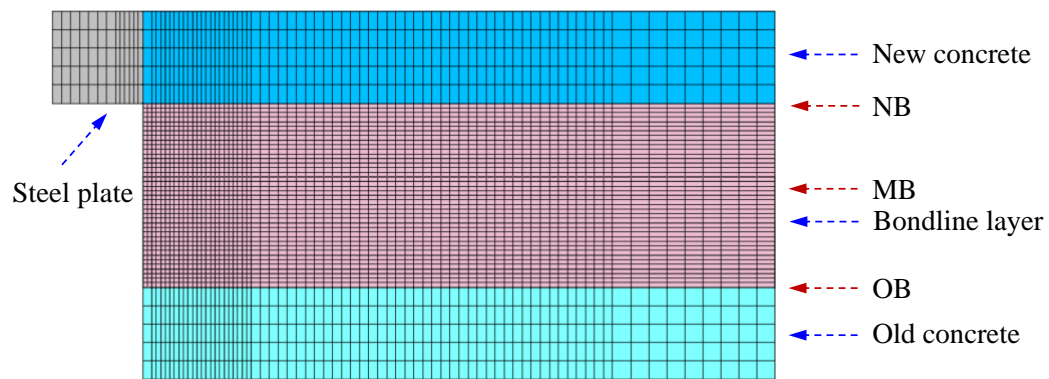
Figure 3.2 The mesh near the push end at the bondline layer
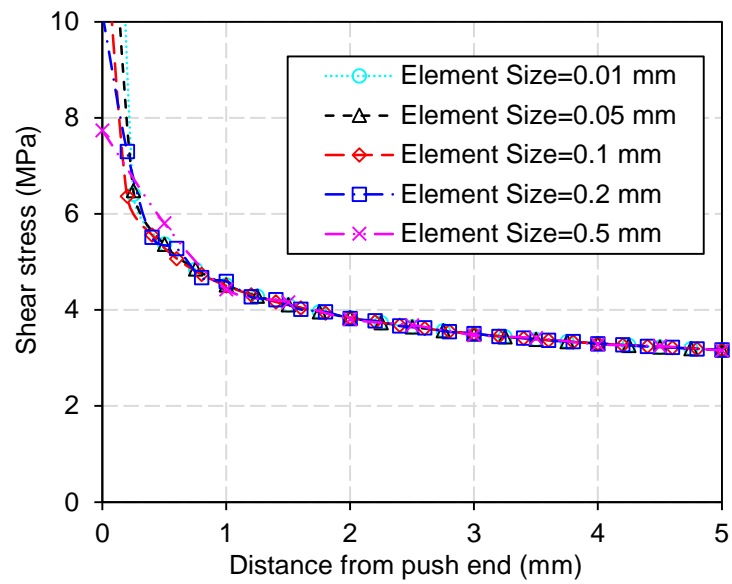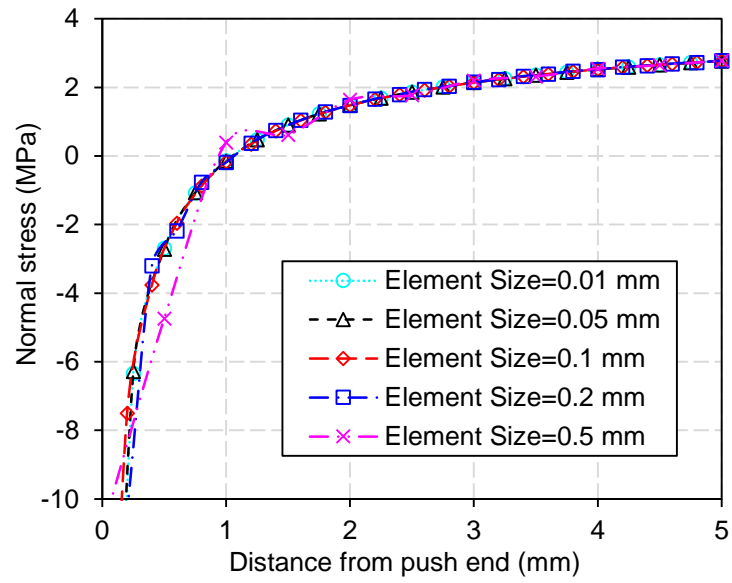
(a) NB interfacial stresses
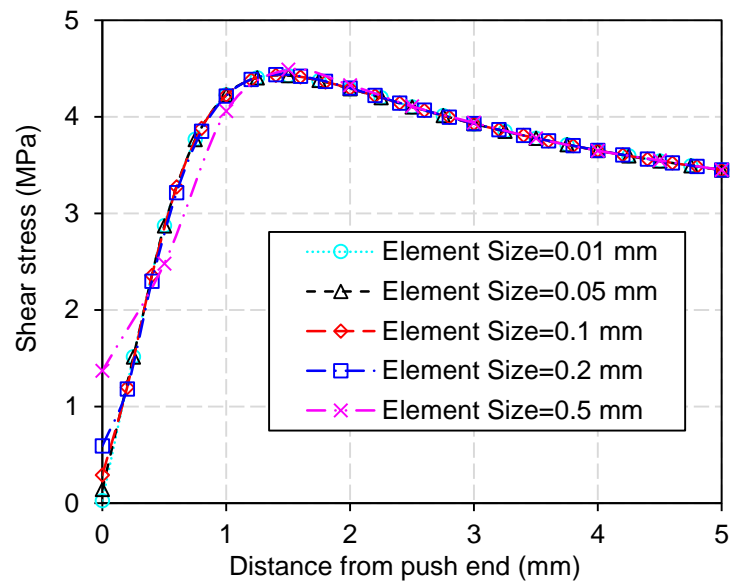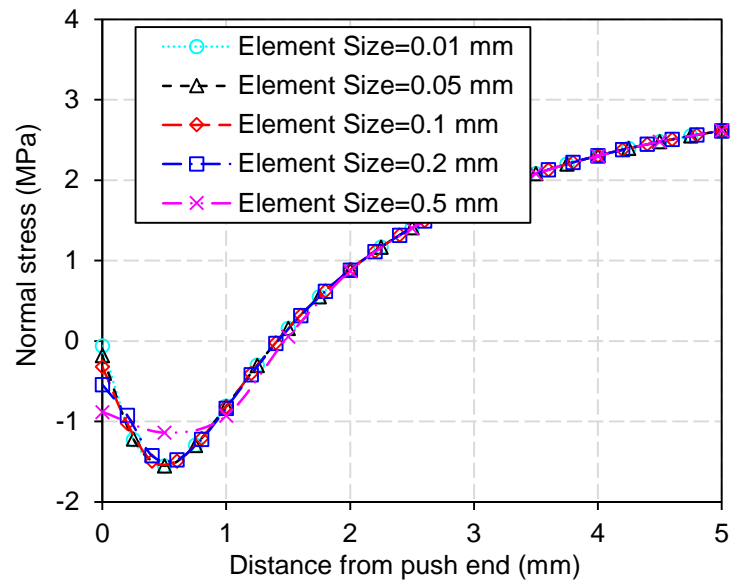
(b) MB interfacial stresses
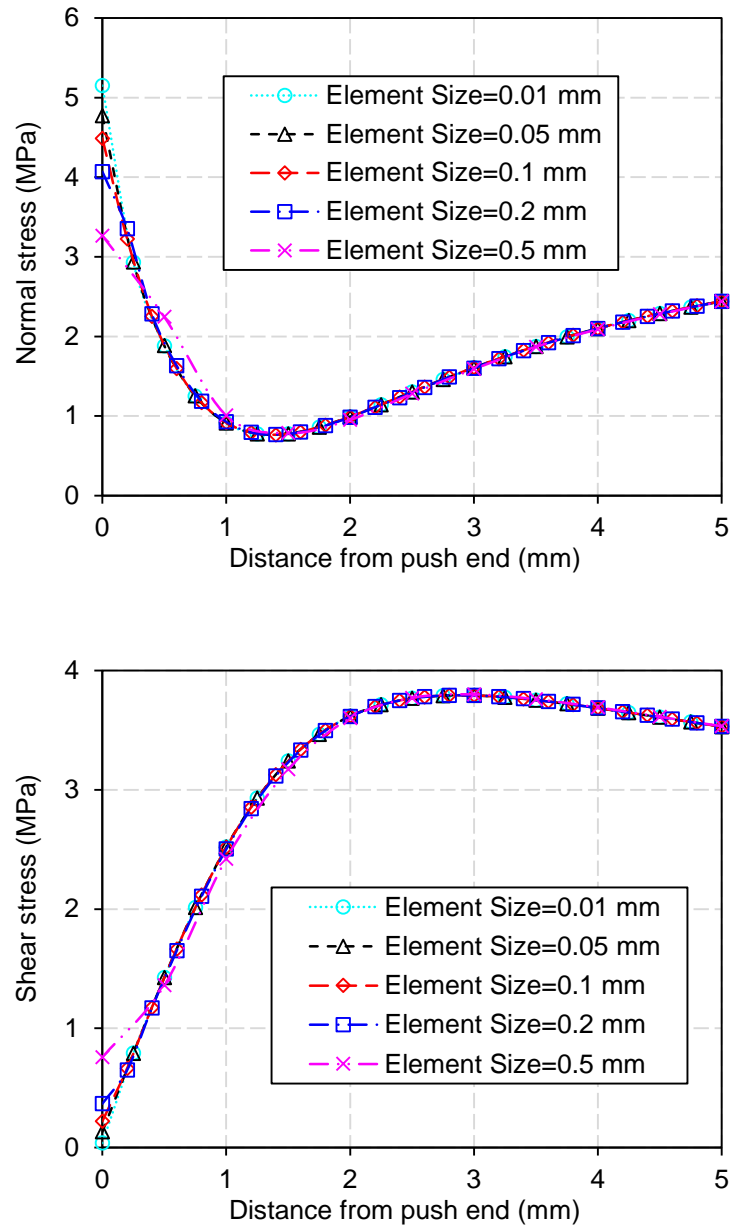
(c) OB interfacial stresses

Figure 3.3 Convergence study
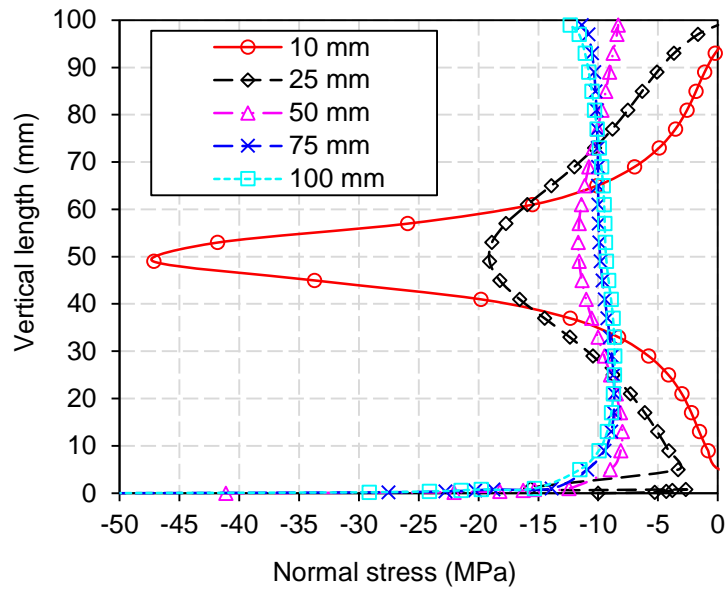
(a) Normal stress on the concrete surface at the loading end
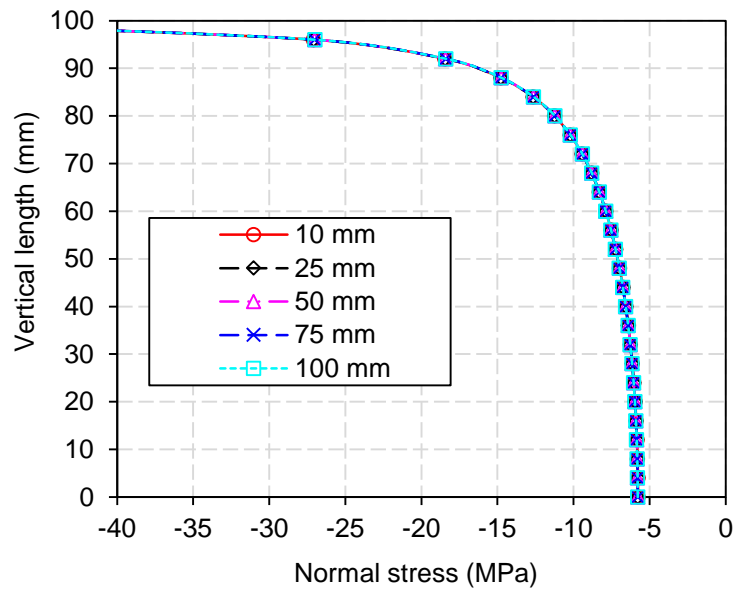
(b) Normal stress on the concrete surface at the support

Figure 3.4 Effect of the thickness of the steel loading plate or support plate
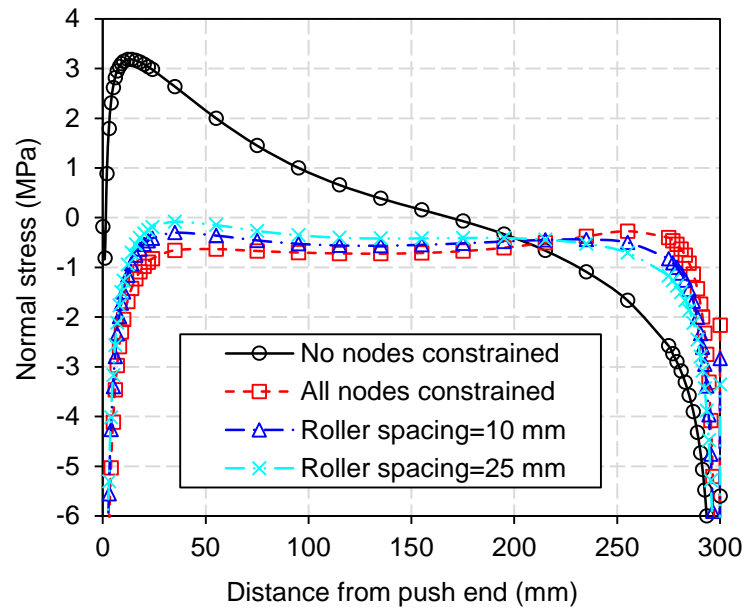
(a) Normal stress
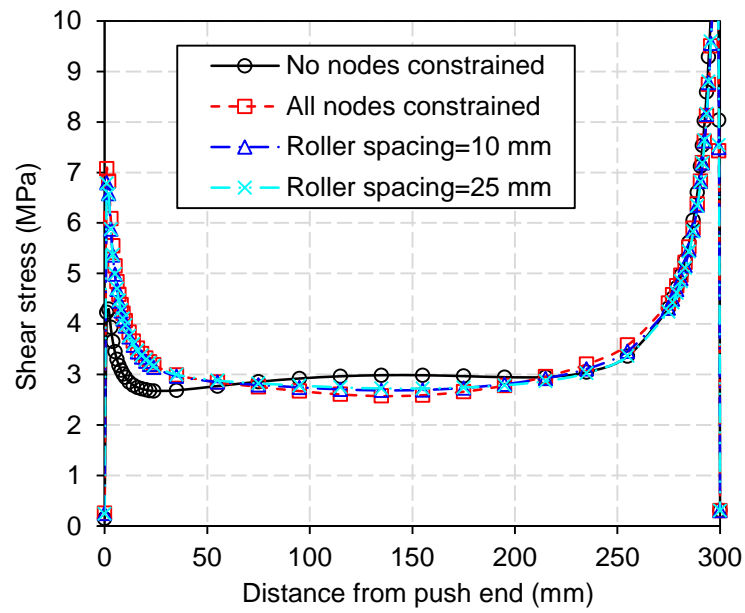
(b) Shear stress

Figure 3.5 Effect of roller support
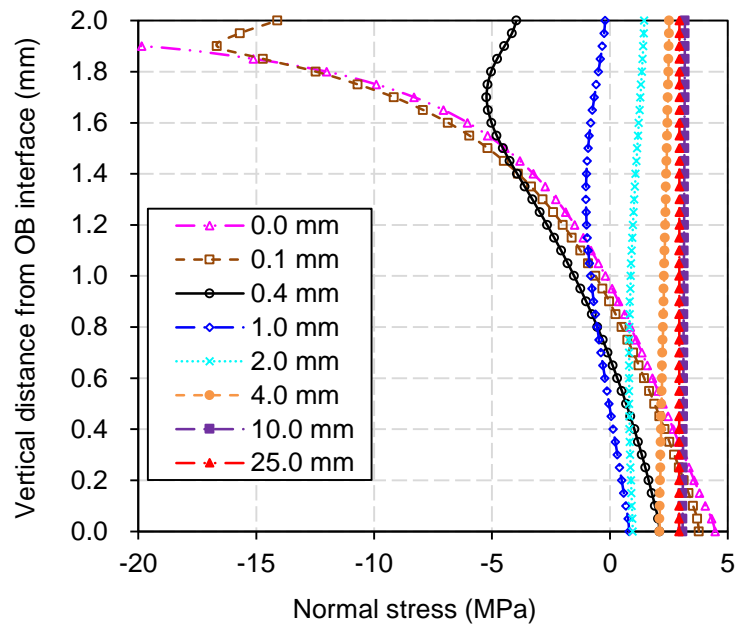
(a) Normal stress at various cross sections near the push end
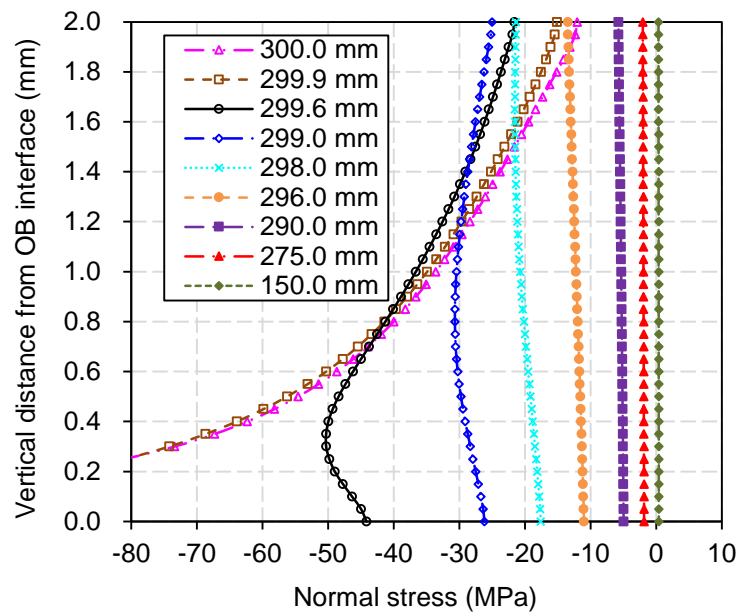
(b) Normal stress at various cross sections near the support end
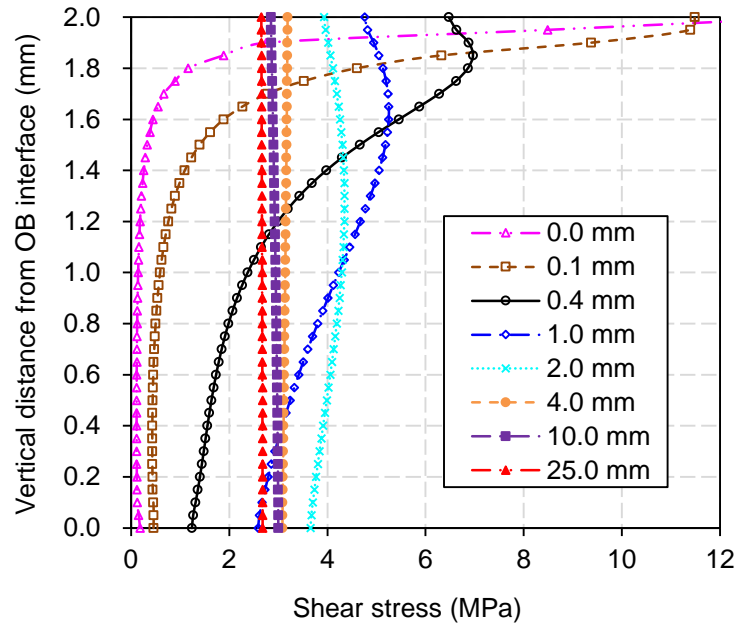
(c) Shear stress at various cross sections near the push end
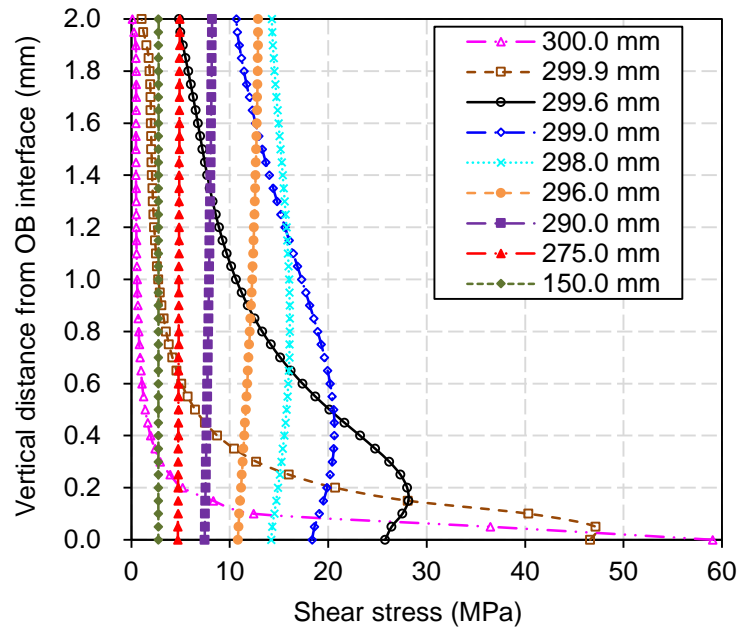
(d) Shear stress at various cross sections near the support end

Figure 3.6 Stress variation across the bondline layer
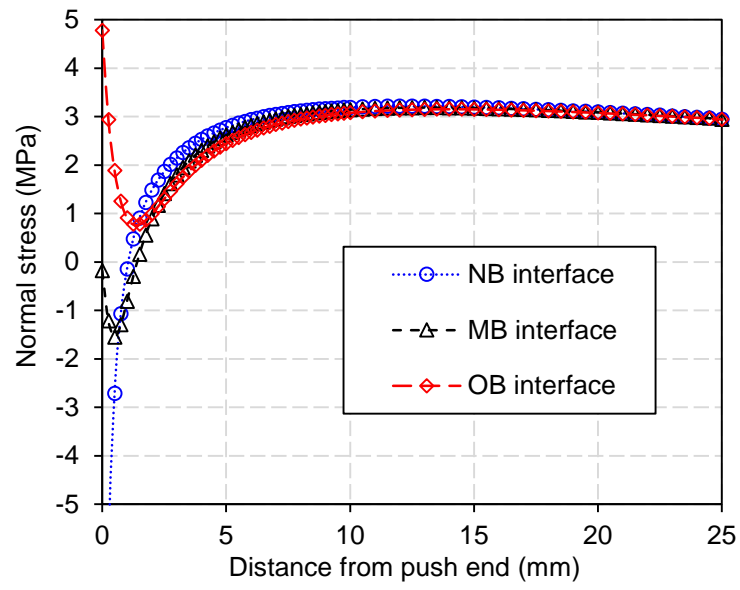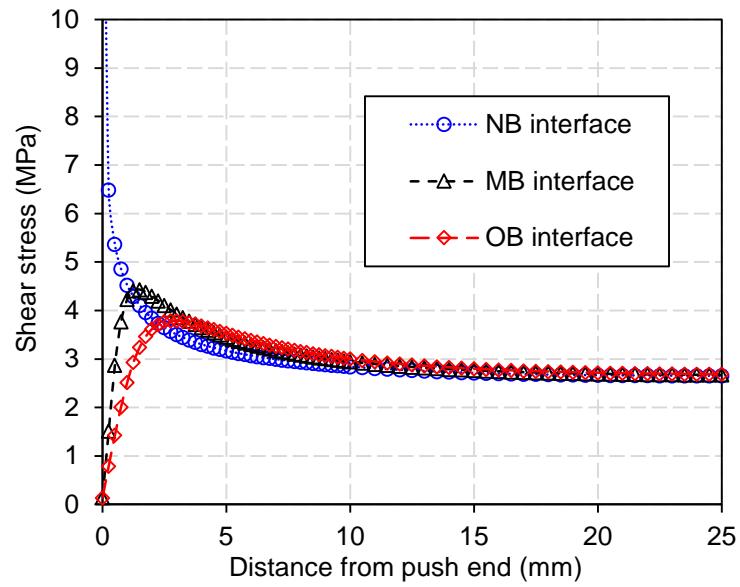
(a) Normal stress

(b) Shear stress

Figure 3.7 Stress comparison among NB, MB and OB interfaces
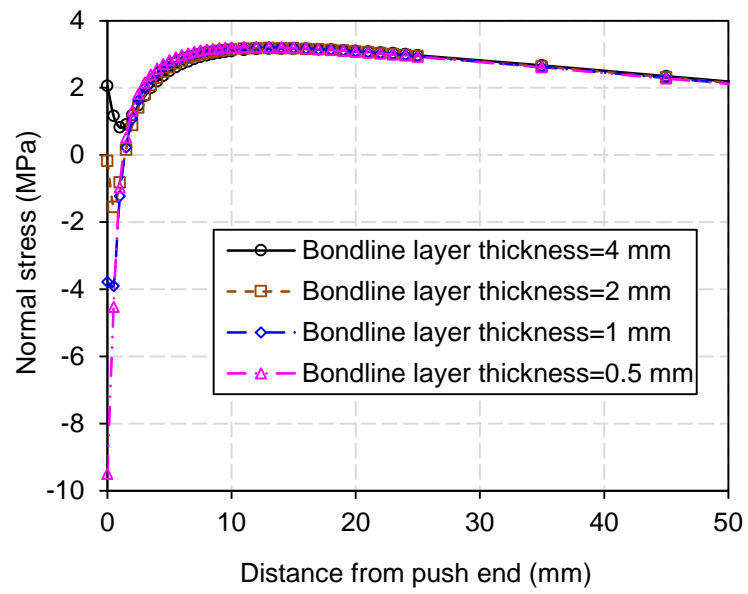
(a) Normal stress
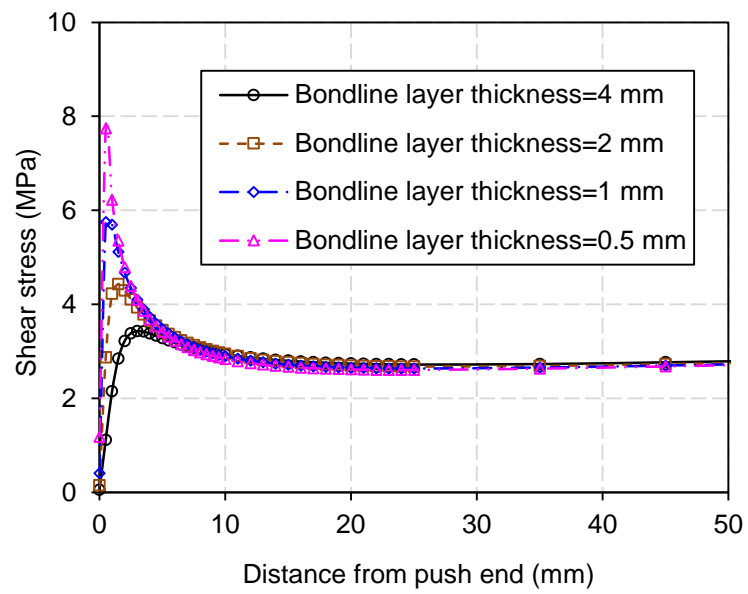
(b) Shear stress

Figure 3.8 Effect of bondline layer thickness

(a) Normal stress
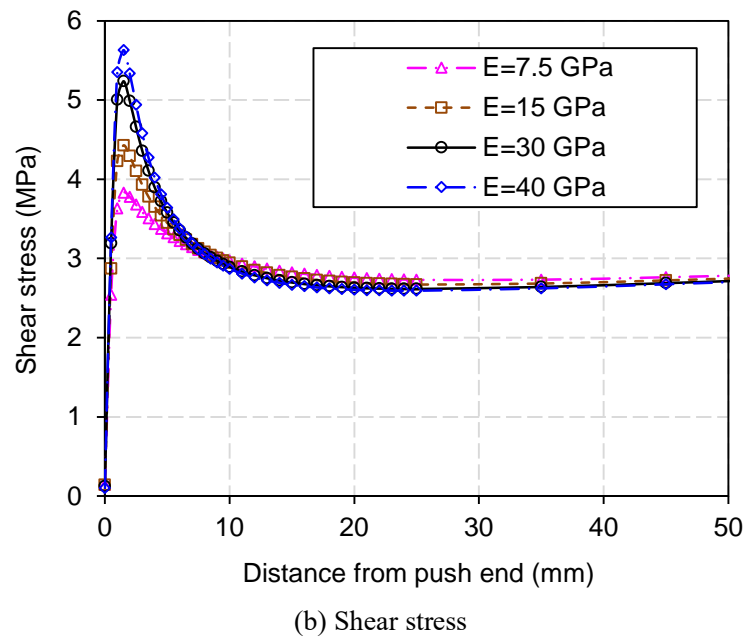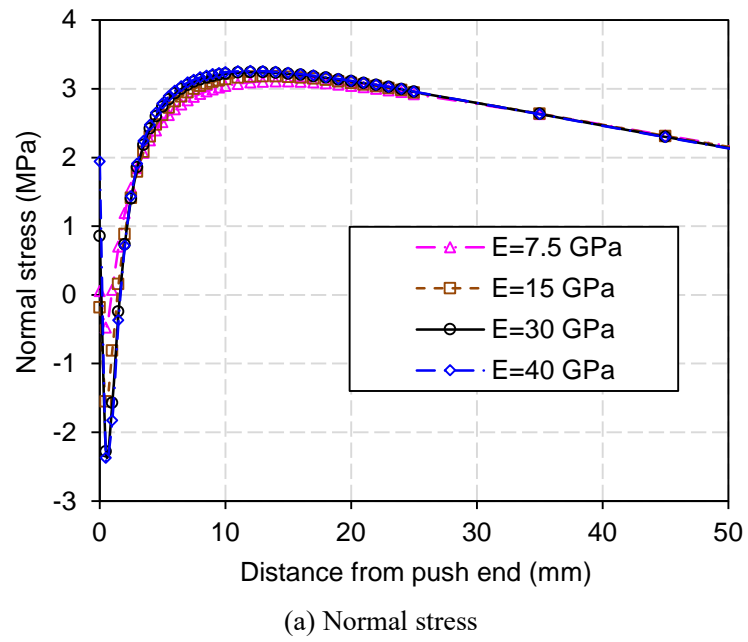
(b) Shear stress

Figure 3.9 Effect of elastic modulus of bondline layer
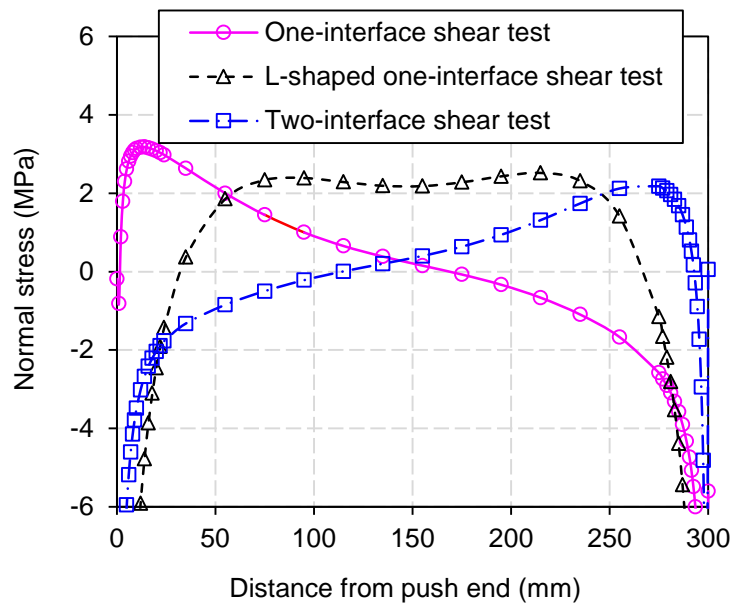
(a) Normal stress
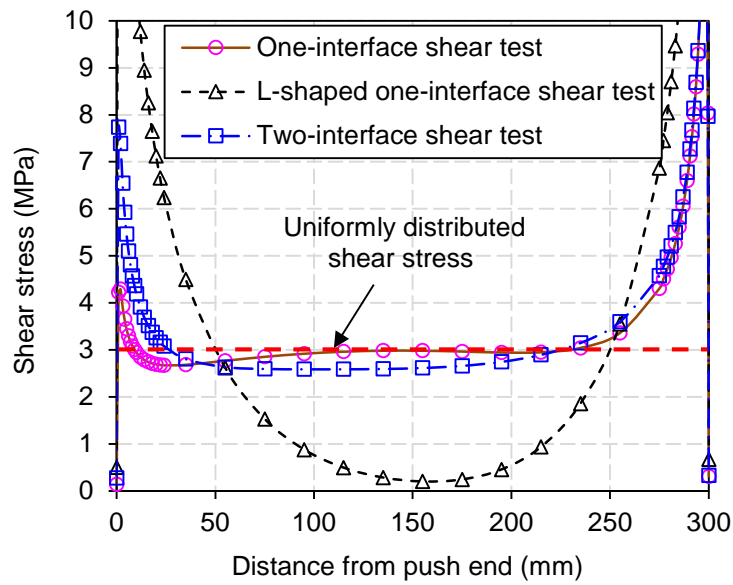
(b) Shear stress

Figure 3.10 Interfacial stresses in various shear test setups

(With a bond length =300 mm and a concrete thickness ratio=1.0)
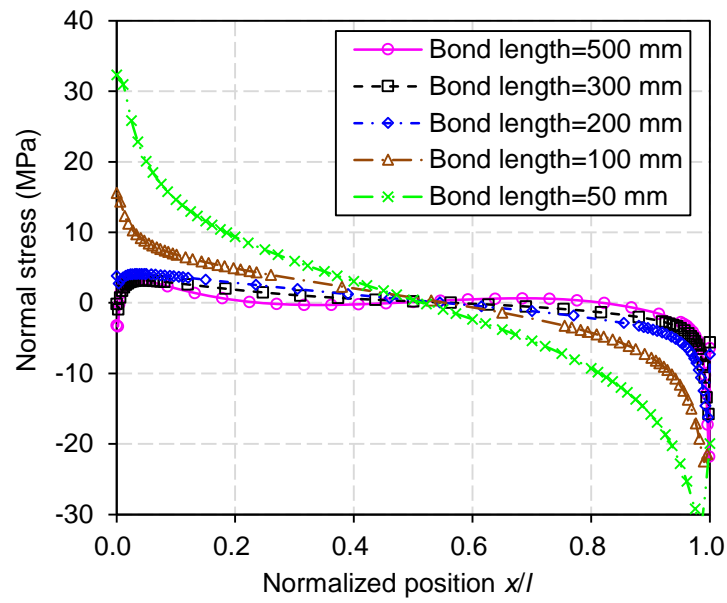
(a) Normal stress distribution
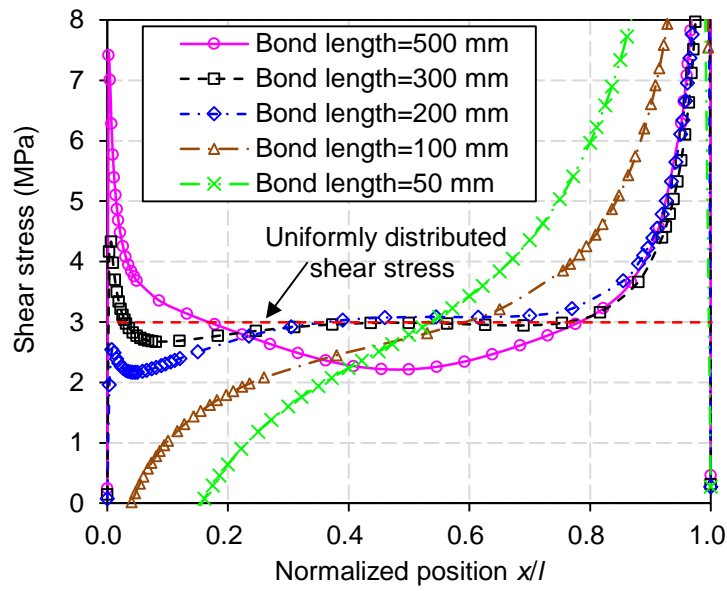
(b) Shear stress distribution

Figure 3.11 One-interface shear test: various bond lengths
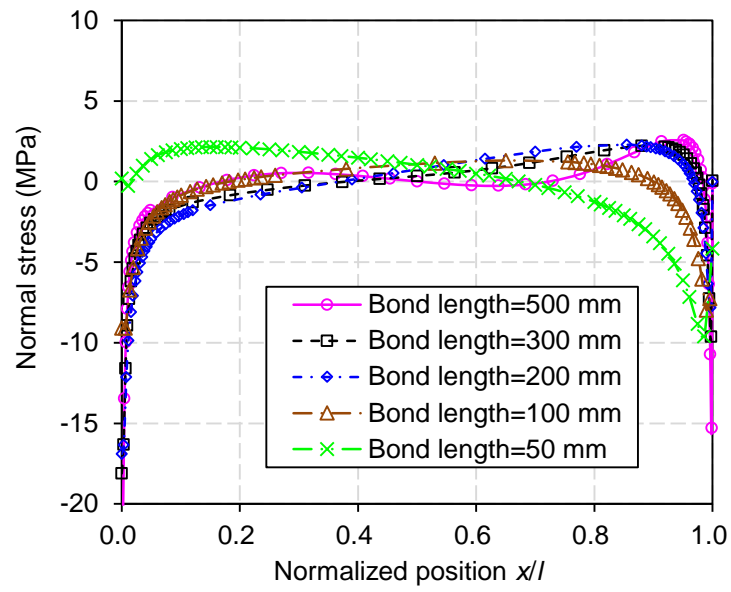
(a) Normal stress distribution
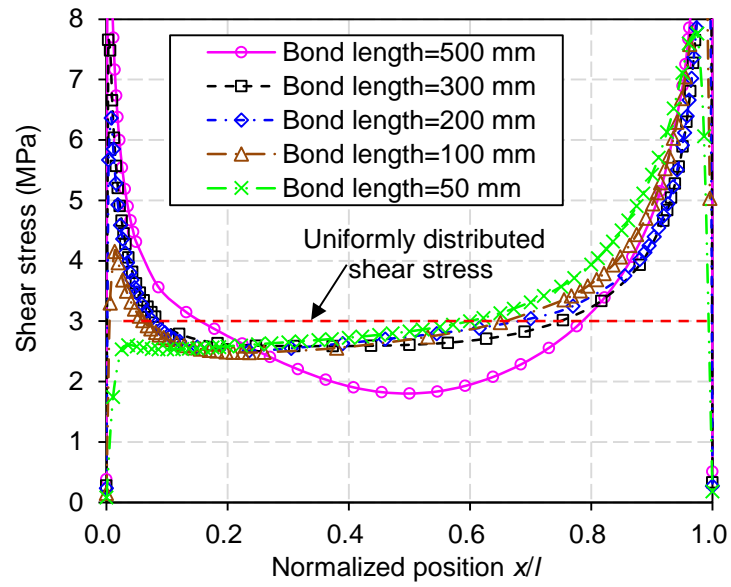
(b) Shear stress distribution

Figure 3.12 Two-interface shear test: various bond length
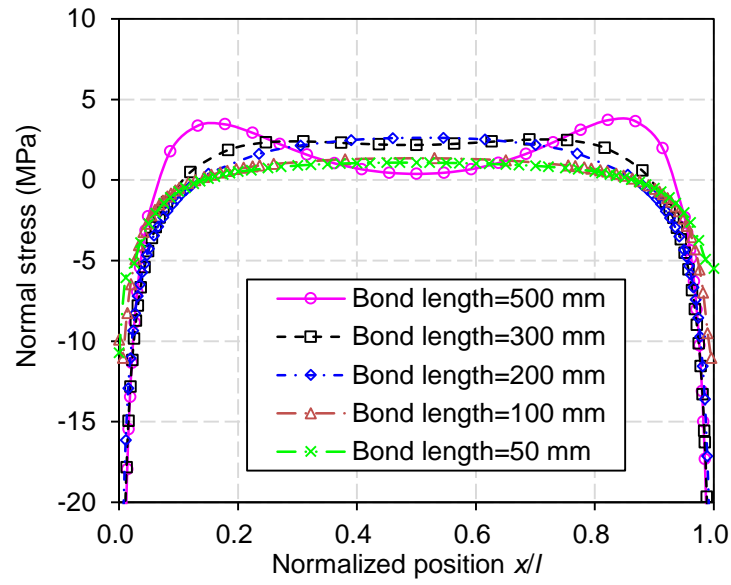
(a) Normal stress distribution
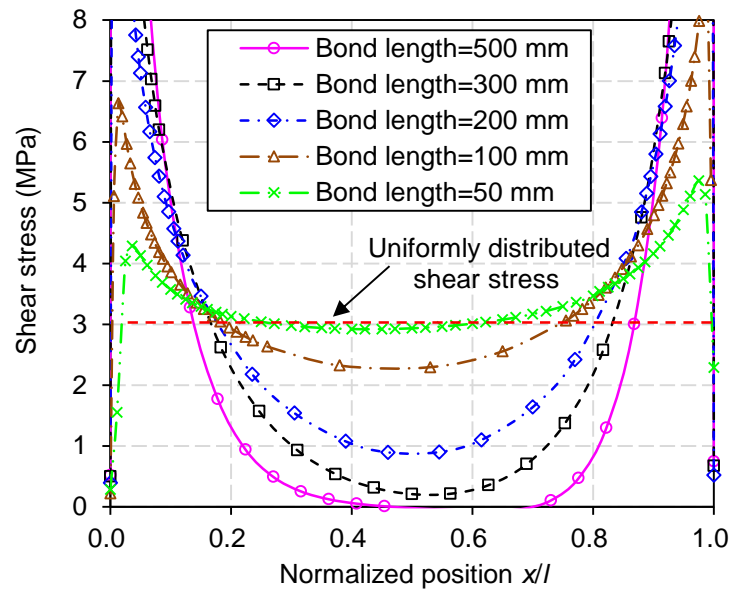
(b) Shear stress distribution

Figure 3.13 L-shaped one-interface shear test: various bond length

(a) Normal stress distribution

(b) Shear stress distribution
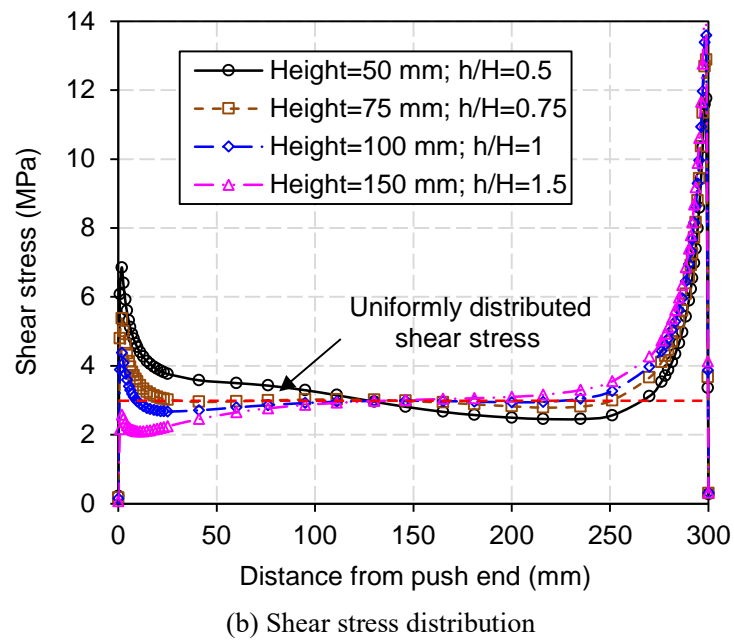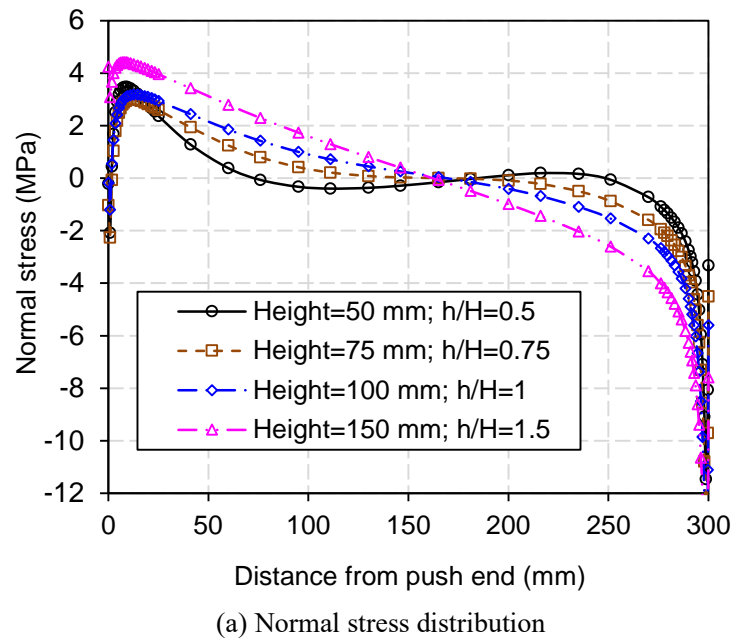
Figure 3.14 One-interface shear test: various concrete block heights

(a) Normal stress distribution

(b) Shear stress distribution
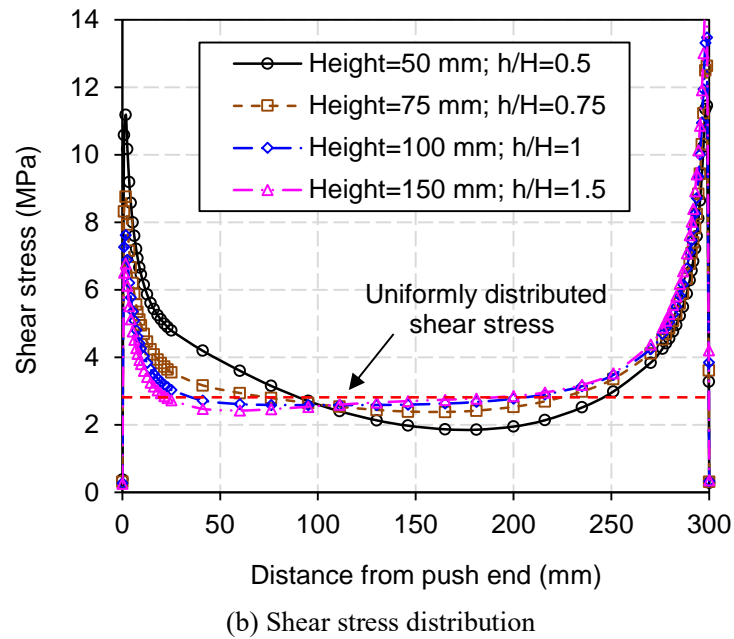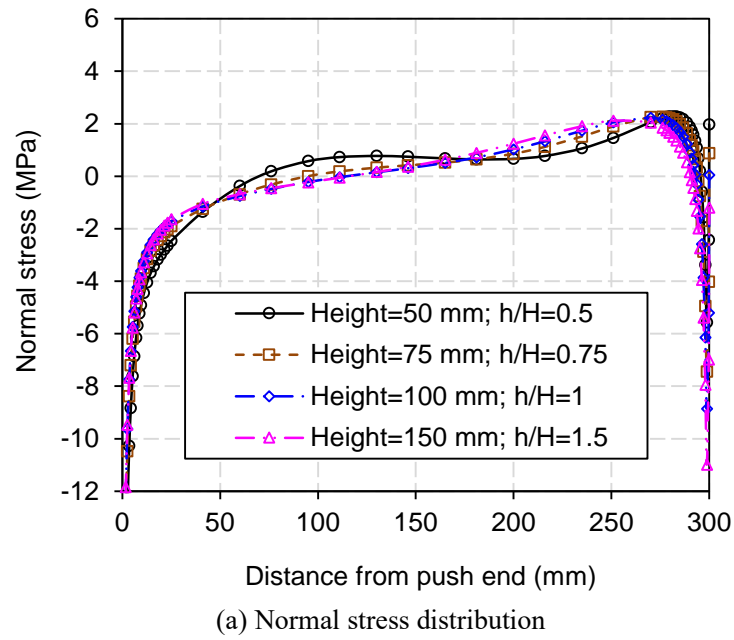
Figure 3.15 Two-interface shear test: various concrete block heights

(a) Normal stress distribution

(b) Shear stress distribution
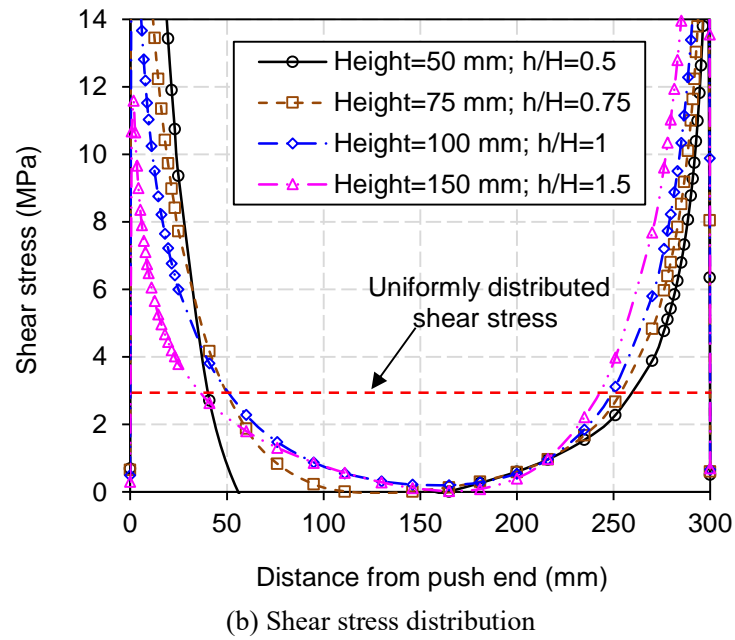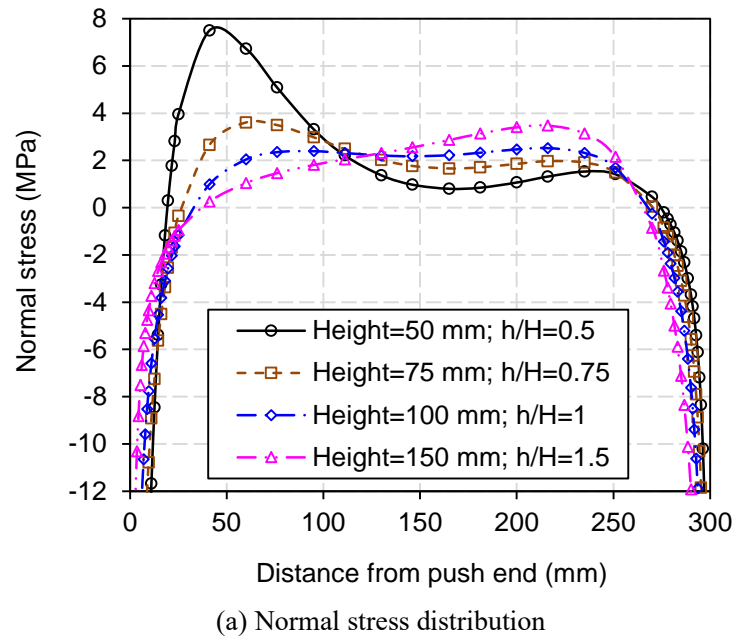
Figure 3.16 L-shaped one-interface shear test: various concrete block heights
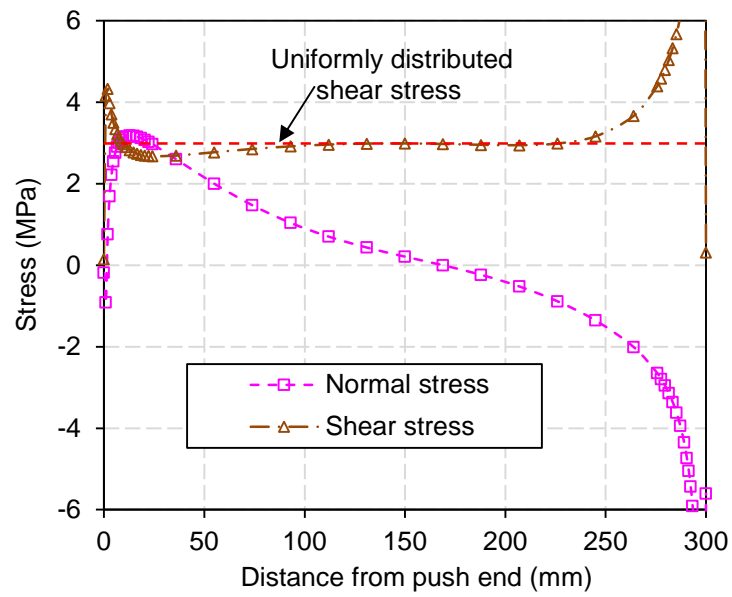
(a) One-interface shear test

(b) Two-interface shear test

88
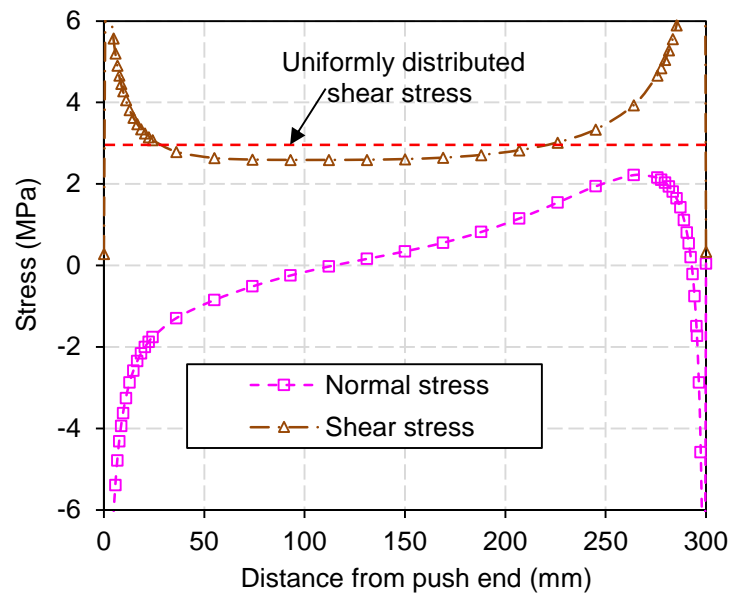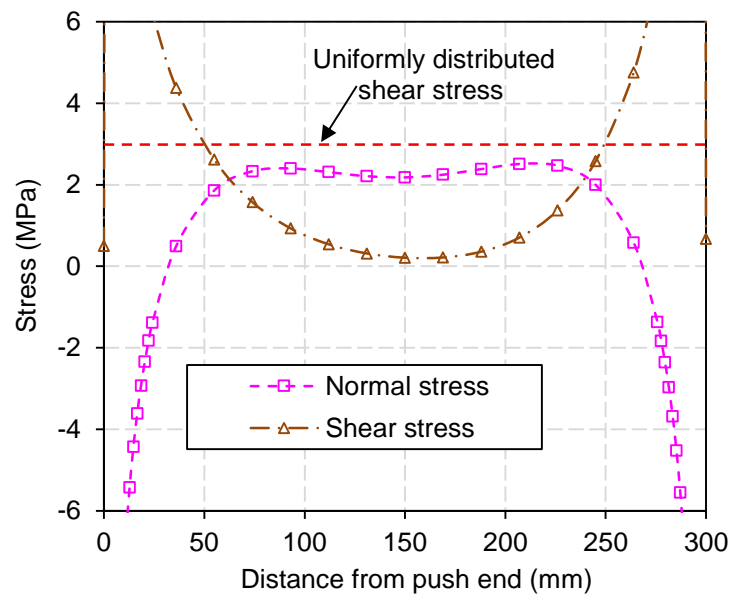
(c) L-shaped one-interface shear test

Figure 3.17 Interfacial stresses for the three test setups

(With a roller support, a bond length=300 mm and a concrete block height ratio=1.0)
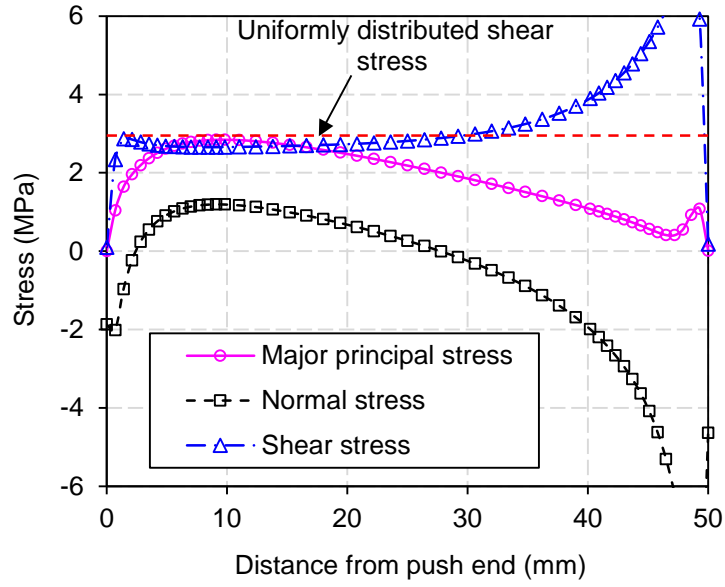
(a) One-interface shear test

(b) Two-interface shear test

90
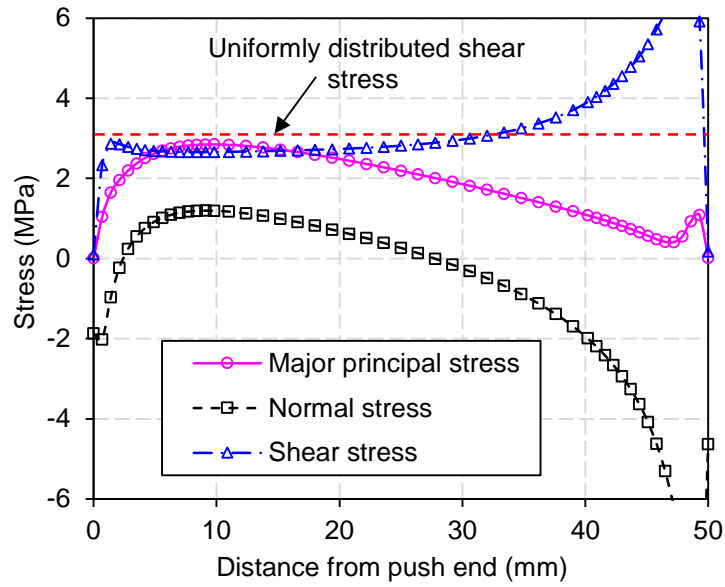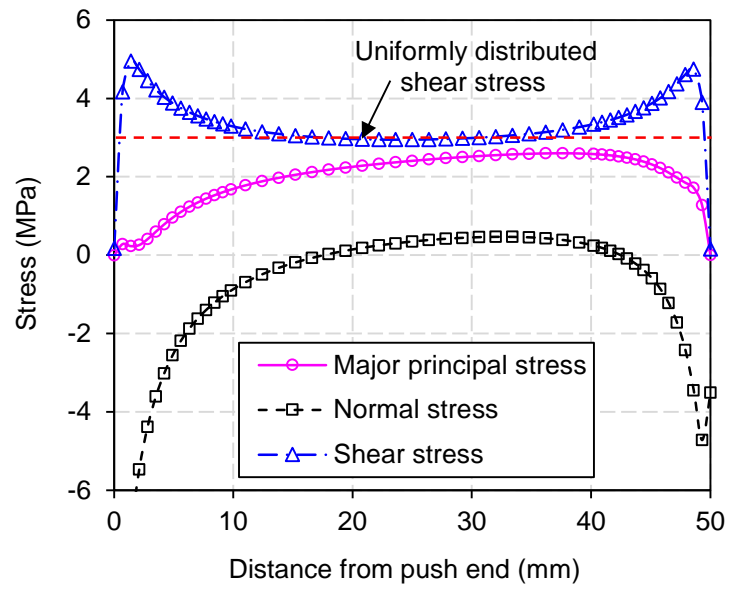
(c) L-shaped one-interface shear test

Figure 3.18 Interfacial stresses of suggested shear test setups

(With a roller support, a bond length=50 mm and a concrete block height ratio=1.0)

CHAPTER 4

VALIDITY OF A MODIFIED SHEAR TEST FOR CONCRETE-TO-CONCRETE INTERFACES

4.1 INTRODUCTION

According to the analyses and findings presented in Chapter 3, an appropriate test method for investigating the shear performance of concrete-to-concrete interfaces should produce a uniform interfacial shear stress distribution and allow the stable propagation of interfacial debonding (Tabor, 1978; Saucier *et al*., 1991; Gohnert, 2003; Randl, 2013; Santos, 2013). In all the existing test methods for concrete-to-concrete interfaces, the induced interfacial shear stress distributions are all non-uniform to a certain degree, and significant normal stress along the interface is inevitable. The FE analysis presented in the previous chapter indicates that by optimizing the parameters of the L-shaped one-interface test specimen, a generally uniform interfacial shear stress distribution with minimal normal stresses can be achieved. However, as the interfacial tensile and shear stresses are concentrated at the ends of the bondline, interfacial splitting or debonding of a brittle manner is likely to initiate at these locations, causing sudden premature failure of the test specimen. Therefore, it is difficult to achieve stable debonding propagation along the bondline, which is necessary to investigate the local interfacial damage evolution behaviour after reaching the peak interfacial stress.

Based on the conclusions of Chapter 3, a modified shear test method is proposed in this chapter to overcome the shortcomings of the existing methods and experimentally obtain a relatively accurate local bond-slip relationship at the concrete-to-concrete interface. The feasibility and reliability of the proposed test method, especially the

rationality of the layout of external reinforcement, the bond length of concrete-to-concrete interfaces, the measurement of interfacial slip, as well as the data processing method, have yet to be verified at the experimental level, which will be focused in this chapter.

4.2 THE MODIFIED L-SHAPED ONE-INTERFACE SHEAR TEST METHOD

4.2.1 Deficiencies of the Existing L-shaped One-interface Shear Test

A typical L-shaped one-interface shear test specimen consists of two anti-symmetrically bonded L-shaped concrete blocks, with the concrete-to-concrete interface located at the centreline of the specimen (Hofbeck *et al*., 1969; Mattock, 1976; Walraven *et al*., 1987; Júlio *et al*., 2010). During testing, a compressive load concentric to the interface is applied to the specimen, nominally generating a shear force at the interface. The specimen can be fabricated with or without dowel reinforcement crossing the interface, as shown in Figure 4.1 (a) and Figure 4.1 (b), respectively.

For specimens without dowel reinforcement, the shear resistance is solely provided by the concrete-to-concrete interface. Hence, the main advantage of this kind of specimens is that the interfacial behaviour is directly measured. However, as mentioned previously, the brittle failure induced by local cracking at the interface ends prevents the accurate measurement of interfacial elastic behaviour (test may end before the peak load), as well as the debonding process, as illustrated in Figure 4.2. Consequently, the complete interfacial bond-slip relationship for concrete-to-concrete interfaces cannot be developed based on this type of tests. On the other hand, for specimens with dowel reinforcement, the abrupt fracture of the interface is prevented by the dowel reinforcing bars, thereby enabling the measurement of the softening behaviour of the interface.

However, the measured behaviour is the mixed responses of the interface and the reinforcement, since the contributions of the concrete-to-concrete interface and the reinforcement are deeply entangled, as shown in Figure 4.3. The situation is further complicated by the local stress concentrations induced by the reinforcement crossing the interface, which affect the stress distribution and may cause local fractures. As a result, the mechanical response of the concrete-to-concrete interface cannot be quantified by this type of test.

Taken collectively, both test methods have critical deficiencies in the measurement of bond-slip behaviour of concrete-to-concrete interfaces. To overcome these defects, a modified test method is proposed as follows.

4.2.2 Modification of the L-shaped One-interface Shear Test

In order to take advantage of the stabilising effect of reinforcing bars while avoiding the entanglement between the dowel reinforcement and the concrete-to-concrete interface, in the modified test method, the reinforcing bars are placed outside of and in parallel with the concrete-to-concrete interface, as shown in Figure 4.4. The transverse reinforcement in the traditional L-shaped one-interface test has a two-fold influence on the interfacial behaviour. First, it develops a local dowel reaction under shear action that leads to severe non-uniformity in stresses along the interface. Second, it suppresses brittle interfacial debonding but instead induces a gradual debonding process. To understand the complete local bond-slip relationship, this stress non-uniformity should be avoided while the gradual debonding process should be preserved. Therefore, the transverse reinforcement is removed in the proposed test specimen to avoid local dowel effects. Meanwhile, longitudinal reinforcement that is parallel to but outside of the interface is used in the proposed test specimen to achieve a gradual debonding process. Thereby, the softening behaviour of the interface can be measured, and the

reinforcement and the concrete-to-concrete interface are physically separated. This modified specimen may be referred to as the L-shaped one-interface specimen with parallel reinforcement.

In order to isolate the contribution of the concrete-to-concrete interface, the contribution of the parallel reinforcement needs to be identified and subtracted from the total resistance. This can be achieved by fabricating a companion specimen, which is identical to the modified specimen except that the interface is unbonded. By testing this unbonded companion specimen, the contribution of the parallel reinforcement can be achieved. This process is schematically shown in Figure 4.5, where the load-slip curves of the modified bonded and reinforced (BR) specimen and the companion unbonded and reinforced (UR) specimen can be separately obtained. Through these two load-slip curves, the load-slip response of the bonded (B) concrete-to-concrete interface can be isolated as indicated in the figure.

As mentioned above, the feasibility and reliability of the modified test method proposed here have yet to be validated. In particular, attentions should be paid to the influence of the parallel reinforcing bars on the interfacial stress distribution, the rationality of the bond length of specimens, the measurement of interfacial slip, and the data processing method. These are described in detail in the following sections.

4.3 VALIDATION PROGRAMME

4.3.1 Specimen Design

Using the modified test method, a pair of companion specimens, one with a bonded interface and two parallel reinforcing bars (referred to as 'BR', see Figure 4.6 (a)) and the other with an unbonded interface and parallel reinforcing bars (referred to as 'UR',

see Figure 4.6 (b)) were used to evaluate the behaviour of concrete-to-concrete interfaces. Since the two companion specimens were identical except for the interfacial bond, the response of the concrete-to-concrete interface could be calculated as the difference between the measured responses of the BR and UR specimens, assuming that the inter-specimen variations are negligible. Additionally, another specimen with a bonded interface but without the parallel reinforcing bars (referred to as 'B'), as shown in Figure 4.6 (c), was used as a reference.

According to the FE simulations presented in Chapter 3, the bond length of the modified specimen should be determined based on the criterion that the interfacial shear stress distribution is most uniform. In this way, the local interfacial shear stresses and slips along the interface are closely represented by the measured global interface-average shear stress-slip relationship. The numerical results suggested that a bond length of 50 mm was most appropriate. Accordingly, to experimentally examine the influence of bond length on the shear stress distribution, specimens with bond lengths of 50 mm and 80 mm were fabricated for comparison. Their detailed geometric layouts are shown in Figures 4.7 and 4.8, respectively. It can be seen from the two figures that for the specimen with a bond length of 50 mm, the overall length, width and height were 200 mm, 100 mm, and 100 mm, respectively. For specimens with a bond length of 80 mm, these values were 230 mm, 100 mm, and 100 mm, respectively. That is to say, the height of the specimens changes accordingly only because of the different bond lengths. Moreover, steel loading plates with a thickness of 50 mm were adopted to minimize the stress concentration on the upper and lower surfaces of the specimen, as suggested in Chapter 3. For each bond length, two companion specimens and one reference specimen were prepared; a total of six specimens were fabricated for the two bond lengths. The specimens are assigned names indicating their specimen role and the bond length: 'UR-L50' indicates the specimen with parallel reinforcement, unbonded interface, and a

bond length of 50 mm. Details of the specimens are listed in Table 4.1.

The purpose of the parallel steel reinforcing bars is to prevent the brittle interfacing debonding, and the contribution of the interface is obtained by finding the difference between the BR and UR specimens. Therefore, if the contribution of the steel bars is too large, the difference is not obvious and difficult to measure. On the other hand, if the steel bars are too weak, the brittle debonding cannot be effectively prevented. Thus, the diameter of the steel reinforcing bars was determined based on the consideration that the resistance provided by the steel bars should be on par with the shear resistance provided by the concrete-to-concrete interface. Namely, $f_y A_s \approx \tau_c A_c$, where f_y and A_s are the yield stress and area of the steel bars, and τ_c and A_c are the interface-average shear strength and area of the concrete-to-concrete interface. Therefore, by assuming a representative value of 300 MPa for f_y and 1.5 MPa for τ_c and knowing that A_c is 5000 and 8000 mm^2 for specimens with bond lengths of 50 and 80 mm, the steel bar diameter was about 4 mm and will be selected in the tests.

4.3.2 Materials and Specimen Preparation

Practically, the concrete strength in existing structures, especially old concrete structures in need of rehabilitation, is relatively low. Therefore, a low-strength concrete mix was used to fabricate the old concrete block for the modified test specimens. Specifically, the target 28-day compressive cube strength of the old concrete was around 20 MPa, which was the minimum strength allowed for reinforced concrete structures according to the Chinese "Code for design of concrete structures (GB 50010-2010, 2010)". Further, the strength of the new concrete used for strengthening should be higher than that of the old concrete, as stipulated by the Chinese "Technical Specification for Strengthening Concrete Structures" (CECS 25:90, 1991). Therefore, a mix producing a target 28-day compressive cube strength of 40 MPa was used for the

new concrete block for the specimens. For the concrete mixes, ordinary medium-coarse river sand was used as the fine aggregate, crushed stone with a particle size of 4 to 18 mm was used as the coarse aggregate, and ordinary Portland cement of grades 42.5 or 32.5 was adopted as the binder. The mixing proportions of the new and old concretes are detailed in Table 4.2. During preparation of the specimens, six 100 mm concrete cubes (three for the old concrete and three for the new concrete) were cast simultaneously to evaluate the concrete compressive strength; the corresponding standard compressive strength of a 150 mm cube can be evaluated by multiplying the compressive strength of a 100 mm cube by a coefficient of 0.95 (GB/T 50081-2002, 2003). The measured 100 mm cube strengths for the old and new concretes were 22.8 MPa and 43.7 MPa, and therefore the standard cube compressive strengths for the old and new concretes were 21.7 MPa and 41.5 MPa, respectively. The used mixes for the old and new concretes satisfied the design requirements.

Two steel bars with a 4-mm diameter were used as the parallel reinforcement. The setup of the tension test of the steel bars is shown in Figure 4.9, and a total of three steel bars were tested. The average values of the yield stress, tensile strength, and elastic modulus of the steel bars were 274.11 MPa, 377.81 MPa, and 182.01 GPa, as listed in Table 4.3.

All the specimens consisted of two L-shaped concrete blocks. The L-shaped old concrete block was first cast and cured for 28 days while the parallel reinforcing bars were held in place, as shown in the left prat of Figure 4.10. Subsequently, the L-shaped new concrete block was cast onto the old one and the reinforcing bars and cured for another 28 days, thereby forming a concrete-to-concrete interface (see right prat of Figure 4.10).

4.3.3 Test Setup and Measurement

The WDW-100-type electronic universal testing machine at Tongji University was used as the loading frame for the tests, as shown in Figure 4.11. This machine has a loading range of 0 ~ 100 kN, and a displacement-control loading rate ranging from 0.05 mm/min to 500 mm/min. Two 50-mm-thick steel loading plates were used, as illustrated in Figure 4.6. The axial compression was applied using displacement control with a rate of 0.05 mm/min until complete interfacial debonding occurred. This very low loading rate ensured that the concrete-to-concrete interface was subjected to quasi-static loading, as well as providing a sufficient time span for the digital image correlation (DIC) system to capture enough images, as explained below.

The load was recorded by the loading machine, and the interfacial slip was measured using both a clip extensometer and a DIC system. A close-up view of the clip extensometer is shown in Figure 4.12 (a). The literature indicated that the maximum interfacial slip corresponding to the shear failure of the concrete-to-concrete interface was typically no larger than 0.2 mm (Chilwesa *et al*. 2017). Therefore, the accuracy of the clip extensometer should be sufficiently high. Specifically, the YYJ-4/10 clip extensometer used in this test has an accuracy of 0.1 μm and a measuring range of 0 ~ 6 mm. In addition, the clip extensometer has a small size, which is suitable for the small specimens with only 50 mm bond length in this test. A schematic of using the extensometer to measure the interfacial slip at the centre location of the interface is shown in Fig. 4.12 (b). It can be seen that, before the test, the clip extensometer was fixed on small iron sheets on both sides of the concrete-to-concrete interface and the clip extensometer initially opened for a certain distance. During the loading process, the opening of the clip extensometer became larger and the changed distance would be automatically recorded, which was considered as the slip of concrete-to-concrete

interfaces. It is noted that the extensometer could only measure the relative slip of two spots that are 20 mm apart, due to the limitation of the attachment setup. Accordingly, the slip measured by the extensometer was essentially the relative displacement of two spots that were each 10 mm away from the concrete-to-concrete interface. Considering that the displacement field around the interface may be non-uniform, i.e., the displacement at a spot 10 mm away from the interface may be different from that at a spot 2 mm away, a DIC system was also employed in this test to measure the entire displacement field of the specimen.

4.3.4 The Digital Image Correlation System

As mentioned above, the clip extensometer actually measured the slip of 10 mm from both sides of the concrete-to-concrete interface. Whether this slip can represent the slip of the interface requires further examination. In addition, in order to better observe the interfacial crack initiation and propagation of the specimen during the test, the DIC system was also employed to measure the displacement field of the specimen.

The DIC system continuously captures images of the prepared specimen surface during the testing at pre-set intervals and from a fixed location. Through post-processing, each captured digital image except for the first one can be converted to displacement and strain fields, representing the state of the specimen at the time that image was taken (Blaber *et al*. 2015). According to the number of cameras used, DIC technology can be categorized into 2D (two-dimensional) method, which uses images taken from a single camera to calculate the displacement and strain fields on a plane, and 3D (three-dimensional) method, which uses images taken from two cameras to calculate the displacement and strain fields in a volume. In comparison between the two methods, the 2D method requires less computational cost and is easier to setup, but it is only suitable for the analysis of a surface with good flatness (Murienne and Nguyen, 2016).

In this study, due to the good flatness of the specimen surface, the 2D DIC method using a single digital camera was employed to take images of one surface of the specimen, while the extensometer was mounted on the opposite surface. Then the images were post-processed to obtain the displacement field of the specimen surface.

Before testing, the specimen surface needs to be prepared with a random pattern by spraying black speckles on white substrates. As a result, each pixel in the captured digital image has a random grey-scale value, and the entire image can be mathematically represented by a large matrix, within which each sub-matrix with a size of a certain number of pixels is unique and can be traced even after deformation. During the post-processing, the locations of all the sub-matrices in an image are compared to those in the initial image of the undeformed surface (specimen), and thereupon the displacement field can be calculated. The strain field can be readily obtained by differentiating the displacement field (Pan *et al*., 2009). It is noted that the displacement field calculated by the DIC system is pixel-based; the pixel-to-length relationship must be established for the DIC system to derive real displacement and strain fields.

An important prerequisite for the DIC system to accurately measure the displacement field is capturing quality images of clear speckles (Kumar *et al*., 2019). Therefore, all specimens should satisfy the following four requirements: 1) before the test, the surface should be prepared with a speckle pattern with obvious grey differences; 2) the speckle image taken by the camera should be clear and identifiable, and the diameter of a single grey spot should be roughly the same; 3) in order to keep the grey level of the speckle image unchanged, stable lighting conditions must be maintained during the test, and artificial light source with constant brightness should be used; 4) the positions of the camera and the specimen during the test should be kept unchanged to maintain the validity of the pixel-to-length relationship (Pan *et al*., 2009; Kumar *et al*., 2019). In

addition, for the 2D method, it is also necessary to ensure that the camera shooting direction is perpendicular to the surface to minimize the perspective effect and the corresponding errors.

The surface of the shear specimens was prepared as follows. At 48 hours before the test, a layer of white matt paint was uniformly sprayed on the surface of the specimen. After the proper cure of the white paint, black matt paint was sprayed on the white substrate to obtain black speckles with a diameter of about 0.5 mm and a density of about $50/cm^2$. A typical finished surface is shown in Figure 4.13.

The DIC system mainly consisted of a digital camera fixed on a tripod and a white light source. During the test, the CMOS high-resolution camera (Nikon D7100, with 18-105 mm lens) was set up directly in front of the specimen, and the white light source was set on the right side so that the light directly hit the surface of the specimen, as shown in the Figure 4.14. In order to ensure a clear image and obvious black-and-white contrast, the camera parameters were set as: aperture priority mode, with an aperture value of F4.5, ISO (photosensibility) about 1000. The camera was set to automatically take pictures at a 10-s interval until the end of the test.

After the test, the commonly used open-source program Nccor (Blaber *et al*. 2015) was used to post-process the images. The Nccor program is an algorithm with graphical user-interface (GUI). The opening, calculation and result export of the program all rely on MATLAB software platform (Harilal and Ramji, 2014).

4.3.5 FE Modelling

The influence of the two parallel reinforcing bars on the interfacial stress distribution of the modified L-shaped one-interface shear test specimen cannot be quantified using

the current instrumentation. Therefore, FE modelling was employed to simulate the behaviour of the test specimens. The difference between the current FE model and the model shown in Figure 3.1 (c) mainly lay in two aspects: one is the addition of steel bars parallel to the bondline; the other is to reduce the bond length from 300 mm to 50 mm according to the specimen design in this test. As an elastic analysis, four-node quadrilateral plane stress elements were used to simulate the reinforcing bars, and the elastic modulus was taken as 182.01 GPa, based on the tensile tests of the steel bars. The cylinder compressive strength of the concrete, obtained by multiplying the cube compressive strength by a coefficient of 0.79, according to the Chinese "Code for design of concrete structures (GB 50010-2010, 2010)" as well as the literature (Elwell and Fu, 1995), was assigned to the concrete in the model. The elastic modulus of the concrete was obtained using the ACI equation $E_c = 4730\sqrt{f_c}$ (in MPa) from the concrete cylinder compressive strength (ACI, 2008). The other details of the model were the same with those in the FE model shown in Chapter 3 and are not repeated.

4.4 RESULTS AND DISCUSSIONS

4.4.1 Failure Mode

Debonding failure at the concrete-to-concrete interface occurred in all the specimens. For group B specimens, the failure was brittle due to the absence of reinforcement, as shown in Figure 4.15 (a). During loading, cracks first propagated at the ends of the interface. Subsequently, the cracks propagated rapidly through the interface until the complete separation of the new and old concrete blocks. For group BR specimens, the specimens behaved similarly to group B specimens before the initiation of interfacial cracks/debonding. After the initiation of interfacial cracks at the ends of the concrete-to-concrete interface, the presence of parallel steel bars prevented the abrupt separation

of the new and old concrete blocks. Instead, the specimens experienced a gradual propagation of the interfacial cracks until final complete debonding, resulting in separation of the old and new concrete blocks, as shown in Figure 4.15 (b). For group UR without bonding of the new and old concrete, the load was solely resisted by the steel bars. No obvious damage was observed at the interface between new and old concrete blocks. The tests for the UR specimens were terminated when the slip reached 0.3 mm.

Figure 4.16 shows the shear strain fields obtained from the DIC system, along the 50 mm interface and 2 mm to each side of the interface, for a typical BR specimen; they qualitatively show the interfacial debonding process. It is obvious from these results that the shear strain was generally uniformly distributed along the interface before the initiation of debonding, as shown in Figure 4.16 (a)-(c) by the strain fields under an applied load below 8.5 kN. When the applied load was about 10.5 kN (Figure 4.16 (d)), a strain concentration can be seen at the lower end of the interface indicating interfacial debonding initiation. With the further increase of the applied load in Figure 4.16 (e)-(g), the shear strain concentration propagated along the interface, and meanwhile the interfacial crack was observed to propagate along the interface. Finally, at a load level of 15.5 kN (Figure 4.16 (h)), the crack propagated through the concrete-to-concrete interface and complete debonding occurred. It can be seen from the failed specimen that a single main crack path was formed at the concrete-to-concrete interface while no branching cracks nor smeared secondary cracks parallel to the main crack were observed. Similar trend of crack initiation and propagation was observed for the other specimens.

4.4.2 Effect of Parallel Steel Bars

The FE results of the modified L-shaped one-interface shear test specimens, with the

parallel steel bars placed at different distances, on both sides, from the concrete-to-concrete interface are shown in Figure 4.17. Figure 4.17 (a) shows the normal stress distributions. The results indicate that the normal stress distribution along the interface is basically the same for the specimens with parallel steel bars at different distances and the specimen without the steel bars. That is, the steel bars have little impact on the interfacial normal stress distribution. By contrast, as shown in Figure 4.17 (b), the interfacial shear stress in specimens with the steel bars is lower than that without the steel bars. This is because the steel bars carry part of the shear load, which needs to be identified and subtracted from the total load to isolate the contribution of the interface. Moreover, the shear stress distribution is little affected by the location of the bars, as indicated by Figure 4.17 (b). Therefore, for the designed specimens, the distance between the steel bars and the concrete-to-concrete interface was determined as 10 mm.

4.4.3 Evaluation of the DIC Accuracy by Clip Extensometer Measurements

According to the test setup introduced in section 4.3.4, the relative slip of two spots 10 mm away from and on each side of the interface can be measured by the extensometer, and the entire displacement field of the specimen can be measured by the DIC system. In order to evaluate the accuracy of the DIC displacement measurements, the relative slip measured by the clip extensometer and the relative displacement of the same two spots obtained from the DIC measured displacement field are compared for three BR-L50 specimens. The results are plotted in Figure 4.18. It is noted that although the parallel steel bars prevent the specimens from separating after the peak, however, this debonding process was instantaneously. Neither the clip extensometer nor the DIC system can capture sufficient valid data in the softening stage. Therefore, only the slip before the peak load was analyzed here.

It can be seen that from the beginning of loading to the peak load around 17 kN, the

slip-load curves measured by the clip extensometer are generally linear indicating an elastic behaviour of the specimen. In comparison, the slip measured by the DIC system fluctuated around the values measured by the clip extensometer, with an average difference between the two of about 0.0009 mm. This difference was acceptable relative to the slip of approximately 0.02 mm corresponding to the peak load, which was only 4.5%. This result indicates that the DIC measurements are reliable for quantitative purposes, as also suggested in other studies (Zheng and Dawood, 2016). However, compared with the slip measured by the clip extensometer, the slip measured by DIC system has certain fluctuations. Nevertheless, the data measured by the DIC system are very helpful in analyzing the slip distribution for these specimens.

4.4.4 The Displacement Field at the Vicinity of the Interface

Conceptually, the concrete-to-concrete interface refers to the distinct boundary between the new and old concrete, which is formed during the cure of the new concrete. Practically, however, such a distinct boundary is nonexistent; instead, the 'interface' is more a flat region of a certain thickness than a zero-thickness plane. Therefore, the judicious choice of the representative slip at the interface is indeed a subject worth investigation. The conventional instrument such as a clip extensometer can only measure the relative displacement of two spots. In the present study, with the ability of measuring the entire displacement field by the DIC system, the vicinity of the interface is thoroughly investigated and a rigorous choice of the most representative slip for the interface is suggested.

The investigated vicinity of the interface is illustrated as the shaded area in Figure 4.19, a region along the entire interface and to the 10 mm each side of it. The displacement field of this region measured by the DIC system was used to investigate the displacement field of the 'interface'. In Figure 4.19, if the coordinates of point A are

(x_0, y_A), the coordinates of the interface-mirrored point B are defined as (-x_0, y_B), where x_0 is the distance away from the interface. Then the relative displacement between the two points A and B is calculated as the distance between y_A and y_B.

Figure 4.20 presents the distribution of the slip distribution for specimen BR-L50 at the loading stages of 0.25P, 0.5P, 0.75P and P, where P denotes the peak load. The 'Distance from the interface' axis in Figure 4.20 corresponds to the x-axis in Figure 4.19, ranging from 0 to 10 mm; the 'Bond length' axis in Figure 4.20 corresponds to the y-axis in Figure 4.19, ranging from 0 to 50 mm. The 'Slip' axis is the absolute relative displacement, or slip, between the points and their interface-mirrored points.

It can be seen from Figure 4.20 that, under different load levels, the displacement distribution in this region was basically the same and no obvious variation can be found, only the value of z-axis increased. This is because with the increase of loading, the slip in this area was increasing. Examining the slip distribution indicates that, in general, along the x-axis, the slip was smaller at locations closer to the interface. Taking the slip distribution at 0.25P (Figure 4.20 (a)) as an example, the average slip was about 0.0042 mm along $x = 0$, while that was about 0.0053 mm along $x = 10$ mm, marking a difference of about 0.0009 mm. Under the peak load (Figure 4.20 (d)), the difference between the average slips along $x = 0$ and $x = 10$ was about 0.0037 mm. The reason for the inconsistent slip value may be due to the combined effect of shear deformation of the concrete block, as well as the small rigid rotation of the specimen under the action of vertical loading, although the size of the specimen had been designed to avoid such unnecessary rotation as much as possible in this test. Figures 4.21 and 4.22 show the slip distributions at various load levels for specimens B-L50 and UR-L50, respectively. It can be seen that before reaching the peak load, the slip distributions of specimen B-L50 and UR-L50 are very similar to that of specimen BR-L50. The slip was also smaller

at locations closer to the interface, the difference between the average slips along $x = 0$ and $x = 10$ was about 0.0041 mm and 0.0036 mm at the peak load, respectively. Meanwhile, this difference basically shows a linear increase trend with the load increased linearly.

With the current experimental data, it is quite difficult to exactly quantitatively determine the contribution from the shear deformation of the concrete blocks, or the small rigid rotation of the specimen for this slip difference. In spite of this, the slip near the concrete-to-concrete interface can be calculated by the following equation with the slip recorded by the clip extensometer before the peak load:

$$s(t) = s_c(t) - 0.0038 \cdot \frac{P(t)}{P_{\max}} \tag{4.1}$$

where $s(t)$ is the slip near the concrete-to-concrete interface at time t and the unit *is mm*, $s_c(t)$ is the slip recorded by the clip extensometer at time t and the unit, $P(t)$ is the shear load of the specimen at time t while $P_{\max}$ is the peak load. Here, 0.0038 is an average slip difference for the three specimens mentioned above with an unit of *mm*.

After the peak load, on the one hand, neither the DIC system nor the clip extensometer captured sufficient data for the softening stage of the interface. On the one hand, the slip corresponding to the residual load was around 0.1 mm, and the slip difference of 0.0038 mm was only 3.8% of this value. Therefore, it is considered to be acceptable to adopt the slip measured by the clip extensometer directly as the slip after the peak load.

Analysing the variation of the slip along the *y*-axis in Figure 4.20 indicates that, although there are minor fluctuations, the distribution is generally uniform. Figures 4.21 and 4.22 show that fluctuations of the slip along the bond length are more obvious for specimen B-L50 than for specimen UR-L50, due to that there is no bond at the interface

for specimen UR-L50. This indicates that, with a proper design of the test specimen, the goal of basically uniform slip along the interface can be achieved. The numerical results presented in chapter 3 indicate that the bond length has a significant impact on the shape of slip distribution. The shape of slip distribution at the concrete-to-concrete interface under shear loading is the main focus of this thesis, which will be analyzed and discussed in detail in the following Section.

4.4.5 Distributions of Slip and Opening/Closing Displacement for Different Bond Lengths

The influence of the bond lengths, 50 and 80 mm, on the interfacial slip and opening/closing displacement are further investigated through the DIC measurements of BR-L50 and BR-L80. The tangential slip and normal opening/closing displacement at the interface can be obtained from the DIC measurements. Specifically, the displacements along two parallel lines of $x = -0.05$ and $x = 0.05$ measured by the DIC system were used to investigate the relative displacements. The slip was obtained as discussed above, and the opening/closing displacement was obtained by calculating the difference of the x-displacements. Figure 4.23 shows the slip distributions along the interface for specimens with bond lengths of 50 mm (specimen BR-L50) and 80 mm (specimen BR-L80), respectively, at applied loads of 0.5 P, 0.75P and P. Generally, the slip distribution is much more uniform for the 50 mm bond length than for the 80 mm, which is in agreement with the conclusions obtained from the FE analysis presented in Chapter 3. Therefore, it is more appropriate to select the specimen with a bond length of 50 mm when investigating the bond-slip behaviour of concrete-concrete interfaces.

The distributions of the normal opening/closing displacement along the interface measured by the DIC system are shown in Figure 4.24, for both the 50 and 80 mm bond lengths. Closing displacements were observed at the ends of the interface while

negligible opening displacements are seen in the middle part of the bonded interface for both specimens. For the specimens with different bond lengths of 50 mm and 80 mm, the opening displacements are similar. By contrast, at the ends of the interface, the closing displacements for the two specimens are slightly different. Therefore, this modified specimen is appropriate for the bond-slip investigation because no large opening displacement appears at the interface ends, indicating no premature interfacial debonding.

It can be indicated from Figure 4.17 and Figures 4.20 ~ 4.24 that the slip measured by the clip extensometer at the middle point of the bond length (25 mm away from both ends), except for the areas at both ends of the interface, can basically represent the average shear slip over the entire bond length (approximately from 0.2 to 0.8 of normalized position). The normal stress, as well as the opening displacement at this point can also be ignored because these values here are very small.

In addition, the experimental results and the FE results clearly show that when cracks initiate at the ends of the interface, since no other diagonal cracks have been observed. Therefore, except for the small area of the ends, the behaviour of the L-shaped one-interface shear test is governed by shear, and this test set-up can be employed effectively to study the shear behaviour of concrete-concrete interfaces.

4.4.6 Load-Slip Responses

From the previous analysis, the specimen with a bond length of 50 mm is more appropriate than the specimen with a bond length of 80 mm in achieving uniform distribution of interfacial stress or slip. Therefore, the following analysis of the load-slip responses will only focus on those specimens with a bond length of 50 mm. For all specimens, the load was the total force applied to the specimen, and the slip measured

by the extensometer is directed used. Figure 4.25 shows the load-slip curves of the three UR-L50 specimens. The shear stress at the unbonded interface of the specimens UR-L50 is assumed to be zero, and the measured load is solely contributed by the parallel reinforcing bars. In the initial stage, the load increased linearly with the increase of the interfacial slip, as the parallel reinforcing bars were in the linear elastic stage. When the slip exceeded around 0.015 mm, an evident yielding behaviour was seen due to the yielding of the parallel reinforcement. The loading was terminated at a slip of 0.30 mm in this test. It can also be obtained from Figure 4.25 that the stiffness of the specimen UR was approximately 433 kN/mm. Based on the data in Table 4.3, the stiffness of the two steel bars under compression are about 458 kN/mm. Therefore, the elastic stiffness of the specimen UR-L50 was close to the sum of the elastic stiffness of the two parallel steel bars.

Figure 4.26 shows the load-slip curves of specimens BR-L50, which start from a linear stage when the slip was below 0.02 mm. In this stage, the concrete-to-concrete interface was in the elastic stage. At the slip of 0.02 mm, the peak load was reached, indicated by a sudden increase of the slip to over 0.10 mm accompanied by a sudden drop of the load by approximately 50%; meanwhile, interfacial cracks were observed. This sudden debonding was cushioned by the parallel reinforcing bars, and the potential brittle failure was thus prevented. Subsequently, the slightly increasing load with the increase of the slip was a combined result of the softening behaviour of the concrete-to-concrete interface and the yielding behaviour of the parallel reinforcing bars.

The load-slip responses of specimens UR-L50 and BR-L50 can then be used to isolate the behaviour of the concrete-to-concrete interface, as illustrated in Figure 4.5. The so-obtained curves based on the results are shown in Figure 4.27. In the elastic stage, the linear ascending load-slip response was only attributed to the resistance of the concrete-

to-concrete interface. Subsequently, with the increasing slip, the load decreased rapidly after the peak, but still maintained a small value without sudden interruption of the shear test. As a comparison, Figure 4.28 presents the load-slip relationship obtained from specimens B-L50 without the parallel reinforcement. It is seen that the linear ascending behaviour was basically identical to the isolated load-slip response. After the peak load at the critical slip around 0.02 mm, the load dropped sharply, and the shear test ended.

4.5 CONCLUSIONS

This chapter has proposed a novel test method by adding reinforcement that is parallel to, instead of crossing, the interface to the L-shaped one-interface specimen. Therefore, the reinforcement and the bonded interface are physically separated, and the softening behaviour of the interface can be measured. This method takes advantage of the stabilising effect of the reinforcing bars while avoiding the entanglement between the dowel and interface. Accordingly, in order to isolate the response of the interface, a companion specimen that is identical with the modified specimen except with unbonded interface is needed to obtain the contribution of the parallel reinforcement, which is excluded from the response of the modified specimen.

An experimental programme was carried out to validate the modified test specimen in producing an acceptably uniform interfacial shear stress distribution and the modified test method in obtaining a complete local bond-slip relationship of the interface. Three configurations of specimens, including the modified test specimen, the companion specimen with an unbonded interface, and a reference specimen without the parallel reinforcement, were prepared and tested. Specifically, a DIC system was used to measure the interfacial slip distribution as an estimate of the interfacial shear stress

distribution, and an extensometer was used to measure the slip at the mid-point of the interface.

Test results demonstrated that the presence of parallel steel bars indeed prevented the abrupt separation of the new and old concrete blocks, and the specimens could experience a gradual propagation of the interfacial cracks until final complete debonding. Only one main crack path along the concrete-to-concrete interface and no diagonal cracks nor a second crack parallel to the main crack was observed in all specimens. By contrast, the reference specimen without the parallel reinforcement experienced brittle interfacial fracture upon reaching the peak load. Interfacial slip distributions measured by the DIC system indicated that the interfacial slip was basically uniform along the interface for the modified specimens, and the slip measured by the clip extensometer could represent the average interfacial slip of the concrete-to-concrete interface with acceptable accuracy. Additionally, another specimen with a bond length of 80 mm was tested to further validate the specimen design. Comparison of the interfacial slip distributions between the 50 and 80 mm bond length specimens indicated that a 50 mm bond length leads to a more uniform slip distribution, thereby verifying the specimen design.

The load-slip responses of the modified specimen and the companion specimen with unbonded interface were used to isolate the behaviour of the concrete-to-concrete interface. The resulting load-slip response included a linear ascending branch, a still sudden but not fatal descending branch, and a final gradual descending branch. The linear ascending branch was basically identical to that measured from the reference specimen, validating the isolated response of the interface. This newly proposed modified test method is able to produce nearly uniform interfacial shear stress distribution and provide the interfacial softening behaviour. Therefore, the local bond-

slip relationship could be approximated from such a test method. It is used to examine the interfacial behaviour of concrete-to-concrete interfaces through a comprehensive test programme as elaborated in the next chapter.

4.6 REFERENCES

American Concrete Institute (ACI). (2008). *Building code requirements for structural concrete and commentary*. ACI 318, Farmington Hills, MI.

Blaber, J., Adair, B., & Antoniou, A. (2015). Ncorr: open-source 2D digital image correlation matlab software. *Experimental Mechanics*, 55(6), 1105-1122.

CECS 25:90. (1991). *Technical Specification for Strengthening Concrete Structures*. Beijing, China Jihua Press.

Chilwesa, M., Minelli, F., Reggia, A., & Plizzari, G. (2017). Evaluating the shear bond strength between old and new concrete through a new test method. *Magazine of Concrete Research*, 69(9), 425-435.

Elwell, D. J., & Fu, G. (1995). Compression testing of concrete: cylinders vs. cubes. No. FHWA/NY/SR-95/119. *Transportation Research and Development Bureau*, New York State Department of Transportation.

GB 50010-2010. (2010). *Code for desing of concrete structures*. Beijing, China Architecture & Building Press.

GB/T 50081-2002. (2003). *Standard for test method of mechanical properties on ordinary concrete*. Beijing, China Architecture & Building Press.

Gohnert, M. (2003). Horizontal shear transfer across a roughened surface. *Cement and Concrete Composites*, 25(3), 379-385.

Harilal, R. & Ramji, M. (2014). Adaptation of open source 2D DIC software Ncorr for solid mechanics applications. *9th International Symposium on Advanced Science and Technology in Experimental Mechanics*.

Hofbeck, J. A., Ibrahim, I. O., & Mattock, A. H. (1969). Shear transfer in reinforced concrete. *ACI Journal*, 66(2), 119-128.

Júlio, E. N. B. S., Dias-da-Costa, D., Branco, F. A. B., & Alfaiate, J. M. V. (2010). Accuracy of design code expressions for estimating longitudinal shear strength of strengthening concrete overlays. *Engineering Structures*, 32(8), 2387-2393.

Kumar, S. L., Aravind, H. B., & Hossiney, N. (2019). Digital image correlation (DIC) for measuring strain in brick masonry specimen using Ncorr open source 2D MATLAB program. *Results in Engineering*, 4, 100061.

Mattock, A. H. (1976). Shear Transfer under Monotonic Loading, across an Interface between Concretes Cast at Different Times. University of Washington report SM, 76-3.

Murienne, B. J., & Nguyen, T. D. (2016). A comparison of 2D and 3D digital image correlation for a membrane under inflation. *Optics and Lasers in Engineering*, 77, 92-99.

Pan, B., Qian, K., Xie, H., & Asundi, A. (2009). Two-dimensional digital image correlation for in-plane displacement and strain measurement: A review. *Measurement Science and Technology*, 20(6), 062001.

Randl, N. (2013). Design recommendations for interface shear transfer in *f*ib Model Code 2010. *Structural Concrete*, 14(3), 230-241.

Saucier, F., Bastien, J., Pigeon, M., & Fafard, M. (1991). A combined shear-compression device to measure concrete-to-concrete bonding. *Experimental Techniques*, 15(5), 50-55.

Santos, P. M., & Júlio, E. N. (2013). A state-of-the-art review on roughness quantification methods for concrete surfaces. *Construction and Building Materials*, 38, 912-923.

Tabor, L. J. (1978). The evaluation of resin systems for concrete repair. *Magazine of Concrete Research*, 30(105), 221-225.

Walraven, J. (1987). Influence of concrete strength and load history on the shear friction capacity of concrete members. *PCI Journal*, 32(1), 66-83.

Zheng, B., & Dawood, M. (2016). Debonding of carbon fiber–reinforced polymer patches from cracked steel elements under fatigue loading. Journal of Composites for Construction, 20(6), 04016038.

Table 4.1 Specimen details

Specimen name	Interface	Steel bar	Bond length (mm)	Old concrete cube strength (MPa)	New concrete cube strength (MPa)
BR-L50	Bonded	Y	50	21.7	41.5
UR-L50	Unbonded	Y	50	21.7	41.5
B-L50	Bonded	N	50	21.7	41.5
BR-L80	Bonded	Y	80	21.7	41.5
UR-L80	Unbonded	Y	80	21.7	41.5
B-L80	Bonded	N	80	21.7	41.5

Table 4.2 Mix proportions of the new and old concretes

Concrete	Cement Grade	w/c	Cement (kg/m^3)	Sand (kg/m^3)	Coarse aggregate (kg/m^3)	Water (kg/m^3)
Old concrete	32.5	0.60	375	585	1240	220
New concrete	42.5	0.47	500	555	1080	230

Table 4.3 Mechanical properties of the steel bar

Diameter (mm)	Yield strength (MPa)	Ultimate strength (MPa)	Ultimate load (N)	Elastic Modulus (GPa)
4.01	274.11	377.81	3441	182.01
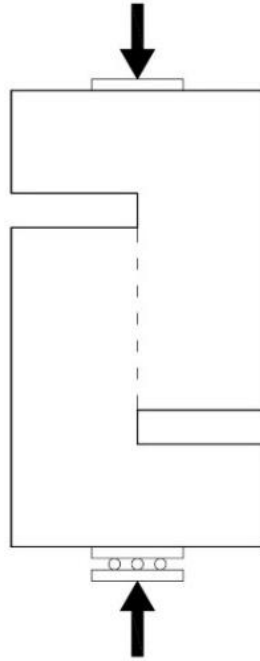
(a) Specimen without dowel reinforcement
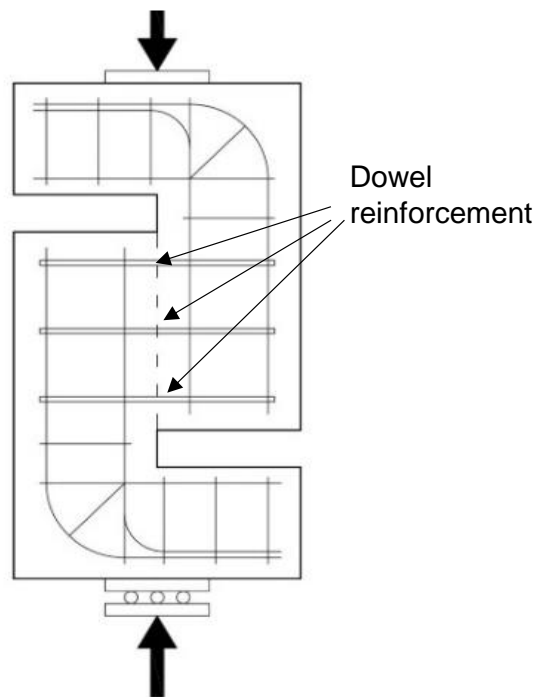
(b) Specimen with dowel reinforcement

Figure 4.1 L-shaped one-interface shear test specimens
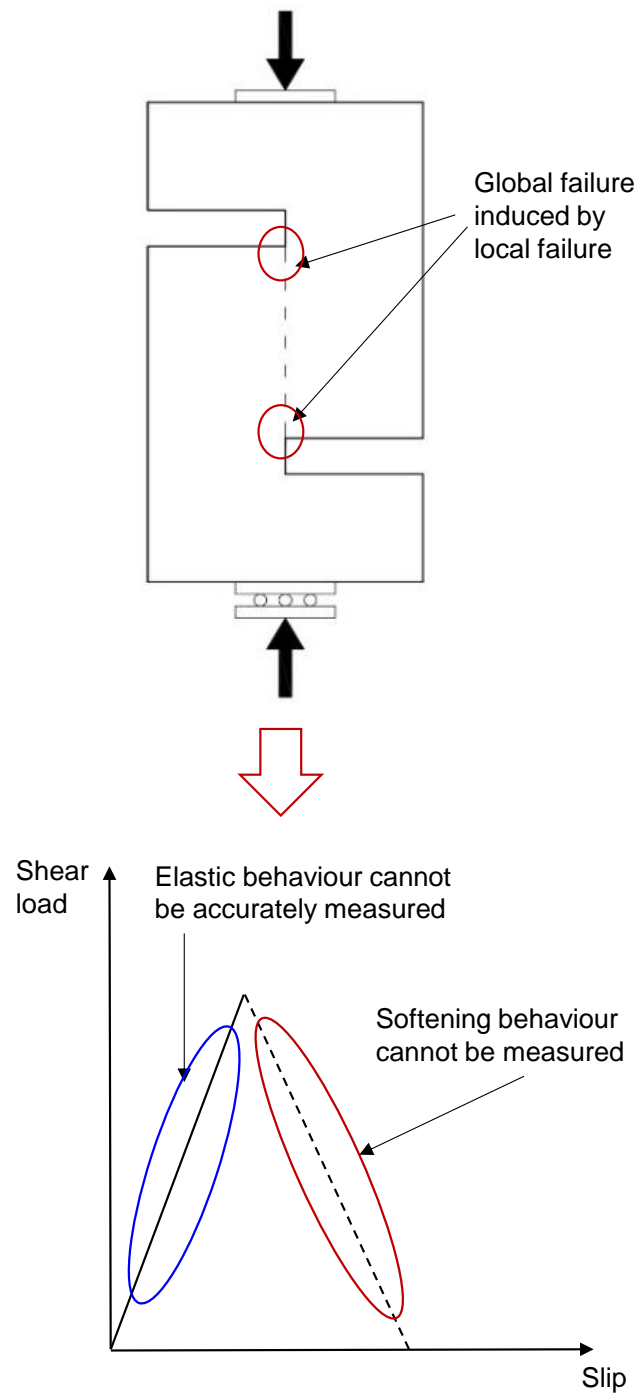
Figure 4.2 Brittle interfacial failure for a specimen without dowel reinforcement
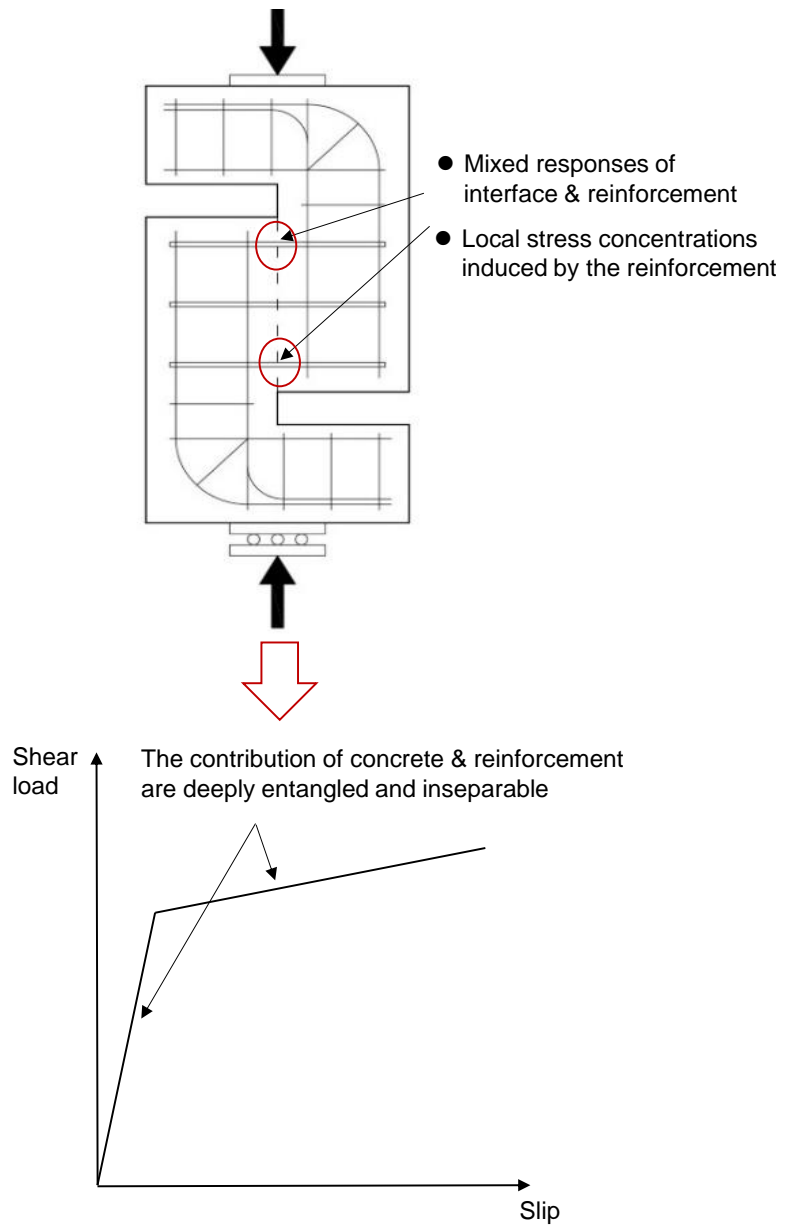
Figure 4.3 The measured mixed response for a specimen with dowel reinforcement
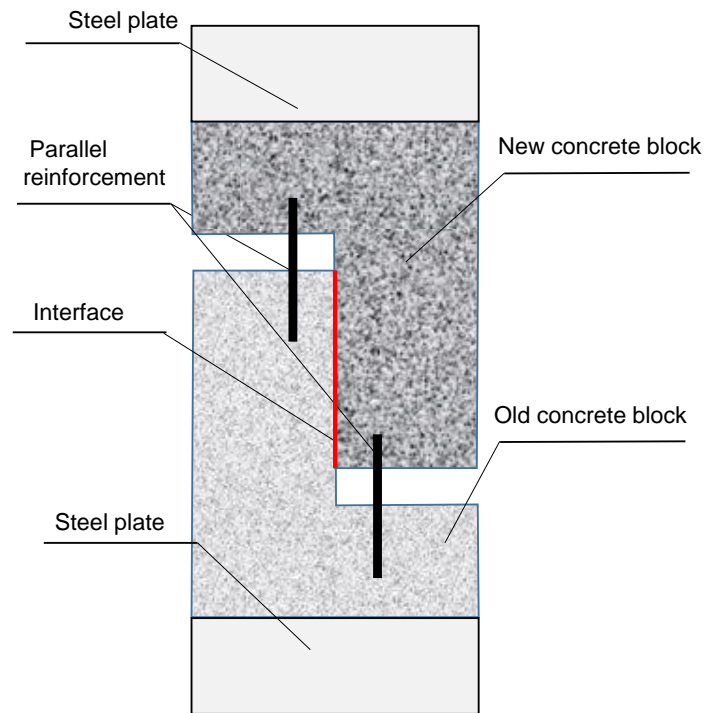
Figure 4.4 Schematic of the modified L-shaped one-interface test specimen
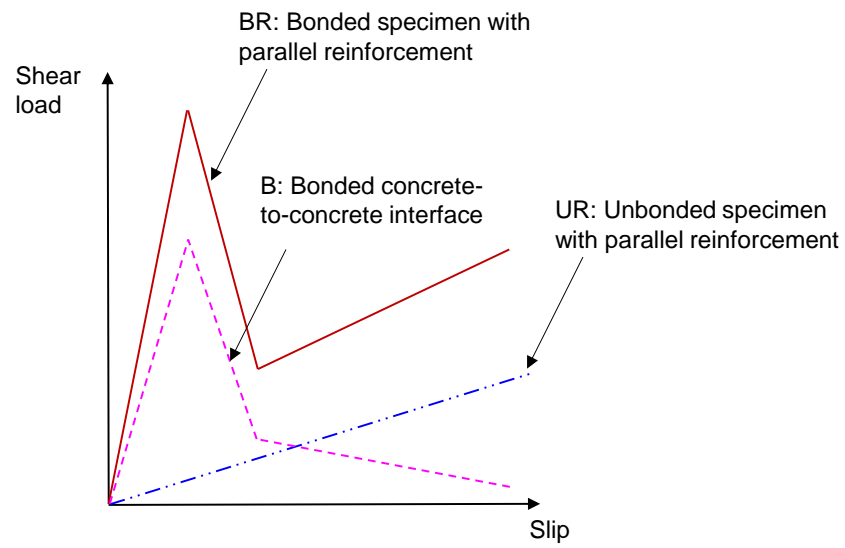
Figure 4.5 Schematic of isolating the response of the concrete-to-concrete interface
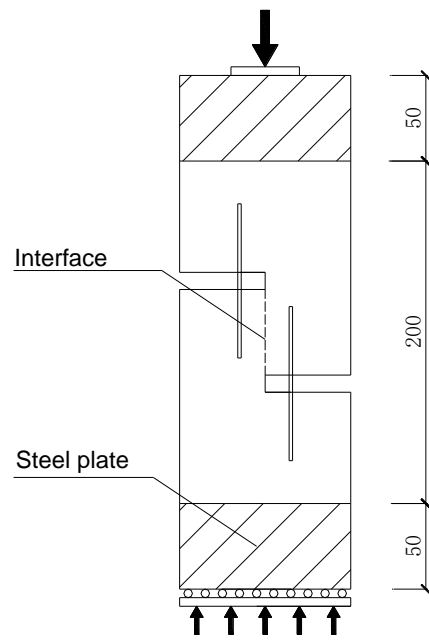
(a) Specimen BR

(b) Specimen UR

123
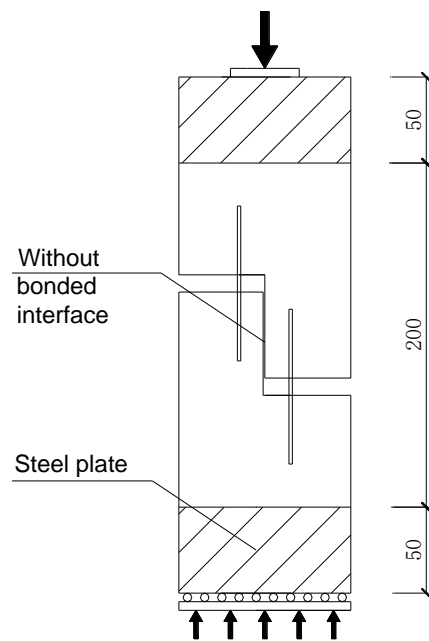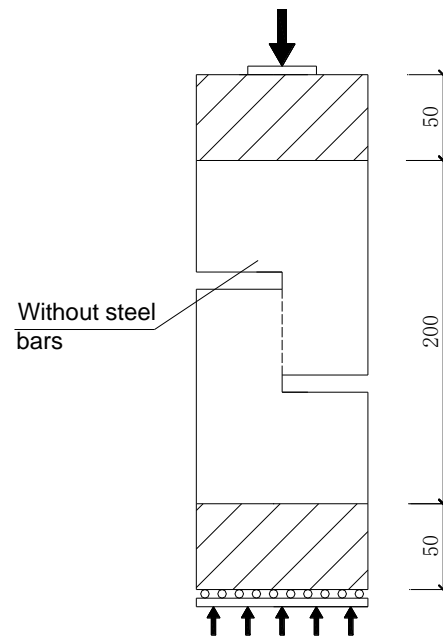
(c) Specimen B

(Dimensions in *mm*)

Figure 4.6 Three types of specimens

124
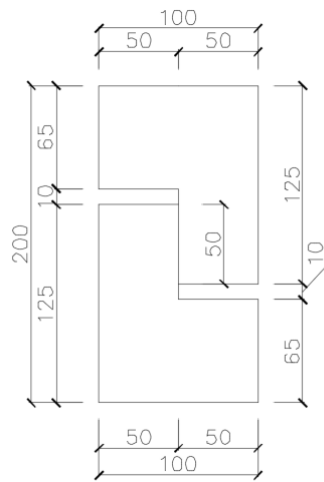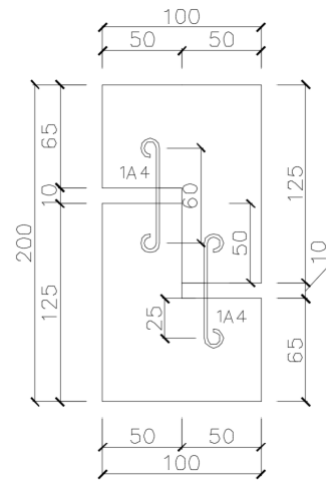
(a) Overview (b) Parallel reinforcement
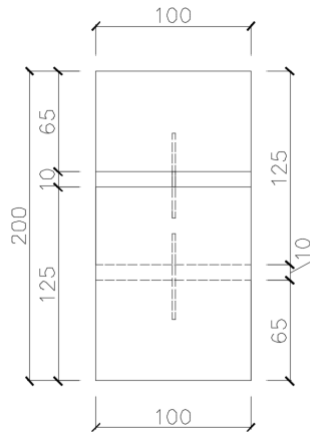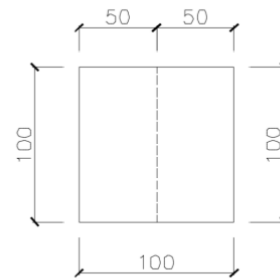
(c) Side view (d) Top view

(Dimensions in *mm*)

Figure 4.7 Geometry of specimens with a 50 mm bond length
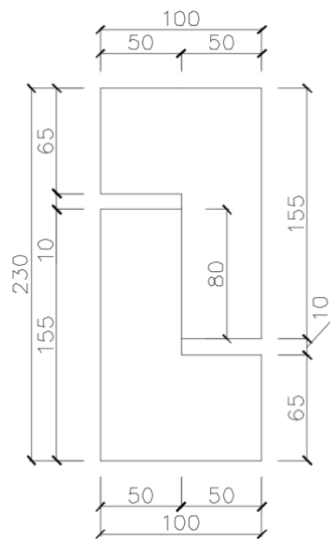
(a) Overview
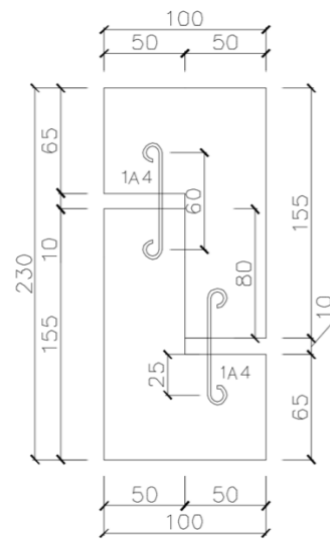
(b) Parallel reinforcement
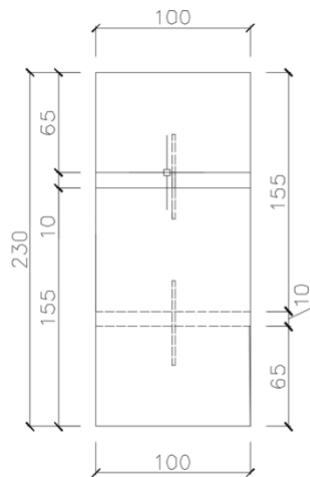
(c) Side view
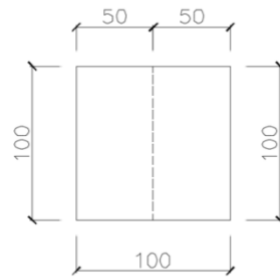
(d) Top view

(Dimensions in *mm*)

Figure 4.8 Geometry of specimens with a 80 mm bond length

Figure 4.9 Tensile test on the steel bar with 4 mm diameter
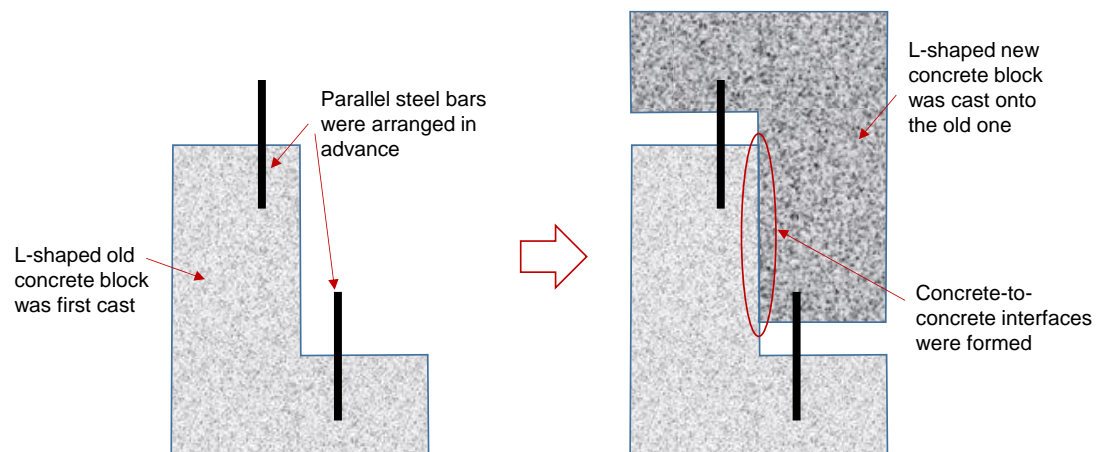
Figure 4.10 Specimen preparation

Loading frame

Specimen

DIC system
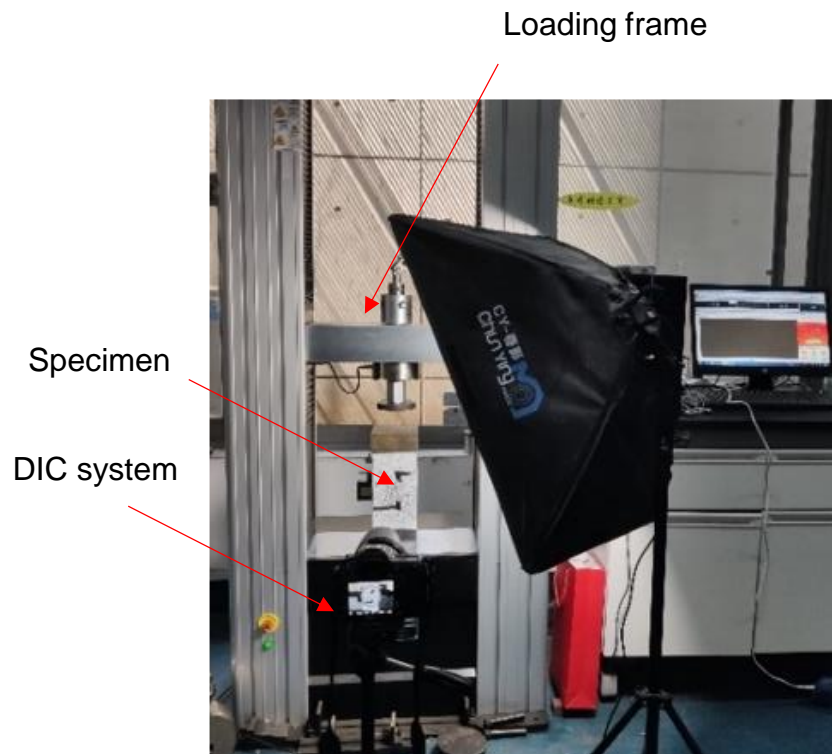
Figure 4.11 WDW-100 universal testing machine
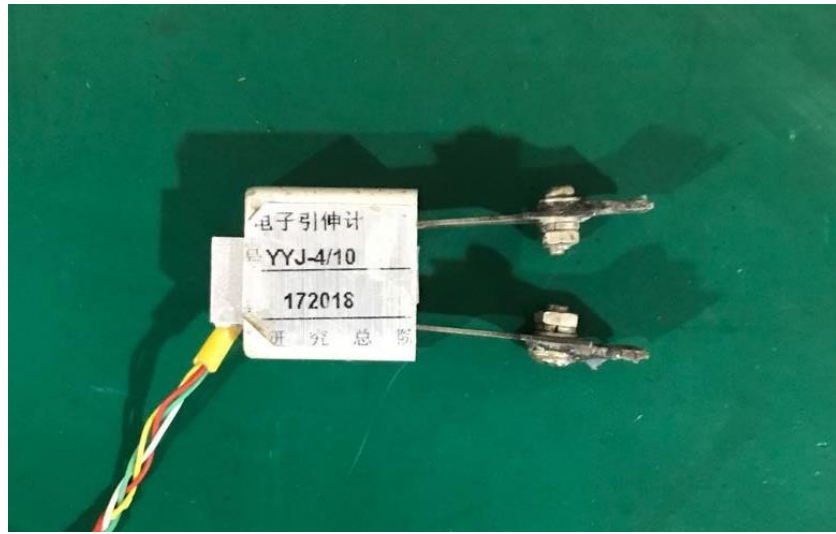
(a) Clip extensometer with an accuracy of 1 μm
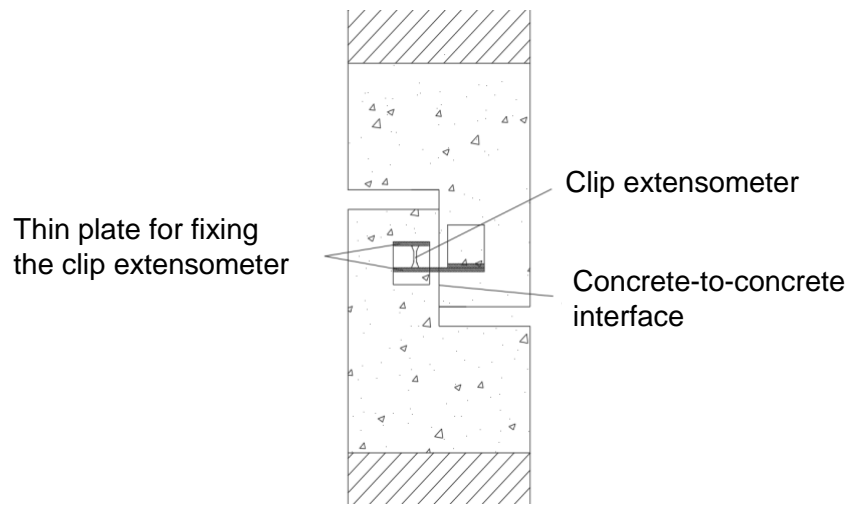
(b) Installation of the clip extensometer

Figure 4.12 Measurement of slips with a clip extensometer

Figure 4.13 Surface preparation of a specimen for DIC measurement
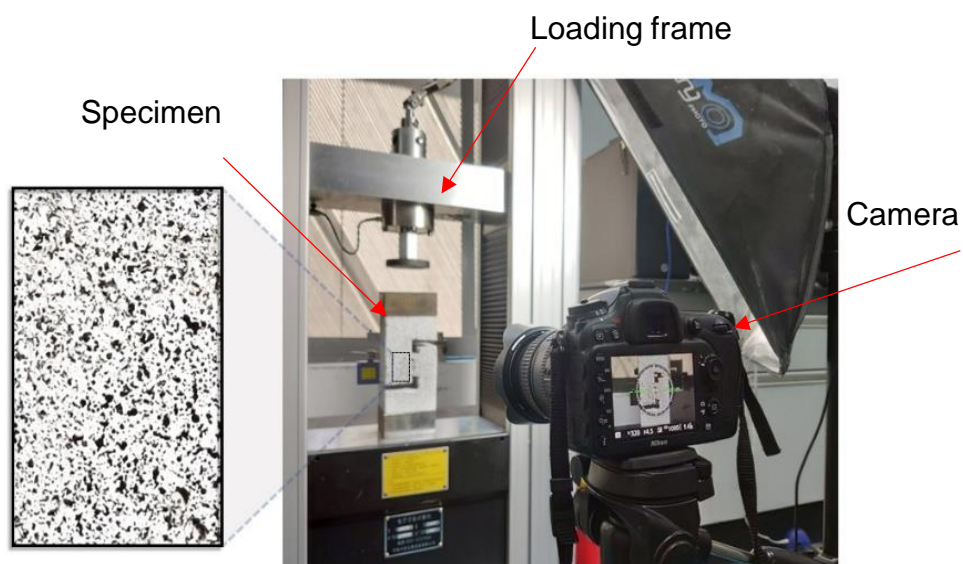
Figure 4.14 Illustration of the DIC setup
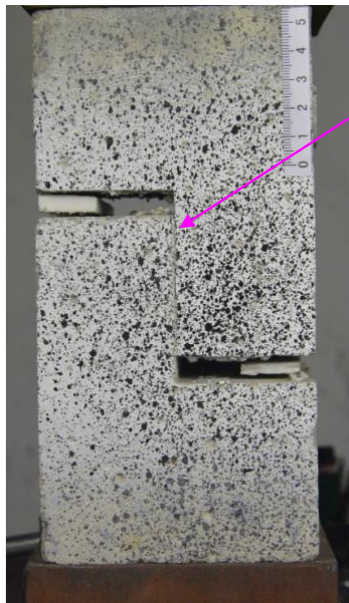
Cracks propagated rapidly downward
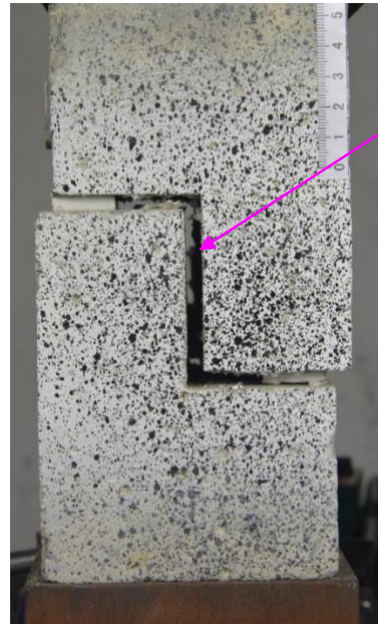
Brittle failure- Complete separation

(a) Group B
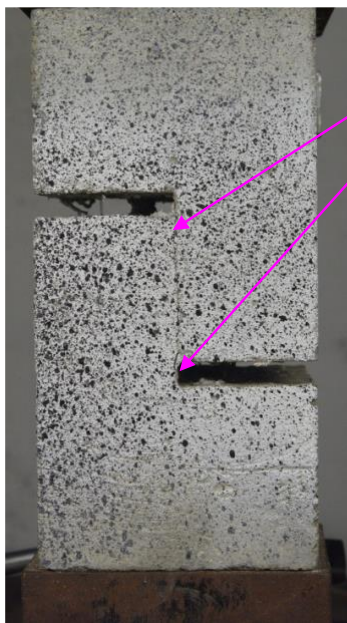
Cracks propagated from ends to the middle
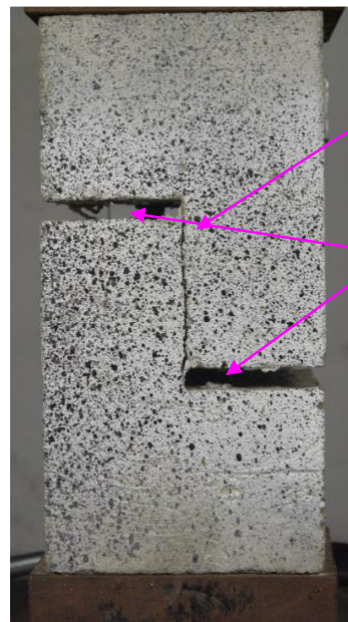
Cracks gradual propagation

The steel bar prevented the abrupt separation

(b) Group BR

Figure 4.15 Failure mode

(a) 3.5 kN (b) 5.5 kN (c) 8.5 kN (d) 10.5 kN

(e) 12.5 kN (f) 13.5 kN (g) 14.5 kN (h) 15.5 kN
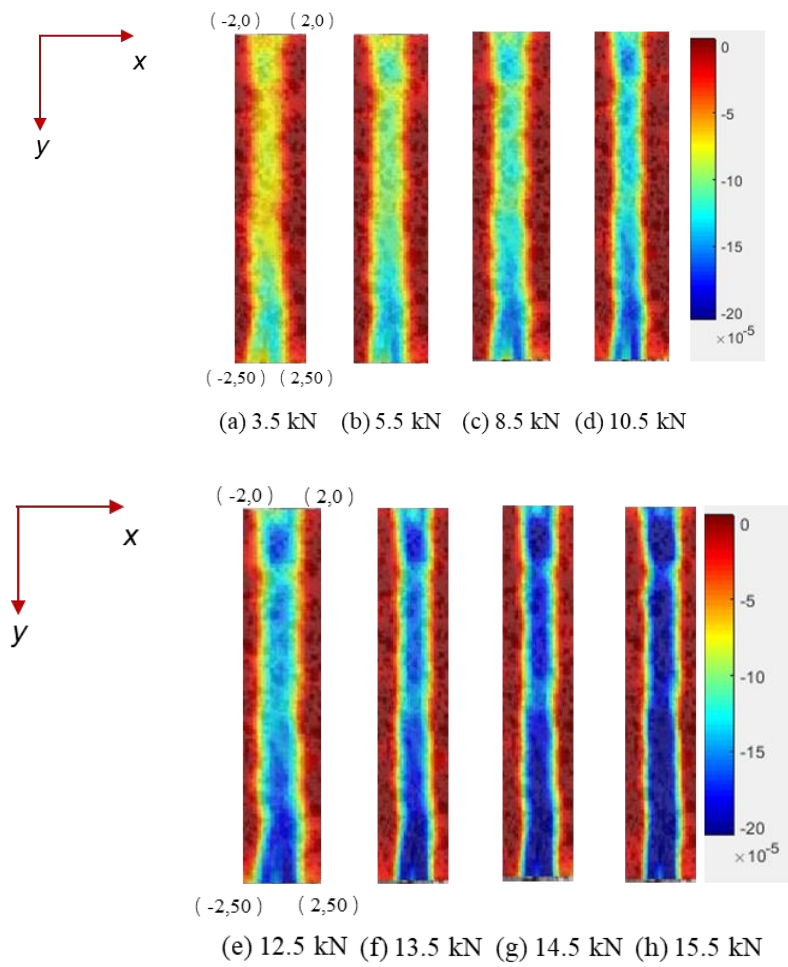
Figure 4.16 Failure process recorded by DIC system
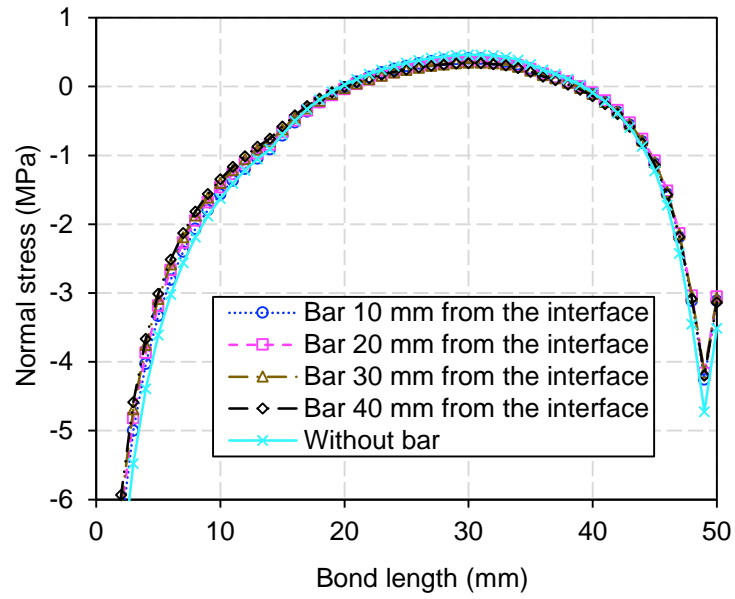
(a) Normal stress
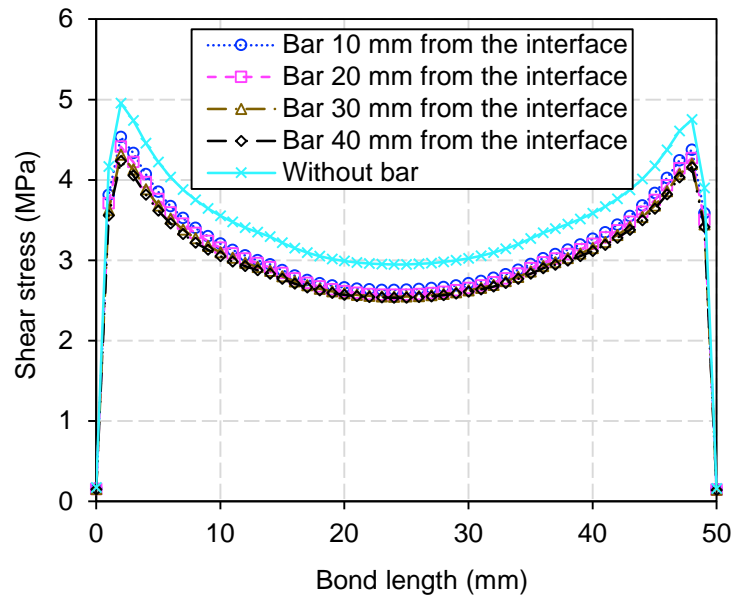
(b) Shear stress

Figure 4.17 Verification by the FE results
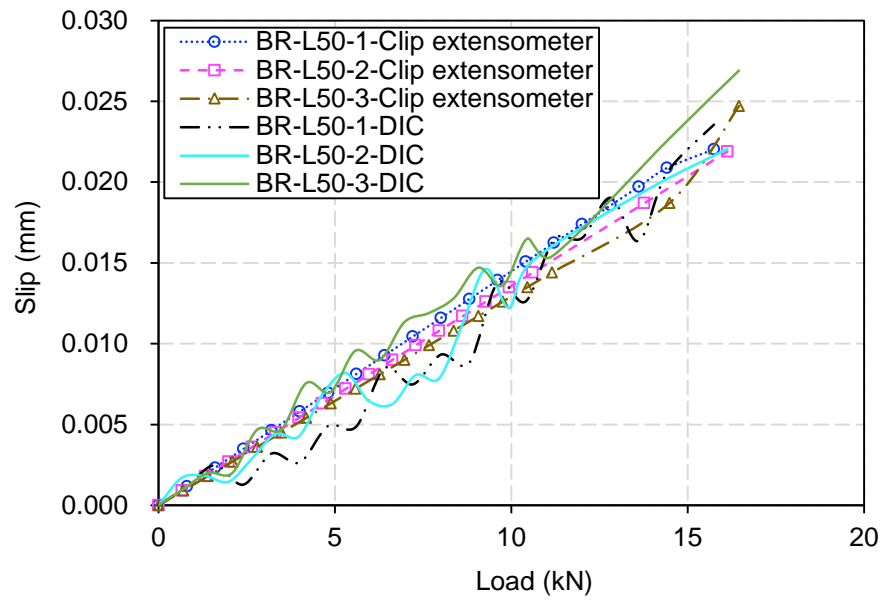
Figure 4.18 Comparisons of DIC results and clip results
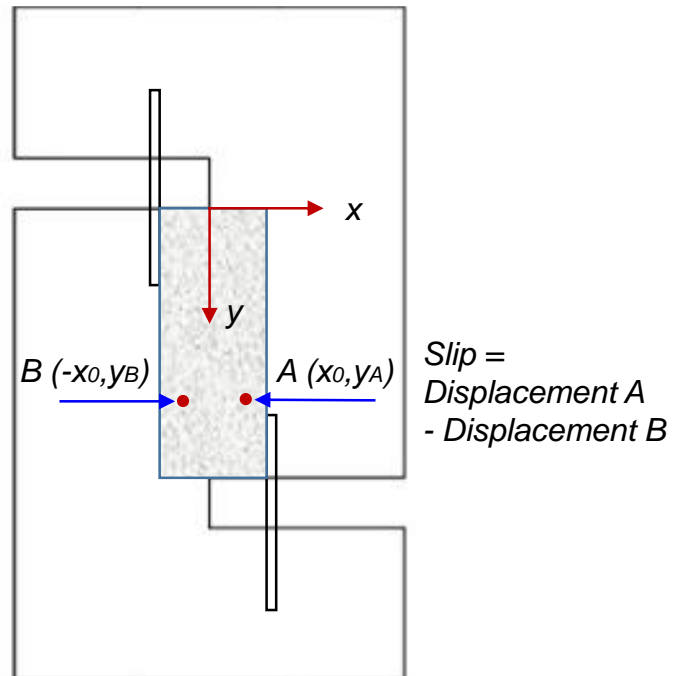
Figure 4.19 Schematic diagram of the interfacial slip from DIC system
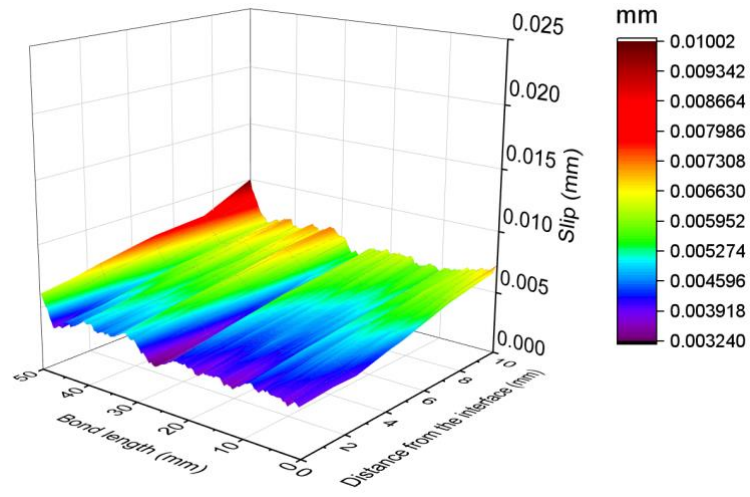
(a) 0.25P
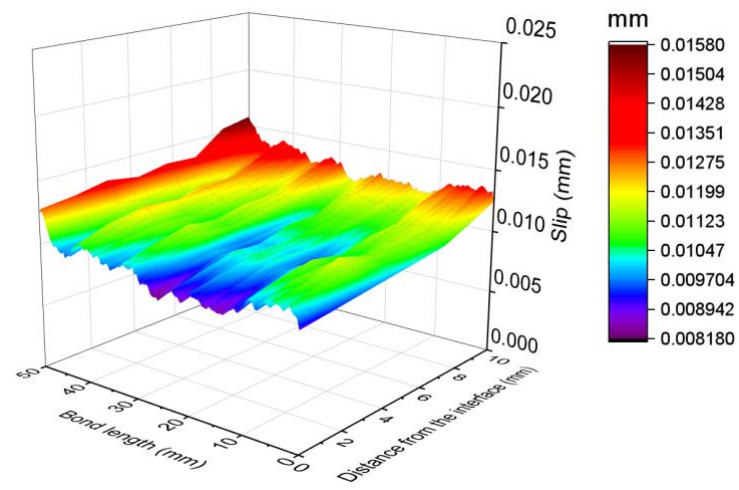
(b) 0.5P
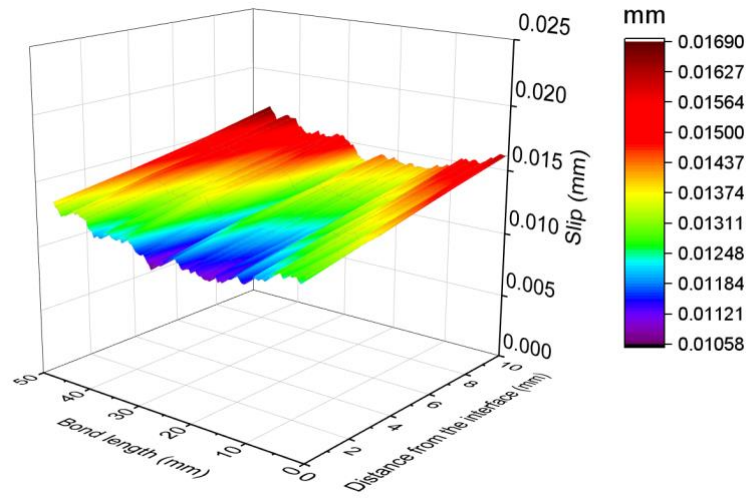
(c) 0.75P
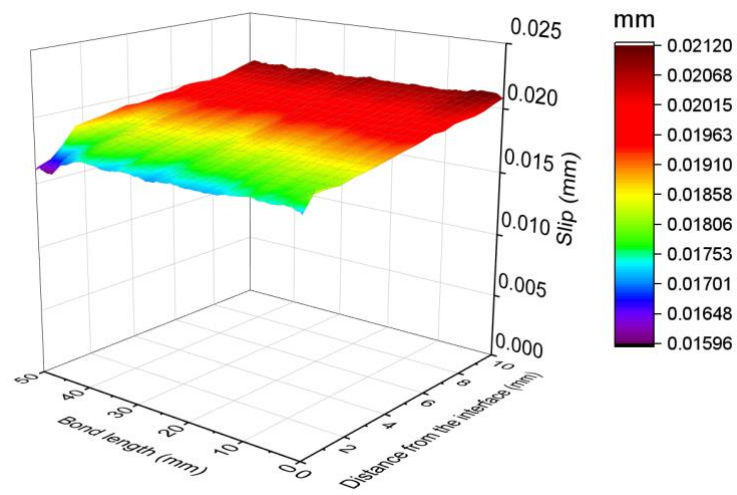
(d) P

Figure 4.20 Slip distribution of specimen BR-L50 at different load levels
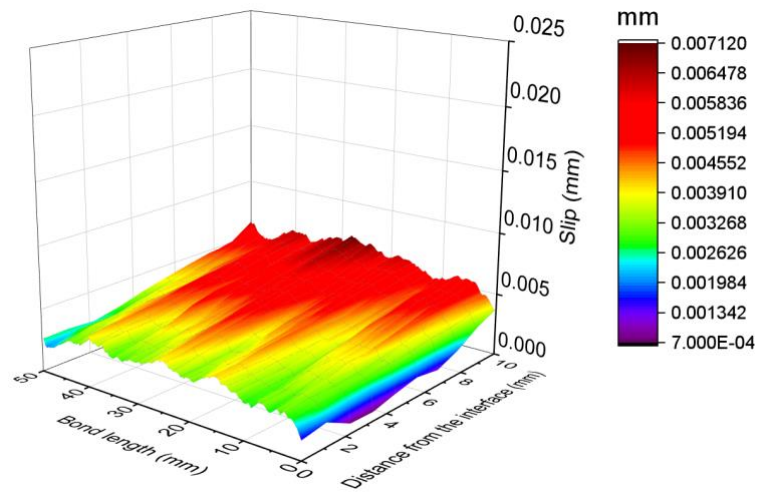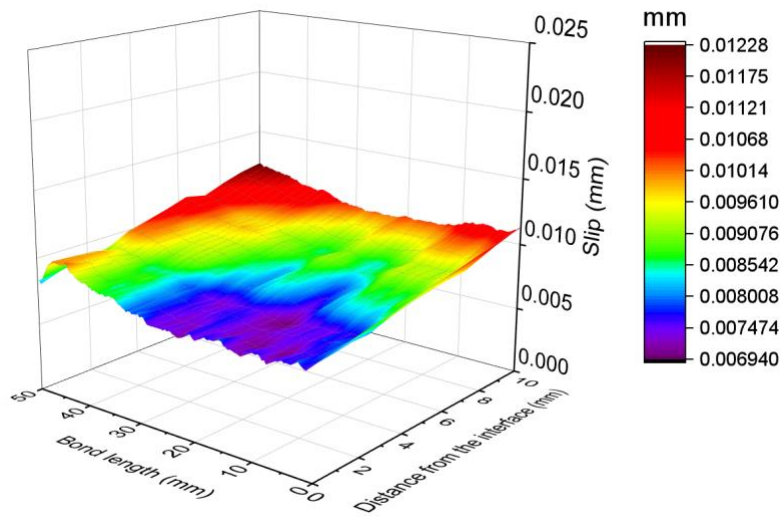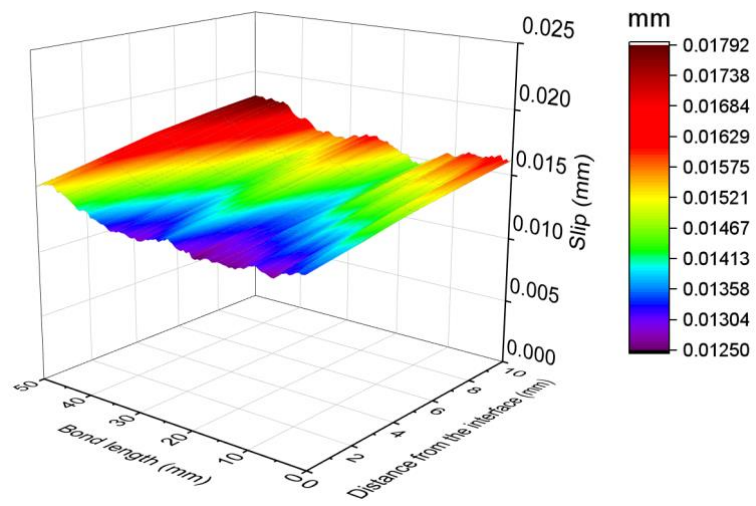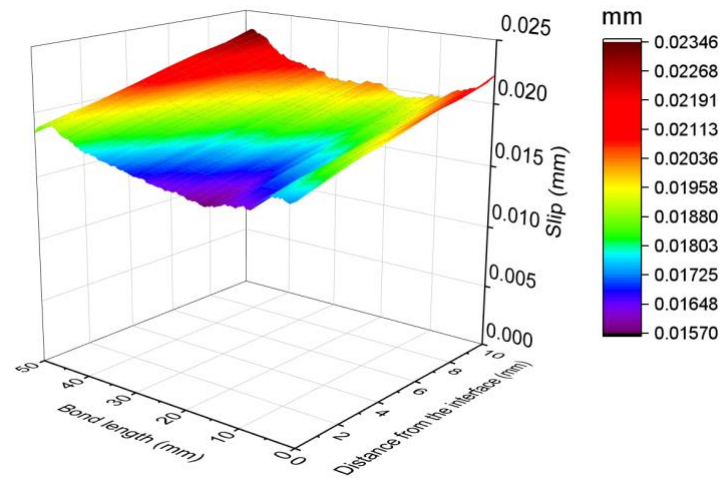
(a) 0.25P

(b) 0.5P

(c) 0.75P

(d) P

Figure 4.21 Slip distribution of specimen B-L50 at different load levels
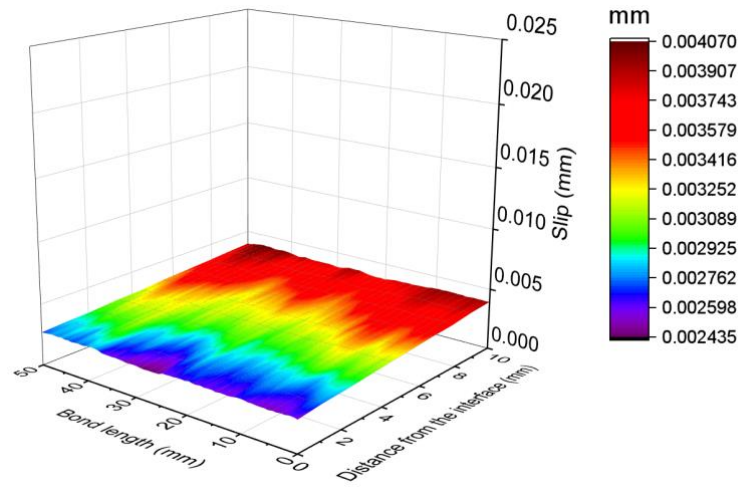
(a) 0.25P
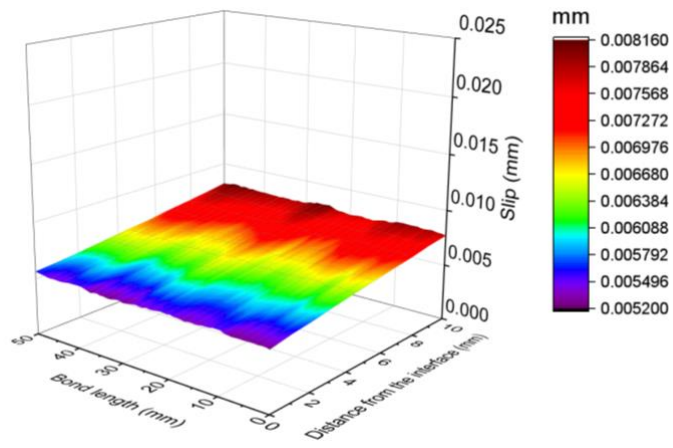
(b) 0.5P
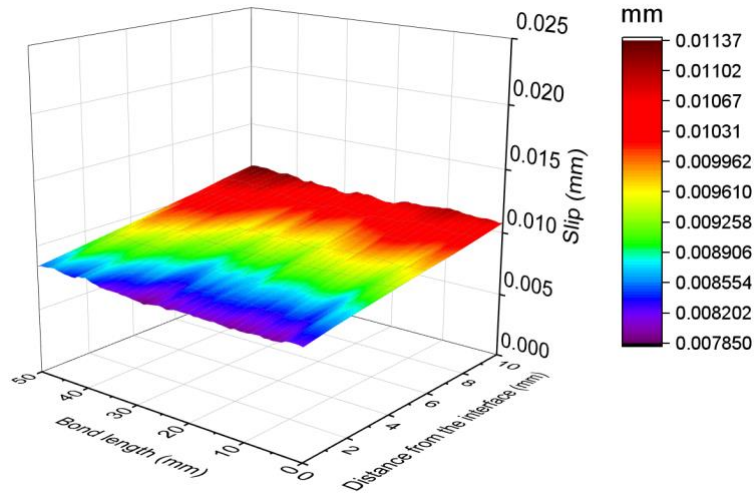
(c) 0.75P
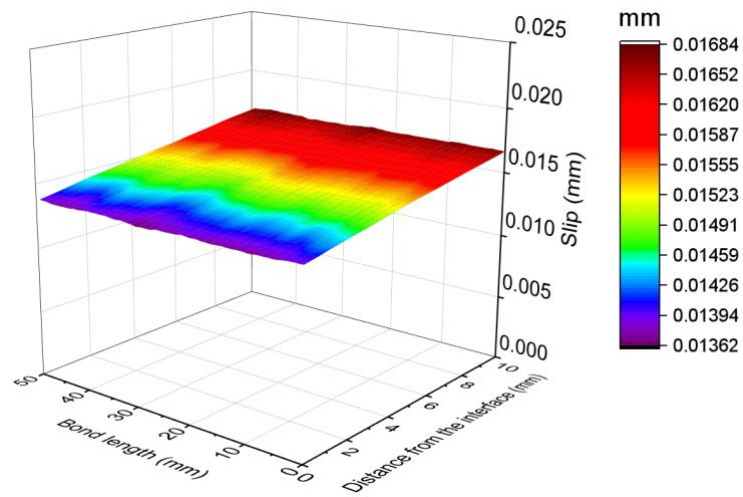
(d) P

Figure 4.22 Slip distribution of specimen UR-L50 at different load levels
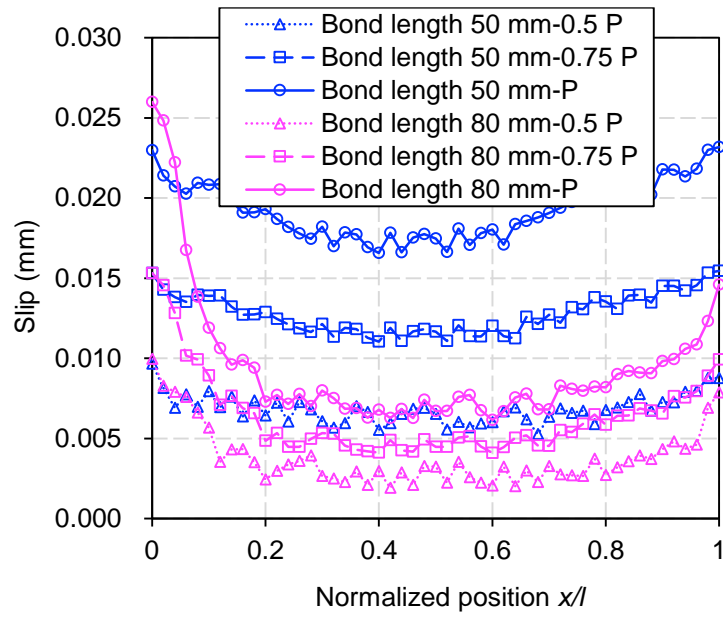
Figure 4.23 Slip distributions of specimens with different bond lengths
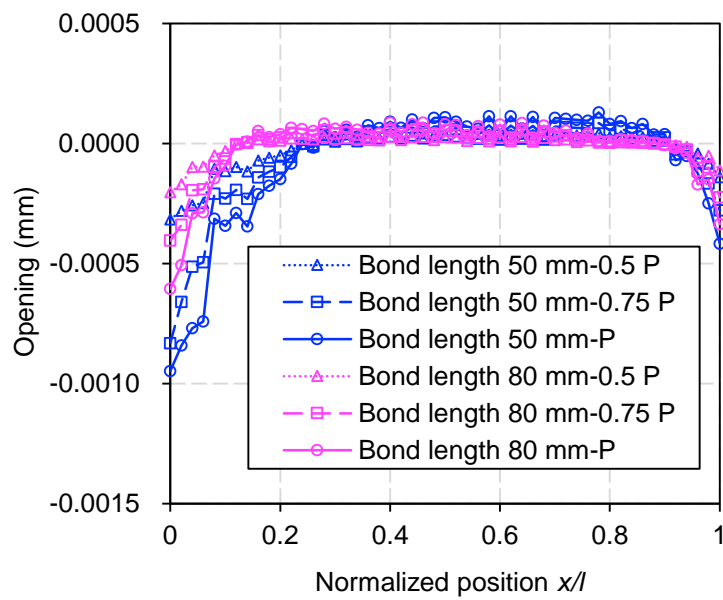
Figure 4.24 Opening/closing distributions of specimens with different bond lengths

142
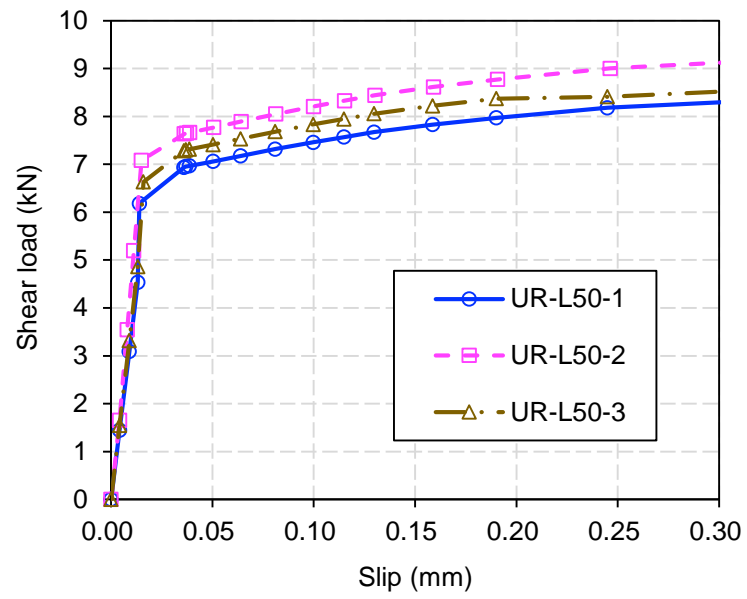
Figure 4.25 Load-slip responses of specimens UR-L50
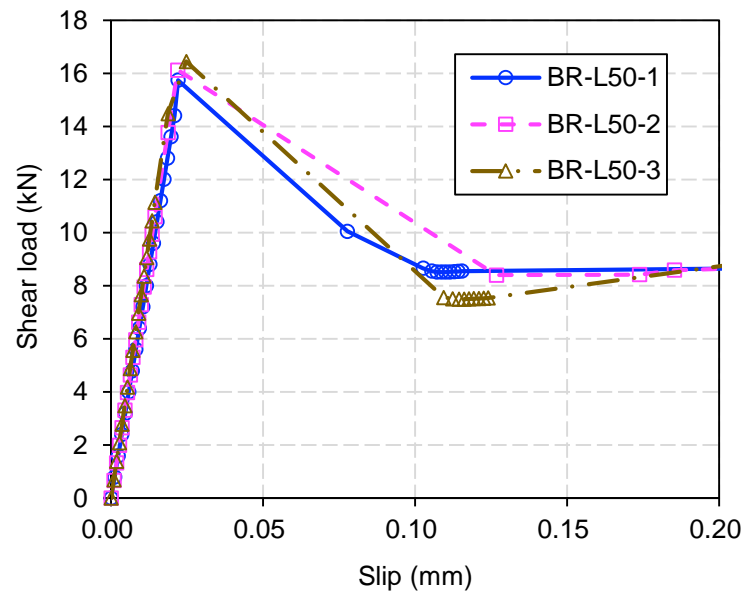
Figure 4.26 Load-slip responses of specimens in BR-L50

143
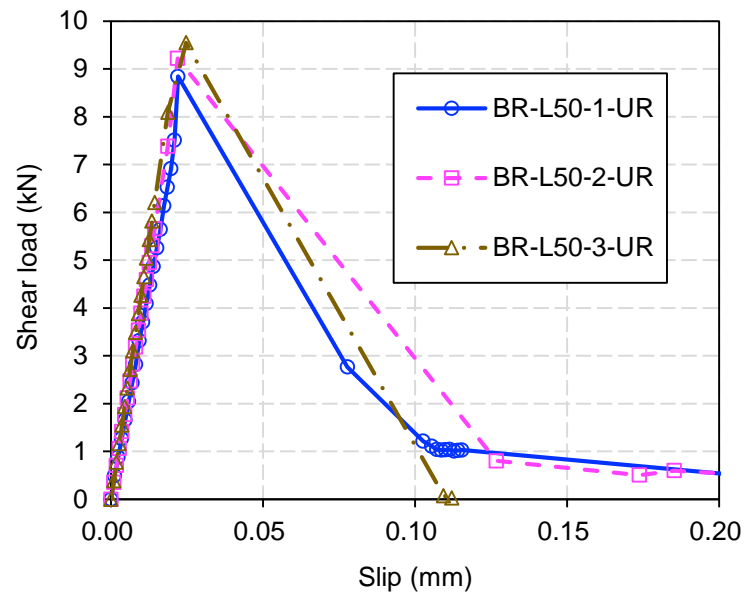
Figure 4.27 Isolated load-slip responses of the concrete-to-concrete interface
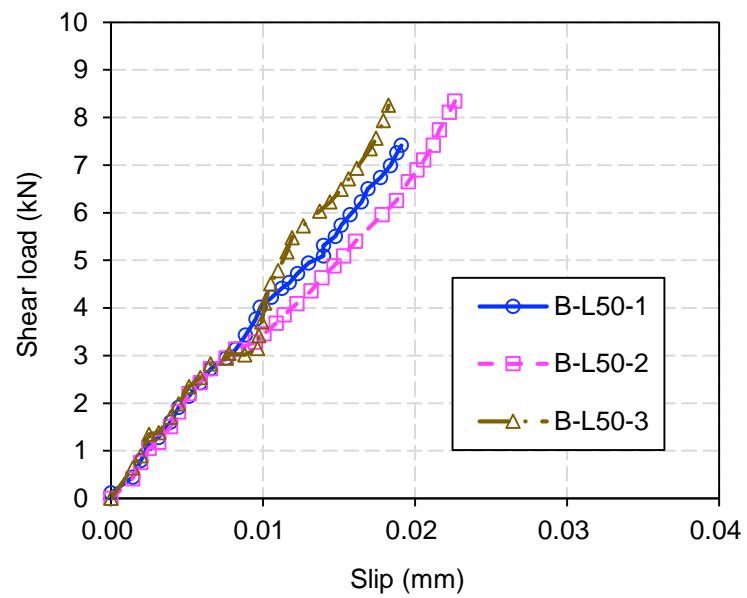
Figure 4.28 Load-slip responses of specimens in B-L50

144

CHAPTER 5

EXPERIMENTAL STUDY OF THE SHEAR
BEHAVIOUR OF CONCRETE-TO-CONCRETE
INTERFACES

5.1 INTRODUCTION

It has been discussed in Chapter 2 that the accurate description of the interfacial behaviour between new and old concretes is critical to the analysis of structures with concrete-to-concrete interfaces. The widely adopted method of describing the interfacial behaviour in terms of its shear strength is insufficient for the description of the complicated interfacial behaviour, which involves interactions between the local bond behaviour and global interfacial response as the stress distribution along the bondline is non-uniform. Therefore, accurate local bond-slip description of the interface is required for the sophisticated analysis of the behaviour of structures with concrete-to-concrete interfaces.

Extensive experimental research has been conducted to quantify the shear bond strength and identify the failure mode of concrete-to-concrete interfaces using different test methods as reviewed in the previous chapters (Gaston and Kriz, 1964; Birkeland and Birkeland, 1966; Tsoukantas and Tassios, 1989; Loov and Patnaik, 1994; Randl, 1997; Mattock, 2001; Santos and Júlio, 2014; Mohamad *et al.*, 2015). As a result, several empirical models were proposed to predict the global-average bond strength of concrete-to-concrete interfaces. However, since the stress distribution is not uniform along the interface, the local stress is different from the global-average stress behaviour. Thus, such models are highly empirical and limited to specific interface configurations

instead of being extendable to the analysis of concrete-to-concrete interfaces with various configurations. Moreover, limited research has been conducted to investigate the influences of parameters such as surface roughness and compressive stress on the concrete-to-concrete interfacial behaviour.

This chapter presents an experimental study using the modified shear test specimen designed specifically considering the local stress distribution to evaluate the local bond-slip relationship of concrete-to-concrete interfaces. The test parameters include concrete strength, surface roughness of the old concrete, and applied compressive stress. The results will be directly used to develop a local bond-slip model for concrete-to-concrete interfaces.

5.2 EXPERIMENTAL PROGRAMME

5.2.1 Specimen Details

The design of test specimens has been discussed in detail in Chapter 4, and the L-shaped one-interface specimen with a bond length of 50 mm was adopted in this test since it produces a generally uniform shear stress distribution and a moderate level of compressive stress along the bondline. According to the casting procedure, the two concrete blocks were defined as old concrete block and new concrete block, respectively. The size of the specimen shown in Figure 4.7 in the previous chapter was adopted in this test. The bond area between the new and old concrete was 50 mm × 100 mm, while the overall size of the specimen composed of two parts of concrete was 100 mm × 200 mm × 50 mm.

This test aimed to explore the main factors affecting the shear behaviour of concrete-to-concrete interfaces. The parameters examined in this study included the strengths of

the new and old concretes, old concrete surface roughness, and applied compressive stress, which were the main factors affecting the shear behaviour of the concrete-to-concrete interface (Kahn and Mitchell, 2002; Júlio *et al.*, 2006; Chilwesa *et al.*, 2017). While the influence of interfacial agents, curing conditions, and other parameters mentioned in Chapter 2 were considered to be less dominant and hence beyond the scope of the present study. The strength of concrete was generally believed to affect the cohesion at concrete-to-concrete interfaces, thus affecting the shear behaviour at the interface. The concrete surface roughness will affect the interlock between the two parts of concrete (Momayez *et al.*, 2005; Santos and Júlio, 2013) while the applied compressive stress further enhances the frictional action at concrete-to-concrete interfaces (Mohamad *et al.*, 2015).

Since the present study is the first attempt to study the bond-slip relationship of concrete-to-concrete interfaces, the focus is placed on normal strength concrete while high-strength concrete is not considered. Therefore, only the concrete with a cube compressive strength below 60 MPa was considered. In addition, the actual application of concrete cube compressive strength below 20 MPa in practice was relatively rare. Based on the above considerations, a series of tests was conducted on concrete with three different cube compressive strengths, namely 20 MPa, 40 MPa and 60 MPa, to explore the influence of concrete strength on the bond-slip relationship of concrete-to-concrete interfaces. The actual cube compressive strengths of new and old concrete were measured according to the Chinese standard GB 50010-2010 (2010) on the day of testing and the 28th day; the strengths are listed in Table 5.1 along with the standard deviation.

There have been many studies investigating the effect of concrete surface roughness on interfacial properties. One of the commonly used method of quantifying the roughness

is the sand patch test method (Santos and Júlio, 2013), which is explained in detail in Section 5.2.3. The *f*ib Model Code 2010 (2013) suggests that a concrete surface can be defined as smooth for a sand-patch roughness less than 1.5 mm, rough for that between 1.5 mm and 3 mm, and very rough for that over 3 mm. In the reported studies, the sand-patch roughness predominantly ranged from 1.0 mm to 3.5 mm (Santos and Júlio, 2013). Therefore, three levels of surface sand-patch roughness, 1.0 mm, 2.0 mm and 3.0 mm were selected in the present experiment to represent the smooth, rough and very rough concrete surfaces. Regarding the applied compressive stress at the interface, Mohamad *et al.* (2015) indicated that when the compressive stress is below 1.5 MPa, the shear strength increases if the compressive stress increase. While when the compressive stress is above 1.5 MPa, the effect on the interface was similar. In addition, applying a very high compressive stress to the concrete-to-concrete interface is practically difficult. Therefore, in the present study, the compressive stress at the interface was limited to below 1.5 MPa, i.e., three levels of applied compressive stress, 0.5 MPa, 1.0 MPa and 1.5 MPa were used.

Four series of specimens with parallel reinforcement and bonded interface were prepared, amounting to a total of 28 L-shaped One-interface shear specimens. Series-I was designed to study the effect of new concrete strength and old concrete strength, including 10 specimens; new and old concrete cube compressive strengths of about 20 MPa, 40 MPa, and 60 MPa are covered, while the actual cube compressive strengths of new and old concrete are listed in Table 5.1. Both the measured strengths of new concrete and old concrete satisfied the design requirements. All specimens of Series-Ⅰ had a concrete surface roughness of 0 mm and no applied compressive stress. Two repetitions were prepared for each specimen configuration.

Series-II was used to study the effect of concrete surface roughness, covering three

different roughness levels of 1 mm, 2 mm, and 3 mm. The old and new concrete cube compressive strengths of the specimens in Series-II were 20 and 40 MPa, respectively. Since no compressive stress was applied, the test results of this series can be compared with those of Series-I.

Series-III was employed to study the effect of applied compressive stresses. Accordingly, the specimens had a varying applied compressive stress of 0.5 MPa, 1.0 MPa and 1.5 MPa, while the old and new concrete cube compressive strengths were 20 MPa and 40 MPa, respectively. The concrete surface roughness was 0 mm. Therefore, the test results of this series can also be compared with those of Series-I.

Series-IV was designed to study the combined effect of surface roughness and applied compressive stress. Therefore, the specimens had different combinations of concrete surface roughness and applied compressive stress level, i.e., 1 mm & 0.5 MPa, 2 mm & 1.0 MPa, and 3 mm & 1.5 MPa. The old and new concrete cube compressive strengths were also 20 MPa and 40 MPa, respectively.

All specimens of the four series had the same companion specimen with parallel reinforcement and unbonded interface; two repetitions were also prepared for the companion specimen. Based on the test results of the four series and companion specimens, the complete interfacial shear load-total slip response of the concrete-to-concrete interfaces, excluding the contribution of the steel reinforcement, can be obtained.

Each specimen was given a name indicating the old concrete strength denoted by 'O', the new concrete strength denoted by 'N', the surface roughness denoted by 'R', the applied compressive stress denoted by 'S', followed by a digital number indicating the different repetition. Accordingly, 'O20-N40-R1-S0.5-I' indicates the first repetition of

the specimen with an old concrete cube compressive strength of 20 MPa, a new concrete cube compressive strength of 40 MPa, a surface roughness of 1 mm, and an applied compressive stress of 0.5 MPa. It should be noted that the actual values of the concrete cube compressive strength, surface roughness, and applied compressive stress may vary slightly from the design values, and they are listed in Table 5.2.

5.2.2 Materials

Three concrete mixes were used in this test for the cube compressive strengths of 20 MPa, 40 MPa and 60 MPa. The material used to prepare concrete includes aggregates, sands, cement, water and additives. The largest particle size of 16 mm aggregates and well-graded natural medium sands were adopted. Cement with 42.5 and 52.5 ordinary Portland cement was employed, while the additives were powder polycarboxylic acid water reducing agent. According to different mixing ratios, the additives were 0.05%, 0.10%, and 0.15% of the cement weight, respectively.

The mix ratios of the three types of concrete are shown in Table 5.3. Three 150 mm × 150 mm × 150 mm cubes were prepared for each type of concrete during casting. In the design of practical engineering, the cylinder compressive strength is often employed. According to the Chinese standard GB 50010-2010 (2010), the 150 mm × 300 mm concrete cylinder compressive strength can be obtained by multiplying cube compressive strength with a factor of 0.79 in subsequent analysis.

The design of companion specimens in this test was exactly the same as described in Chapter 4, including the use of 4-mm diameter steel bars as the parallel reinforcement outside of the concrete-to-concrete interfaces. Therefore, the test results of the material properties of the steel bar were the same as indicated in Chapter 4.

150

5.2.3 Specimen Preparation

Figure 5.1 shows the casting process of the test specimens in an assembled aluminium alloy mould. In order to improve the quality of casted specimens, aluminium moulds that can be connected by bolts were customized for this test. The adoption of bolted formwork minimizes the risk of specimen damage during demoulding. When preparing specimens, the casting of old concrete was completed first, as shown in Figure 5.1 (b), and cured for 28 days. Then, before casting the new concrete block, the three baffle plates in the middle of the aluminium mould were removed and two high-density foam plates were placed through the parallel bars, as shown in Figure 5.1 (c). The new concrete was thereafter cast and fully vibrated. In order to further avoid damage to the specimens, the specimen was demoulded after 24 hours after the casting, and cured for another 28 days.

In addition, for specimens in Series-II and Series-IV that require surface roughness, the old concrete surface was roughened before casting the new concrete block. Since the area of the bond interface is small, it is difficult to produce the surface roughness by mechanical equipment such as high-pressure water gun without causing unwanted damage. Therefore, in this experiment, the manual chiselling method, which is a simple and commonly used method (He *et al.*, 2017), was adopted to generate the roughness of the old concrete surface. During the surface treatment, the surface roughness of the concrete was evenly distributed as much as possible by finely chiseling the surface. The surface of the old concrete after the chisel-roughening is shown in Figure 5.2 (b). The loose aggregate, gravel, dust on the surface of concrete were then cleaned by the wire brush and water.

After roughness treatment of concrete surface, the roughness of the surface needs to be measured. The commonly used roughness evaluation methods include the sand patch

test method, digital surface roughness meter measurement, and 3D laser scanning method (Santos and Julio, 2013). The sand patch test method, which is relatively simple to operate, was adopted in the present test. The roughened surface was first smeared with standard sand, as shown in Figure 5.2 (c), and the total volume of the smeared sand was then measured as shown in Figure 5.2 (d). The surface roughness parameter, R, was then determined by dividing the sand volume, V, by the surface area, A_c, as follows:

$$R = \frac{V}{A_c} \tag{1}$$

A higher value of the roughness parameter indicates a rougher surface. In this test, the average roughness was designed as 1 mm, 2 mm and 3 mm, and the error range of the roughness was controlled within 0.2 mm.

5.2.4 Test Setup and Instrumentation

Figure 5.3 shows the test setup. The WDW-100 electronic universal testing machine at Tongji University was used as the testing frame. The DIC system and clip extensometers were adopted in this test to measure the interfacial slip, as discussed in detail in Chapter 4.

For Series-III and Series-IV specimens requiring interfacial compressive stress, a device shown in Figure 5.4 (a) was used to apply the stress. The detailed design of this device is shown in Figure 5.4 (b); the two thick steel plates with a thickness of 20 mm were used to apply uniform pressure at the interface through tightening the four steel bolts with a diameter of 8 mm. In order to minimize the friction, Teflon sheets were placed between the steel plates and the specimen. Tensile tests of the bolts were conducted to obtain the modulus to achieve accurate application of the compressive stress to the interface. The load-displacement curves of the tests two bolts are shown in

Figure 5.5, from which it was measured that the elastic modulus of the bolt was 153.7 GPa. Therefore, for the designed compressive stresses of 0.5 MPa, 1 MPa, 1.5 MPa for the specimens, the target strains of the bolts should be 80.9, 161.8, and 243 $\mu\varepsilon$ ($\times 10^{-6}$), respectively. The strain of the bolt should be kept constant during the loading process. Therefore, strain gauges were used the monitor the strains of the four bolts, which are presented in Figure 5.6. It is seen that a constant strain has been generally maintained for all the bolts in all specimens. It should be noted that, for Series-III and Series-IV specimens requiring the application of compressive stress, the DIC system was not used since the device for compressive stress blocked the view of the DIC cameras.

5.3 TEST RESULTS AND DISCUSSIONS

5.3.1 Failure Mode

Figure 5.7 (a) and (b) show the typical crack development at the smooth and rough interfaces, respectively, of the specimen during loading. Figure 5.8 (a), (b), and (c) show the fractured surfaces of the smooth, rough, and compressed interfaces, respectively. For Series-I specimens with smooth concrete surface, all specimens failed by separation at the concrete-to-concrete interface as a result of the gradual debonding propagation, as shown in Figure 5.7 (a). During loading, the global load-displacement relationship was linear initially before the initiation of the crack. Debonding first appeared at the end of the interface, which was accompanied by a fracturing noise. Due to the parallel reinforcing bars, the cracks of all the specimens did not propagate through the bondline immediately, nor did the global load drop to zero. Thereafter, further increase of the global displacement resulted in the propagation of the debonding along the bondline, i.e., it experienced a gradual process of debonding propagation and decrease of the global load. Finally, one straight crack developed through the bondline, leading to the failure of the specimen and relatively smooth fractured surfaces, as shown in Figure 5.8

(a).

Specimens with a rough concrete surface in Series-II experienced a similar course of crack initiation and propagation to that of specimens with a smooth interface as described above, except the crack propagated through the bondline was slightly curved when the specimen failed, as shown in Figure 5.7 (b). Figure 5.8 (b) shows the fractured surface of the interface, and it is observed that a considerable amount of old concrete remained on the fractured surface of the new concrete block. This indicates that the crack cut through the concrete substrate instead of strictly following the geometry of the interface during the debonding process.

Specimens with compressed interfaces in Series-III and Series-IV experienced similar crack development to that of the specimens in Series-I and Series-II, with only one main crack developing along the concrete-to-concrete interface. The friction at the interface of these specimens was substantial, with the increase of surface roughness and the application of compressive stress. Moreover, the failure process exhibited stronger ductility than specimens in the other series. Moreover, obvious scratches on the fractured surfaces due to friction under compressive stress can be observed, as indicated in Figure 5.8 (c).

5.3.2 Global Shear Load-Slip Responses

The relationship between the global shear load to the slip measured by the clip-extensometer for all the specimens are shown in Figures 5.9 (a~e). It can be seen from these figures that all specimens exhibit a shear-load plateau at the end of the loading process, indicating that the parallel steel bars played a major role in the post-peak behaviour of the specimens. The corresponding global shear load-slip relationship excluding the contribution of the reinforcing bars are presented in Figures 5.10 (a~e),

using the test data of the companion specimens as explained in Chapter 4. Comparing these results indicates obviously different performance for specimens with different concrete strengths, surface roughness, and interfacial compressive stresses.

First, the peak shear load (P_{max}) of the specimens, as indicated in Figure 5.10 (a~b), was higher if the strength of either the old or new concrete was higher. Similarly, the maximum shear load was higher if the concrete surface roughness (R) or the applied compressive stress (σ_n) was higher, seen in Figure 5.10 (c~e). These results are consistent with the previous studies showing that the concrete strength, surface roughness, and compressive stress affect the mechanical behaviour of the concrete-to-concrete interface (Kahn and Mitchell, 2002; Júlio *et al*., 2006; Chilwesa *et al*., 2017).

Second, the residual load (P_r), as indicated in Figure 5.10 (a~b), for series-I specimens was minimal, because the friction at the concrete-to-concrete interface after debonding was trivial. For specimens with a higher surface roughness, the residual load was higher Figure 5.10 (c), although still relatively small compared to the maximum load. This indicates that the concrete surface roughness alone does not significantly improve the post-peak behaviour of the concrete-to-concrete interface without the application of compressive stress. For specimens with applied compressive stress at the interface, the residual load was considerable; it increased with the increase of the applied compressive stress, as shown in Figure 5.10 (d). Specifically, for specimens with the same interfacial compressive stress, the residual load increased considerably if the interfacial roughness increased, as shown in Figure 5.10 (e). This shows that the roughness has a considerable impact on the residual load if combined with the applied compressive stress. Tables 5.4 ~ 5.7 summarises the characteristic values of the global shear force-slip behaviour for all the specimens; it clearly shows the influence of the concrete strength, surface roughness, and compressive stress on the concrete-to-concrete interfacial behaviour.

5.3.3 Slip Distribution

In Chapter 4, the distribution of slip at the interface for different specimen designs has been discussed in detail. The current test was focused on the influence of surface roughness on the interfacial slip distribution. Figure 5.11 and Figure 5.12 show the typical slip distributions measured by the DIC system along the bonded interface for specimens with smooth and rough surfaces, respectively, at different load levels.

For Series-I specimens where the concrete surface was smooth, the slip was slightly higher at the interface ends and generally uniformly distributed in the middle segment, as shown in Figure 5.11. For the Series-II specimens where the concrete surface was rough, the slip distribution was generally uniform when the shear force was small but became increasingly non-uniform as the shear force increases, as shown in Figure 5.12, attributing to the random pattern of the old concrete surface generated in the surface preparation. Therefore, the assumption that the interface is subjected to uniform shear stress and slip distributions is accurate for specimens with rough interfaces under small shear loads but not large shear loads. Nevertheless, the uniform shear stress and slip assumptions may still be the most reasonable assumption for large shear loads as the real distributions are random. For Series-III and Series-IV specimens with compressive stress at the interface, the interfacial slip data was not available since DIC system was unable to take images of the specimen surface. This is expected to be addressed in the future research.

5.3.4 Local Bond-Slip Behaviour

The local bond-slip relationship can be converted from the global shear load-slip relationship based on the assumption of uniform shear stress and slip distributions. Accordingly, the local interfacial shear stress can be approximated by the interface-

average shear stress, and the slip measured using the clip-extensometer is taken as the local slip. Thereby, the local bond-slip relationship for all the test specimens can be obtained.

Figure 5.13 shows the bond-slip curves for the four series of specimens, all of which follow a typical tri-linear shape including a linear elastic stage, a softening stage, and a residual stress stage. Overall, the interfacial stiffness of the initial linear elastic stage and the maximum interfacial shear stress are dependent on the concrete strength, surface roughness, and the applied compressive stress. For the softening stage, although brittle failure was prevented by the parallel reinforcing bars, the load drop and the slip increase were still sudden, losing the data between the maximum stress point and the beginning of the residual stage. Nevertheless, a linear softening stage based on the test data may still be used to represent the damage evolution of the specimen, as adopted in the present study. Subsequent to the softening stage, a residual stress stage characterized by a gradually softening behaviour was observed for all specimens. As indicated by the results shown in Figure 5.13, for the specimens without interfacial compressive stress, the residual stress was minimal regardless of the concrete strength or surface roughness; for the specimens with an applied compressive stress, a considerable level of residual stress existed in the residual stress stage. Therefore, the residual stress level was dependent on the interfacial compressive stress but not the concrete strength nor the surface roughness. Tables 5.4-5.7 summarise the maximum shear stress, slip corresponding to the maximum shear stress, residual stress and corresponding slip, and interfacial fracture energy (area under the curve) of the bond-slip curves for all specimens.

5.3.5 Effect of Concrete Strength

Figure 5.14 shows the interfacial shear stress (τ_{max}), residual stress (τ_r), and fracture

energy (G_f) for specimens with different new concrete strengths to demonstrate the effect of new concrete strength on the behaviour of concrete-to-concrete interfaces. For these specimens, the cube compressive strength of old concrete was 22.8 MPa, the concrete surface roughness was 0 mm, and no compressive stress was applied.

Test results show that the average interfacial maximum stresses were 1.44 MPa, 1.81 MPa, and 2.73 MPa, respectively, for specimens with a new concrete cube compressive strength of 23.2 MPa, 42.5 MPa, and 59.6 MPa. It can be seen that the new concrete strength has a positive impact on the interfacial maximum stress. Similarly, for the specimens with three different new concrete strengths, the average interfacial fracture energies were 0.107 N/mm, 0.130 N/mm, and 0.157 N/mm, respectively. Therefore, the new concrete strength also has a positive impact on the interfacial fracture energy.

Figure 5.15 shows the interfacial maximum stress, residual stress, and fracture energy for specimens with different old concrete cube compressive strength. Again, for these specimens, the cube compressive strength of new concrete was 42.5 MPa, the concrete surface roughness was 0 mm, and no compressive stress was applied. Test results show that the interfacial maximum stresses were 1.81 MPa, 2.10 MPa, and 2.76 MPa, respectively, for specimens with old concrete strengths of 22.8 MPa, 43.1 MPa, and 57.3 MPa. That is to say, when the cube compressive strength of old concrete was increased from 22.8 MPa to 43.1 MPa, the maximum stress did not increase much, while the maximum stress increased greatly when the cube compressive strength of old concrete changed from 43.1 MPa to 57.3 MPa. Similarly, the average interfacial fracture energy was also increased significantly when the cube compressive strength of old concrete changed from 43.1 MPa to 57.3 MPa. This is because for the old concrete with 57.3 MPa cube compressive strength, 52.5 ordinary Portland cement was adopted, while the high strength cement can effectively improve the bond strength of the

concrete-to-concrete interface.

By contrast, the levels of residual stresses for series Series-I specimens were quite low and fluctuated and did not show a clear correlation with the new or old concrete strength. This may be due to the existence of a certain degree of sliding friction even though the concrete surface was smooth. Due to the action of parallel steel bars, the specimen was not completely separated after the crack propagated along the bondline, so that the friction between the new and old concrete could promote certain residual stresses. However, this friction was small and random, and the residual stress showed fluctuations.

5.3.6 Effect of Concrete Surface Roughness

To investigate the influence of the concrete surface roughness on the interfacial behaviour, Figure 5.16 shows the interfacial maximum shear stress, residual stress and fracture energy for specimens with different surface roughness. For these specimens, the old concrete strength was 21.5 MPa, the new concrete strength was 43.1 MPa, and no compressive stress was applied.

Test results show that the average maximum stresses were 1.81 MPa, 2.80 MPa, 3.41 MPa and 3.97 MPa, respectively, for specimens with concrete surface roughness of 0 mm, 1 mm, 2 mm and 3 mm. This result indicates that the interfacial bond strength is positively correlated with the surface roughness. Similarly, the interfacial fracture energy also showed a positive correlation with the increase of surface roughness. By contrast, it is seen that for the various surface roughness, the average residual stress varied between 0.31 MPa and 0.36 MPa without a clear correlation with the surface roughness. The average residual stress was still relatively small, around 0.36 MPa, when the roughness was as high as 3 mm. Therefore, the surface roughness has a limited

effect on the residual stress of the specimen.

It can be clearly observed from the fractured surface of this series specimens that part of the old concrete fell off and remained on the surface of new concrete block, which can explain the reason why the surface roughness could improve the bond strength. After the chiselling of the surface of the old concrete block, the new concrete was cast onto the uneven surface and an interface with both adhesion and mechanical interlock was formed. In addition, due to the unevenness of the interface, the interfacial bond area between old and new concrete was also increased, positively affecting the interfacial capacity. As a result, both the interfacial maximum shear stress and the fracture energy were positively correlated to the surface roughness.

On the other hand, in the absence of applied compressive stress, effective frictional action between the fractured surfaces was unable to form. As a result, the residual stress at the interface was not affected by the surface roughness. This is similar to the previous analysis on the influence of concrete strength on the residual stress of the concrete-to-concrete interface. In general, without the interfacial compressive stress, the residual stress at the interface was nearly negligible, regardless of the concrete strength and surface roughness. However, when the interface is compressed, a strong correlation between the surface roughness and residual stress can be observed, as discussed below.

5.3.7 Effect of Interfacial Compressive Stress

Figure 5.17 shows the interfacial maximum stress, residual stress, and fracture energy for specimens with different applied compressive stress. For specimens in this series, the old and new concrete strength was kept as 19.8 MPa and 40.8 MPa, and the surface roughness was remained to be 0 mm.

From the test results, it can be found that the influence of interfacial compressive stress on the bond strength is significant. When the compressive stresses were 0 MPa, 0.5 MPa and 1.0 MPa, the average maximum stresses were 1.81 MPa, 2.10 MPa and 2.43 MPa, respectively. When the compressive stress was 1.5 MPa, the average maximum stress was 2.78 MPa, corresponding to capacity increases of approximately 16.2 %, 34.6 % and 53.8 % compared to those with compressive stresses of 0 MPa, 0.5 MPa and 1.0 MPa, respectively. Therefore, the applied compressive stress has a clear positive correlation with the interfacial maximum shear stress.

In terms of the residual stresses, they were 0.31 MPa to 0.81 MPa, 1.20 MPa and 1.30 MPa, respectively, for specimens with interfacial compressive stresses of 0, 0.5, 1.0, and 1.5 MPa, showing a clear positive correlation in contrast to the influence of concrete strength and surface roughness. This is due to the direct increase of the frictional stress at the interface under the increase of compressive stress. Accordingly, the interfacial fracture energy was also proportional to the compressive stress. The interfacial fracture energy of the specimen with an interfacial compressive stress of 1.5 MPa was 0.47 N/mm, 266.4% more than that of the specimen without interfacial compressive stress.

Observing the fractured surface of specimens in this series, clear scratches on the concrete-to-concrete interface can be found. Therefore, it can be considered that with the interfacial compressive stress, friction plays an important role in improving the maximum stress and residual stress at the concrete-to-concrete interface. However, the compressive stress is highly entangled with the surface roughness. They need to be taken collectively in understanding their influence on the interfacial behaviour. For instance, when the surface roughness was small, the influence of the compressive stress on the maximum stress of the interface was relatively limited. As for the residual load, the impact of the interfacial compressive stress was still considerable for smooth

surfaces, indicating that the residual stress was mainly contributed by the frictional action.

In order to further understand the shear behaviour of the concrete-to-concrete interface, Figure 5.18 shows the variation of interfacial maximum stress, residual stress and fracture energy under various combinations of surface roughness and interfacial compressive stress. In these specimens, the strengths of old concrete and new concrete remain unchanged to be 23.4 MPa and 43.7 MPa. With the simultaneous increase of surface roughness and applied compressive stress, the interfacial maximum stress increased obviously from 1.81 MPa to 3.16 MPa, 4.42 MPa and 5.84 MPa, respectively. This is consistent with the effect of increasing either the roughness or compressive stress alone. The average residual stress increased from 0.31 MPa to 2.47 MPa when both the roughness and compressive stress were increased, due to the substantial increase of the frictional stress between the fractured surfaces.

Examining Figures 5.14-5.18 collectively, it can be found that increasing each of the old or new concrete strength, surface roughness, and interfacial compressive stress enhances the interfacial shear resistance. Practically, in order to achieve reliable bond between the new and old concrete, surface preparation can be used to roughen the old concrete, and relatively high new concrete strength could further enhance the bond. It may be practically inconvenient to actively apply interfacial compressive stress, in addition to that generated by the applied load. Nevertheless, considering that in practical applications interfacial cracking or debonding is not permitted, the residual stress at the interface is less critical than the maximum interfacial shear stress, which could be effectively enhanced by surface roughening and the increase of new concrete strength.

5.4 CONCLUSIONS

A modified shear test method has been proposed to investigate the local bond-slip relationship at the concrete-to-concrete interfaces and validated, as discussed in Chapter 4. A comprehensive experimental programme based on this newly proposed test method has been conducted to quantify the bond-slip behaviour at the concrete-to-concrete interface. Based on the literature review, the main factors affecting the interfacial shear are the strengths of the old and new concrete, old concrete surface roughness, and applied interfacial compressive stress. Accordingly, four series of the modified test specimens were prepared; the test parameters included the three main factors. The failure mode, global force-slip behaviour, interfacial slip distribution, and local bond-slip relationship of the specimens were examined, and the following conclusions can be drawn:

All specimens failed by separation at the concrete-to-concrete interface as a result of gradual interfacial debonding propagation. During the loading process, the shear load increased linearly to the peak level, which was followed by a sudden drop of the load and sudden increase of the slip. Thereafter, gradual interfacial debonding took place until complete separation at the interface.

The local bond-slip relationship of the concrete-to-concrete interface follows a typical tri-linear shape, including a linear elastic stage that terminates at the maximum shear stress, a subsequent softening stage that terminates at a residual stress level, and a residual stress stage with the stress approaching zero as the slip increases.

The interfacial stiffness and strength both increase with the old and new concrete strengths, surface roughness, and applied compressive stress. The residual stress level is dependent on the applied compressive stress but not the concrete strength nor the

surface roughness. Specifically, for the interface without applied compressive stress, the residual stress is minimal; for the interface with applied compressive stress, a considerable level of residual stress exists after the softening stage.

Therefore, it has been experimentally demonstrated that the interfacial bond-slip relationship is dependent on the three testing parameters examined in the tests. Moreover, the typical bond-slip relationship can be represented by a few key parameters, including the interfacial stiffness, shear strength, and residual stress level. The obtained test results can be used to calibrate appropriate models for these key parameters, and a complete bond-slip model for the concrete-to-concrete interface could be achieved, as discussed in the next chapter.

5.5 REFERENCES

Birkeland, P. W., & Birkeland, H. W. (1966). Connections in precast concrete construction. *PCI Journal*, 63(3), 345-368.

Chilwesa, M., Minelli, F., Reggia, A., & Plizzari, G. (2017). Evaluating the shear bond strength between old and new concrete through a new test method. *Magazine of Concrete Research*, 69(9), 425-435.

*f*ib model code for concrete structures 2010 (2013). Berlin, Germany.

Gaston, J. R., & Kriz, L. B. (1964). Connections in precast concrete structures--scarf joints. *PCI Journal*, 9(3), 37–59.

GB 50010-2010. (2010). *Code for desing of concrete structures*. Beijing, China Architecture & Building Press.

Gohnert, M. (2003). Horizontal shear transfer across a roughened surface. *Cement and Concrete Composites*, 25(3), 379-385.

He, Y., Zhang, X., Hooton, R. D., & Zhang, X. (2017). Effects of interface roughness and interface adhesion on new-to-old concrete bonding. *Construction and Building Materials*, 151, 582-590.

Júlio, E. N., Branco, F. A., Silva, V. D., & Lourenço, J. F. (2006). Influence of added concrete compressive strength on adhesion to an existing concrete substrate. *Building and Environment*, 41(12), 1934-1939.

Kahn, L. F., & Mitchell, A. D. (2002). Shear friction tests with high-strength concrete. *ACI Structural Journal*, 99(1), 98-103.

Loov, R. E., & Patnaik, A. K. (1994). Horizontal shear strength of composite concrete beams. *PCI Journal*, 39(1), 48-69.

Mattock, A. H. (2001). Shear friction and high-strength concrete. *ACI Structural Journal*, 98(1): 50-59.

Mohamad, M. E., Ibrahim, I. S., Abdullah, R., Rahman, A. A., Kueh, A. B. H., & Usman, J. (2015). Friction and cohesion coefficients of composite concrete-to-concrete bond. *Cement and Concrete Composites*, 56, 1-14.

Momayez, A., Ehsani, M. R., Ramezanianpour, A. A., & Rajaie, H. (2005). Comparison of methods for evaluating bond strength between concrete substrate and repair materials. *Cement and Concrete Research*, 35(4), 748-757.

Randl, N. (1997) Investigations on transfer of forces between old and new concrete at different joint roughness. PhD. thesis. Austria: University of Innsbruck.

Santos, P. M., & Júlio, E. N. (2014). Interface shear transfer on composite concrete members. *ACI Structural Journal*, 111(1), 113-120.

Santos, P. M., & Júlio, E. N. (2013). A state-of-the-art review on roughness quantification methods for concrete surfaces. *Construction and Building Materials*,

38, 912-923.

Tsoukantas, S. G., & Tassios, T. P. (1989). Shear resistance of connections between reinforced concrete linear precast elements. *ACI Structural Journal*, 86(3), 242-249.

Table 5.1 Concrete strengths on the testing day and the 28th day

Series	Specimen	$f_{cu,o}$ (MPa)	STD (MPa)	$f_{cu,ot}$ (MPa)	STD (MPa)	$f_{cu,n}$ (MPa)	STD (MPa)	$f_{cu,nt}$ (MPa)	STD (MPa)
Series-I	O20-N40-R0-S0-I	20.3	1.3	22.8	1.4	41.5	2.3	42.5	2.6
	O20-N40-R0-S0-II	20.3	1.3	22.8	1.4	41.5	2.3	42.5	2.6
	O20-N20-R0-S0-I	20.3	1.3	22.8	1.4	21.8	1.8	23.2	1.9
	O20-N20-R0-S0-II	20.3	1.3	22.8	1.4	21.8	1.8	23.2	1.9
	O20-N60-R0-S0-I	20.3	1.3	22.8	1.4	57.9	3.2	59.6	3.3
	O20-N60-R0-S0-II	20.3	1.3	22.8	1.4	57.9	3.2	59.6	3.3
	O40-N40-R0-S0-I	41.0	2.4	43.1	2.2	41.5	2.3	42.5	2.6
	O40-N40-R0-S0-II	41.0	2.4	43.1	2.2	41.5	2.3	42.5	2.6
	O60-N40-R0-S0-I	54.2	2.8	57.3	3.0	41.5	2.3	42.5	2.6
	O60-N40-R0-S0-II	54.2	2.8	57.3	3.0	41.5	2.3	42.5	2.6
Series-II	O20-N40-R1-S0-I	19.2	1.5	21.5	1.7	42.4	2.1	43.1	3.0
	O20-N40-R1-S0-II	19.2	1.5	21.5	1.7	42.4	2.1	43.1	3.0
	O20-N40-R2-S0-I	19.2	1.5	21.5	1.7	42.4	2.1	43.1	3.0
	O20-N40-R2-S0-II	19.2	1.5	21.5	1.7	42.4	2.1	43.1	3.0
	O20-N40-R3-S0-I	19.2	1.5	21.5	1.7	42.4	2.1	43.1	3.0
	O20-N40-R3-S0-II	19.2	1.5	21.5	1.7	42.4	2.1	43.1	3.0
Series-III	O20-N40-R0-S0.5-I	18.9	1.3	19.8	1.4	40.1	2.5	40.8	2.8
	O20-N40-R0-S0.5-II	18.9	1.3	19.8	1.4	40.1	2.5	40.8	2.8
	O20-N40-R0-S1.0-I	18.9	1.3	19.8	1.4	40.1	2.5	40.8	2.8
	O20-N40-R0-S1.0-II	18.9	1.3	19.8	1.4	40.1	2.5	40.8	2.8
	O20-N40-R0-S1.5-I	18.9	1.3	19.8	1.4	40.1	2.5	40.8	2.8
	O20-N40-R0-S1.5-II	18.9	1.3	19.8	1.4	40.1	2.5	40.8	2.8
Series-IV	O20-N40-R1-S0.5-I	21.8	1.7	23.4	2.0	43.2	2.1	43.7	2.5
	O20-N40-R1-S0.5-II	21.8	1.7	23.4	2.0	43.2	2.1	43.7	2.5
	O20-N40-R2-S1.0-I	21.8	1.7	23.4	2.0	43.2	2.1	43.7	2.5
	O20-N40-R2-S1.0-II	21.8	1.7	23.4	2.0	43.2	2.1	43.7	2.5
	O20-N40-R3-S1.5-I	21.8	1.7	23.4	2.0	43.2	2.1	43.7	2.5
	O20-N40-R3-S1.5-II	21.8	1.7	23.4	2.0	43.2	2.1	43.7	2.5

Note: $f_{cu,o}$=Cube compressive strength of old concrete on the 28th day; $f_{cu,ot}$=Cube compressive strength of old concrete on the day of testing; $f_{cu,n}$=Cube compressive strength of new concrete on the 28th day; $f_{cu,nt}$=Cube compressive strength of new concrete on the day of testing; STD=Standard deviation.

Table 5.2 Test parameters of the specimens

Series	Specimen	$f_{cu,o}$ (MPa)	$f_{cu,n}$ (MPa)	R (mm)	σ_n (MPa)	Remarks
Series-I	O20-N40-R0-S0-I	22.8	42.5	0	0	Reference
	O20-N40-R0-S0-II	22.8	42.5	0	0	Reference
	O20-N20-R0-S0-I	22.8	23.2	0	0	Varying concrete strength
	O20-N20-R0-S0-II	22.8	23.2	0	0	
	O20-N60-R0-S0-I	22.8	59.6	0	0	
	O20-N60-R0-S0-II	22.8	59.6	0	0	
	O40-N40-R0-S0-I	43.1	42.5	0	0	
	O40-N40-R0-S0-II	43.1	42.5	0	0	
	O60-N40-R0-S0-I	57.3	42.5	0	0	
	O60-N40-R0-S0-II	57.3	42.5	0	0	
Series-II	O20-N40-R1-S0-I	21.5	43.1	0.9	0	Varying surface roughness
	O20-N40-R1-S0-II	21.5	43.1	0.9	0	
	O20-N40-R2-S0-I	21.5	43.1	2.2	0	
	O20-N40-R2-S0-II	21.5	43.1	2.2	0	
	O20-N40-R3-S0-I	21.5	43.1	3.2	0	
	O20-N40-R3-S0-II	21.5	43.1	3.2	0	
Series-III	O20-N40-R0-S0.5-I	19.8	40.8	0	0.5	Varying compressive stress
	O20-N40-R0-S0.5-II	19.8	40.8	0	0.5	
	O20-N40-R0-S1.0-I	19.8	40.8	0	1.0	
	O20-N40-R0-S1.0-II	19.8	40.8	0	1.0	
	O20-N40-R0-S1.5-I	19.8	40.8	0	1.5	
	O20-N40-R0-S1.5-II	19.8	40.8	0	1.5	
Series-IV	O20-N40-R1-S0.5-I	23.4	43.7	1.0	0.5	Varying surface roughness and compressive stress
	O20-N40-R1-S0.5-II	23.4	43.7	1.0	0.5	
	O20-N40-R2-S1.0-I	23.4	43.7	1.9	1.0	
	O20-N40-R2-S1.0-II	23.4	43.7	1.9	1.0	
	O20-N40-R3-S1.5-I	23.4	43.7	3.1	1.5	
	O20-N40-R3-S1.5-II	23.4	43.7	3.1	1.5	

Note: $f_{cu,o}$=Cube compressive strength of old concrete on the day of testing; $f_{cu,n}$=Cube compressive strength of new concrete on the day of testing; R = Surface roughness; σ_n = Applied compressive stress

Table 5.3 Mix proportions for the three grades of concrete

Type	w/c	Cement of Grade 42.5 (kg/m^3)	Cement of Grade 52.5 (kg/m^3)	Water (kg/m^3)	Sand (kg/m^3)	Aggregate (kg/m^3)	Superplasticizer
C20	0.65	334	-	217	780	1036	0.05%
C40	0.45	510	-	230	600	1072	0.10%
C60	0.32	-	544	174	554	1100	0.15%

Table 5.4 Influence of concrete strength

Specimen	$f_{cu,o}$ (MPa)	$f_{cu,n}$ (MPa)	P_{max} (kN)	τ_{max} (MPa)	δ_1 (mm)	P_r (kN)	τ_r (MPa)	δ_2 (mm)	G_f (N/mm)
O20-N40-R0-S0-I	22.8	42.5	8.843	1.769	0.019	1.16	0.232	0.078	0.131
O20-N40-R0-S0-II	22.8	42.5	9.222	1.844	0.018	1.905	0.381	0.112	0.128
O20-N20-R0-S0-I	22.8	23.2	8.126	1.625	0.007	1.117	0.223	0.088	0.104
O20-N20-R0-S0-II	22.8	23.2	6.313	1.263	0.008	0.938	0.188	0.149	0.109
O20-N60-R0-S0-I	22.8	59.6	13.837	2.767	0.009	0.893	0.179	0.101	0.158
O20-N60-R0-S0-II	22.8	59.6	13.46	2.692	0.019	1.009	0.202	0.098	0.155
O40-N40-R0-S0-I	43.1	42.5	9.592	1.918	0.018	1.322	0.264	0.101	0.162
O40-N40-R0-S0-II	43.1	42.5	11.385	2.277	0.023	1.351	0.270	0.131	0.158
O60-N40-R0-S0-I	57.3	42.5	14.243	2.849	0.008	2.012	0.402	0.126	0.251
O60-N40-R0-S0-II	57.3	42.5	13.318	2.664	0.019	1.931	0.386	0.131	0.230

Note: $f_{cu,o}$ = Cube compressive strength of old concrete; $f_{cu,n}$ = Cube compressive strength of new concrete; P_{max} = Peak load; τ_{max} = Maximum shear stress; δ_1 = slip corresponding to the maximum shear stress; P_r = Residual load; τ_r = Residual shear stress; δ_2 = slip corresponding to the residual shear stress; G_f = Interfacial fracture energy

Table 5.5 Influence of concrete surface roughness

Specimen	R (mm)	P_{max} (kN)	τ_{max} (MPa)	δ_1 (mm)	P_r (kN)	τ_r (MPa)	δ_2 (mm)	G_f (N/mm)
O20-N40-R0-S0-I	0	8.843	1.769	0.019	1.16	0.232	0.078	0.131
O20-N40-R0-S0-II	0	9.222	1.844	0.018	1.905	0.381	0.112	0.128
O20-N40-R1-S0-I	0.9	15.296	3.059	0.017	1.372	0.274	0.071	0.168
O20-N40-R1-S0-II	0.9	12.748	2.550	0.010	1.058	0.212	0.106	0.184
O20-N40-R2-S0-I	2.2	15.968	3.194	0.010	1.408	0.282	0.102	0.219
O20-N40-R2-S0-II	2.2	18.113	3.623	0.020	1.332	0.266	0.120	0.261
O20-N40-R3-S0-I	3.2	18.167	3.633	0.015	1.761	0.352	0.122	0.296
O20-N40-R3-S0-II	3.2	21.508	4.302	0.012	1.745	0.349	0.126	0.290

Note: R = Surface roughness; P_{max} = Maximum load; τ_{max} = Maximum shear stress; δ_1= slip corresponding to the maximum shear stress; P_r = Residual load; τ_r = Residual shear stress; δ_2= slip corresponding to the residual shear stress; G_f = Interfacial fracture energy

Table 5.6 Influence of applied compressive stress

Specimen	σ (MPa)	P_{max} (kN)	τ_{max} (MPa)	δ_1 (mm)	P_r (kN)	τ_r (MPa)	δ_2 (mm)	G_f (N/mm)
O20-N40-R0-S0-I	0	8.843	1.769	0.019	1.16	0.232	0.078	0.131
O20-N40-R0-S0-II	0	9.222	1.844	0.018	1.905	0.381	0.112	0.128
O20-N40-R0-S0.5-I	0.5	10.065	2.013	0.013	3.676	0.735	0.107	0.280
O20-N40-R0-S0.5-II	0.5	10.933	2.187	0.017	4.408	0.882	0.092	0.311
O20-N40-R0-S1.0-I	1.0	11.888	2.378	0.015	6.027	1.205	0.103	0.426
O20-N40-R0-S1.0-II	1.0	12.435	2.487	0.019	5.937	1.187	0.122	0.432
O20-N40-R0-S1.5-I	1.5	13.21	2.642	0.021	6.342	1.268	0.125	0.444
O20-N40-R0-S1.5-II	1.5	14.579	2.916	0.011	6.655	1.331	0.126	0.505

Note: σ = Applied compressive stress; P_{max} = Maximum load; τ_{max} = Maximum shear stress; δ_1= slip corresponding to the maximum shear stress; P_r = Residual load; τ_r = Residual shear stress; δ_2= slip corresponding to the residual shear stress; G_f = Interfacial fracture energy

Table 5.7 Influence of surface roughness and compressive stress

Specimen	R (mm)	σ (MPa)	P_{max} (kN)	τ_{max} (MPa)	δ_1 (mm)	P_r (kN)	τ_r (MPa)	δ_2 (mm)	G_f (N/mm)
O20-N40-R0-S0-I	0	0	8.843	1.769	0.019	1.16	0.232	0.078	0.131
O20-N40-R0-S0-II	0	0	9.222	1.844	0.018	1.905	0.381	0.112	0.128
O20-N40-R1-S0.5-I	1	0.5	15.063	3.013	0.009	4.575	0.915	0.109	0.413
O20-N40-R1-S0.5-II	1	0.5	16.565	3.313	0.010	4.934	0.987	0.117	0.467
O20-N40-R2-S1.0-I	2	1.0	22.966	4.593	0.013	8.701	1.740	0.136	0.761
O20-N40-R2-S1.0-II	2	1.0	21.228	4.246	0.017	9.005	1.801	0.122	0.693
O20-N40-R3-S1.5-I	3	1.5	29.961	5.992	0.012	11.832	2.366	0.109	0.965
O20-N40-R3-S1.5-II	3	1.5	28.433	5.687	0.020	12.907	2.581	0.124	0.898

Note: R = Surface roughness; σ = Applied compressive stress; P_{max} = Maximum load; τ_{max} = Maximum shear stress; δ_1= slip corresponding to the maximum shear stress; P_r = Residual load; τ_r = Residual shear stress; δ_2= slip corresponding to the residual shear stress; G_f = Interfacial fracture energy

(a) Aluminum alloy mould

(b) Old concrete casting

(c) Ready for new concrete casting

(b) Complete specimen

Figure 5.1 Preparation of test specimens

(a) Smooth surface
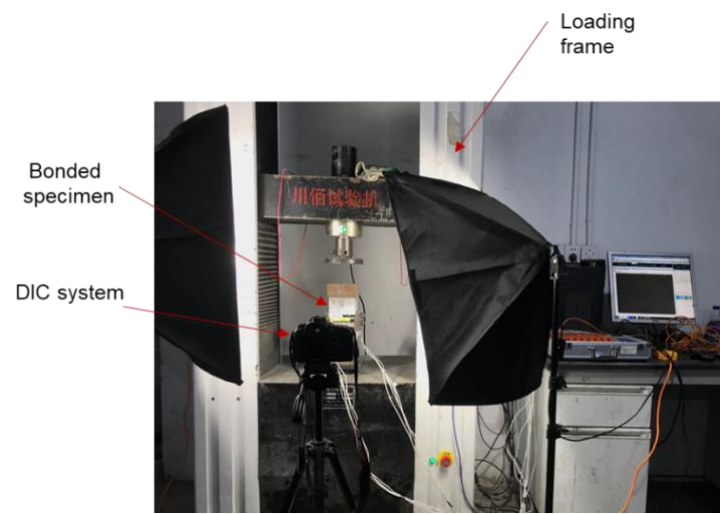

(b) Chisel-roughened surface

(c) Sand-filling of the rough surface

(d) Volume measurement of the filling sand

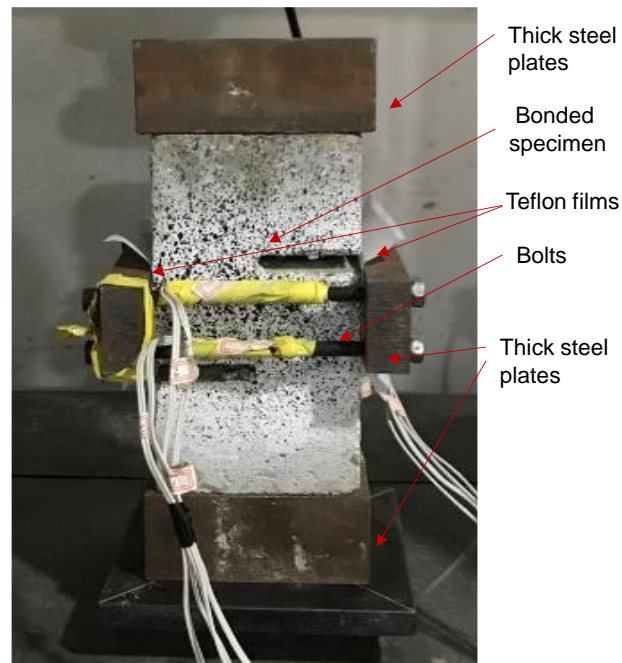Figure 5.2 Roughening of the old concrete surface
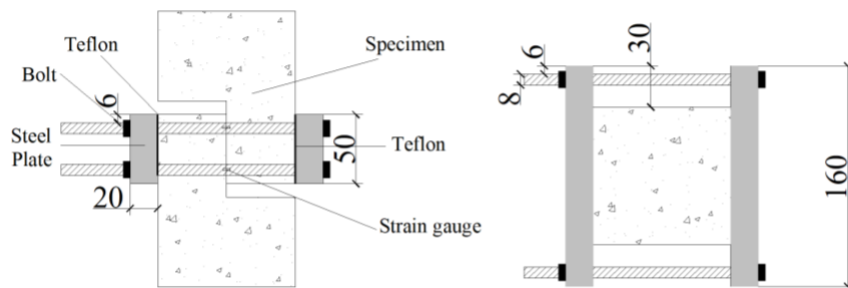
(a) Test set-up

(b) Specimen ready for testing

Figure 5.3 Test setup

(a) Photo of compressive stress application device

(b) Dimensions of the applied compressive stress device

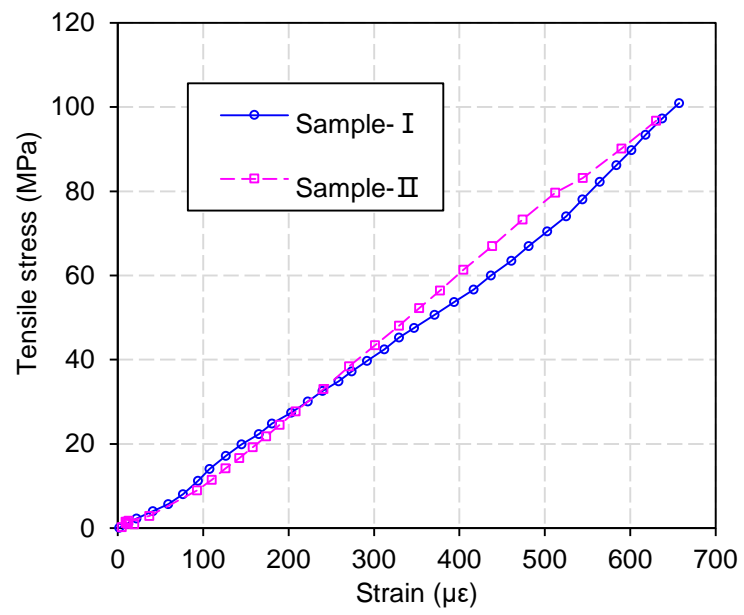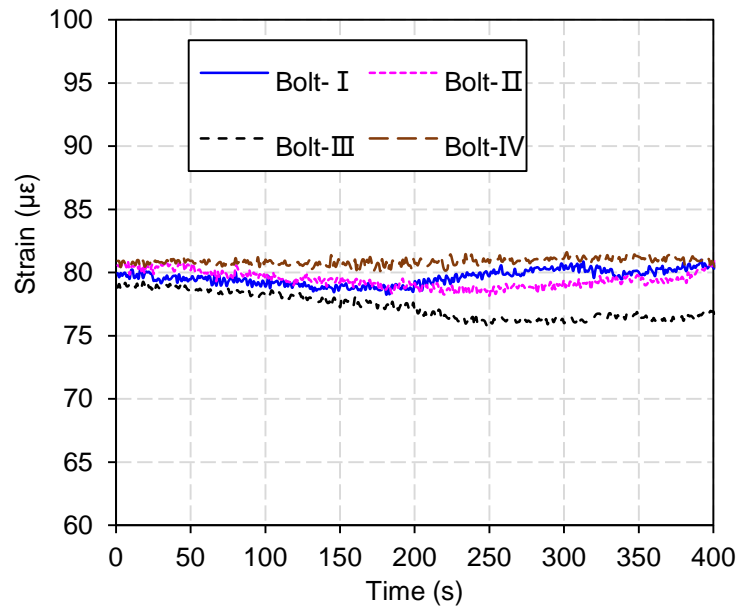Figure 5.4 Arrangements for the series-III and series-IV
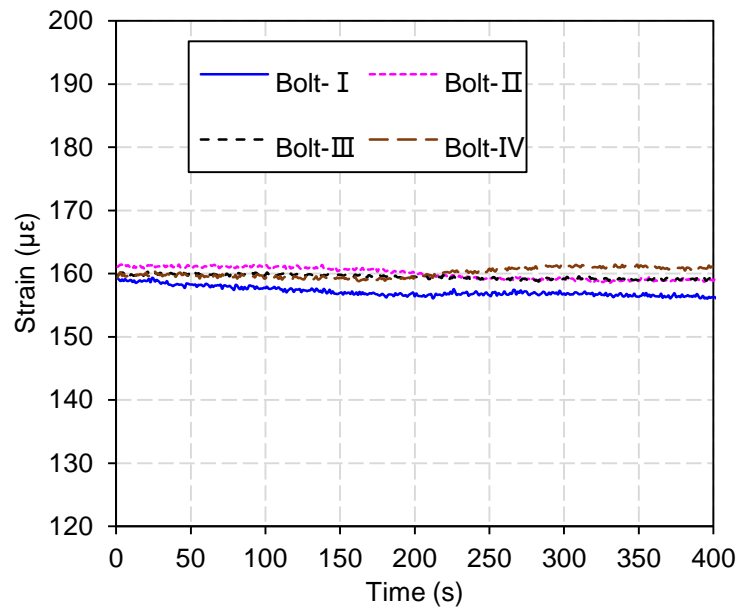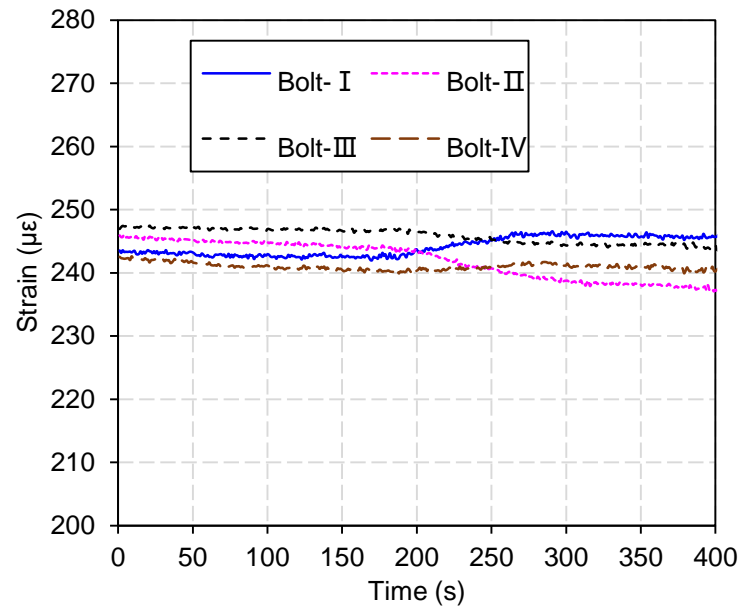
Figure 5.5 Tensile stress-strain curve relationship of the bolts

(a) Specimen O20-N40-R0-S0.5-Ⅰ (σ=0.5 MPa)
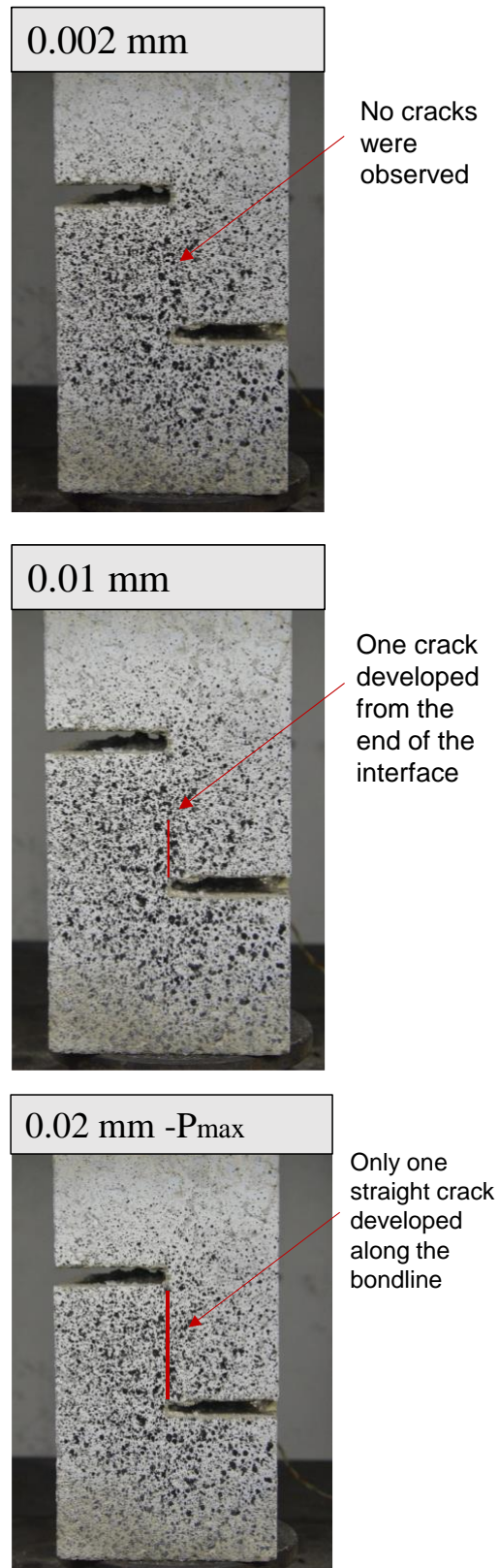

(b) Specimen O20-N40-R0-S1.0-Ⅰ (σ=1.0 MPa)

(c) Specimen O20-N40-R0-S1.5-Ⅰ (σ=1.5 MPa)

Figure 5.6 Bolt stresses during loading

0.002 mm

No cracks were observed

0.01 mm

One crack developed from the end of the interface

0.02 mm -P_{max}

Only one straight crack developed along the bondline

(a) Specimen with a smooth old concrete surface (Specimen O20-N40-R0-S0-Ⅰ)

0.002 mm

No cracks were observed

0.01 mm

One crack developed from the end of the interface

0.02 mm -P_{max}

Only one slightly curved crack propagated along the bondline
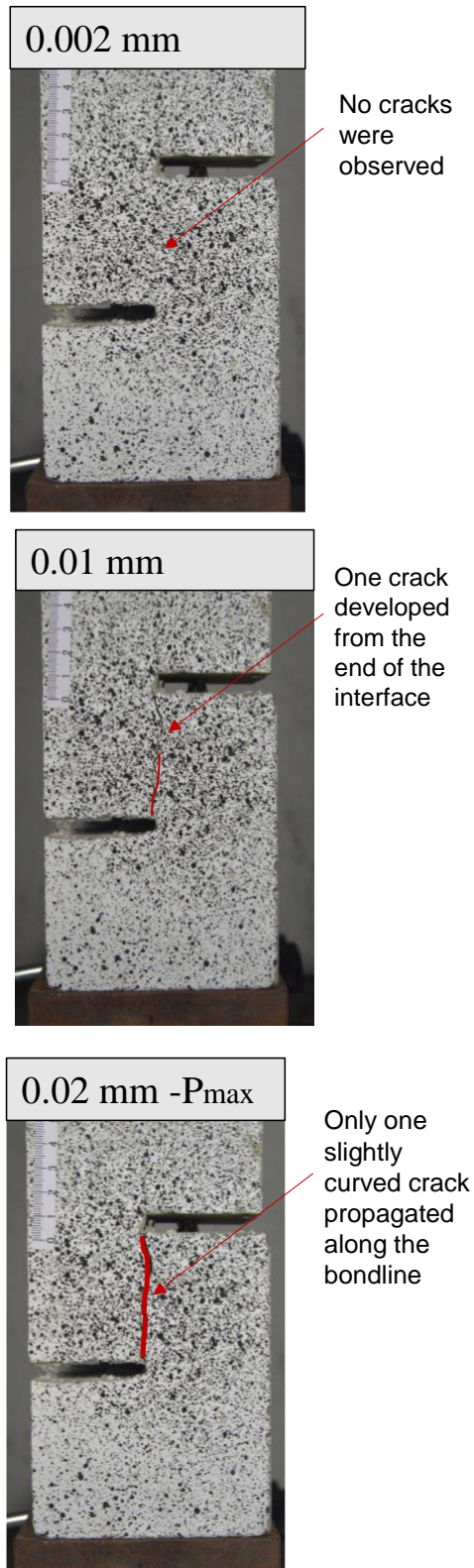
(b) Specimen with a rough old concrete surface (Specimen O20-N40-R2-S0-Ⅰ)
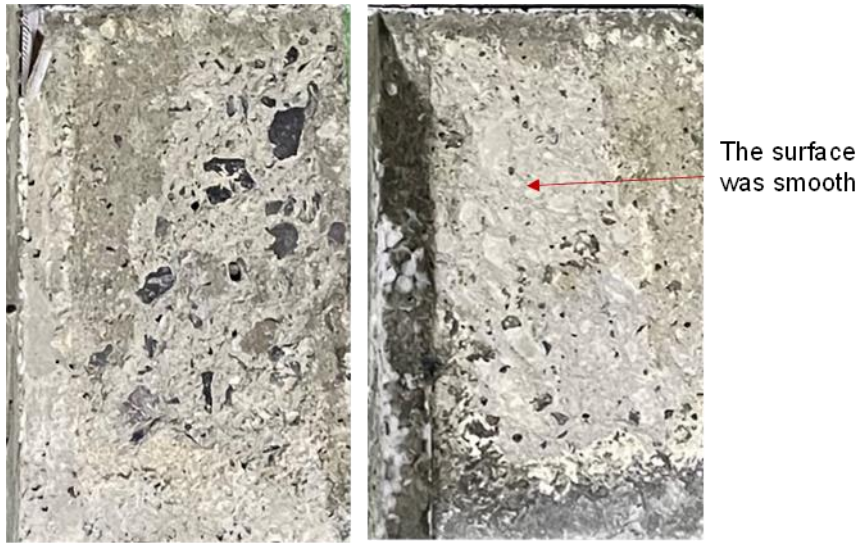
Figure 5.7 Typical crack development process

(a) Specimen with smooth old concrete surface (Specimen O20-N40-R0-S0-Ⅰ)
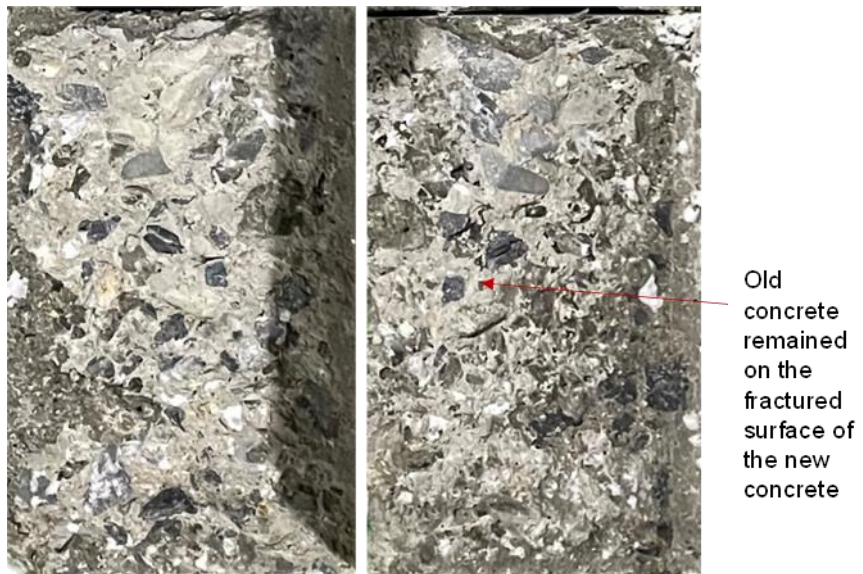
(b) Specimen with rough old concrete surface (Specimen O20-N40-R2-S0-Ⅰ)

(c) Specimen with applied compressive stress (Specimen O20-N40-R0-S1.5-Ⅱ)

Figure 5.8 Fractured surfaces of the interfacial bond area after shear loading
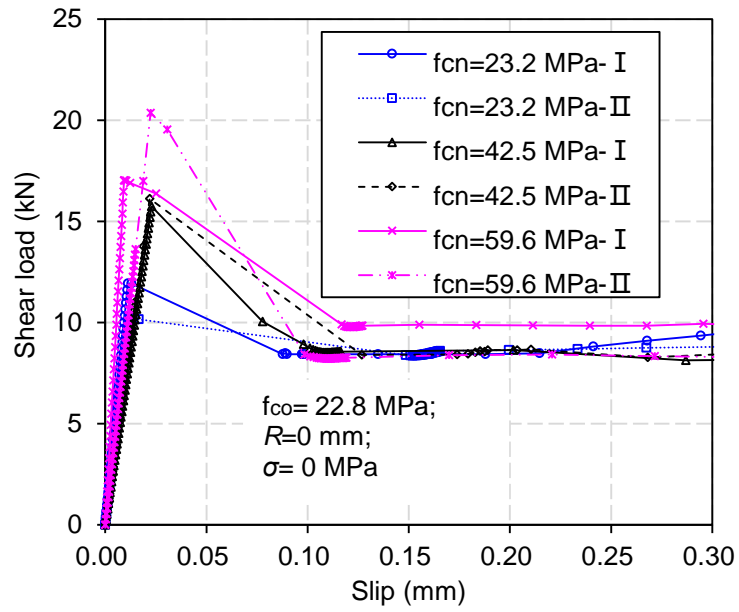
(a) Effect of new concrete strengths
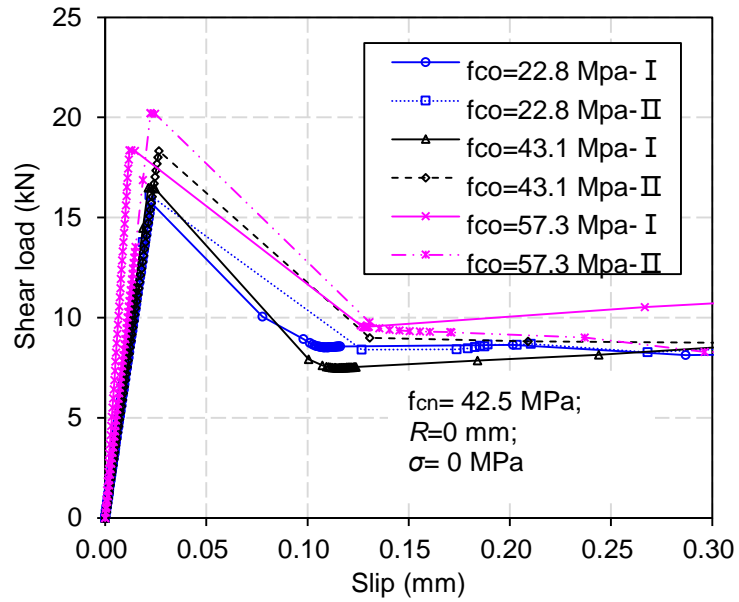
(b) Effect of old concrete strengths
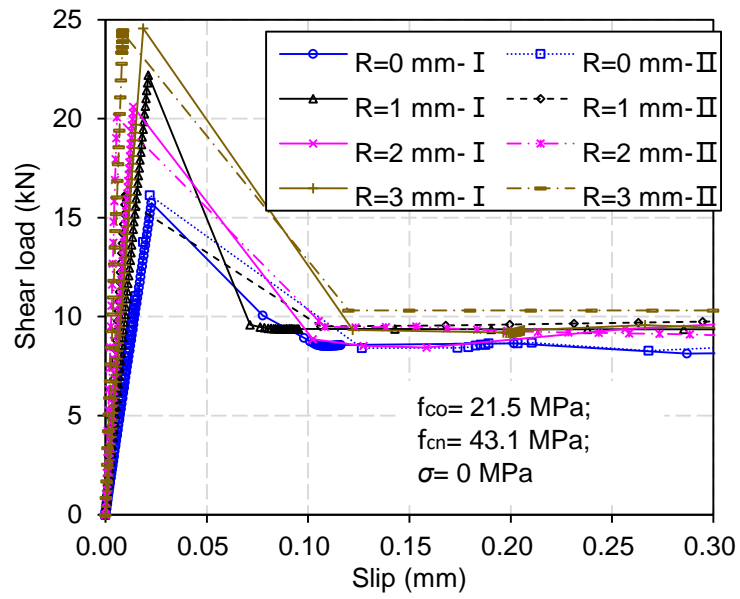
(c) Effect of old concrete surface roughness

(d) Effect of applied compressive stress

187
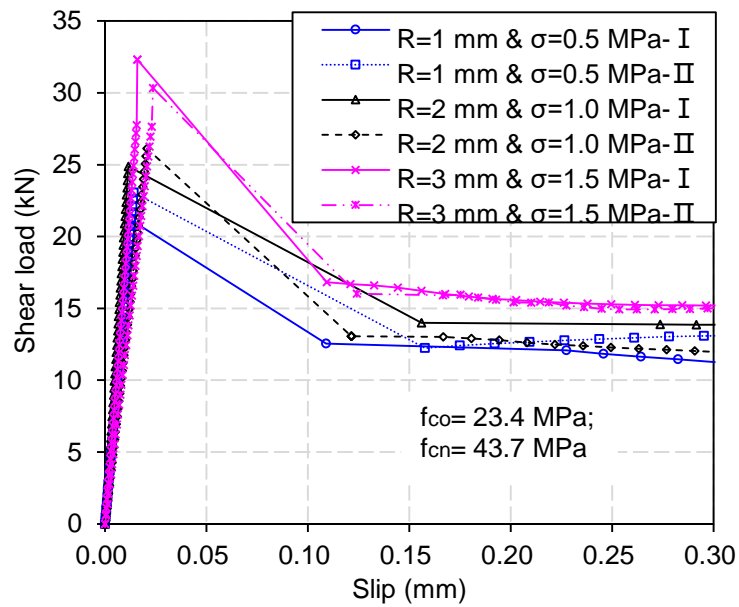
(e) Effect of surface roughness and applied compressive stress

Figure 5.9 Load- slip curves of specimens with parallel reinforcement

(a) Effect of new concrete strengths

(b) Effect of old concrete strengths

(c) Effect of old concrete surface roughness

189
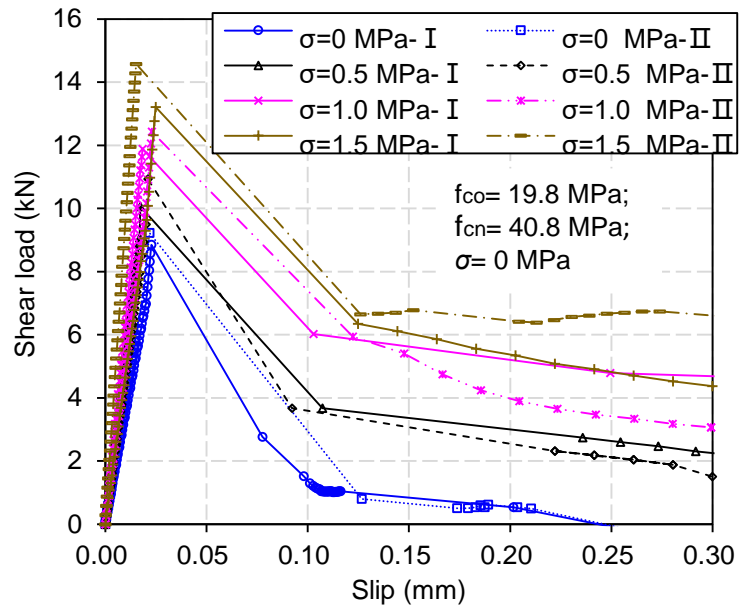
(d) Effect of applied compressive stress
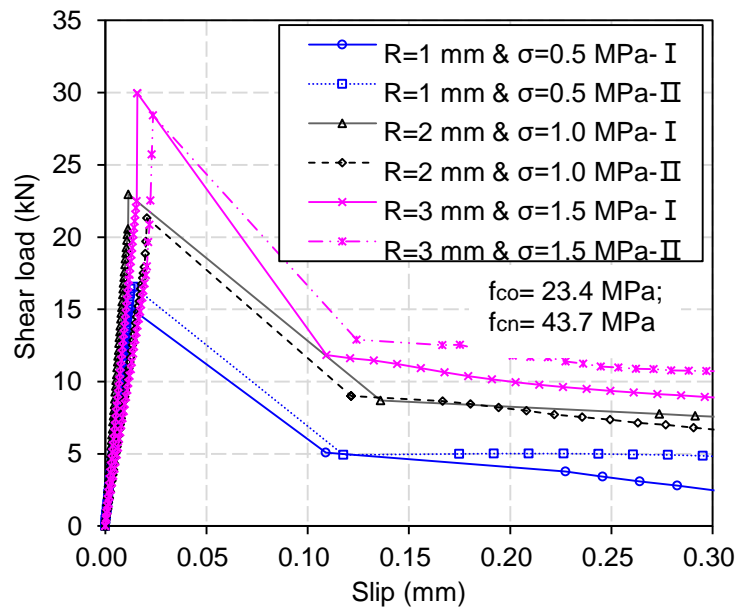
(e) Effect of surface roughness and applied compressive stress

Figure 5.10 Load-slip curves of isolated concrete-to-concrete interfaces
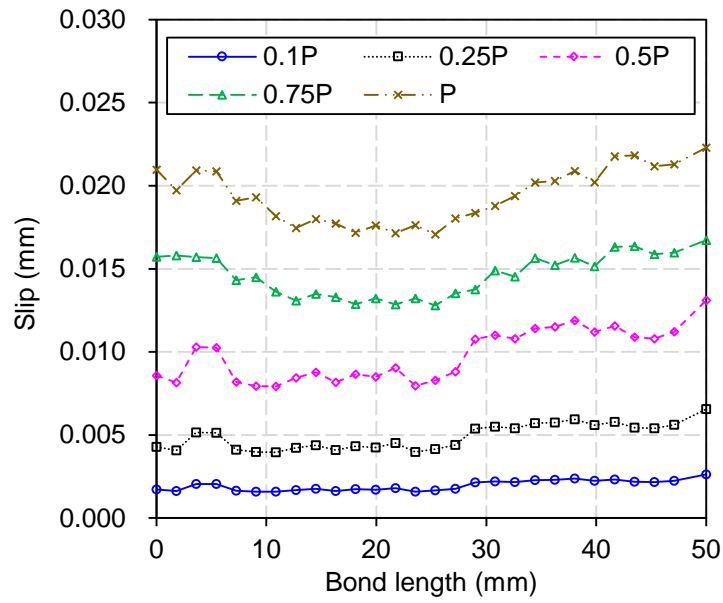
Figure 5.11 Slip distribution of specimen O20-N40-R0-S0-I along the interface at various load levels
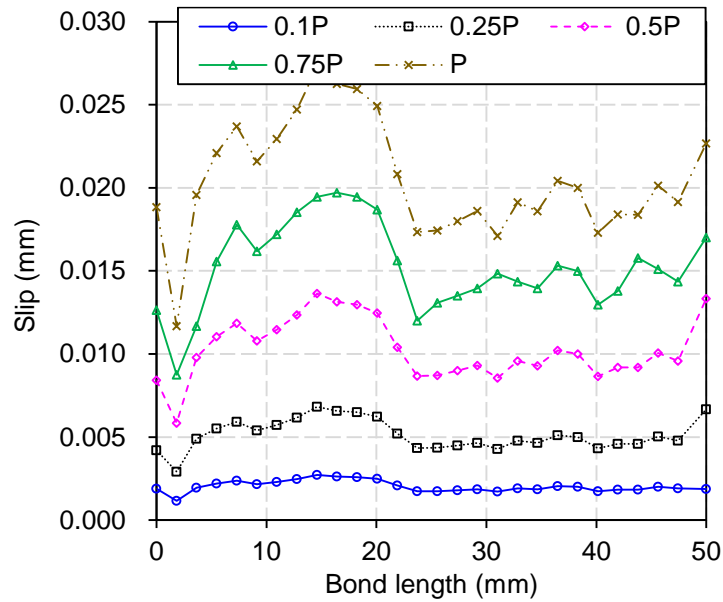
Figure 5.12 Slip distribution of specimen O20-N40-R2-S0-I along the interface at various load levels(with rough interface)
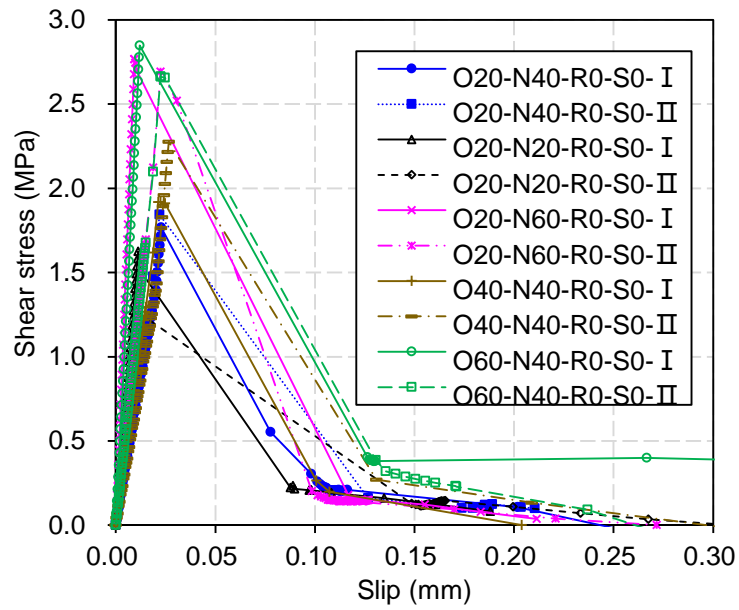
(a) Series-I

(b) Series-II
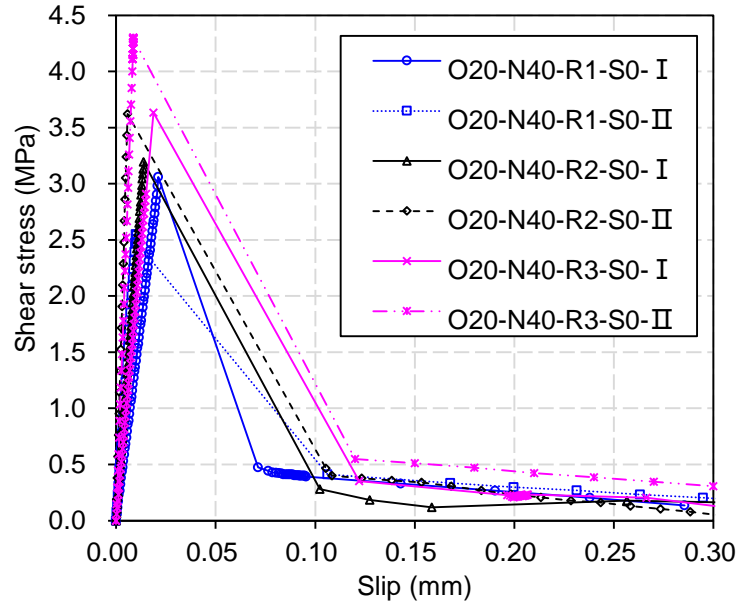
(c) Series-III

(d) Series-IV
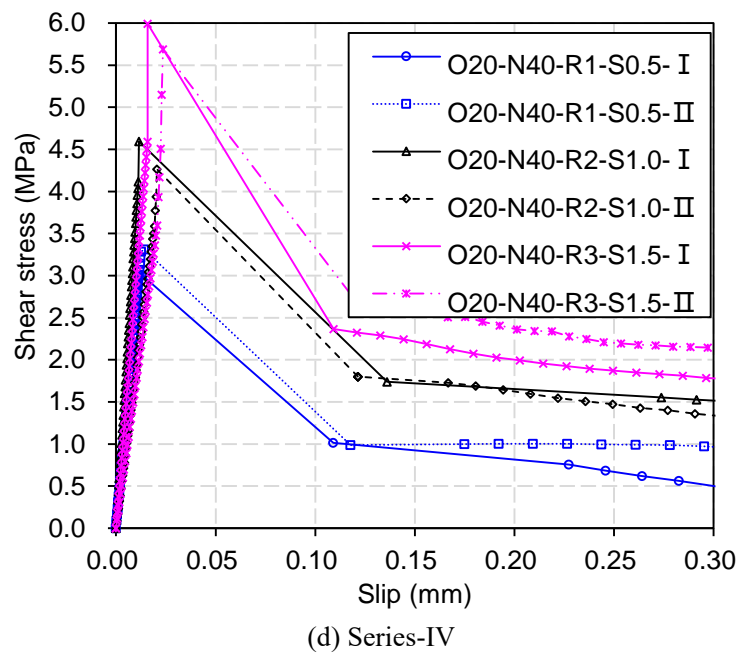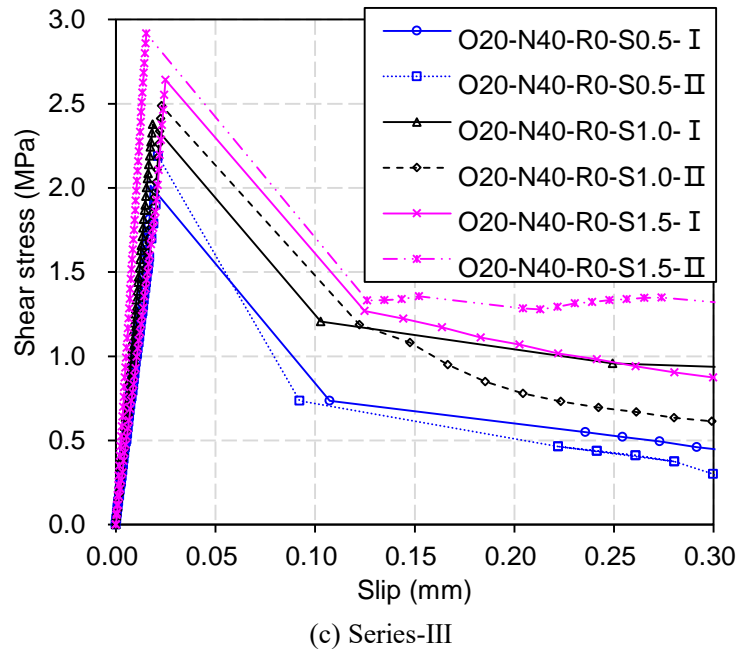
Figure 5.13 Shear bond-slip curves
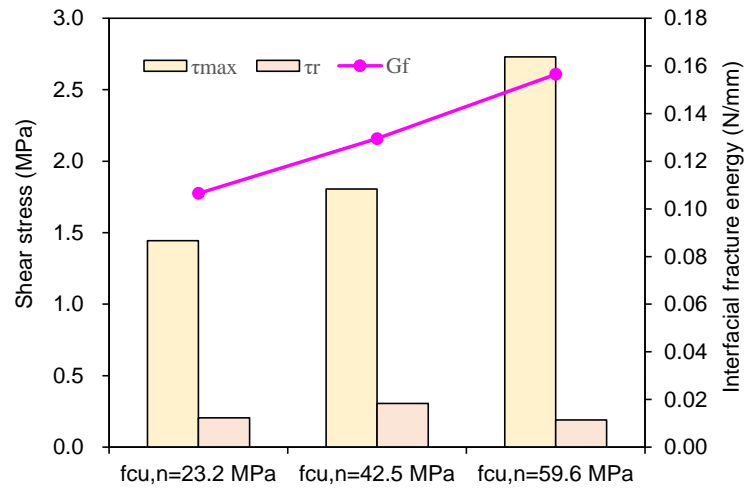
Figure 5.14 Effect of new concrete strength
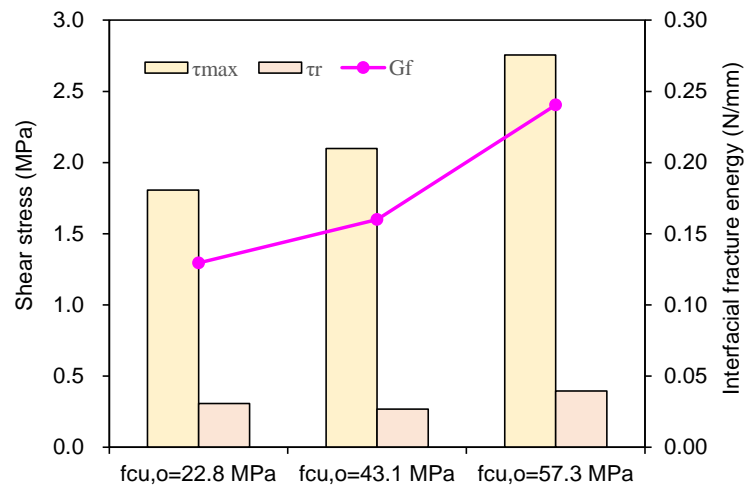
Figure 5.15 Effect of old concrete strength
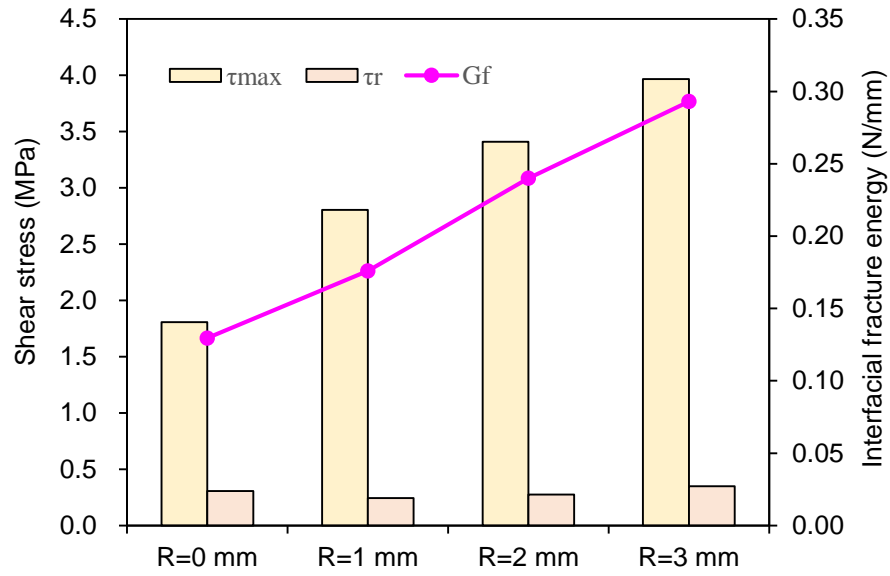
Figure 5.16 Effect of old concrete surface roughness
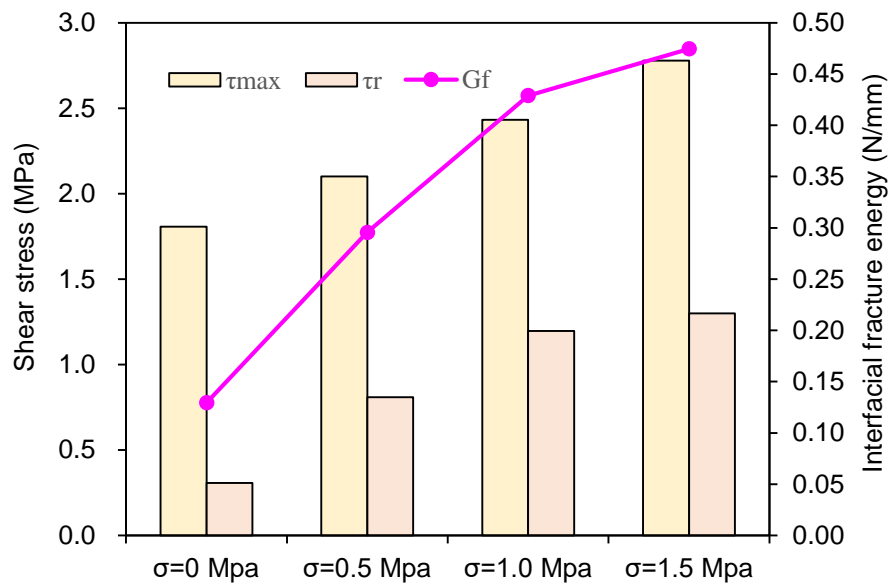
Figure 5.17 Effect of applied compressive stress
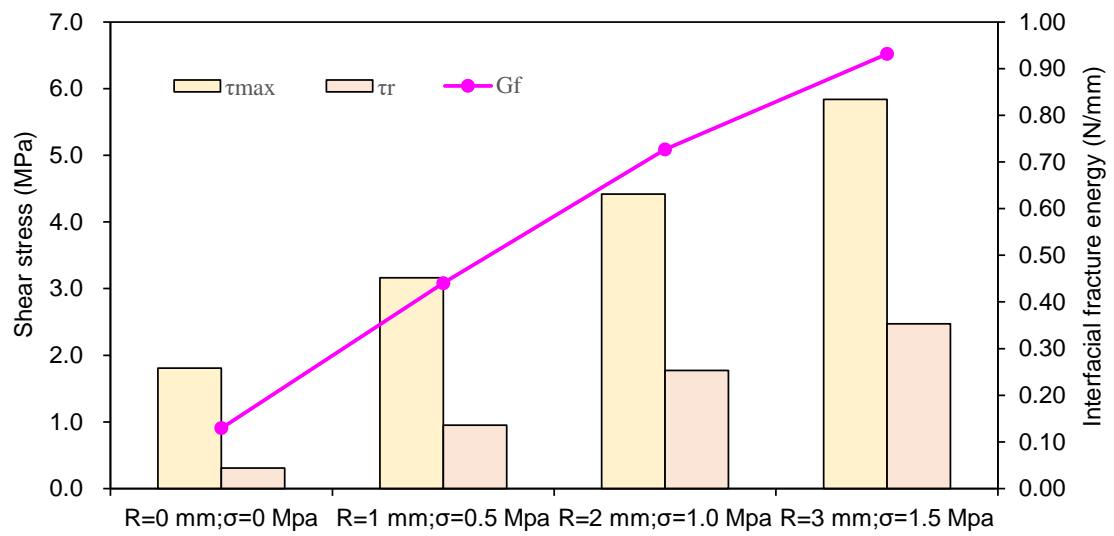
Figure 5.18 Effect of combined old concrete surface roughness and applied
compressive stress

CHAPTER 6

DEVELOPMENT OF A BOND-SLIP MODEL FOR CONCRETE-TO-CONCRETE INTERFACES

6.1 INTRODUCTION

Establishing an accurate Mode-II shear stress-slip, commonly referred to as bond-slip, model for the concrete-to-concrete interface is critical for understanding the mechanical behaviour and the accurate numerical simulations of structural members with such interfaces. At present, the most extensively investigated interfacial bond-slip model for concrete materials is the FRP-concrete interfacial bond-slip model. Lu *et al*. (2005) developed a bond-slip model for FRP-concrete bonded interfaces based on the macro-scale and meso-scale FE model. Specifically, the authors established an accurate local bond-slip model and developed the shear strength model for FRP-concrete interfaces. However, the local bond-slip behaviour for concrete-to-concrete interfaces has been little investigated and an accurate local bond-slip model has not been achieved yet.

The existing research is concerned with either the bond-slip model at the aggregate-mortar interface, or the Mode-I tensile stress-opening model at the interface between new and old concrete. For example, Stankowski *et al*. (1993a; 1993b) developed a model describing the interface between the aggregate and matrix, considering the normal-shear stress coupling, dilatancy, and elastic pre-peak adhesion. The tensile properties of concrete-to-concrete interfaces were studied based on a three-point bend test by Shah and Kishen (2010a; 2010b). The crack opening length and propagation area, fracture energy, and size effects on the interface were fully analysed. Based on the introduced crack hinge concept, a bi-linear softening model was defined and verified

by performing an FE simulation.

The experimental results presented in Chapter 5 clarified the influence of three variables, namely, concrete strength, concrete surface roughness and applied normal stress, on the shear behaviour of concrete-to-concrete interfaces. The effects on the failure mode, load-slip curve and interfacial slip distribution were discussed. This chapter describes the formulation of a bond-slip model for concrete-to-concrete interfaces, based on the experimental results presented in Chapter 5.

6.2 THEORETICAL BACKGROUND

6.2.1 Bond Strength Models for Concrete-to-Concrete Interfaces

It has been widely adopted that the strength of concrete-to-concrete interfaces subjected to shear stress can be predicted by the "shear-friction theory". This theory was first proposed by Birkeland and Birkeland (1966) and subsequently modified by Mattock and Hawkins (1972), Walraven et al., (1987) and Randl (1997, 2013), who suggested that the shear strength of concrete-to-concrete interfaces was composed of cohesion, friction, and dowel action. The load transfer mechanisms at concrete-to-concrete interfaces, as stated by Zilch and Reinecke (2000), could be defined as follows:

$$\tau(s) = \tau_a(s) + \tau_{sf}(s) + \tau_{sr}(s) \qquad (6.1)$$

where $\tau_a(s)$, $\tau_{sf}(s)$, and $\tau_{sr}(s)$ represent the adhesion, shear friction, and dowel action of the shear reinforcement, respectively.

In particular, adhesion is generated by the chemical bond between the new and old concrete aggregate and related to the strength of concrete, especially the tensile strength of concrete (Santos and Júlio, 2014; Mohamad et al., 2015). After the debonding,

adhesion is completely lost, and the shear stress is solely dependent on mechanical interactions at the fractured interface. If the interface is subjected to compressive stress, frictional stress is induced upon slip; otherwise, if no compressive stress is applied, the shear stress after debonding is trivial as observed from the experimental results in Chapter 5. If the interface is reinforced with dowel reinforcement, as the increase of the interfacial slip, the dowel is subjected to a combined action of tension and shear, often referred to as dowel action. Randl (2013) proposed a model of the interfacial shear strength by considering the dowel action as follows:

$$v_u = \tau_{coh} + \mu\sigma_n + \alpha\rho\sqrt{f_c f_y} \tag{6.2}$$

where v_u is the maximum shear stress at the interface; τ_{coh} is the bond stress due to concrete cohesion and adhesion; μ is the coefficient of friction; σ_n is the applied compressive stress; α is a coefficient related to the dowel reinforcement; ρ is the shear reinforcement ratio; f_c and f_y are the concrete cylinder compressive strength and the yield strength of the steel bar, respectively.

Many studies have proposed modifications to the above method of evaluating the interfacial shear strength to improve the accuracy and extend the scope of application by considering more factors. Moreover, the shear friction theory has been adopted in many design codes to analyse the shear strength of concrete-to-concrete interfaces, as reviewed in Chapter 2. However, as discussed previously, most of these models are based on inappropriate shear test methods where the interfacial shear stress distribution is highly non-uniform. Therefore, the shear strength models of concrete-to-concrete interfaces are inaccurate in representing the local interfacial behaviour and unsuitable for more sophisticated analyses of structures containing such interfaces.

6.2.2 Interfacial Fracture Energy

In addition to the bond strength, fracture energy is a key parameter for concrete-to-concrete interface defining the interfacial debonding evolution. When cracks are formed in concrete, the work absorbed by the total fractured area is the work done by the external force (Bazant *et al.*, 1984):

$$W = S \int_0^{w_{cr}} \sigma dw \tag{6.3}$$

where S is the fracture area and w_{cr} is the maximum crack opening displacement when the interfacial stress decreases to zero. The work of the external forces absorbed by a unit of fracture area is defined as the fracture energy G_f:

$$G_f = \int_0^{w_{cr}} \sigma dw \tag{6.4}$$

The fracture energy can be generally taken as equal to the area under the bond-slip curve. It can be directly measured through concrete fracture tests. Moreover, relevant research has indicated that the fracture energy of concrete is related to the concrete strength, aggregate particle size, and mixing ratio of the concrete, among other factors, (Stankowski *et al.* 1993a). Therefore, analytical models have been proposed to estimate the fracture energy in addition to the experimental measurement.

The blunt crack zone model (Bazant *et al.* (1984) has been widely adopted to estimate the concrete fracture energy in studies involving concrete fracture mechanics. The fracture energy G_f required for the formation of crack per unit length is defined as:

$$G_f = w_c \frac{f_t^2}{2E_c}\left(1 - \frac{E_c}{E_t}\right)$$ (6.5)

where w_c is the width of the crack zone, f_t is the concrete tensile strength, E_c is the elastic modulus while E_t is the strain-softening modulus. The fracture energy is related to the elastic modulus and tensile strength of the concrete, as well as the width of the crack zone.

The test results presented in Chapter 5 show that the interfacial behaviour is mainly affected by the strengths of the new and old concretes, surface roughness, and applied compressive stress. Similar research on the interfacial fracture energy of concrete aggregate-mortar interfaces indicated that the interface roughness and strength of the material considerably influenced the fracture energy, which affected the shape of the softening stage of the bond-slip curve and ultimate displacement (Stankowski *et al.* 1993a). In the study on the FRP-concrete bonded interface, Lu *et al.* (2005) conducted a series of parametric analyses in the FE model and proposed a model for estimating the interfacial fracture energy G_f:

$$G_f = \alpha \beta_w^2 \sqrt{f_t} f\left(K_a\right)$$ (6.6)

where α is the specific parameter, β_w is the FRP-concrete width coefficient, f_t is the concrete tensile strength, K_a is the shear stiffness of the adhesive layer, and $f(K_a)$ is the factor indicating the influence of adhesive layer shear stiffness on the failure energy. These parameters were determined through regression. According to this model, the failure energy of concrete-to-concrete interfaces should be related to the tensile strength of the concrete and the shear modulus of the interface bond layer. Since concrete-to-concrete interfaces generally do not have a specific adhesive layer (unless the interface

201

agent is applied), the concrete surface roughness considerably influences the interface shear fracture energy.

6.3 BOND-SLIP MODEL

6.3.1 Experimental Observation of Bond-Slip behaviour

The shear bond-slip curves obtained in the tests in Chapter 5 showed that the shear bond-slip relationship of concrete-to-concrete interfaces under the action of shear mainly includes three stages: the linearly elastic stage, the softening stage, and the residual stress stage. Under various concrete strengths, surface roughness's, and interfacial compressive stresses, the former two stages of the bond-slip curves are similar, but the stress level in the residual stress stage is almost zero for smooth surface with no compressive stress and is non-zero otherwise. Based on these experimental observations, the bond-slip model, with two types, that is, a tri-linear model and a bi-linear model, is proposed to approximate the local bond-slip behaviour with or without a residual stress stage, respectively, as shown in Figure 6.1. The relatively simple bi-linear model is only suitable for the concrete-to-concrete interface without interfacial compressive stress, while the tri-linear model is suitable for other scenarios. It should be kept in mind that the bi-linear model is a special case of the trilinear model-with a zero residual stress. When either the bilinear or the trilinear form is used, the peak local interfacial shear stress and the fracture energy are equal.

The bi-linear model (Figure 6.1 (a)) is expressed as follows:

$$\tau = \tau_{\max} \frac{\delta}{\delta_1} \qquad if \qquad \delta \le \delta_1 \qquad\qquad (6.7a)$$

$$\tau = \tau_{\max} \frac{\delta_f - \delta}{\delta_f - \delta_1} \qquad if \qquad \delta_1 \le \delta \le \delta_f \qquad (6.7b)$$

$$\tau = 0 \qquad if \qquad \delta \ge \delta_f \qquad\qquad (6.7c)$$

$$\delta_f = \frac{2G_f}{\tau_{max}} \tag{6.7d}$$

where τ_{max} is the shear strength, δ_1 is the slip corresponding to the shear strength, δ_f is the ultimate slip, and G_f is the interfacial fracture energy. The ultimate slip is a dependent parameter that can be determined from the fracture energy and bond strength. The tri-linear model (Figure 6.1 (b)) is expressed as follows:

$$\tau = \tau_{max}\frac{\delta}{\delta_1} \qquad if \qquad \delta \leq \delta_1 \tag{6.8a}$$

$$\tau = (\tau_{max} - \tau_r)\frac{\delta_2 - \delta}{\delta_2 - \delta_1} + \tau_r \qquad if \qquad \delta_1 < \delta \leq \delta_2 \tag{6.8b}$$

$$\tau = \tau_r \qquad if \qquad \delta_2 < \delta \leq \delta_f \tag{6.8c}$$

$$\tau_r = \frac{2G_f - \tau_{max}\delta_2}{2\delta_f - \delta_1 - \delta_2} \tag{6.8d}$$

where τ_r is the residual shear stress, δ_2 is the slip corresponding to the beginning of the residual stress stage, and the other parameters are the same with those in the bi-linear model. The residual shear stress is a dependent parameter that can be determined from the other parameters: the interfacial fracture energy G_f, the shear strength τ_{max}, the slip corresponding to the shear strength δ_1, the slip corresponding to the beginning of the residual stress stage δ_2, and the ultimate slip δ_f. The determination of the values of these key parameters are discussed in detail below.

6.3.2 Interfacial Shear Strength

The interfacial shear strengths at the interfaces with various concrete strengths, surface roughness's, and compressive stress obtained from the test data are summarised in Table 6.1. It is seen that the shear strength increases with the tensile strengths of the old and new concretes, interface roughness, and applied compressive stress. According to the shear-friction theory, the shear strength of concrete-to-concrete interfaces is derived from two sources: cohesion and friction, which are respectively represented by the first and the second parts on the RHS (right-hand side) of Eq. 6.9 given below. As it was

found from the test results that the interfacial shear strength is proportional to the tensile strength of the old and new concretes and the interface roughness, the cohesion part is chosen to be the product of these three variables with coefficients for calibration. The friction part is chosen to be the product of the applied compressive stress and the friction coefficient. Therefore, the interfacial shear strength is proposed to have the following form:

$$\tau_{max} = \left(\alpha_1 + \alpha_2 R^{\alpha_3}\right) f_{t,o}^{\alpha_4} f_{t,n}^{\alpha_5} + \mu\sigma_n \tag{6.9}$$

where $f_{t,o}$ and $f_{t,n}$ represent the tensile strengths of old and new concretes, R is the surface roughness, σ_n is the applied compressive stress, α_1, α_2, α_3, α_4 and α_5 are coefficients to be calibrated by the test data, and the friction coefficient μ can be determined from *fib* model code (2013), as shown in Table 6.2. The tensile strength of old and new concretes $f_{t,o}$ and $f_{t,n}$ (*MPa*) can be predicted from the equation suggested by CEB-FIP code (1993) as follows:

$$f_t = 1.4\left(\frac{f_c - 8}{10}\right)^{\frac{2}{3}} \tag{6.10}$$

where f_c (*MPa*) is the cylinder compressive strength, which can be can be obtained by multiplying cube compressive strength with a factor of 0.79 (GB 50010-2010, 2010).

Regression analysis was performed using the test data presented in Table 6.1. The best-fitting values for the coefficients α_1, α_2, α_3, α_4 and α_5 are 0.964, 0.337, 0.803, 0.203 and 0.743, respectively. Therefore, the interfacial shear strength could be evaluated using the following equation:

$$\tau_{max} = \left(0.964 + 0.337 R^{0.803}\right) f_{t,o}^{0.203} f_{t,n}^{0.743} + \mu\sigma_n \tag{6.11}$$

This equation is calibrated with the concrete tensile strength f_t ranging from 1.2 MPa to 3.5 MPa, the surface roughness R ranging from 0 mm to 3 mm, and the applied normal stress σ_n ranging from 0 MPa to 3 MPa. The interfacial shear strengths predicted using Eq. 6.11 are listed in Table 6.1; comparison between the predictions and the experimental data indicates close agreement, as shown in Figure 6.2. The average ratio between the predictions and the test results is 1.008, and the standard deviation (STD) and coefficient of variation (CoV) are 0.096 and 0.096, respectively, as shown in Table 6.1.

6.3.3 Interfacial Fracture Energy

The interfacial fracture energy for the tested specimens were determined from the area under the corresponding bond-slip curve shown in Figure 5.16, and the calculated values of the interfacial fracture energy for all the tested specimens are listed in Table 6.1. For the bi-linear model, the fracture energy is straightforward. However, for the tri-linear model, the residual stress stage essentially represents the frictional behaviour of the interface after debonding, i.e., when the interface has fractured. Therefore, the area below the tri-linear bond-slip curve is the combined fracture and frictional energy. On the other hand, the frictional behaviour is integral to the interfacial behaviour especially when interfacial compressive stress is involved. As a convenient treatment, the frictional energy is incorporated into the fracture energy for the tri-linear bond-slip model. Since the frictional stress is defined constant in the tri-linear bond-slip model, the interfacial ultimate slip is infinite, which is impractical and results in an infinite frictional energy. Therefore, an artificial ultimate slip of 0.3 mm is defined in the present study to achieve comparable fracture and frictional energies, which will be further discussed in the following sub-section. Accordingly, the fracture energy for the tri-linear bond-slip model is calculated as the area below the bond-slip curve with an

ultimate slip of 0.3 mm.

Because the interfacial fracture energy is related to the tensile strengths of old and new concretes, surface roughness, and interfacial compressive stress, the following equation is proposed for the evaluation of the interfacial fracture energy based on the forms of the previous models:

$$G_f = \beta_1 f_{t,n}{}^{\beta_2} f_{t,o}{}^{\beta_3} (1 + \beta_4 R_m)^{\beta_5} \left(1 + \beta_6 \sigma_n\right)^{\beta_7} \tag{6.12}$$

where β_1, β_2, β_3, β_4, β_5, β_6, and β_7 are coefficients to be calibrated by the test data, and the other parameters are the same with those in Eq. 6.11. Regression analysis was performed using the test data in Table 6.1, and the best-fitting values for coefficients β_1, β_2, β_3, β_4, β_5, β_6, and β_7 are 0.084, 0.462, 0.354, 0.647, 0.548, 8.926 and 0.464, respectively. Therefore, the interfacial fracture energy can be estimated by the following equation:

$$G_f = 0.084 f_{t,n}{}^{0.462} f_{t,o}{}^{0.354} \left(1 + 0.647 R\right)^{0.548} \left(1 + 8.926 \sigma_n\right)^{0.464} \tag{6.13}$$

This equation is calibrated with the concrete tensile strength f_t ranging from 1.2 MPa to 3.5 MPa, the average roughness R ranging from 0 mm to 3 mm, and the applied compressive stress σ_n ranging from 0 MPa to 3 MPa.

Figure 6.3 shows the close agreement between the predictions using Eq. 6.12 and the experimental data. Specifically, the average ratio between the predictions and the test data is 1.031. The standard deviation (STD) and the coefficient of variation (CoV) are 0.099 and 0.096, respectively, as shown in Table 6.1.

6.3.4 Characteristic Interfacial Slips

For the bi-linear model, the slip corresponding to the shear strength δ_1 need to be determined. For the tri-linear model, the slip corresponding to the shear strength δ_1, the slip corresponding to the beginning of the residual stress stage δ_2, and the ultimate slip δ_f need to be determined. By reviewing the obtained bond-slip curves for all specimens listed in Table 6.1, no clear correlation was found between the characteristic slips with the tensile strengths of new and old concretes, interface roughness, or interfacial compressive stress. Instead, the values of the slips are fairly close for all specimens with various configurations. Therefore, the slips are determined to be constant values in the current study based on the test data. The ultimate slip δ_f for the trilinear model is determined by the tested bond-slip curves of those specimens with interfacial compressive stress. For this type of specimen, the tested bond-slip curve ends with approximately a constant stress. It should be considered that the interface has been completely debonded with large slip, while this stress was only provided by the friction. Combined with the test results, 0.3 mm was taken as the ultimate slip δ_f. The values of these slips are expected to vary for different concrete-to-concrete interfaces. Therefore, calibration may be needed to determine their values for other interfaces. Nevertheless, the predictions obtained using the current model are in good agreement with the experimental results.

Therefore, the following values of the characteristic slips closely represent the interfacial behaviour:

For both the bi-linear and tri-linear model

$$\delta_1=0.016 \text{ mm} \tag{6.14}$$

Only for the tri-linear model

$$\delta_2 = 0.10 \text{ mm} \qquad\qquad (6.15)$$

$$\delta_f = 0.30 \text{ mm} \qquad\qquad (6.16)$$

The proposed shear bond-slip model for concrete-to-concrete interfaces includes Eqs. 6.7, 6.8, 6.11, 6.13-6.16. The prediction results of the shear bond-slip model were compared with the test results. Figure 6.4 presents the comparison between the predicted versus experimental bond-slip curves. Only some representative specimens O20-N40-R0-S0 of Series-I, O20-N40-R2-S0 of Series-II, O20-N40-R0-S0.5 of Series-III, O20-N40-R1-S0.5 of Series-IV were displayed in this figure. The comparison between the experimental bond-slip curves and the predicted curves for all specimens are shown in Appendix Figure A6.1 to Figure A6.4.

It can be observed that a close agreement has been achieved between the predictions with the proposed bond-slip model and the test data. This is not surprising since the same test data were used to determine the key parameters of the bond-slip relationships. It can also be indicated that for the specimen without applied normal stress, both the bi-linear model and the tri-linear model are applicable within a certain allowable error range.

6.4 COMPARISONS BETWEEN FE AND TEST RESULTS FOR LOAD-SLIP BEHAVIOUR

In this section, the tested L-shaped one interface specimens are simulated using FE models incorporating the developed bond-slip models. Specifically, the concrete was simulated by the damage-plasticity constitutive model, and the concrete-to-concrete interface is modelled using cohesive elements. The predicted results are compared with the experimental data to validate the bond-slip model.

6.4.1 Constitutive Modelling of Concrete

The damage-plasticity model built-in ABAQUS (Lubliner *et al.*, 1989; Lee and Fenves, 1998) was employed to simulate the concrete blocks. The model is characterised with uncoupled damage and plasticity evolution. The concrete tensile cracking was simulated using the crack band model built-in the framework of the damage-plasticity model.

For concrete under uniaxial compression, the axial stress-axial strain relationship suggested by Saenz (1964) was adopted:

$$\sigma_c = \frac{\alpha \varepsilon_c}{1+[(\alpha \varepsilon_p / \sigma_p)-2](\varepsilon_c / \varepsilon_p)+(\varepsilon_c / \varepsilon_p)^2} \tag{6.17}$$

where σ_c and ε_c denote the axial stress and axial strain, respectively; σ_p and ε_p are the peak axial stress and the corresponding axial strain, which are equal to the uniaxial cylinder compressive strength f_c and the corresponding axial strain of concrete; α is the elastic modulus of concrete. Equation $E_c = 4730\sqrt{f_c}$ from the ACI Code (2008) was employed to predict the elastic modulus of concrete, based on the uniaxial compressive strength if the experimental data are not available to determine the elastic modulus.

When concrete under uniaxial tension, the tensile strength of concrete f_t (*MPa*) can be predicted with the data of the compressive strength f_c (*MPa*), according to equation 6.10 mentioned above. The concrete tensile softening model proposed by Hordijk (1991) was used for the tensile softening behaviour of concrete as follows:

$$\frac{\sigma_t}{f_t} = [1 + \left(c_1 \frac{w_t}{w_{cr}}\right)^3] e^{\left(-c_2 \frac{w_t}{w_{cr}}\right)} - \frac{w_t}{w_{cr}}(1 + c_1^3)e^{-c_2} \tag{6.18}$$

where σ_t is the tensile stress, c_1 and c_2 are coefficients taken as 3.0 and 6.93, respectively, w_t is the crack opening displacement, and w_{cr} is the crack opening displacement at the complete release of stress or fracture energy. The value of w_{cr} (*mm*) can be calculated from the tensile fracture energy using the following equation (Hordijk, 1991):

$$w_{cr} = 5.14 \frac{G_F}{f_t} \tag{6.19}$$

The tensile fracture energy G_F (*N/m*), which was proposed by CEB-FIP (1993) was adopted:

$$G_F = \left(0.0469 d_a^2 - 0.5d + 26\right)\left(\frac{f_c}{10}\right)^{0.7} \tag{6.20}$$

where d_a (*mm*) is the maximum aggregate size and f_c is the compressive strength in *MPa*.

The compressive and tensile damage evolution for concrete were considered in the proposed FE model. Two damage variables d_c and d_t were employed to simulate the concrete damage when under compression or tension. According to Yu *et al.* (2010), for concrete subjected to compression, the damage variable d_c is set to zero before reaching the strength, and it is determined using the following equation in the post-peak regime:

$$d_c = 1 - \frac{\sigma_c}{f_c} \tag{6.21}$$

The shear retention factor considerably influences the shear behaviour after concrete cracking (Chen *et al.* 2012; Zhang and Teng, 2014). Following shear retention model

was used, which was proposed by to Rots (1988), to simulate the shear resistance degradation of cracked concrete:

$$\gamma = \left(1 - \frac{\varepsilon_{cr}}{\varepsilon_{cr,u}}\right)^n \qquad (6.22)$$

$$d_t = 1 - \gamma \qquad (6.23)$$

where ε_{cr} is the concrete cracking strain corresponding to crack opening displacement w_t (Eq. 6.18), $\varepsilon_{cr,u}$ is the maximum principal concrete cracking strain at crack opening width w_{cr} (Eq. 6.18), and n is a parameter that reflects the shear resistance feature of cracked concrete. In the present study, a value of $n=5$ was selected according to (Chen $et\ al.$ 2012).

The relationship between ε_{cr} and w_t and that between $\varepsilon_{cr,u}$ and w_{cr} can be obtained through the equation provided by Bazant and Planas (1997), as follows:

$$w = \int_{h_c} \varepsilon_{cr} dh \qquad (6.24)$$

The crack band width h_c is defined as the characteristic length of the element, which was $\sqrt{2}e$ (e is the side length of the element) for a plane stress four-node square element in a two-dimensional FE model (Zhang and Teng, 2014).

6.4.2 Bond-slip Model for Concrete-to-Concrete Interfaces

(1) Tangential bond-slip model

In the analysis of the tested specimens, the tangential behaviour at the concrete-to-concrete interface was simulated by the developed bond-slip model described in Section

6.3. The key parameters of the model include the maximum shear stress τ_{max}, fracture energy G_f, and the characteristic slips δ_1 and δ_f, as shown in Figure 6.1.

(2) Normal bond-opening model

The bond-opening behaviour in the normal direction at the interface is simulated using a bi-linear bond-separation model (Teng *et al*. 2015), which consists of a linear elastic stage up to the interfacial maximum tensile stress at the corresponding opening and a linear softening stage terminated at a maximum opening where the tensile stress vanishes. The maximum opening can be determined from the interfacial fracture energy. The maximum tensile stress, elastic modulus and fracture energy of the interface were assumed to be 50% of those of the base concrete, as suggested by Zanotti and Randl, (2019).

(3) Mixed-mode cohesive law

The tangential and normal models are combined into a mixed-mode cohesive law, which could predict the interfacial normal and shear behaviour under coupled slip and opening. The following equation defines the linear-elastic interfacial behaviour before reaching the peak stress (initiation of damage):

$$\sigma = \left\{ \begin{matrix} \sigma_n \\ \sigma_s \\ \sigma_t \end{matrix} \right\} = \begin{bmatrix} K_{nn} & 0 & 0 \\ 0 & K_{ss} & 0 \\ 0 & 0 & K_{tt} \end{bmatrix} \left\{ \begin{matrix} \varepsilon_n \\ \varepsilon_s \\ \varepsilon_t \end{matrix} \right\} = K\varepsilon \qquad (6.25)$$

where σ_n, σ_s and σ_t represent the normal and two shear stresses, ε_n, ε_s and ε_t represent the normal and two shear strains; and K_{nn}, K_{ss} and K_{tt} denote the elastic stiffness values of the normal and two shear directions, respectively. K_{nn} was set equal to the initial slope of the bond-separation model, and K_{ss} and K_{tt} were set equal to the initial slope of the shear bond-slip model.

The reaching of the peak nominal stress or initiation of damage quadratic is defined by the quadratic criterion as shown in Equation 6.26. In this case, the damage is assumed to initiate when the combination of the normal and shear stresses satisfy the below equation:

$$\left\{\frac{\langle t_n \rangle}{t_n^0}\right\}^2 + \left\{\frac{t_s}{t_s^0}\right\}^2 + \left\{\frac{t_t}{t_t^0}\right\}^2 = 1 \tag{6.26}$$

where t_n^0, t_s^0 and t_t^0 represent the maximum normal and shear stresses, respectively.

$\langle \rangle$ is the Macaulay bracket denoting that only tensile stress is considered in the damage initiation criterion.

The mode-mix definition based on non-accumulated energies was adopted to define the damage evolution. The linear criterion was adopted, as suggested by Teng *et al.* (2015):

$$\frac{G_n^*}{G_{\mathrm{I}}} + \frac{G_s}{G_{\mathrm{II}}} + \frac{G_t}{G_{\mathrm{II}}} = 1 \tag{6.27}$$

where G_n, G_s, and G_t represent the work done in the normal, first, and second shear directions, respectively. G_{I} and G_{II} are the interfacial fracture energies under tension and shear, respectively.

Equation 6.28 represents the effective separation under the mixed mode. Since the interface is subjected to a combined normal tensile stress and tangential shear stress, δ_m is introduced to represent the effective displacement under the mixed mode. Equation 6.28 was developed by Camanho *et al.* (2003).

$$\delta_m = \sqrt{\langle \delta_n \rangle^2 + \delta_s^2 + \delta_t^2} \tag{6.28}$$

Equation 6.29 represents the linear damage evolution proposed by Camanho *et al.* (2003).

$$D = \frac{\delta_m^f (\delta_m^{max} - \delta_m^0)}{\delta_m^{max} (\delta_m^f - \delta_m^0)}$$

(6.29)

Here, D is the damage variable, δ_m^{max} is the maximum effective displacement reached during the history of loading, δ_m^f is the effective displacement at complete failure, and δ_m^0 is the effective displacement at the initiation of damage.

6.4.3 Element Type and Mesh

Four-node plane stress elements with reduced integration (CPS4R) were used to model the concrete. The interface between the concrete-to-concrete interfaces were modelled as zero thickness cohesive zone, as schematically shown in Figure 6.5. The dimension of the FE model was the same as the specimen described in Chapter 5. The mesh and the boundary condition were the same with those in the FE model shown in Chapter 3 and are not repeated.

6.4.4 Comparisons between FE Predictions and Test Results

With the above FE model and the bond-slip models presented in Section 6.3 (i.e., the bi-linear model for specimen without applied compressive stress and the tri-linear model for other specimens), the load-slip curves for the tested specimens were predicted. Figure 6.6 presents the comparison between the prediction and experimental data for four representative specimens of the four series, i.e., O20-N40-R0-S0 of Series-I, O20-N40-R2-S0 of Series-II, O20-N40-R0-S0.5 of Series-III, O20-N40-R1-S0.5 of Series-IV. The comparisons for other specimens are similar and are shown in Figure A6.5 to Figure A6.8 in Appendix A.

It can be seen from the comparison that the shear load-slip behaviour obtained by the FE model is in good agreement with the test data. This indicates that based on the developed bond-slip model for concrete-to-concrete interfaces, the shear capacity of the interfaces can be accurately predicted. Most of the predicted elastic stiffness are close to the experimental data, although some of the calculated elastic stiffnesses are slightly lower than the test data. This is mainly due to that the scatter of the slips corresponding to the maximum stress, as shown between the results of the nominally identical specimens in Figure 6.6. Additionally, the slips are also different for specimens with different configurations. Since the differences are slight, the value of the characteristic slip corresponding to the maximum shear stress is taken as the same value for all specimens. Therefore, slight deviations between the predictions and experimental data can be observed for the interfacial stiffness.

Regarding the softening stage, the predictions generally agree well with the test results. For specimens without normal stress, as shown in Figure 6.6 (a) and (b), both the bi-linear model and tri-linear model predictions are close to the measured load-slip curves. The former gives a zero-stress debonded response while the latter gives a residual frictional stress. By contrast, for specimens with compressive stress at the interface, as shown in Figure 6.6 (c) and (d), only the tri-linear model can predict the residual stress after debonding. While the linear elastic and softening stages are well predicted by the tri-linear model, some degree of inaccuracy is seen for the residual load. The experimental data often show a slightly declining residual load as the slip increases, while the residual load predicted by the FE model is constant due to the constant residual stress of the proposed tri-linear model. As a result, further improvement of the bond-slip model is expected in future research.

Figure 6.7 depicts the predicted versus experimental slip distributions for specimen

O20-N40-R0-S0-I at various load levels. It can be seen from the comparison results that FE results can also generally provide accurate interfacial slip distributions at different loading levels based on the bi-linear bond-slip model, as discussed in Chapter 5. Figure 6.8 shows the predicted interfacial stress distributions at different loading levels, which are very difficult to be obtain experimentally. The FE results show that the peak stress of the entire interface is the largest at peak load. After the peak point, the stress of the entire interface decreases. This indicates that the concrete-to-concrete interface has experienced the process of reaching shear strength first and then softening. The predicted results also show that, the overall interfacial stress distribution in the middle part is relatively uniform, except the two ends of the interface, which verifies the rationality of the experimental design.

6.5 CONCLUSIONS

Establishing an accurate bond-slip model for the concrete-to-concrete interface is critical for understanding the mechanical behaviour and the accurate numerical simulations of structural members with such interfaces. However, an accurate local bond-slip model has not been achieved yet. The experimental results presented in Chapter 5 identified the three key parameters for the interfacial bond-slip behaviour, including concrete strength, surface roughness and applied normal stress. This chapter has described the formulation of a bond-slip model for concrete-to-concrete interfaces based on the experimental results.

Based on the test results, for concrete-to-concrete interfaces without normal stress, the relatively simple bi-linear model is suitable; for the other interfaces, the tri-linear model can be used. The shear strength is related to the tensile strengths of the old and new concretes, surface roughness, and applied compressive stress. An expression of the

shear strength has been developed based on the existing interfacial shear strength models. A regression analysis was performed to calibrate the coefficients in this expression. Similarly, the fracture energy is also related to these parameters, and a form of fracture energy has been developed based on the existing models for interfacial fracture energy. The coefficients of the fracture energy expression were then calibrated based on regression of the test data.

By contrast, reviewing the obtained bond-slip curves for all specimens indicates no clear correlation between the characteristic slips and the tensile strengths of new and old concretes, surface roughness, or interfacial compressive stress. Instead, the values of the slips are fairly close for all specimens with various configurations. Therefore, the slips are determined to be constant values in the bond-slip model. The values of these slips are expected to vary for different concrete-to-concrete interfaces. Therefore, calibration may be needed to determine their values for other interfaces. Nevertheless, the predictions obtained using the current model are in good agreement with the experimental results.

Finally, FE analyses of the tested L-shaped one interface specimens were conducted to verify the developed bond-slip model. Specifically, the concrete was simulated by the damage-plasticity constitutive model, and the concrete-to-concrete interface was modelled using cohesive elements governed by the developed bond-slip models. The shear load-slip behaviour obtained by the FE model was compared to the experimental data, and the predicted interfacial stiffness, shear strength, and the critical slips were all in good agreement with the test data, indicating that based on the developed bond-slip model for concrete-to-concrete interfaces, the interfacial behaviour can be predicted with good accuracy. Therefore, the developed bond-slip model could be used to more accurately predict the behaviour of concrete members containing interfaces.

217

In this chapter, a bond-slip model and a set of key parameters has been proposed. The effects of concrete strength, surface roughness and normal stress on the values of the key parameters have been investigated through an experimental programme using the modified test method. Based on the test data, a set of equations was proposed to determine the values of the key parameters. It is noted that the number of test specimens was quite limited. For example, only normal strength concrete was considered. Meanwhile, both the surface roughness and external normal stress were limited within a certain range. Therefore, more test data are needed in the future to improve the accuracy and applicability of the proposed equations for determining the values of the key parameters.

6.6 REFERENCES

American Concrete Institute (ACI). (2008). *Building code requirements for structural concrete and commentary*. ACI 318, Farmington Hills, MI.

Bažant, Z. P. (1984). Size effect in blunt fracture: concrete, rock, metal. *Journal of Engineering Mechanics*, 110(4), 518-535.

Bazant Z. P., Planas J. (1977). Fracture and size effect in concrete and other quasibrittle materials. CRC Press.

Birkeland, P. W., & Birkeland, H. W. (1966). Connections in precast concrete construction. *PCI Journal Proceedings*, 63(3), 345-368.

Camanho, P. P., Davila, C. G., de Moura M. F. (2003). Numerical simulation of mixed-mode progressive delamination in composite materials. *Journal of Composite Materials*, 37, 1415-1438.

GB 50010-2010. (2010). *Code for desing of concrete structures*. Beijing, China Architecture & Building Press.

CEB-FIP. (1993). *Model Code 90*, Lausanne, Switzerland.

Chen, G. M., Chen, J. F., & Teng, J. G. (2012). On the finite element modelling of RC beams shear-strengthened with FRP. *Construction and Building Materials*, 32, 13-26.

*f*ib model code for concrete structures 2010. (2013). Berlin, Germany.

Lee, J., & Fenves, G. L. (1998). Plastic-damage model for cyclic loading of concrete structures. *Journal of Engineering Mechanics*, 124(8), 892-900.

Lu, X. Z., Teng, J. G., Ye, L. P., & Jiang, J. J. (2005). Bond–slip models for FRP sheets/plates bonded to concrete. *Engineering Structures*, 27(6), 920-937.

Lubliner, J., Oliver, J., Oller, S., & Oñate, E. (1989). A plastic-damage model for concrete. *International Journal of Solids and Structures*, 25(3), 299-326.

Mattock, A. H., & Hawkins, N. M. (1972). Shear transfer in reinforced concrete Recent research. *PCI Journal*, 17(2), 55-75.

Mohamad, M. E., Ibrahim, I. S., Abdullah, R., Rahman, A. A., Kueh, A. B. H., & Usman, J. (2015). Friction and cohesion coefficients of composite concrete-to-concrete bond. *Cement and Concrete Composites*, 56, 1-14.

Randl, N. (1997) Investigations on transfer of forces between old and new concrete at different joint roughness. PhD. thesis. Austria: University of Innsbruck.

Randl, N. (2013). Design recommendations for interface shear transfer in fib Model Code 2010. *Structural Concrete*, 14(3), 230-241.

Rots JG. (1988). Computational modeling of concrete fracture. *PhD Thesis*, Delft University of Technology.

Saenz, L. P. (1964). Discussion of equation for the stress-strain curve of concrete by

Desayi and Krishnan. *ACI Journal*, 61(9), 1229-1235.

Santos, P., & Júlio, E. N. (2014). Interface shear transfer on composite concrete members. *ACI Structural Journal*, 111(1), 113-120.

Shah, S. G., & Kishen, J. C. (2010a). Nonlinear fracture properties of concrete–concrete interfaces. *Mechanics of Materials*, 42(10), 916-931.

Shah, S. G., & Kishen, J. C. (2010b). Fracture behavior of concrete–concrete interface using acoustic emission technique. *Engineering Fracture Mechanics*, 77(6), 908-924.

Stankowski, T., Runesson, K., & Sture, S. (1993a). Fracture and slip of interfaces in cementitious composites. I: Characteristics. *Journal of Engineering Mechanics*, 119(2), 292-314.

Stankowski, T., Runesson, K., & Sture, S. (1993b). Fracture and slip of interfaces in cementitious composites. II: Implementation. *Journal of Engineering Mechanics*, 119(2), 315-327.

Teng, J. G., Fernando, D., & Yu, T. (2015). Finite element modelling of debonding failures in steel beams flexurally strengthened with CFRP laminates. *Engineering Structures*, 86, 213-224.

Walraven, J. (1987). Influence of concrete strength and load history on the shear friction capacity of concrete members. *PCI Journal*, 32(1), 66-83.

Yu, T., Teng, J. G., Wong, Y. L., & Dong, S. L. (2010). Finite element modeling of confined concrete-II: Plastic-damage model. *Engineering structures*, 32(3), 680-691.

Zanotti, C., & Randl, N. (2019). Are concrete-to-concrete bond tests comparable?. *Cement and Concrete Composites*, 99, 80-88.

Zhang, S. S., & Teng, J. G. (2014). Finite element analysis of end cover separation in RC beams strengthened in flexure with FRP. *Engineering Structures*, 75, 550-560.
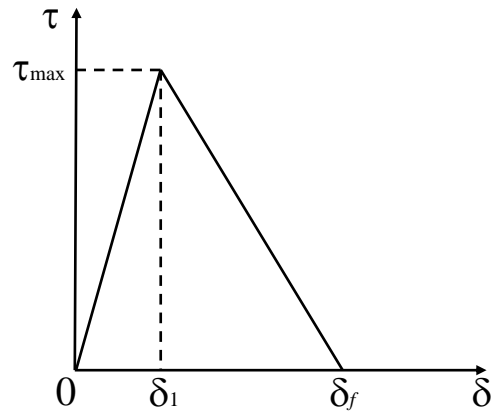
Table 6.1 Comparison between predictions and test results

Series	Specimen	$f_{cu,o}$ (MPa)	$f_{cu,n}$ (MPa)	$f_{t,o}$ (MPa)	$f_{t,n}$ (MPa)	R (mm)	σ (MPa)	τ_{max} (MPa)			G_f (N/mm)		
								Predicted	Test result	Predicted / Test result	Predicted	Test result	Predicted / Test result
Series-I	O20-N40-R0-S0-I	22.8	42.5	1.4	2.6	0	0	2.111	1.769	1.194	0.151	0.131	1.156
	O20-N40-R0-S0-II	22.8	42.5	1.4	2.6	0	0	2.111	1.844	1.145	0.151	0.128	1.177
	O20-N20-R0-S0-I	22.8	23.2	1.4	1.4	0	0	1.345	1.625	0.827	0.114	0.104	1.100
	O20-N20-R0-S0-II	22.8	23.2	1.4	1.4	0	0	1.345	1.263	1.065	0.114	0.109	1.045
	O20-N60-R0-S0-I	22.8	59.6	1.4	3.5	0	0	2.604	2.767	0.941	0.172	0.158	1.088
	O20-N60-R0-S0-II	22.8	59.6	1.4	3.5	0	0	2.604	2.692	0.967	0.172	0.155	1.115
	O40-N40-R0-S0-I	43.1	42.5	2.6	2.6	0	0	2.403	1.918	1.252	0.189	0.162	1.170
	O40-N40-R0-S0-II	43.1	42.5	2.6	2.6	0	0	2.403	2.277	1.055	0.189	0.158	1.197
	O60-N40-R0-S0-I	57.3	42.5	3.4	2.6	0	0	2.523	2.849	0.886	0.206	0.251	0.821
	O60-N40-R0-S0-II	57.3	42.5	3.4	2.6	0	0	2.523	2.664	0.947	0.206	0.230	0.896
Series-II	O20-N40-R1-S0-I	21.5	43.1	1.3	2.6	0.9	0	2.771	3.059	0.906	0.191	0.168	1.137
	O20-N40-R1-S0-II	21.5	43.1	1.3	2.6	0.9	0	2.771	2.550	1.087	0.191	0.184	1.034
	O20-N40-R2-S0-I	21.5	43.1	1.3	2.6	2.2	0	3.478	3.194	1.089	0.241	0.219	1.099
	O20-N40-R2-S0-II	21.5	43.1	1.3	2.6	2.2	0	3.478	3.623	0.960	0.241	0.261	0.921
	O20-N40-R3-S0-I	21.5	43.1	1.3	2.6	3.2	0	3.963	3.633	1.091	0.274	0.296	0.926
	O20-N40-R3-S0-II	21.5	43.1	1.3	2.6	3.2	0	3.963	4.302	0.921	0.274	0.290	0.946
Series-III	O20-N40-R0-S0.5-I	19.8	40.8	1.2	2.5	0	0.5	2.178	2.013	1.082	0.306	0.280	1.092
	O20-N40-R0-S0.5-II	19.8	40.8	1.2	2.5	0	0.5	2.178	2.187	0.996	0.306	0.311	0.985
	O20-N40-R0-S1.0-I	19.8	40.8	1.2	2.5	0	1	2.378	2.378	1.000	0.404	0.426	0.949
	O20-N40-R0-S1.0-II	19.8	40.8	1.2	2.5	0	1	2.378	2.487	0.956	0.404	0.432	0.935
	O20-N40-R0-S1.5-I	19.8	40.8	1.2	2.5	0	1.5	2.578	2.642	0.976	0.480	0.444	1.082
	O20-N40-R0-S1.5-II	19.8	40.8	1.2	2.5	0	1.5	2.578	2.916	0.884	0.480	0.505	0.951
Series-IV	O20-N40-R1-S0.5-I	23.4	43.7	1.4	2.7	1	0.5	3.218	3.013	1.068	0.447	0.413	1.082
	O20-N40-R1-S0.5-II	23.4	43.7	1.4	2.7	1	0.5	3.218	3.313	0.971	0.447	0.467	0.957

|											
O20-N40-R2-S1.0-I	23.4	43.7	1.4	2.7	1.9	1.0	4.327	4.593	0.942	0.696	0.761	0.914
O20-N40-R2-S1.0-II	23.4	43.7	1.4	2.7	1.9	1.0	4.327	4.246	1.019	0.696	0.693	1.004
O20-N40-R3-S1.5-I	23.4	43.7	1.4	2.7	3.1	1.5	5.837	5.992	0.974	0.974	0.965	1.009
O20-N40-R3-S1.5-II	23.4	43.7	1.4	2.7	3.1	1.5	5.837	5.687	1.026	0.974	0.898	1.084
Average=									1.008		1.031	
STD=									0.096		0.099	
CoV=									0.096		0.096	

Table 6.2 Relationship between R and μ

R	Interface	$f$ib Model 2010 μ	This study
0 mm	Very Smooth	-	0.4
1 mm	$<$1.5 mm Smooth	0.5-0.7	0.6
2 mm	$\geq$1.5 mm Rough	0.7-1.0	0.9
3 mm	$\geq$3 mm Very Rough	1.0-1.4	1.2

(a) Bi-linear model
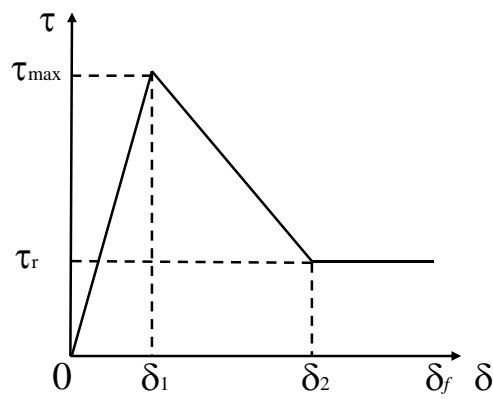
(b) Tri-linear model

Figure 6.1 Proposed bond-slip models
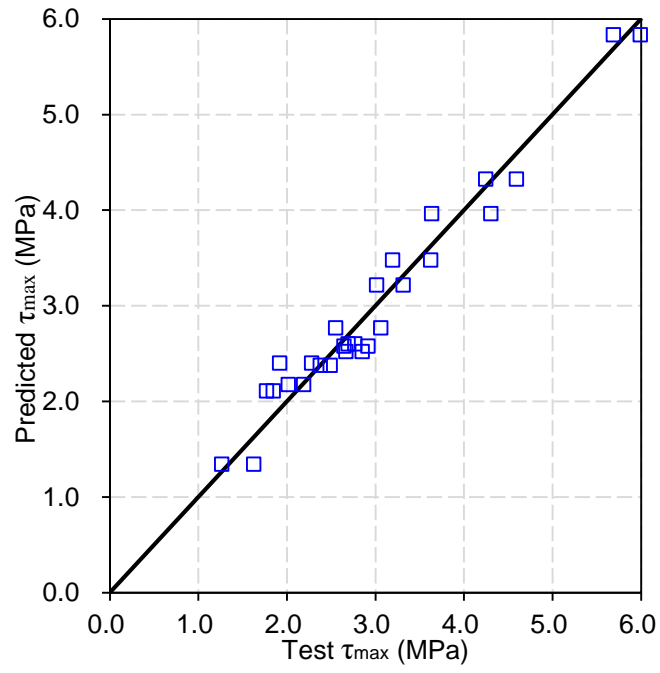
Figure 6.2 Comparison between predicted bond-slip curves and test results for τ_{max}
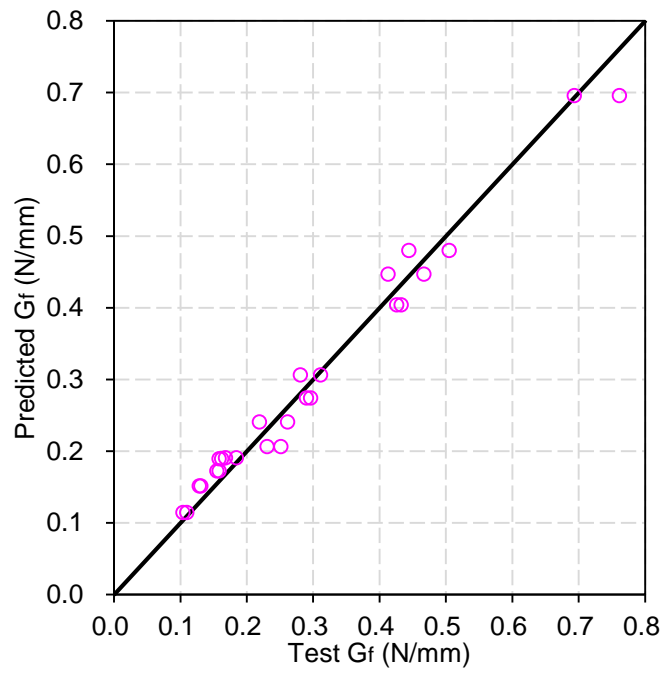
Figure 6.3 Comparison between predictions and test results for G_f
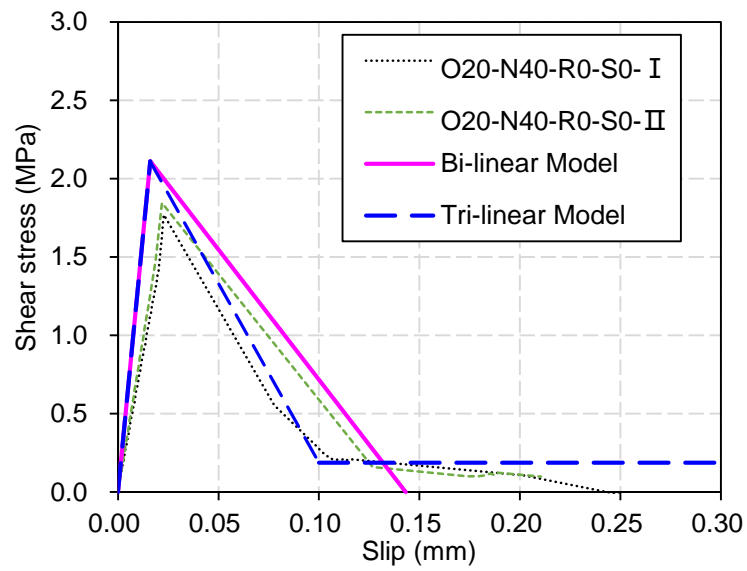
(a) Specimen O20-N40-R0-S0 of Series-I
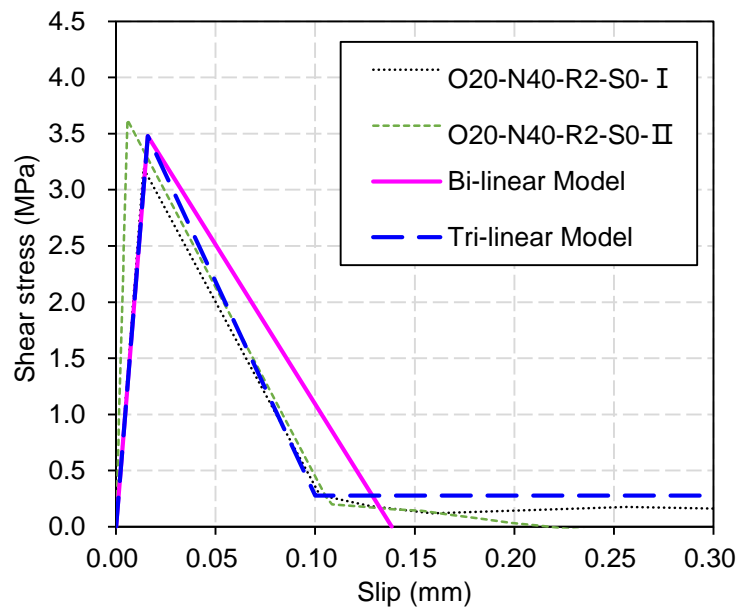
(b) Specimen O20-N40-R2-S0 of Series-II
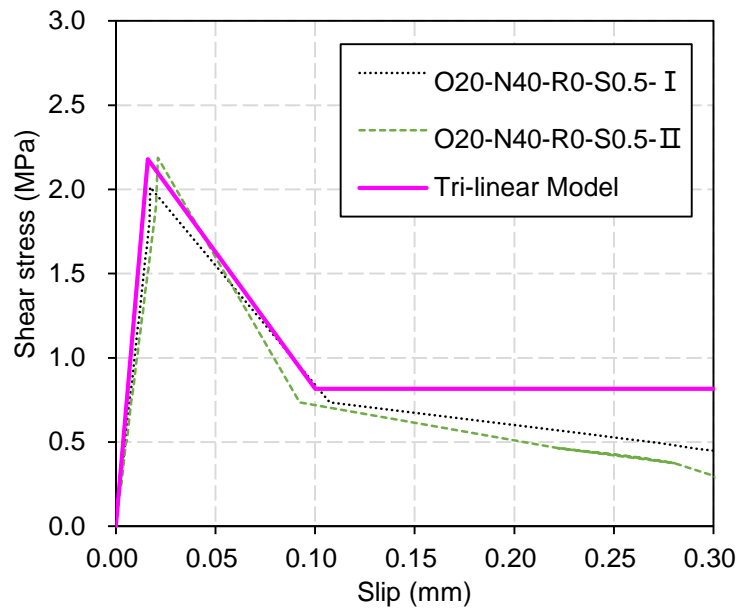
(c) Specimen O20-N40-R0-S0.5 of Series-III
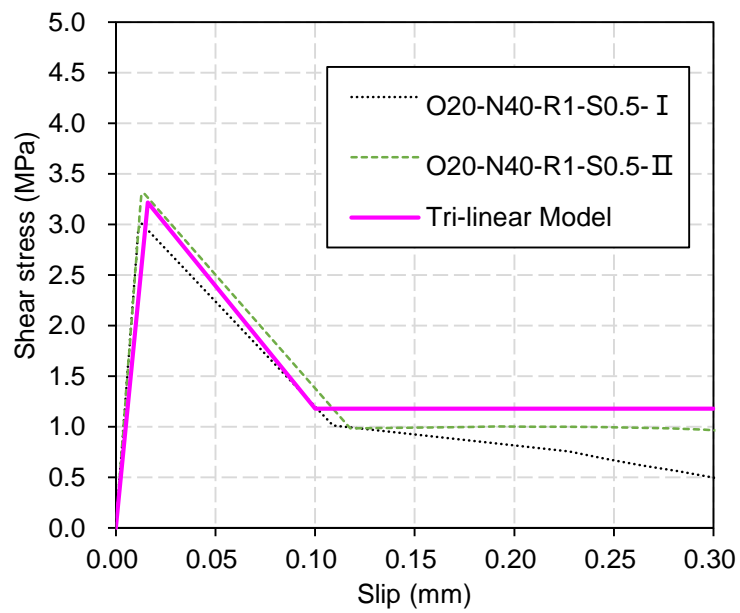
(d) Specimen O20-N40-R1-S0.5 of Series-IV

Figure 6.4 Predicted versus experimental bond-slip curves
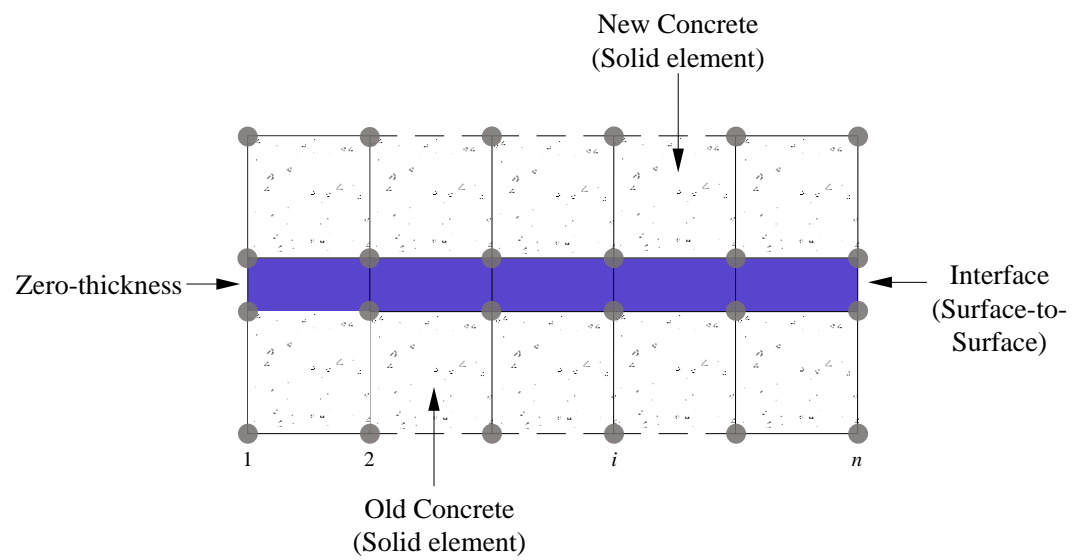
Figure 6.5 Simulation of the concrete-to-concrete interfaces
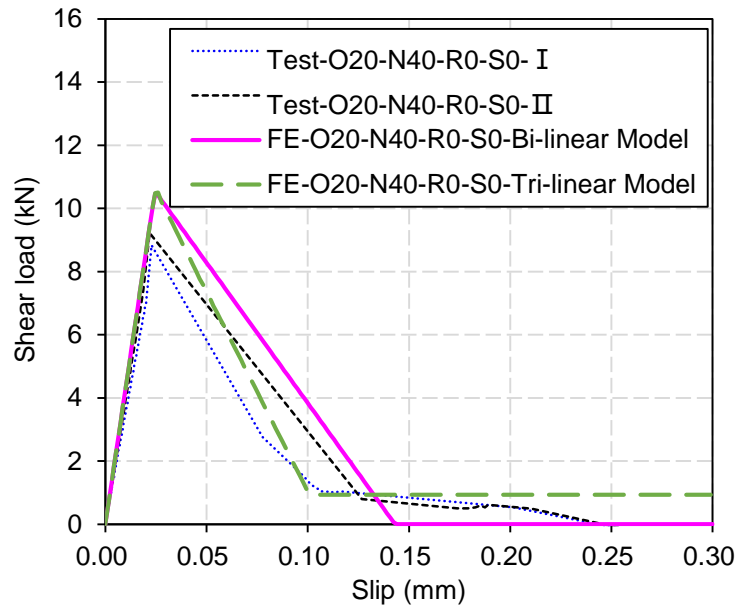
(a) Specimen O20-N40-R0-S0 of Series-I
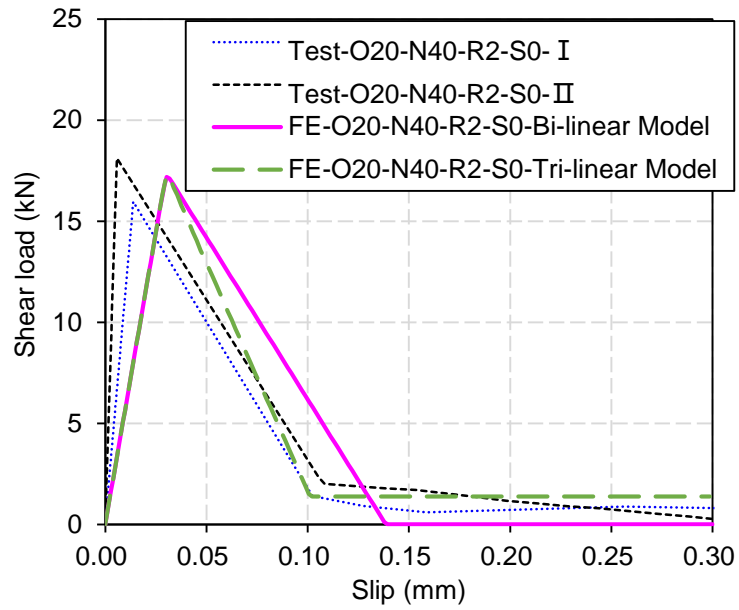
(b) Specimen O20-N40-R2-S0 of Series-II
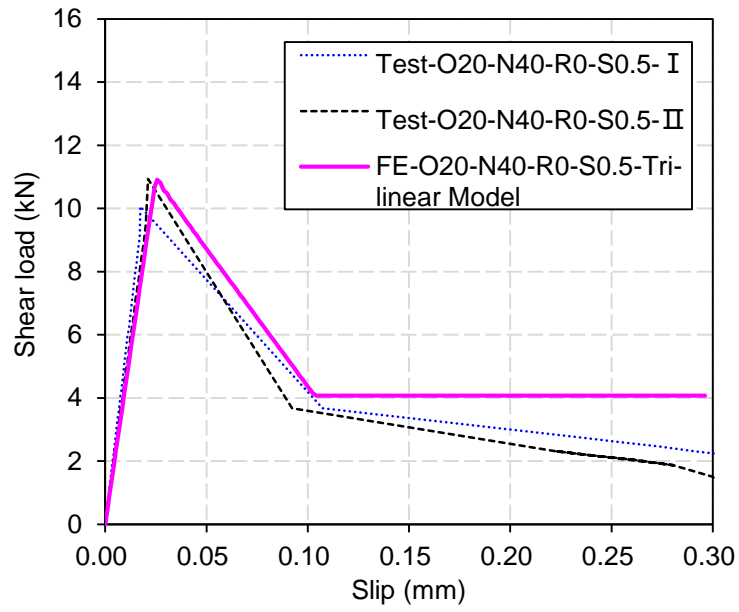
(c) Specimen O20-N40-R0-S0.5 of Series-III
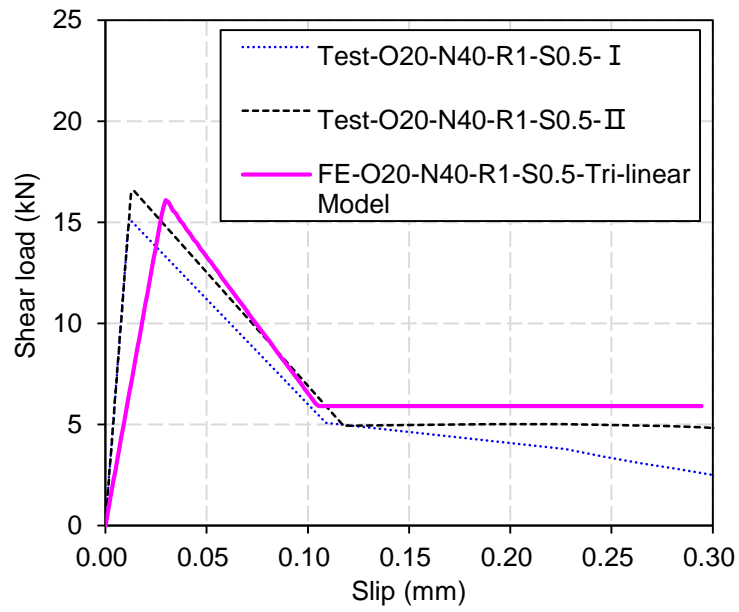
(d) Specimen O20-N40-R1-S0.5 of Series-IV

Figure 6.6 Predicted versus experimental load-slip curves
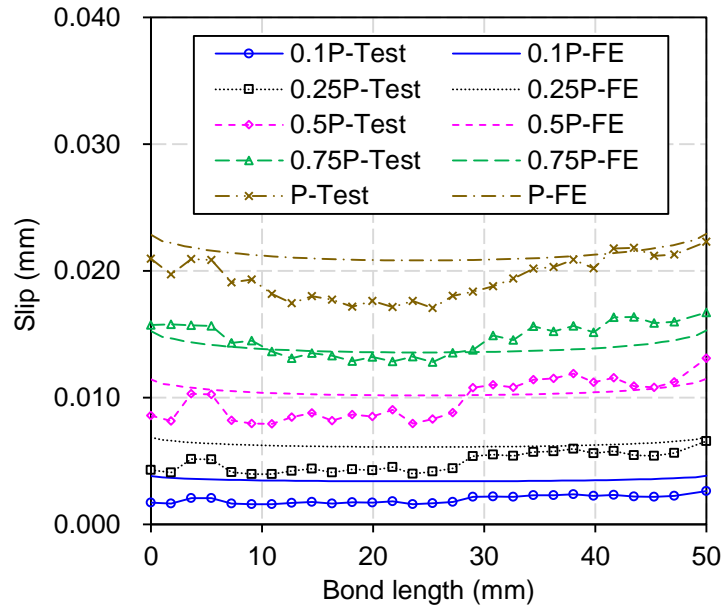
Figure 6.7 Predicted versus experimental slip distributions for specimen O20-N40-R0-S0-I
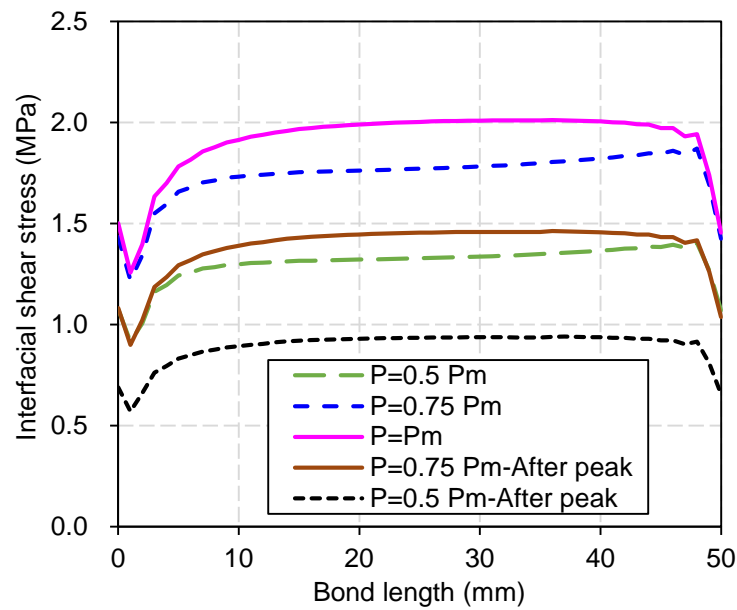
Figure 6.8 Predicted interfacial stress distributions for specimen O20-N40-R0-S0-I

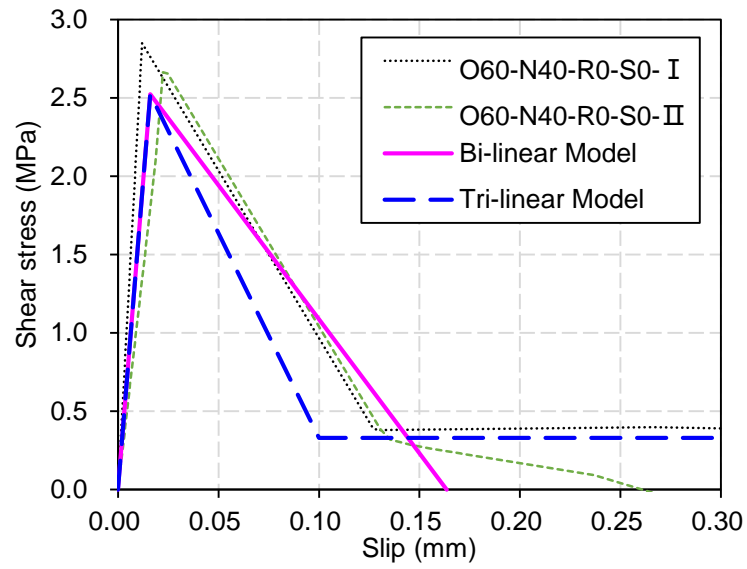# APPENDIX A: ADDITIONAL FIGURES

(a) Specimen O20-N20-R0-S0

(b) Specimen O20-N40-R0-S0
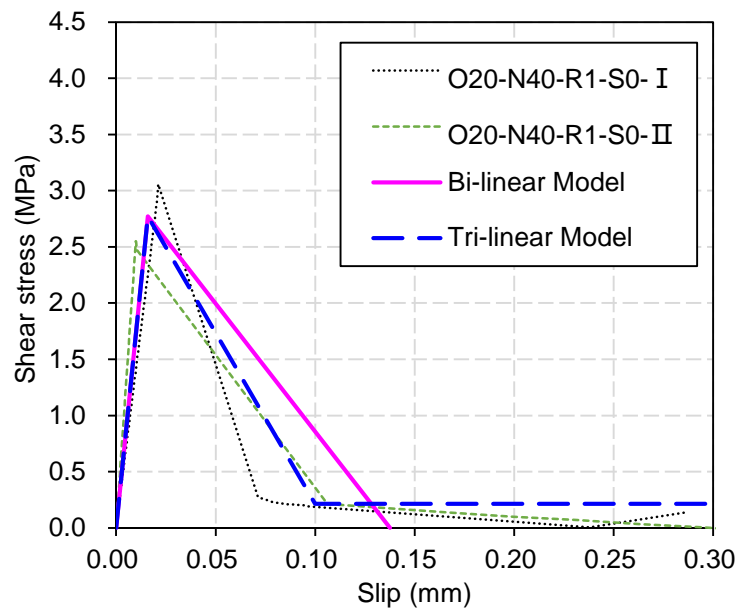
(c) Specimen O20-N60-R0-S0
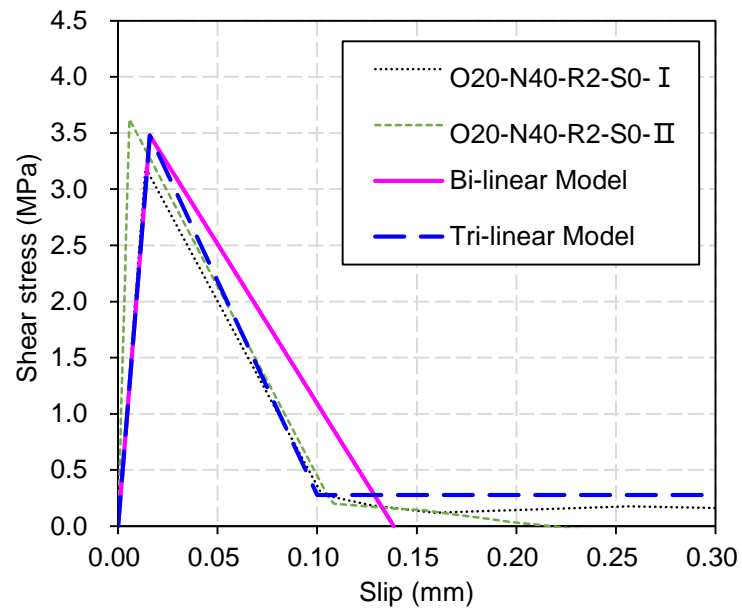

(d) Specimen O40-N40-R0-S0
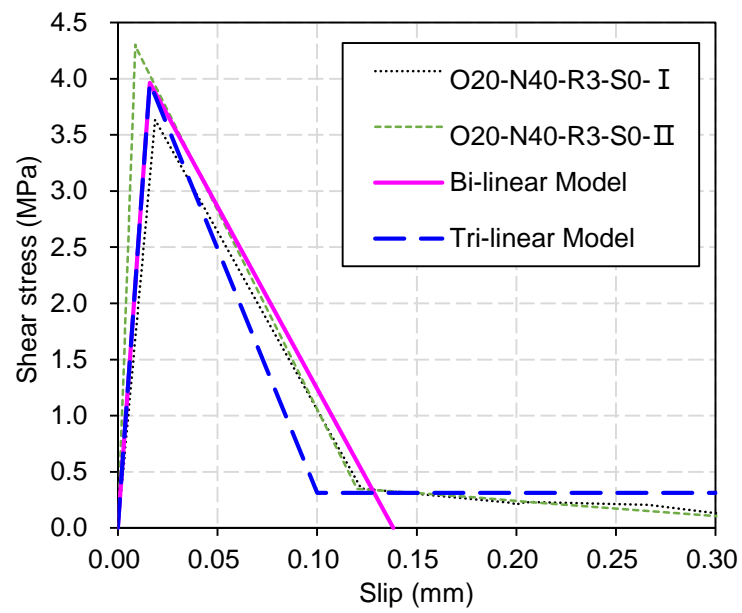
234

(e) Specimen O60-N40-R0-S0

Figure A6.1 Predicted versus experimental bond-slip curves for Series-I specimens
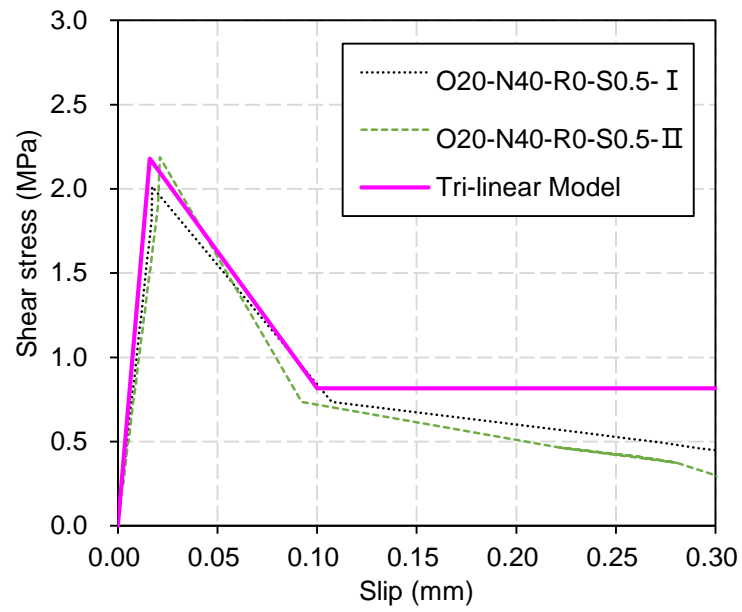

(a) Specimen O20-N40-R1-S0

(b) Specimen O20-N40-R2-S0

(c) Specimen O20-N40-R3-S0

Figure A6.2 Predicted versus experimental bond-slip curves for Series-II specimens

(a) Specimen O20-N40-R0-S0.5

(b) Specimen O20-N40-R0-S1.0

237

(c) Specimen O20-N40-R0-S1.5

Figure A6.3 Predicted versus experimental bond-slip curves for Series-III specimens

(a) Specimen O20-N40-R1-S0.5

(b) Specimen O20-N40-R2-S1.0

(c) Specimen O20-N40-R3-S1.5

Figure A6.4 Predicted versus experimental bond-slip curves for Series-IV specimens

(a) Specimen O20-N20-R0-S0

(b) Specimen O20-N40-R0-S0

(c) Specimen O20-N60-R0-S0

(d) Specimen O40-N40-R0-S0

(e) Specimen O60-N40-R0-S0

Figure A6.5 Predicted versus experimental load-slip curves for Series-I specimens

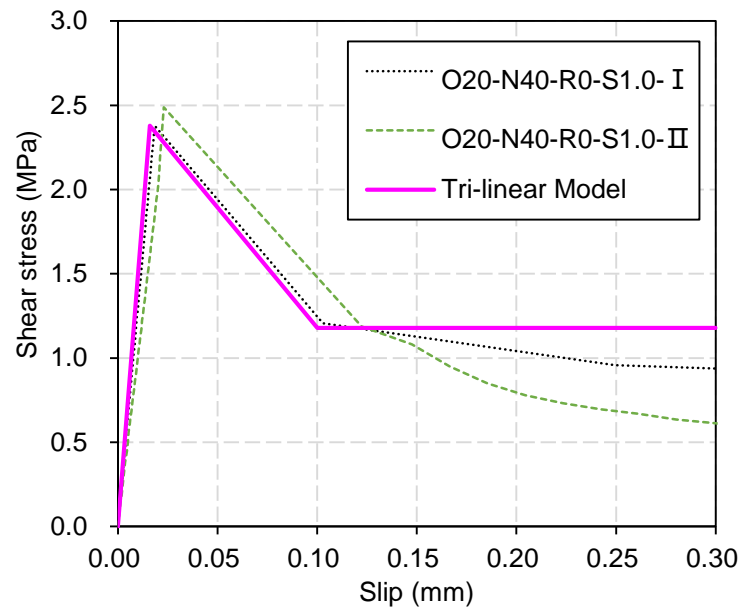(a) Specimen O20-N40-R1-S0

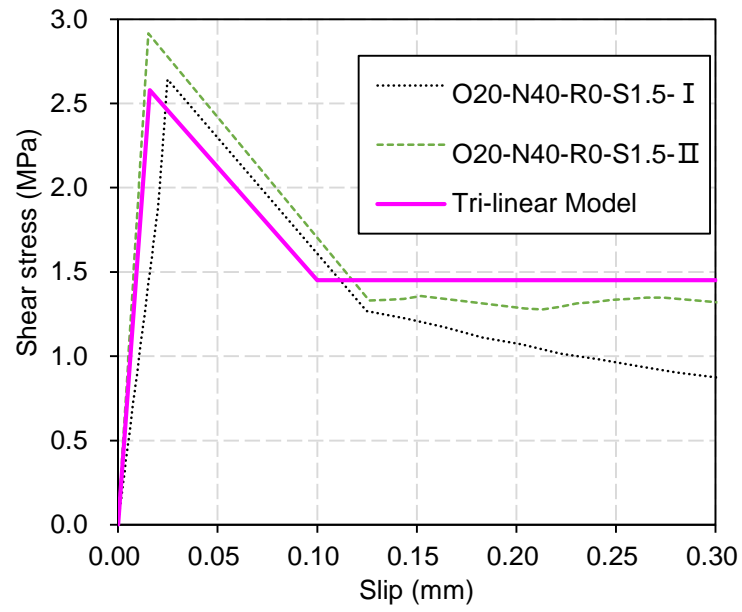(b) Specimen O20-N40-R2-S0

(c) Specimen O20-N40-R3-S0

Figure A6.6 Predicted versus experimental load-slip curves for Series-II specimens
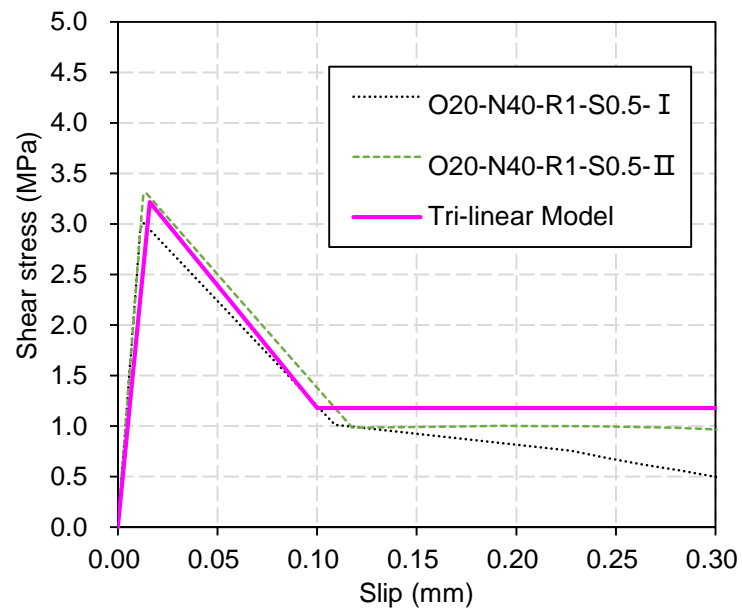
(a) Specimen O20-N40-R0-S0.5
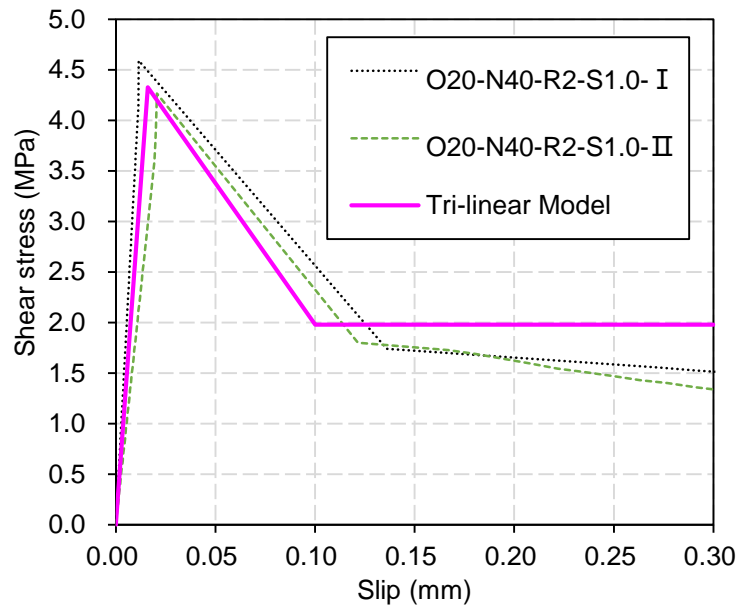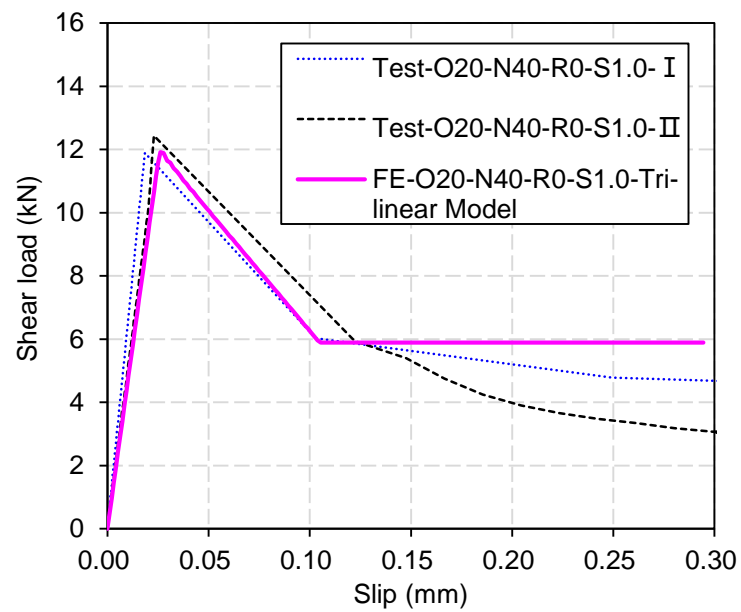

(b) Specimen O20-N40-R0-S1.0
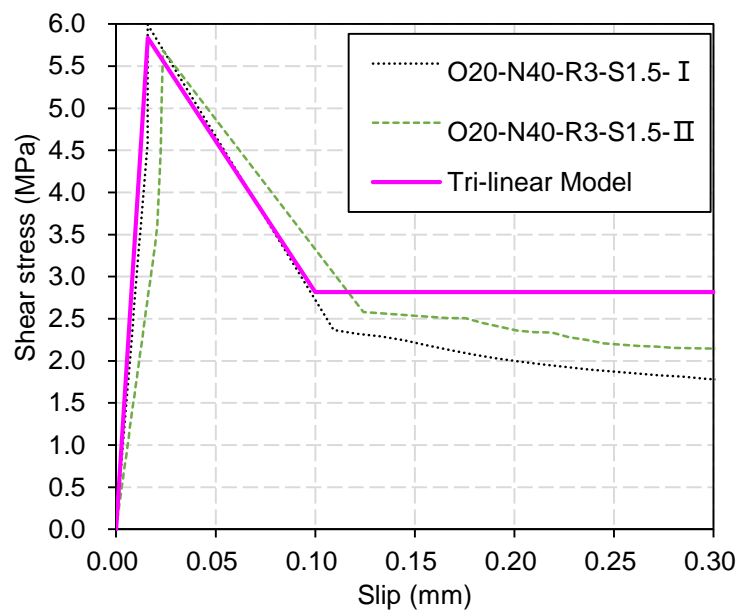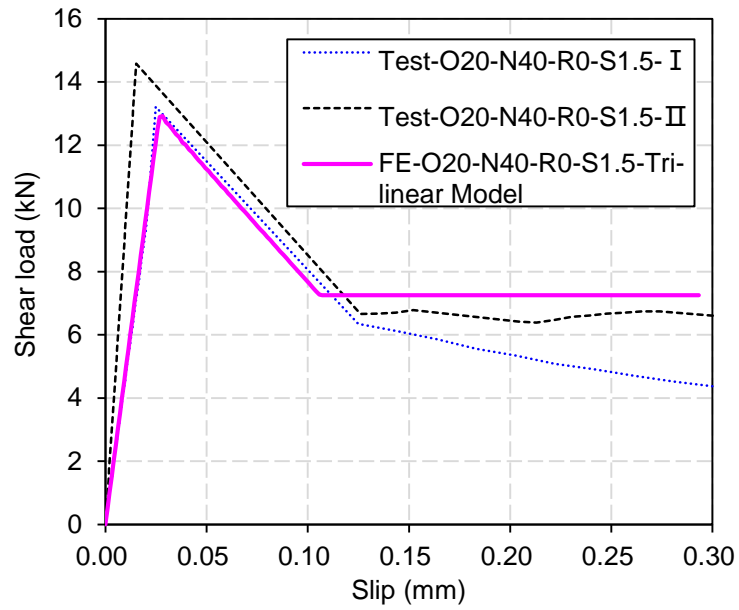
(c) Specimen O20-N40-R0-S1.5

Figure A6.7 Predicted versus experimental load-slip curves for Series-III specimens
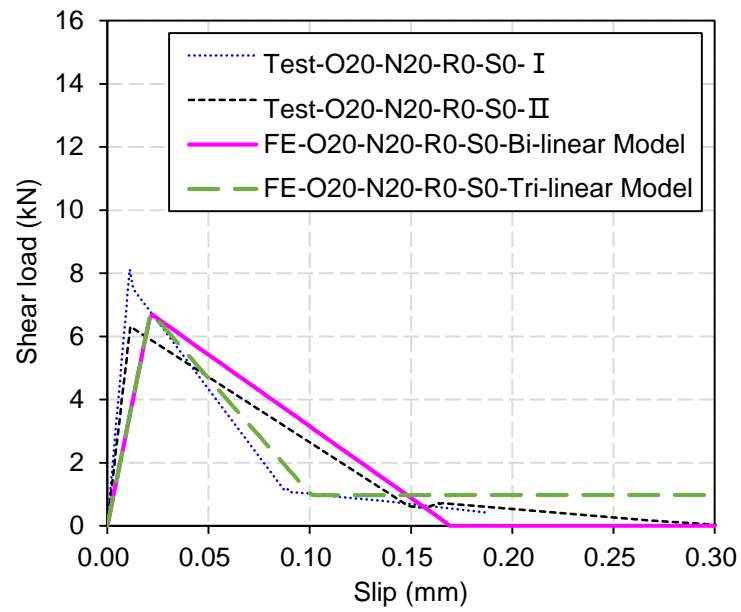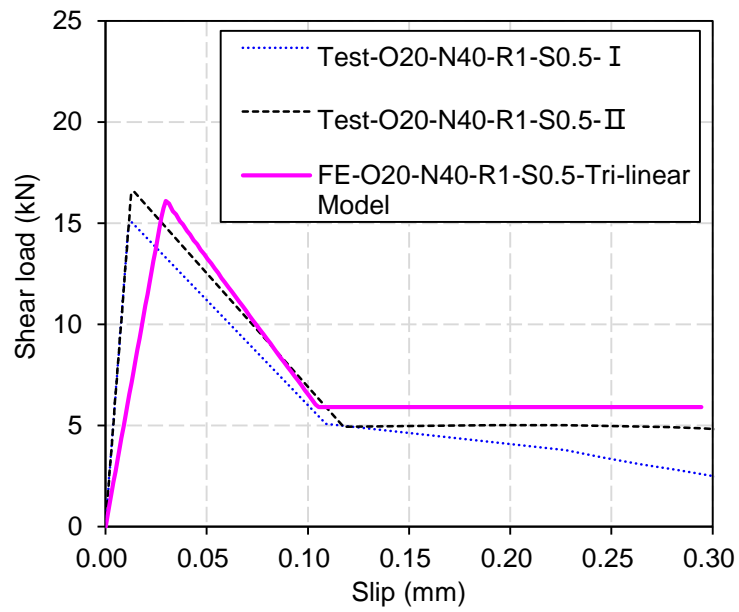

(a) Specimen O20-N40-R1-S0.5
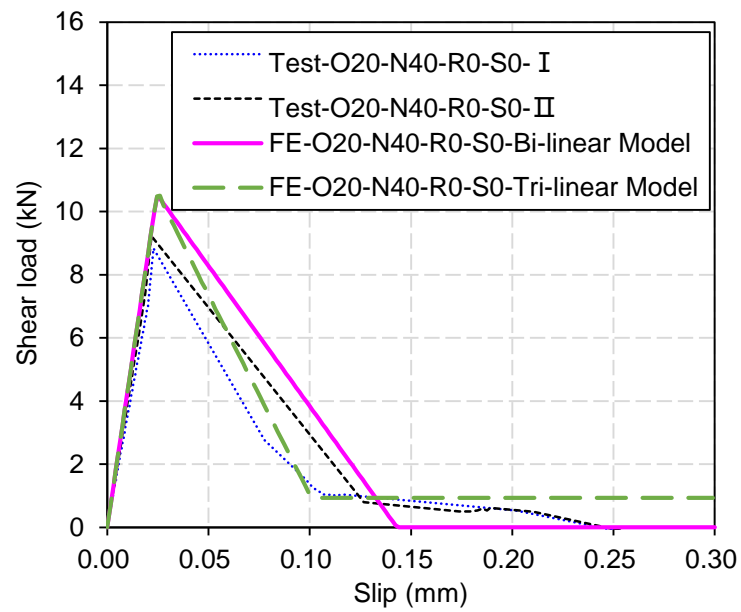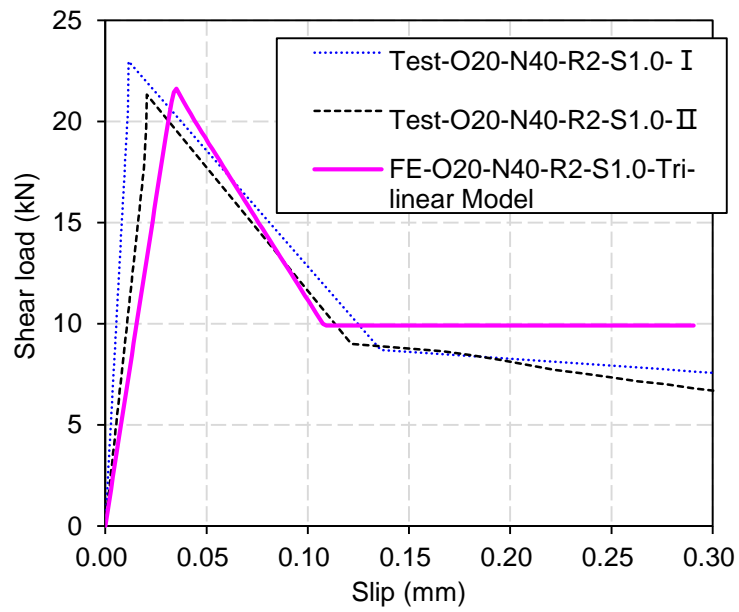
(b) Specimen O20-N40-R2-S1.0
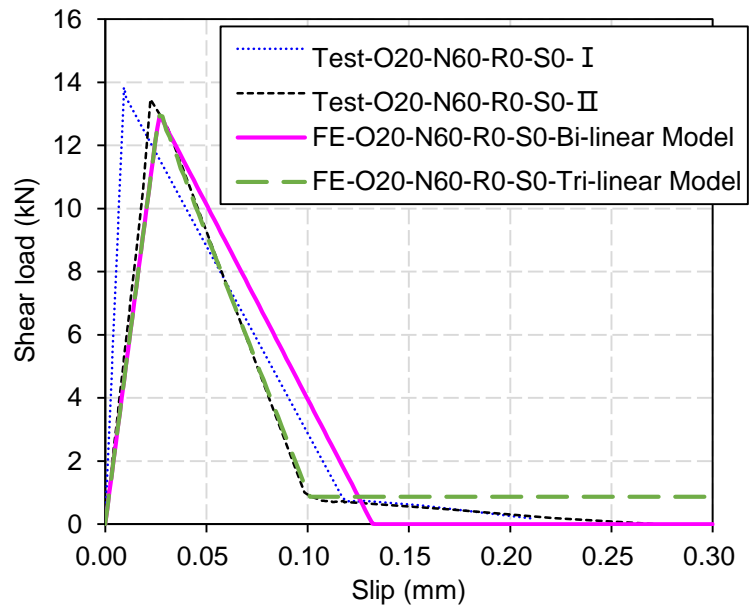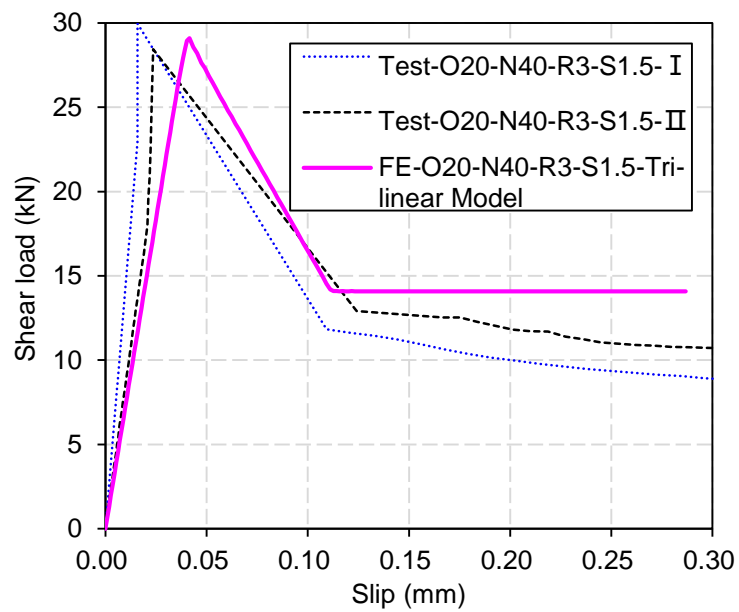

(c) Specimen O20-N40-R3-S1.5

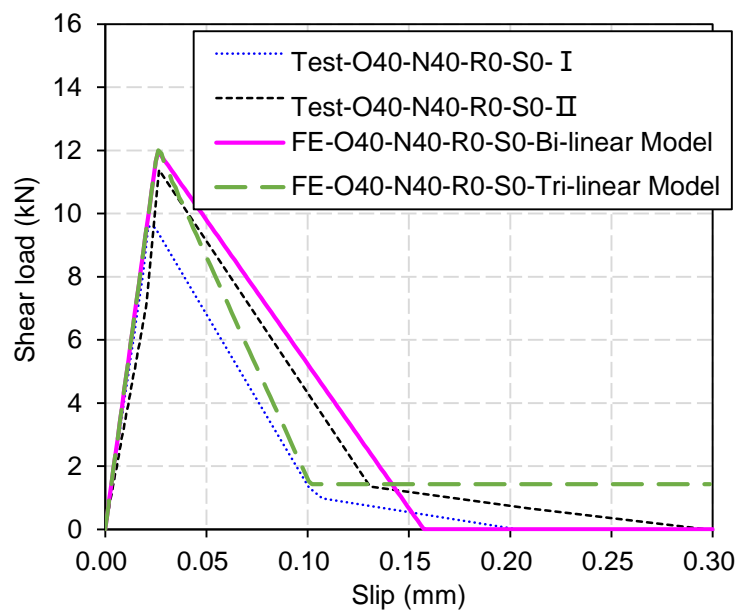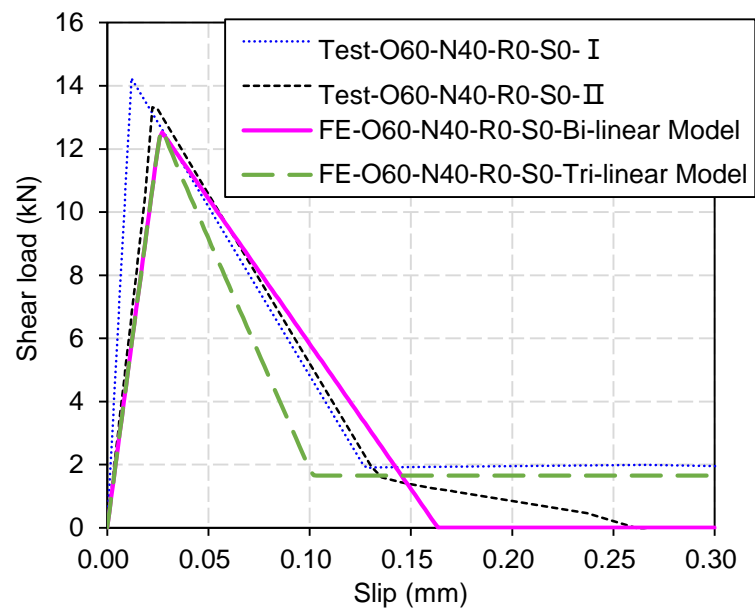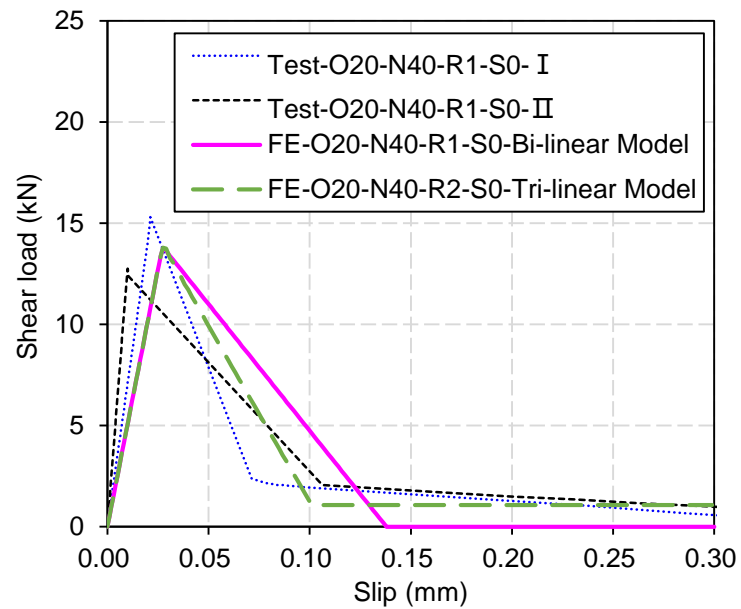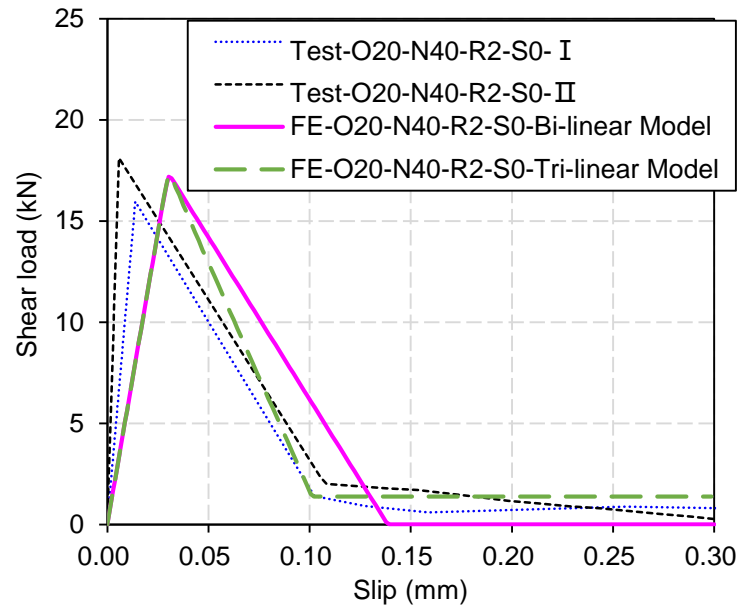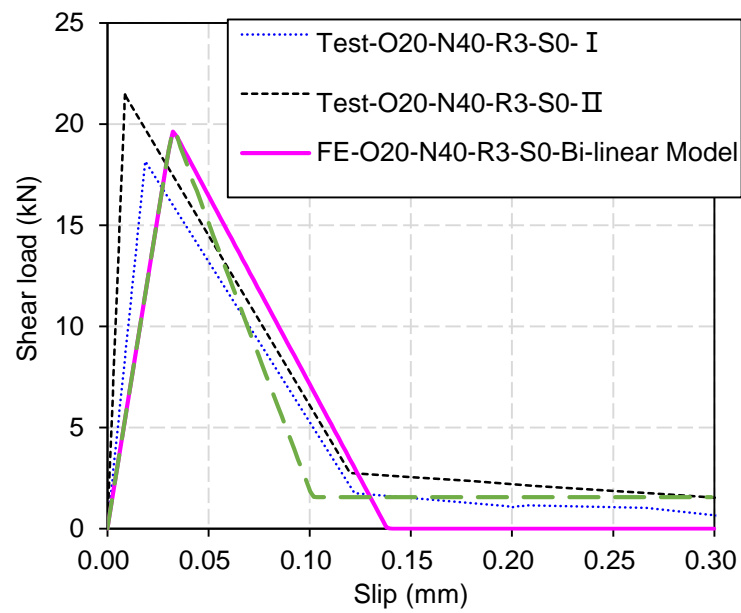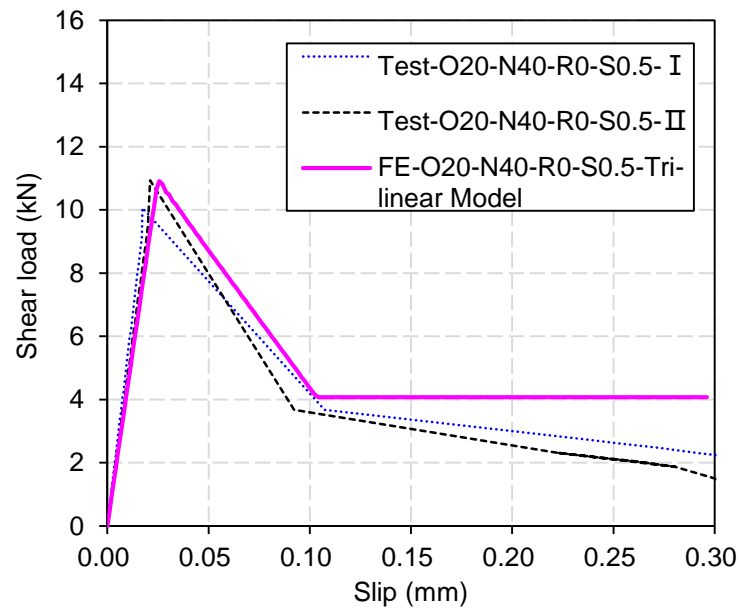Figure A6.8 Predicted versus experimental load-slip curves for Series-IV specimens

CHAPTER 7

FINITE ELEMENT MODELLING OF COMPOSITE BEAMS WITH CONCRETE-TO-CONCRETE INTERFACES

7.1 INTRODUCTION

One of the most common techniques to repair or strengthen reinforced concrete structures is to add new concrete to the existing concrete substrate (Zanotti and Randl, 2019). For example, reinforced concrete building slabs and bridge decks are usually strengthened by adding one concrete overlay on top or bottom of the slabs or decks, and reinforced concrete jacketing is often adopted in the strengthening of columns and beams (Chilwesa *et al*., 2017), whose original cross-section often needs to be enlarged to meet the increased capacity demand. In these cases, concrete-to-concrete interfaces are generated between the parent old concrete and the cast-on-top new concrete, which are critical to the success of the repaired or strengthened structure in terms of durability and structural integrity (Mohamad *et al*., 2015). In addition to strengthening existing reinforced concrete structures, in new constructions, composite concrete members consisting of individual parts usually require the assembly of precast components or on-site casting new components onto the precast part, which generates concrete-to-concrete interfaces that often represent the weak part of the member (Mahmoud *et al*., 2014; Baran, 2015; Achilllopoulou, 2016; Hossain *et al*., 2020). Therefore, the interfacial behaviour between the new and old concretes is a key to the mechanical performance of composite concrete members, as shown in Figure 7.1.

Most of the existing studies pertaining to the analysis of composite concrete structures

focused on steel-to-concrete interfaces (Baskar *et al.*, 2002; Sebastian and McConnel, 2000; Macorini *et al.*, 2006), timber-to-concrete interfaces (Lopes *et al.*, 2012; Zona *et al.*, 2012; Khorsandnia *et al.*, 2018), or FRP-to-concrete interfaces (Chen *et al.*, 2011; Chen *et al.*, 2012; Teng *et al.*, 2013). Much fewer studies were focused on analysing those composite concrete structures containing concrete-to-concrete interfaces. In the limited studies on precast concrete structures containing concrete-to-concrete interfaces, the interface is usually simulated as the base concrete without specific treatment of the interfacial behaviour (e.g., Lin *et al.*, 2013). The analyses presented in Chapters 4 to 6 have demonstrated that such an assumption is inappropriate as the concrete-to-concrete interface is indeed weak compared to the concrete base. Therefore, such assumptions likely lead to unconservative predictions.

In fact, experimental studies have shown that the behaviour of composite concrete structures with interfaces is different to that of cast-in-place concrete structures (e.g., Gohnert, 2003; Li *et al.*, 2015). For instance, in the case of a composite concrete beam, diagonal cracks will further propagate along the interface between the new and old concrete and later extend upward into the post-cast concrete when the beam is under vertical loading. Furthermore, obvious slip can be observed due to the shear stress along the bonded interface (Loov and Patnaik, 1994; Patnaik, 2001; Kahn and Slapkus, 2004; Halicka, 2011; Halicka and Jabłoński, 2016).

In addition, experimental research has been conducted on composite concrete beams with both rough and smooth bonded interfaces (Loov and Patnaik, 1994; Patnaik, 2001; Halicka, 2011). These composite concrete beams were loaded under three- or four-point bending, and smeared cracks appeared at the concrete-to-concrete interfaces when the load was moderate. At the late stage of loading, these fine cracks coalesced into a major crack at the interface and further penetrated into the concrete substrate leading to the

failure of the beam.

Therefore, in modelling such as FE analyses of composite concrete structures, it is necessary to properly simulate the concrete-to-concrete interfaces to achieve accurate prediction of the failure mode or mechanical behaviour of composite concrete structures. This chapter presents the FE analysis of composite concrete structures containing concrete-to-concrete interfaces, which were simulated using the interfacial bond-slip model developed in the previous chapters. The performance of the FE model was evaluated by comparing the predicted results with the experimental data. As a reference, the prediction of the composite beams without considering the interfacial behaviour was conducted to demonstrate the necessity of proper treatment of the interface. Finally, a parametric study was carried out using the verified FE model to identify the key parameters in the design of composite concrete beams.

7.2 FE MODELLING OF COMPOSITE CONCRETE BEAMS

7.2.1 General

A typical composite concrete beam consists of multiple individual parts, either reinforced or unreinforced, that are cast in sequence, thereby generating concrete-to-concrete interfaces between the neighbouring parts. Figure 7.1 schematically shows typical composite concrete beams consisting of an old reinforced concrete part and a new concrete part cast onto the old part, as indicated in the figure.

An FE framework is presented in this chapter to simulate the behaviour of such composite concrete beams with various configurations. A 2D model is considered to be sufficiently accurate for beams with the out-of-plane deformation sufficiently restrained. The framework simulates the concrete material using a damage-plasticity constitutive

model, the steel reinforcement using a linear elastic behaviour followed by plasticity, the concrete-to-concrete interface with the bond-slip model developed in the previous chapters, and the concrete-to-steel reinforcement interface with a well-established bond-slip model that is different from the concrete-to-concrete bond-slip model. Thereupon, composite concrete beams with different geometries can be simulated with this 2D model. The predicted results are compared with the experimental data reported in the literature to validate the model. Moreover, a baseline model without considering the interface has been used to predict the behaviour of the same beams to demonstrate the necessity of properly simulating the concrete-to-concrete interfaces.

7.2.2 FE Mesh

Four-node plane stress elements with reduced integration (CPS4R) and 2-node truss elements (T2D2) were used to simulate the concrete and steel bars, respectively. The bond behaviour between the steel bars and concrete and the interaction behaviour between the concrete-to-concrete interfaces were modelled using four-node cohesive elements (COH2D4), as shown in Figure 7.2. Spring elements (SPRINGA) were adopted to simulate the dowel steel reinforcing bar crossing the interface to predict the dowel action, as schematically shown in Figure 7.2. The mesh convergence study indicated that a mesh size of 1 *mm* × 1 *mm* for solid elements resulted in favourable results. Therefore, this element size was adopted in all the following numerical simulations. The boundary conditions of the FE model were consistent with the experimental conditions.

7.2.3 Constitutive Laws for Steel and Concrete

The constitutive law for concrete is exactly the same with that used in Chapter 6. Therefore, only a brief introduction is presented here, and more details can be found in

Chapter 6.

The damage-plasticity model built-in ABAQUS (2010) was adopted to simulate the constitutive behaviour of concrete (Lubliner *et al*., 1989; Lee and Fenves, 1998). The concrete tensile cracking was simulated using the built-in crack band model in the damage-plasticity model. For concrete under uniaxial compression, the axial stress-axial strain relationship suggested by Saenz (1964) was adopted. The concrete tensile softening model proposed by Hordijk (1991) was used for concrete after reaching the uniaxial tensile strength.

The compressive and tensile damage evolution for concrete were considered in the proposed FE model. Damage variables d_c and d_t were introduced to model the concrete damage under compression and tension, respectively. The shear retention of cracked concrete is highly complex. Therefore, the shear retention factor considerably influences the shear behaviour after concrete cracking (Zhang and Teng, 2014; Chen *et al*. 2012). The shear retention model suggested by Rots (1988) was adopted to model the shear resistance degradation of cracked concrete.

The reinforcing steel was modelled using J_2 elastoplasticity. The corresponding tensile stress-strain relationship follows a bi-linear model with a linear elastic and a plastic hardening branch. The hardening modulus $E_s^{'}$ was taken as $0.005\,E_s$, where E_s is the elastic modulus of the steel. A Poisson's ratio of 0.3 was used for steel.

7.2.4 Bond-Slip Relationship

The interfacial behaviour between the steel reinforcement and concrete was considered in the FE framework. For the normal interfacial behaviour, a perfect bond is assumed. For the tangential behaviour, the bond-slip relationship suggested by the CEB-FIP code

(1993) was used, as shown in Figure 7.3. The relationship includs four stages expressed by the following piecewise equations:

$$\tau = \tau_{max}\left(\frac{s}{s_1}\right)^{\alpha} \qquad 0 \le s \le s_1 \tag{7.1a}$$

$$\tau = \tau_{max} \qquad s_1 \le s \le s_2 \tag{7.1b}$$

$$\tau = \tau_{max} - \left(\tau_{max} - \tau_f\right)\frac{s - s_1}{s_3 - s_2} \qquad s_2 \le s \le s_3 \tag{7.1c}$$

$$\tau = \tau_f \qquad s_3 \le s \tag{7.1d}$$

where τ (MPa) is the local shear stress; s (mm) is the slip; the critical slips separating the stages are taken as $s_1 = s_2 = 0.6$ mm and $s_2 = 1.0$ mm for deformed steel bars, $s_1 = s_2 = s_3 = 0.1$ mm for plain steel bars; the maximum and residual shear stresses are taken as $\tau_{max} = 2.0\sqrt{f_{ck}}$ and $\tau_f = 1.5\tau_{max}$ (MPa) for deformed steel bars, and $\tau_f = \tau_{max} = 0.3\sqrt{f_{ck}}$ for plain steel bars; the coefficient α determining the shape of the bond-slip curve in the initial stage is taken as 0.4 and 0.5 for deformed and plain steel bars, respectively.

The *fib* model code (2013) describes a model for the dowel action of steel, as shown in Figure 7.4. The resistance V_F of the reinforcement acting as the shear force can be calculated as follows:

$$V_F(s) = V_{F,max}\left(\frac{s}{s_{max}}\right)^{0.5} = \kappa_{2,max} A_s \sqrt{f_c f_y}\left(\frac{s}{s_{max}}\right)^{0.5} \le \frac{A_s f_y}{\sqrt{3}} \tag{7.2}$$

where $V_{F,max}$ is the maximum force of the dowel action; s_{max} is the slip when $V_{F,max}$ is attained, with $s \le s_{max} = 0.10d \sim 0.20d$, where d is the diameter of the rebar; and $\kappa_{2,max}$

is the interaction coefficient, which can be derived from the *fib* model code (2013).

For the concrete-to-concrete interfaces, the proposed bond-slip model formulated in Chapter 6 was used and the key parameters of this model can be determined. More modelling details, such as the tangential bond-slip model, normal bond-opening model and the mixed-mode cohesive law, are available in section 6.4.2.

7.3 VALIDATION OF THE FE FRAMEWORK

The performance of the proposed FE framework is evaluated by simulating the flexural behaviour of two types of composite concrete beams with different cross-sections. To validate the developed bond-slip model, beams containing a concrete-to-concrete interface were selected with the criterion that the failure is caused by interfacial debonding. Therefore, if the bond-slip model is suitable for such a concrete-to-concrete interface, both the interfacial debonding and the overall flexural behaviour could be accurately predicted. A rectangular-section beam tested by Halicka (2011) and a T-sectioned beam tested by Halicka and Jabłoński (2016) containing a concrete-to-concrete interface were selected as both beams failed by interfacial debonding in the test. The first type of composite beams has the old and new concrete parts of equal width, forming a rectangular cross-section. Halicka (2011) tested two configurations of such beams, one with transverse reinforcement acting as dowel reinforcement for the interface and the other configuration without such dowel reinforcement, as shown in Figure 7.5 (a). Both configurations were simulated using the proposed framework. The second type of beams has the old and new concrete parts of different widths forming a T-shaped cross-section. The beam tested by Halicka and Jabłoński (2016), as shown in Figure 7.5 (b), was simulated using the proposed framework. These beams were tested up to failure caused by interfacial debonding, and the test data were complete. Therefore,

they were suitable for the evaluation of the performance of the developed framework.

7.3.1 The Rectangular-section Composite Concrete Beam

Halicka (2011) conducted four-point bending tests of composite concrete beams. These composite concrete beams had a rectangular cross-section of 80 mm×140 mm, a total length of 1500 mm, and a span between the supports of 1100 mm. The details of the beams are listed in Table 7.1. One beam with a dowel reinforcement ratio of 0.2%, denoted as beam-RD (R for rectangular and D for dowel reinforcement), and the other without dowel reinforcement, denoted as beam-R, as shown in Figure 7.5 (a), have been simulated using the proposed framework. The FE model of the beams is shown in Figure 7.6. Half model of the composite concrete beam was used due to the symmetry of the beam. As shown in Figure 7.6, the vertical constraint was applied to the support point, and the horizontal constraint was applied at the symmetrical line. A displacement-controlled loading was applied at a location 195 mm away from the symmetric line to simulate the four-point bending, as shown in the figure.

In this test, the yield stresses of the transverse and longitudinal reinforcement were 414 and 481 MPa, respectively. The tensile strength of the old and new concrete for beam-RD was 1.92 MPa and 2.88 MPa, respectively. Meanwhile, the tensile strength of the old and new concrete for beam-R was 2.20 MPa and 3.0 MPa, respectively. No specific treatment was conducted for the old concrete surface during the beam specimen preparation, as reported in the literature. Therefore, the concrete surface roughness was considered as zero in this FE model. Moreover, under the four-point bending test, the applied compressive stress on the concrete-to-concrete surfaces should be minimal and hence the interface was assumed to be free of compressive stress. Accordingly, the concrete-to-concrete interfacial properties can be determined according to section 6.3 and the modelling parameters are listed in Table 7.2. The bi-linear bond-slip model was

selected since no residual stress due to interfacial compressive stress was considered, while these bond-slip relationships for concrete-to-concrete interfaces for beam-RD and beam-R are shown in Figure 7.7.

The load-deflection curves of the two beams measured in the tests are plotted in Figure 7.8. It is seen that below the load level of 15 kN, the behaviour of the two beams is basically identical; when the load level is above 15 kN, beam-RD exhibits a smaller reduction of the flexural stiffness than beam-R. Both beams failed at the peak load of 21 kN with a failure mode of combined interfacial debonding and diagonal cracks. The load-deflection curves predicted using the proposed framework are plotted as the dashed curves in Figure 7.8, which are generally in good agreement with the experimental data. The comparison of key values between FE and experimental results is also listed in Table 7.3. The numerical results indicate that the flexural stiffness of beam-R is slightly smaller than beam-RD when the load level is above 10 kN, and the difference in the flexural stiffness enlarges as the load level increases. The predicted capacity of beam-R is 20 kN, which is slightly smaller than the predicted capacity of 21 kN for beam-RD. After the deflection exceeded about 2.8 mm, the test was terminated. However, the predicted results show that the transverse reinforcement crossing the concrete-to-concrete interface significantly increases the capacity of the composite concrete beam at this stage. When the deflection is 3.5 mm, the predicted capacity of the beam-RD is 20 kN while the beam-R is 15 kN, with a difference of about 33%. It is believed that the concrete-to-concrete interface has completely failed at this moment.

In addition, the load-deflection curve of beam-R predicted without considering the interfacial behaviour is compared with those predicted considering the interfacial behaviour in the figure. It is seen that both the flexural stiffness and capacity are over-

255

predicted because the weak interface was modelled as the base concrete. This clearly indicates the necessity of properly simulating the concrete-to-concrete interface for such composite beams.

Figure 7.9 shows the predicted crack pattern of the beam-R at the peak load, with and without modelling of concrete-to-concrete interfaces, respectively. When the FE model includes the simulation of concrete-to-concrete interfaces, in addition to the flexural cracks in the middle area of the beam, the interfacial debonding along the concrete-to-concrete interface, as well as several diagonal cracks near the support can be observed. These diagonal cracks extend and will develop along the concrete-to-concrete interface, while stopping their upward propagation. This predicted crack pattern is consistent with the experimental observation. However, if the model does not include the simulation of concrete-to-concrete interfaces, that is, the cast-in-situ reinforced concrete beam, only the flexural cracks and few diagonal cracks can be observed. The comparison shows that the accurate simulation of the concrete-concrete interface is crucial to the prediction of mechanical behaviour and failure modes of concrete composite beams.

The interfacial stress distributions along the concrete-to-concrete interface, as well as the stirrup stresses for beam-R will be discussed in the following section 7.4.1.

7.3.2 The T-section Composite Concrete Beam

Halicka and Jabłoński (2016) tested one T-section composite concrete beam, referred to as beam-T herein, and the geometric properties of this composite concrete beam is also listed in Table 7.1. This T-section composite concrete beam had a length of 1800 mm and a span between the supports of 1400 mm under four-point bending. The 80×150 mm web of the beam was the old concrete part, and the 640×50 mm flange was the new concrete part. Accordingly, the concrete-to-concrete interface was located between the

flange and web, as shown in Figure 7.5 (b). The beam had transverse reinforcement crossing the interface with a ratio of 0.21%. The boundary of the FE model for this beam is shown in Figure 7.10. Similar to the modelling of the rectangular-section composite concrete beam, only half of the composite concrete beam was modelled by taking advantage of the symmetry.

According to the test description, the yield strengths of the transverse and longitudinal reinforcement were 340 and 545 MPa, respectively. The tensile strength of the old and new concrete for beam-T was 3.85 MPa and 2.88 MPa, respectively. No surface treatment was applied to the old concrete web, and thus the surface was considered smooth, which indicated that the surface roughness could be considered as zero. This beam was also tested under the four-point bending test, and the applied compressive stress on the concrete-to-concrete surfaces was also assumed to be zero in this FE model. Therefore, the concrete-to-concrete interfacial properties were determined according to section 6.3, and the modelling parameters are listed in Table 7.2. The bi-linear bond-slip model was selected, and the bond-slip relationship for concrete-to-concrete interfaces for beam-T is shown in Figure 7.11.

The load-deflection curve of the beam measured in the test is plotted in Figure 7.12. The tested beam-T behaved similarly with the composite beams-RD and had a capacity of 65 kN. The predicted load-deflection curve is plotted in the figure, and a close match of the flexural stiffness and capacity with the test data is seen. The comparison of key values between FE and experimental results is also listed in Table 7.3. This validates the accuracy of the developed numerical framework in simulating the flexural behaviour of T-section composite concrete beams. Moreover, the load-deflection curve of beam-T predicted without simulating the interface is also shown in the figure. Again, both the flexural stiffness and capacity are over-predicted due to ignoring the weak

interface, which further confirms the necessity of accurately simulating the concrete-to-concrete interface for such composite beams.

7.4 PARAMETRIC STUDY

The parametric study was performed with the validated framework to further explore the influence of the concrete-to-concrete interface on the overall behaviour of the composite concrete beam. The investigated parameters are the mechanical properties and geometric layout of the interface. The former provides guidance for the selection of new concrete strength or treatment of the old concrete surface, such as surface roughening before casting the new concrete. The latter qualitatively compares the cross-section layout design of composite concrete beams. The example beam is the beam-R tested by Halicka (2011) with a rectangular cross-section of 80 mm×140 mm, a total length of 1500 mm, and a span between the supports of 1100 mm under four-point bending load.

7.4.1 Influence of the Interfacial Properties

Identical rectangular-section composite concrete beams with different interfacial properties were simulated using the proposed framework. Three tensile strengths of new concrete were selected as variables, including 0.5 MPa, 1.0 MPa and 3.0 MPa. It is noted that the tensile strength of new concrete for the tested beam-R, which was analysed in section 7.3.1, was 3.0 MPa. Other interfacial parameters, including the strength of old concrete, concrete surface roughness, and the geometry and material parameters of the specimen, were kept unchanged, which are listed in Table 7.1 and Table 7.2. Based on the proposed bi-linear bond-slip model, the corresponding bond-slip relationships for various concrete-to-concrete interfaces are plotted in Figure 7.13 (a). It can be seen that the shear strength of the concrete-to-concrete interface is

258

significantly different from the above three new concrete strengths. The corresponding load-deflection curves predicted with these three interfaces are plotted in Figure 7.13 (b). It is seen that varying the tensile strength of new concrete hardly impacts the flexural stiffness of the composite concrete beam at the initial stage. However, the beam with 0.5 MPa tensile strength of new concrete starts to exhibit flexural stiffness reduction at 6 kN load level, while the stiffness reduction occurs at 10 and 16 kN for the beams with the tensile strength of new concrete of 1.0 MPa and 3.0 MPa. In addition, the ultimate capacity of the composite concrete beam is changed by varying the tensile strength of new concrete for the concrete-to-concrete interface. It is obvious that the ultimate capacity of the composite concrete beam is the largest, with 3.0 MPa tensile strength of new concrete.

Figure 7.14 and Figure 7.15 show the concrete-to-concrete interfacial shear stresses and the stirrup stresses, respectively. The value in the legend of Figure 7.14 represents the mid-span deflection of the concrete composite beam. The position of the stirrup, which acts as the dowel reinforcement, is in the shear zone of the composite concrete beam, as shown in Figure 7.15 (b). Examining these two figures indicates that the reduction of the flexural stiffness is due to the initiation of local interfacial softening at the concrete-to-concrete interface, which was shown in Figure 7.13 (b).

As shown in Figure 7.13 (b), the flexural stiffness reduction occurs at a deflection of 0.6 mm for the specimen with 0.5 MPa tensile strength of new concrete. Figure 7.14 (a) shows that the concrete-to-concrete interface experiences softening when the deflection of the composite concrete beam reaches 0.6 mm. Such softening at the interface leads to the increase of the stress in the dowel reinforcement, as shown in Figure 7.15 (a) that the dowel reinforcement stress increases rapidly after 0.6 mm deflection. That is, since the composite action of the beam relies on the shear transfer at the interface, the

259

reduction of the interfacial stiffness due to softening decreases the flexural stiffness. When the deflection of the composite concrete beam reaches 1.2 mm, it can be seen that the concrete-to-concrete interface has fully debonded. The shear force along this interface should be completely provided by the dowel reinforcement.

Similar observations can be found for the beams with 1.0 and 3.0 MPa tensile strength of new concrete, that the concrete-to-concrete interfacial softening starts around 1.2 and 2.0 mm deflections, respectively, as shown in Figure 7.14 (b) and (c). Accordingly, the dowel reinforcement stress increases sharply at 1.2 and 2.0 mm for the beams, as shown in Figure 7.15 (a). This indicates that increasing the interfacial strength enhances the composite action of the beam and hence delays the reduction of the flexural stiffness. Meanwhile, for the composite concrete beam with 1.0 MPa tensile strength of new concrete, fully debonding of the concrete-to-concrete interface occurs at 2.5 mm. However, for the composite concrete beam with 3.0 MPa tensile strength of new concrete, the concrete-concrete interface is not fully debonding even the deflection reaches 2.5 mm. Therefore, approaches such as increasing the new concrete strength, increasing roughening the old concrete surface before casting the new concrete may considerably enhance the mechanical performance of the resulting composite concrete beams.

7.4.2 Influence of the Cross-section Layout of Composite Beam

Three composite beams with identical cross-section dimensions but different layouts of the old and new concrete parts were simulated using the proposed framework to investigate the differences in their mechanical behaviour. The interfaces for the three beams are located at 100, 70, and 40 mm positions measured from the bottom, as shown in Figure 7.16 (a). These three different concrete-concrete interface positions represent different heights of old and new concrete in composite concrete beams.

The corresponding load-deflection curves are shown in Figure 7.16 (b). The results show that the behaviour of the beams is similar to those in the previous section, which exhibits a linear behaviour up to a certain load level, and the flexural stiffness starts to decrease. It can be found that the concrete-to-concrete interface at different positions does not affect the initial stiffness for the composite concrete beam but will affect the deflection level when flexural stiffness reduction occurs. The flexural stiffness reduction occurs at a deflection of 1.0 mm for the 70 mm interface-location beam, while the stiffness reduction occurs at 1.2 mm 100 and 40 mm interface-location beams. Moreover, the capacities for the 100 and 40 mm interface-location beams are similar, while that for the 70 mm interface-location beam is much smaller.

Figures 7.17 and 7.18 show the interfacial shear stress distributions and the stirrup stress of the three beams at different deflections. The position of the stirrup here is the same as mentioned in the previous section and can be found in Figure 7.15 (b).

It is seen in Figure 7.16 that the 70 mm interface-location beam experiences concrete-to-concrete interfacial softening at a deflection of 1.0 mm prior to those of the other beams around 1.2 mm. Therefore, the stress of the stirrup of the 70 mm interface-location beam increases significantly when the deflection is relatively small, as indicated in Figure 7.17. Also, Figure 7.18 depicts the interfacial shear stress along the beam span with various interface positions. Under small deflections, such as 0.02 mm and 0.6 mm, the interfacial stress of the 70 mm interface-location beam is greater than that of the 40 mm interface-location beam and 100 mm interface-location beam, although the concrete-to-concrete interface is in the elastic stage. When the deflection is 1.2 mm, the 70 mm interface-location beam has already suffered from an interfacial debonding, whereas the other two beams only exhibit interfacial softening.

261

Since the interfacial properties and the dowel reinforcement are identical for the three beams, the reason for the difference is due to the shear force transferred at the interface location. The 70 mm-location interface transfers higher shear force than the other two interface locations under the same applied load. Therefore, this beam experiences an earlier interfacial softening hence the reduction of the composite action and flexural stiffness. Further, due to the higher shear force transferred at the interface, the capacity of the beam is lower than the other two beams whose interfaces resist smaller shear force. Therefore, the accurate prediction of the interfacial behaviour is critical to the design of a composite beam, and an optimal design should achieve a balance between the addition of the new concrete part and the capacity of the interface. That is, if the added new concrete part is small, the flexural stiffness and capacity increase is limited, whereas if the added part is large, the interfacial capacity may pose a limit to the degree of increase for the flexural stiffness and capacity.

7.5 CONCLUSIONS

In this chapter, the behaviour of composite concrete beams containing a concrete-to-concrete interface has been simulated using an FE model, wherein the interface was modelled by the bond-slip model developed in Chapter 6. The flexural behaviour of composite concrete beams depends on the composite action between the old and new concrete, which in turn depends on the shear capacity of the interface. Therefore, accurate prediction of the behaviour of composite concrete beams depends on the accurate simulation of the concrete-to-concrete interfaces. A 2D FE model has been presented in this chapter to simulate composite concrete beams with concrete-to-concrete interfaces. This model incorporates the constitutive modelling of concrete, steel reinforcement, and the concrete-to-concrete and concrete-to-steel interfaces, and therefore it can be used to simulate composite concrete beams of various configurations.

The performance of the model is validated using the experimental data of rectangular-section and T-section composite beams. The predictions of the flexural behaviour and failure mode of these beams are in close agreement with the experimental data. When the interface is not simulated, the model clearly overpredicts the flexural stiffness and capacity.

In addition, a parametric study was carried out using the verified FE model to investigate the influences of the mechanical properties of the interface and the cross-section layout. The results show that increasing the interfacial strength enhances the composite action between the old and new concrete parts hence delaying the stiffness reduction of the composite beam. However, increasing the interfacial strength beyond a limit does not further enhance the flexural stiffness and capacities due to the diagonal cracks. The results for the different cross-section layouts indicate that with identical interfacial capacities, the beam with an interface located away from the centre axis has higher capacity than the beam with an interface located at the centre since the interface in the latter is subjected to higher shear load than that in the former.

7.6 REFERENCES

ABAQUS. *ABAQUS/Standard user's manual*, version 6.10. (2010). Pawtucket (RI): Hibbitt, Karlsson, & Sorensen.

Achilllopoulou, D. V. (2016). Understanding the Basic Mechanisms Acting on Interfaces: Concrete Elements, Materials and Techniques. *Advanced Materials Interfaces*, 205-247.

Baran, E. (2015). Effects of cast-in-place concrete topping on flexural response of precast concrete hollow-core slabs. *Engineering Structures*, *98*, 109-117.

Baskar, K., Shanmugam, N. E., & Thevendran, V. (2002). Finite-element analysis of

steel–concrete composite plate girder. *Journal of Structural Engineering*, 128(9), 1158-1168.

CEB-FIP. (1993). *Model Code 90*, Lausanne, Switzerland.

Chen, G. M., Teng, J. G., & Chen, J. F. (2011). Finite-element modeling of intermediate crack debonding in FRP-plated RC beams. *Journal of Composites for Construction*, 15(3), 339-353.

Chen, G. M., Chen, J. F., & Teng, J. G. (2012). On the finite element modelling of RC beams shear-strengthened with FRP. *Construction and Building Materials*, 32, 13-26.

Chilwesa, M., Minelli, F., Reggia, A., & Plizzari, G. (2017). Evaluating the shear bond strength between old and new concrete through a new test method. *Magazine of Concrete Research*, 69(9), 425-435.

*f*ib model code for concrete structures 2010. (2013). Berlin, Germany.

Gohnert, M. (2000). Proposed theory to determine the horizontal shear between composite precast and in situ concrete. *Cement and Concrete Composites*, *22*(6), 469-476.

Halicka, A. (2011). Influence new-to-old concrete interface qualities on the behaviour of support zones of composite concrete beams. *Construction and Building Materials*, *25*(10), 4072-4078.

Halicka, A., & Jabłoński, Ł. (2016). Shear failure mechanism of composite concrete T-shaped beams. *Proceedings of the Institution of Civil Engineers-Structures and Buildings*, 169(1), 67-75.

Hordijk DA. (1991). Local approach to fatigue of concrete. *PhD thesis*, Delft University of Technology.

Hossain, K. M. A., Hasib, S., & Manzur, T. (2020). Shear behavior of novel hybrid composite beams made of self-consolidating concrete and engineered cementitious composites. *Engineering Structures*, *202*, 109856.

Kahn, L. F., & Slapkus, A. (2004). Interface shear in high strength composite T-beams. *PCI Journal*, 49(4), 102-111.

Khorsandnia, N., Valipour, H., & Bradford, M. (2018). Deconstructable timber-concrete composite beams with panelised slabs: Finite element analysis. *Construction and Building Materials*, 163, 798-811.

Lee, J., & Fenves, G. L. (1998). Plastic-damage model for cyclic loading of concrete structures. *Journal of Engineering Mechanics*, 124(8), 892-900.

Li, W., Xiao, J., Shi, C., & Poon, C. S. (2015). Structural behaviour of composite members with recycled aggregate concrete—An overview. *Advances in Structural Engineering*, 18(6), 919-938.

Lin, Z. S., Ong, K. C. G., Chandra, L. R., Tan, B. H. A., Tam, C. T., & Dai Pang, S. (2013). Finite element study of a DfD beam-column connection. *International Journal of Civil and Environmental Engineering*, 7(3), 244-250.

Lopes, S., Jorge, L., & Cruz, H. (2012). Evaluation of non-linear behavior of timber–concrete composite structures using FE model. *Materials and Structures*, 45(5), 653-662.

Loov, R. E., & Patnaik, A. K. (1994). Horizontal shear strength of composite concrete beams. *PCI Journal*, 48-69.

Lubliner, J., Oliver, J., Oller, S., & Oñate, E. (1989). A plastic-damage model for concrete. *International Journal of Solids and Structures*, 25(3), 299-326.

Macorini, L., Fragiacomo, M., Amadio, C., & Izzuddin, B. A. (2006). Long-term

analysis of steel–concrete composite beams: FE modelling for effective width evaluation. *Engineering Structures*, 28(8), 1110-1121.

Mahmoud, M. A., Elafandy, T. H., Okail, H. O., & Abdelrahman, A. A. (2014). Interfacial shear behavior of composite flanged concrete beams. *HBRC Journal*, 10(2), 206-214.

Mohamad, M. E., Ibrahim, I. S., Abdullah, R., Rahman, A. A., Kueh, A. B. H., & Usman, J. (2015). Friction and cohesion coefficients of composite concrete-to-concrete bond. *Cement and Concrete Composites*, 56, 1-14.

Patnaik, A. K. (2001). Behavior of composite concrete beams with smooth interface. *Journal of Structural Engineering*, 127(4), 359-366.

Rots JG. (1988). Computational modeling of concrete fracture. *PhD Thesis*, Delft University of Technology.

Saenz, L. P. (1964). Discussion of equation for the stress-strain curve of concrete by Desayi and Krishnan. *ACI Journal*, 61(9), 1229-1235.

Sebastian, W. M., & McConnel, R. E. (2000). Nonlinear FE analysis of steel-concrete composite structures. *Journal of Structural Engineering*, 126(6), 662-674.

Teng, J. G., Zhang, S. S., Dai, J. G., & Chen, J. F. (2013). Three-dimensional meso-scale finite element modeling of bonded joints between a near-surface mounted FRP strip and concrete. *Computers & Structures*, 117, 105-117.

Zanotti, C., & Randl, N. (2019). Are concrete-to-concrete bond tests comparable?. *Cement and Concrete Composites*, 99, 80-88.

Zhang, S. S., & Teng, J. G. (2014). Finite element analysis of end cover separation in RC beams strengthened in flexure with FRP. *Engineering Structures*, 75, 550-560.

Zona, A., Barbato, M., & Fragiacomo, M. (2012). Finite-element model updating and probabilistic analysis of timber-concrete composite beams. *Journal of Structural Engineering*, 138(7), 899-910.

Table 7.1 Details of geometric properties of the composite concrete beams

Source	Specimen	L (mm)	b_o (mm)	h_o (mm)	b_n (mm)	h_n (mm)	b_i (mm)	L_i (mm)
Halicka (2011)	Beam-RD	1500	80	100	80	40	80	1500
	Beam-R	1500	80	100	80	40	80	1500
Halicka and Jabłoński (2016)	Beam-T	1800	80	150	640	50	80	1800

Note: L =span of beam; L_e =effective span of beam; b_o =width of old concrete layer; h_o =height of old concrete layer; b_n =width of old concrete layer; h_n =height of old concrete layer; b_i =width of bonded interface; L_i =length of bonded interface.

Table 7.2 Details of material properties of composite concrete beams

Source	Specimen	$f_{t,o}$ /MPa	$f_{t,n}$ /MPa	f_y /MPa	A_s /mm^2	f_{yv} /MPa	A_{sv} /mm^2	s /mm	τ_{max} /MPa	G_f /N/mm	δ_l /mm
Halicka (2011)	Beam-R	2.20	3.00	481	276.3	414	/	/	2.54	0.188	0.016
	Beam-RD	1.92	2.88	481	276.3	414	25.12	75	2.41	0.177	0.016
Halicka and Jabłońs ki (2016)	Beam-T	3.85	2.88	545	326.6	340	25.12	75	2.78	0.226	0.016

Note: $f_{t,o}$ = tensile strength of old concrete; $f_{t,n}$ = tensile strength of new concrete; f_y = yield stress of longitudinal reinforcement; A_s = cross-sectional area of longitudinal reinforcement; f_{yv} = yield stress of the tie reinforcement crossing the shear plane; ; A_{sv} = cross-sectional area of tie reinforcement anchored on each side of the shear plane; s = spacing of reinforcement crossing the shear plane.

Table 7.3 Verification of the FE model

FE Model	Experimental result		FE result	
	Maximum load (kN)	Deflection at maximum load (mm)	Maximum load (kN)	Deflection at maximum load (mm)
Beam-RD	19.70	2.49	19.45	2.55
Beam-R	20.96	2.52	20.07	2.62
Beam-T	64.68	6.12	69.00	6.13
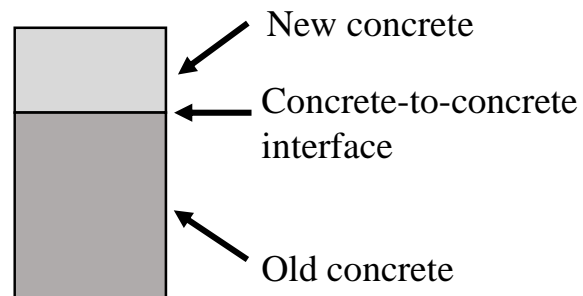
(a) Rectangular-section composite concrete beam
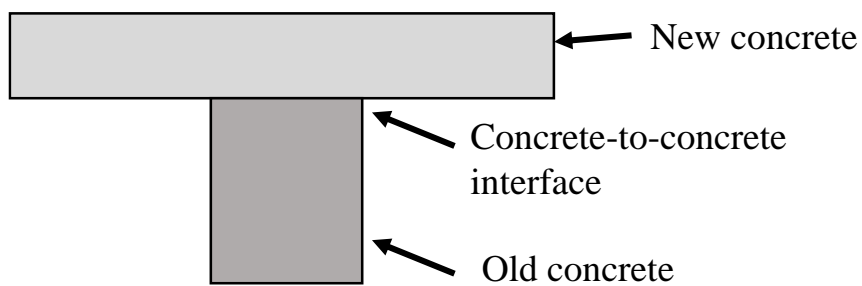
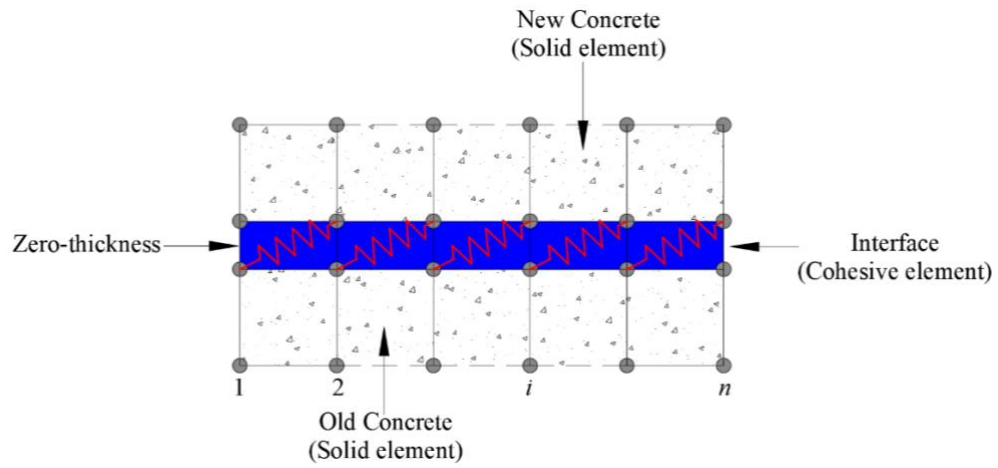(b) T-section composite concrete beam

Figure 7.1 Schematic of composite concrete beams

Figure 7.2 Simulation of the concrete-to-concrete interfaces
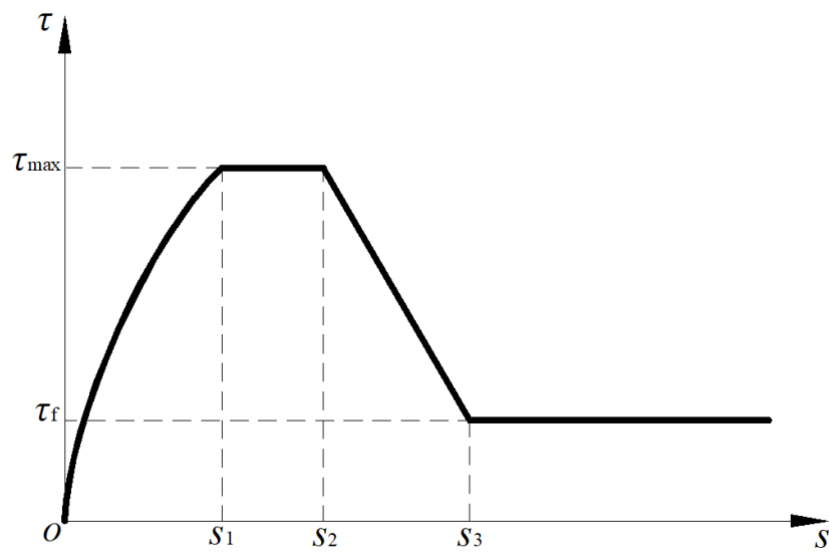
Figure 7.3 Tangential bond-slip model for the concrete-to-steel interface
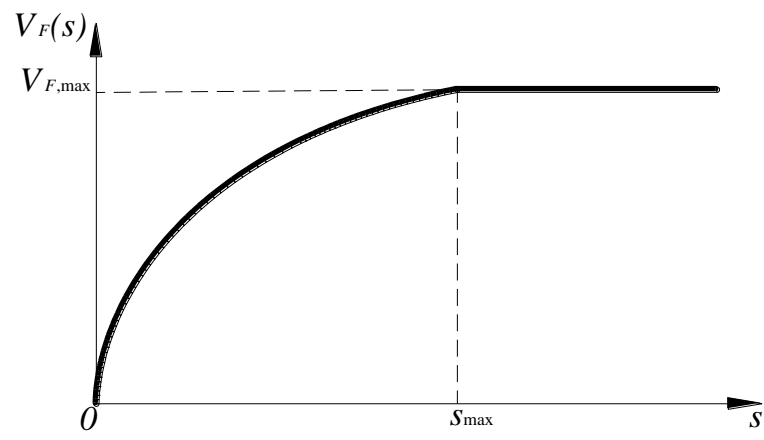
Figure 7.4 Force-displacement model for dowel actions
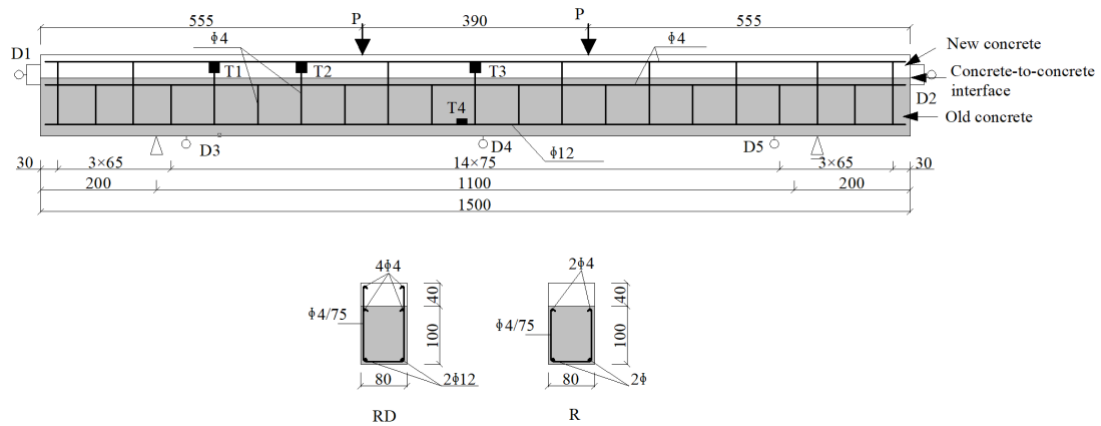
(a) Test conducted by Halicka (2011)
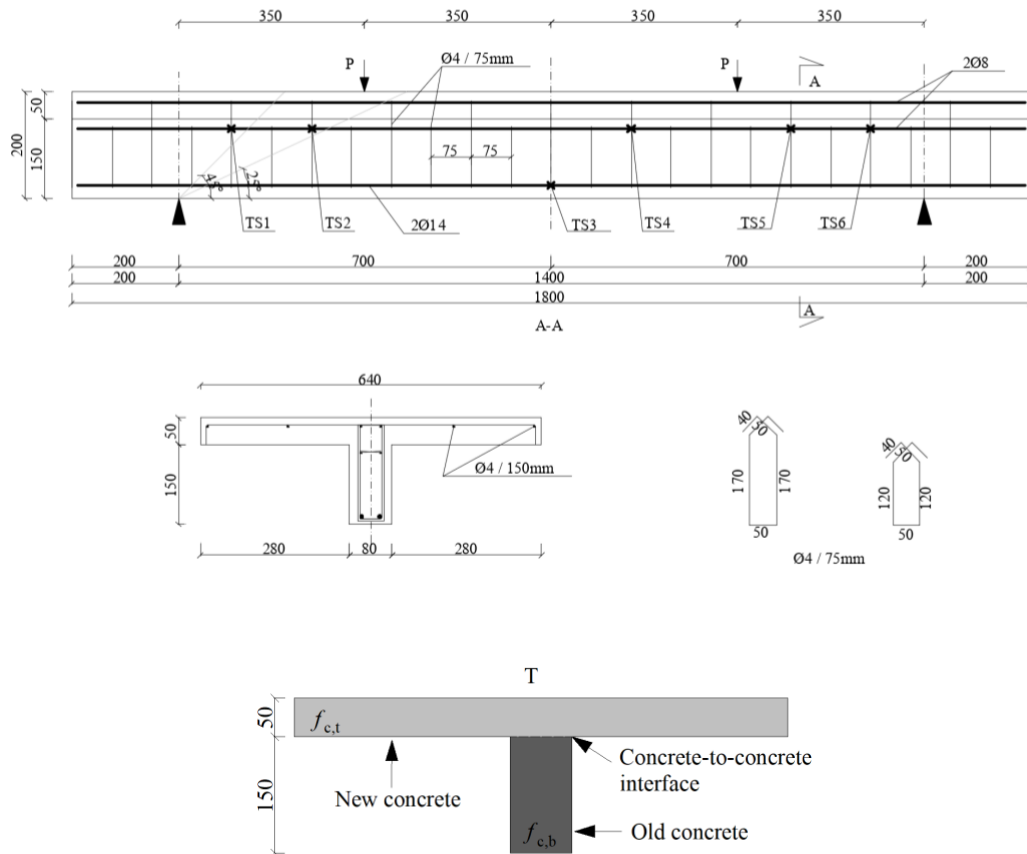
(b) Test conducted by Halicka and Jablonski (2016)

Figure 7.5 Details of test specimens of Halicka (2011) and Halicka and Jablonski (2016)
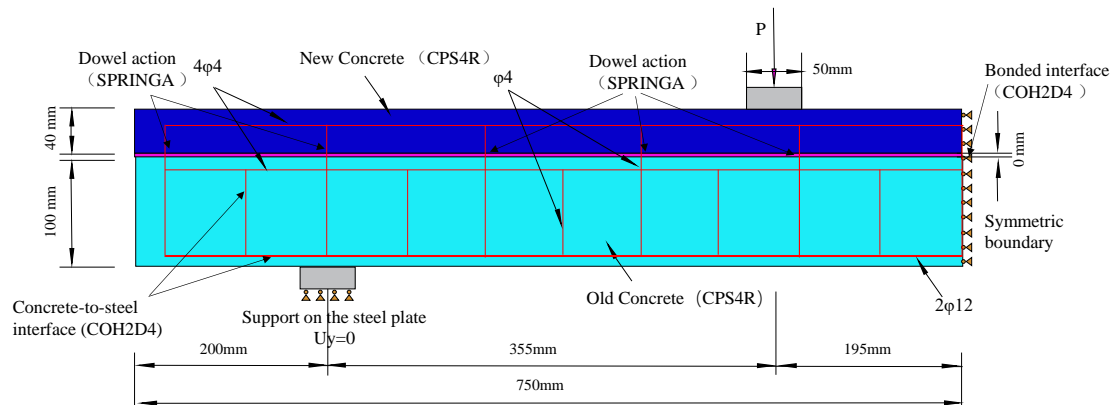
Figure 7.6 FE model of the composite concrete beam tested by Halicka (2011)
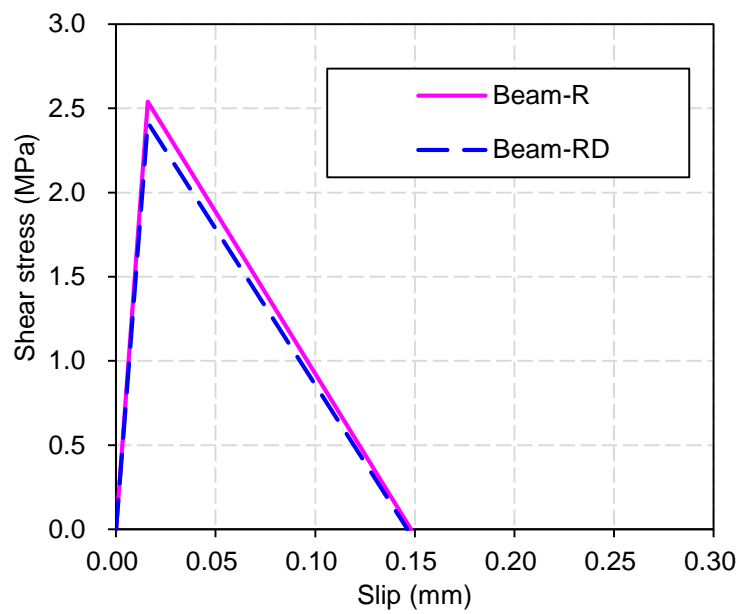
Figure 7.7 Bond-slip relationships for concrete-to-concrete interfaces of beam-R and beam-RD
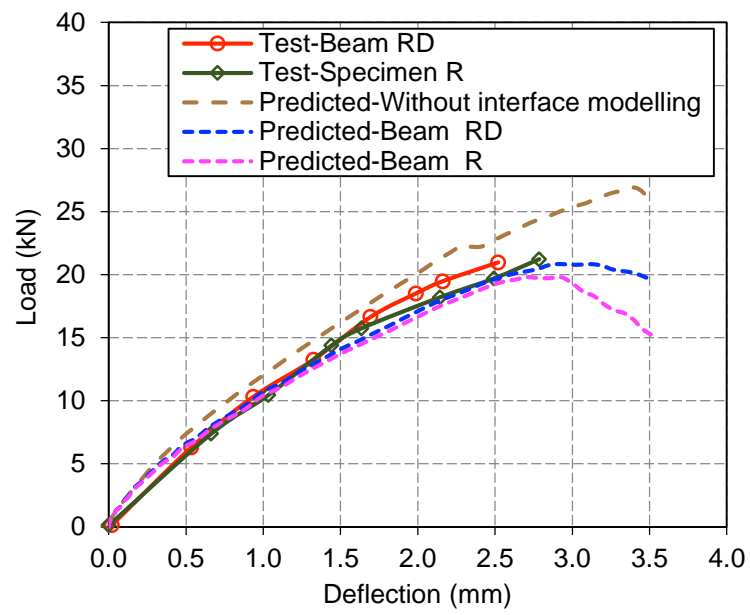
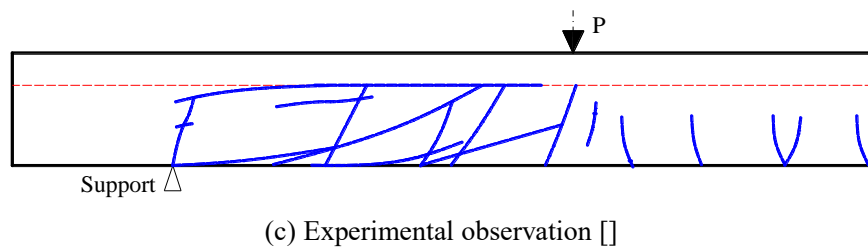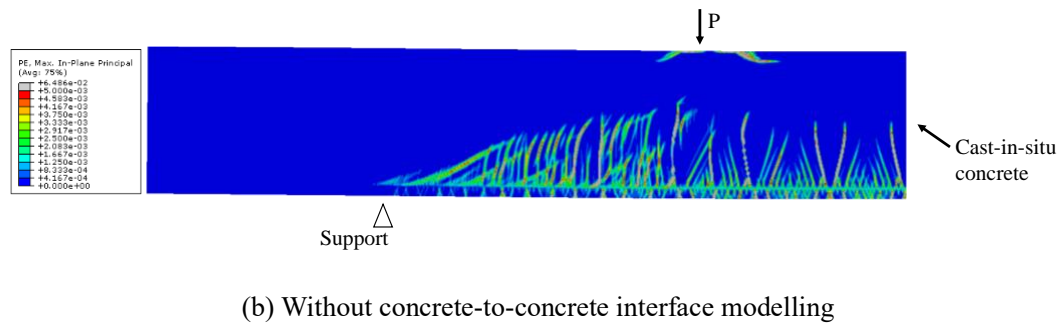Figure 7.8 Comparisons on load-deflection curves of tests conducted by Halicka (2011)

(a) With concrete-to-concrete interface modelling

(b) Without concrete-to-concrete interface modelling
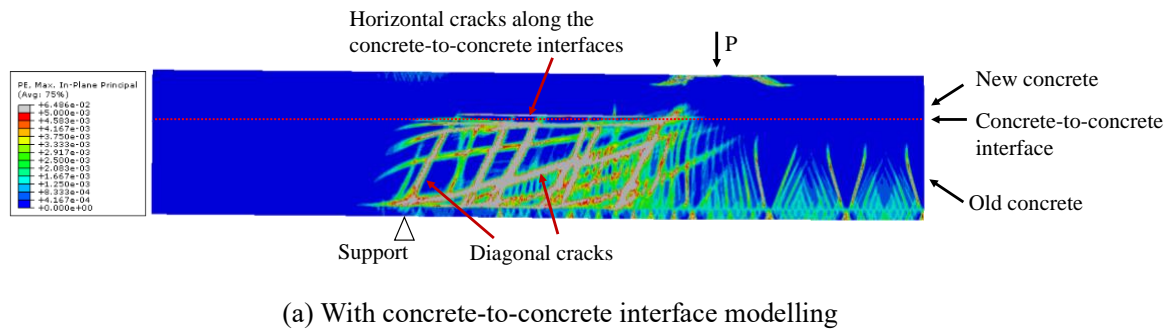

(c) Experimental observation []

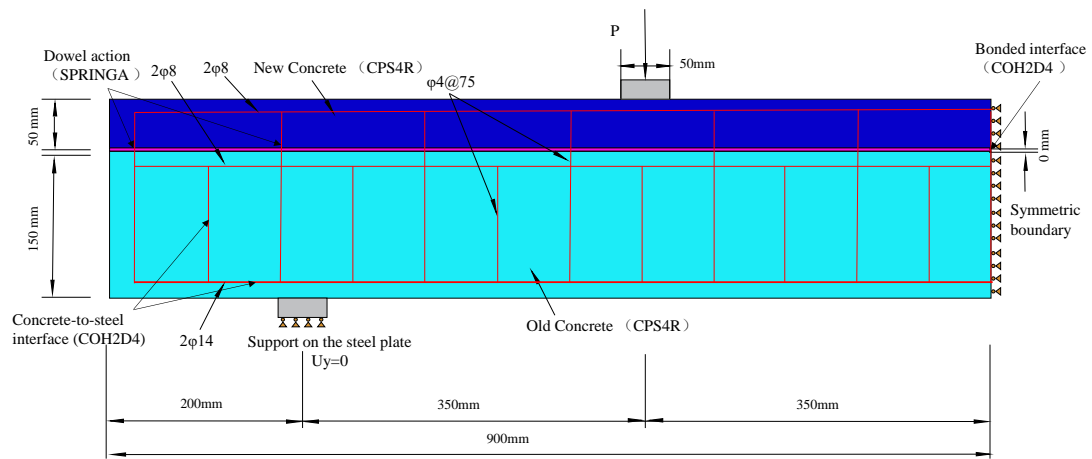Figure 7.9 Crack patterns at failure for beam-R conducted by Halicka (2011)

Figure 7.10 FE model of the composite concrete beam tested by Halicka and Jablonski (2016)
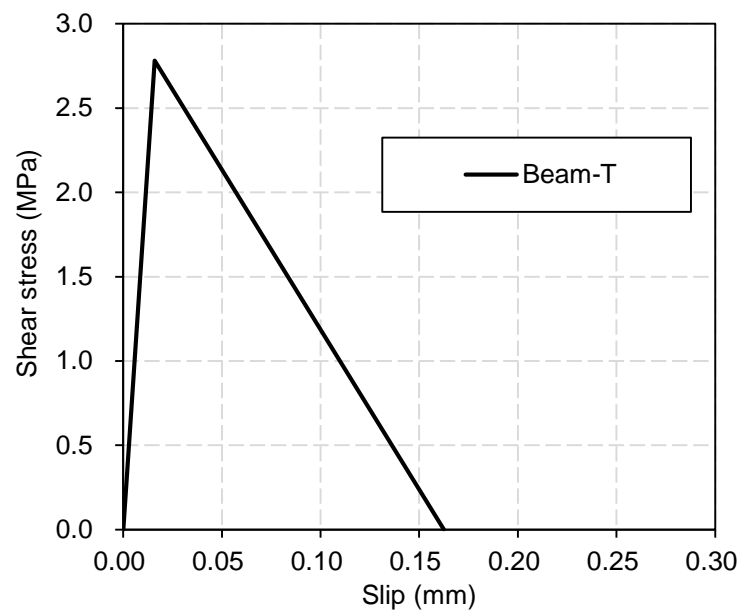

Figure 7.11 Bond-slip relationships for concrete-to-concrete interfaces of beam-T
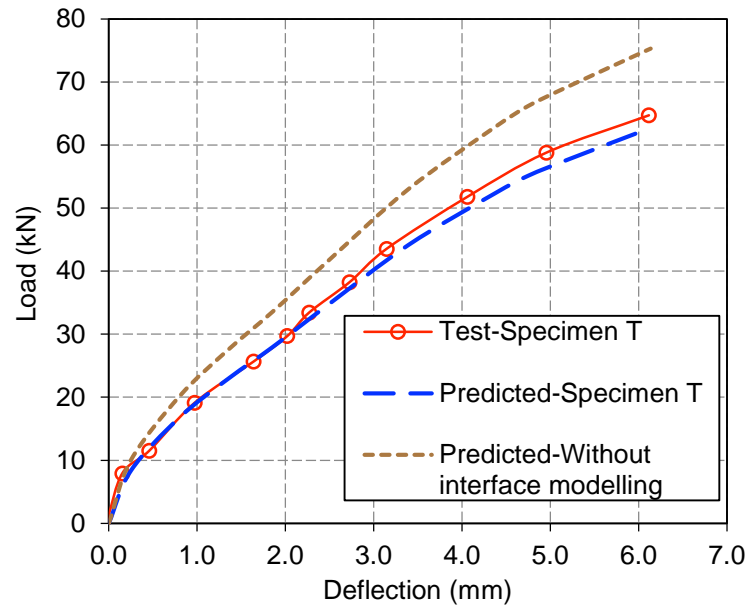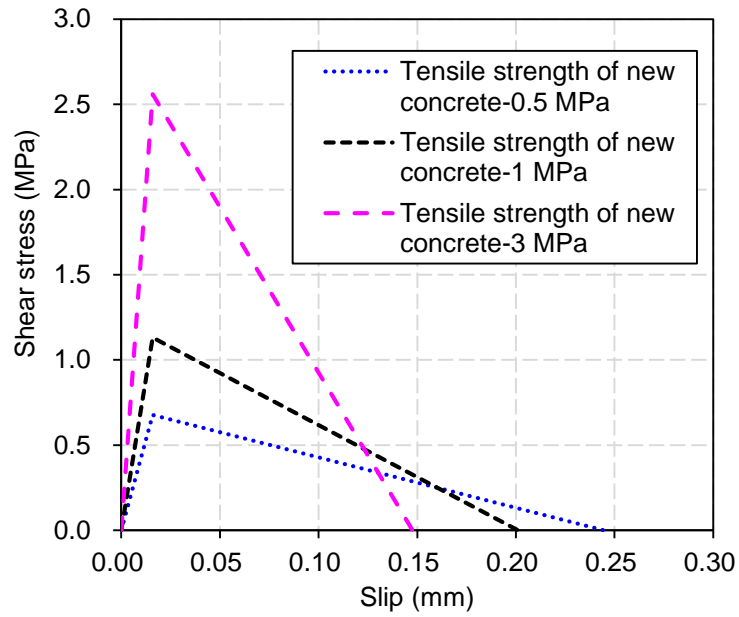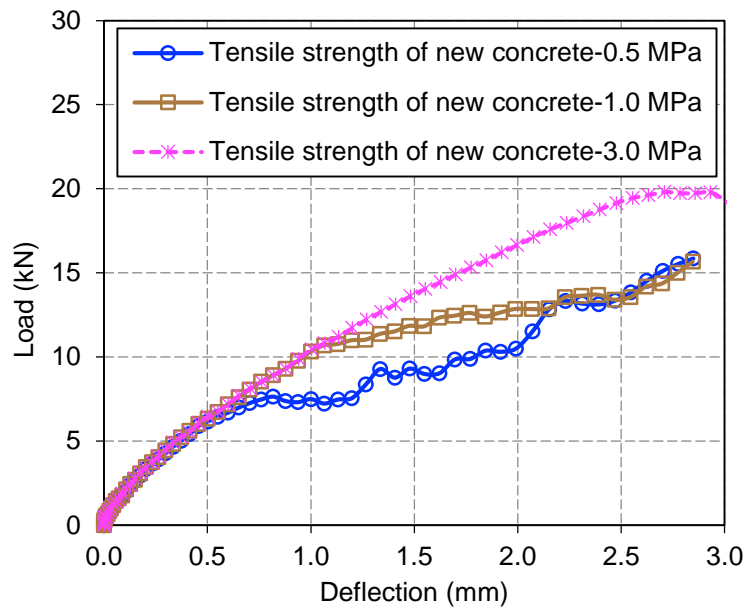
Figure 7.12 Comparisons on load-deflection curves of tests conducted by Halicka and Jablonski (2016)
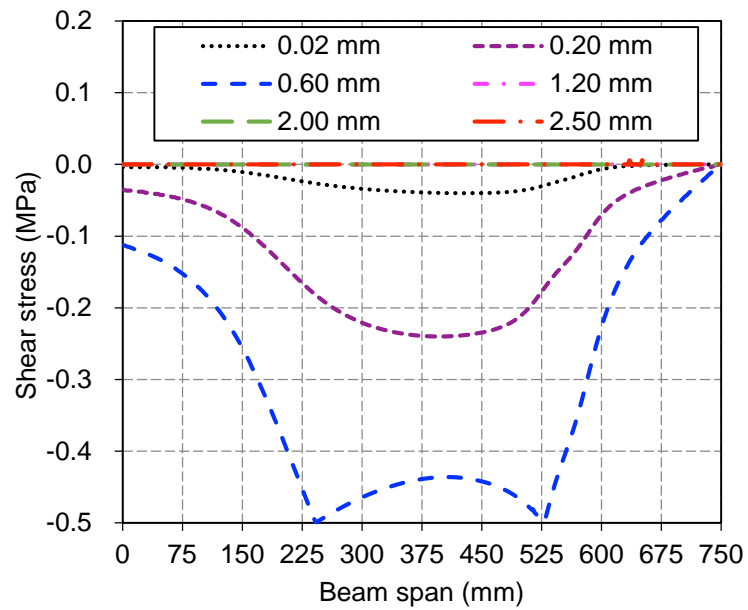
(a) The bond-slip relationships for the four interfaces with various surface roughness

(b) The corresponding load-deflection curves

Figure 7.13 Predicted load-deflection curves of composite beams with different interfaces

(a) Concrete-to-concrete interfaces with 0.5 MPa tensile strength of new concrete
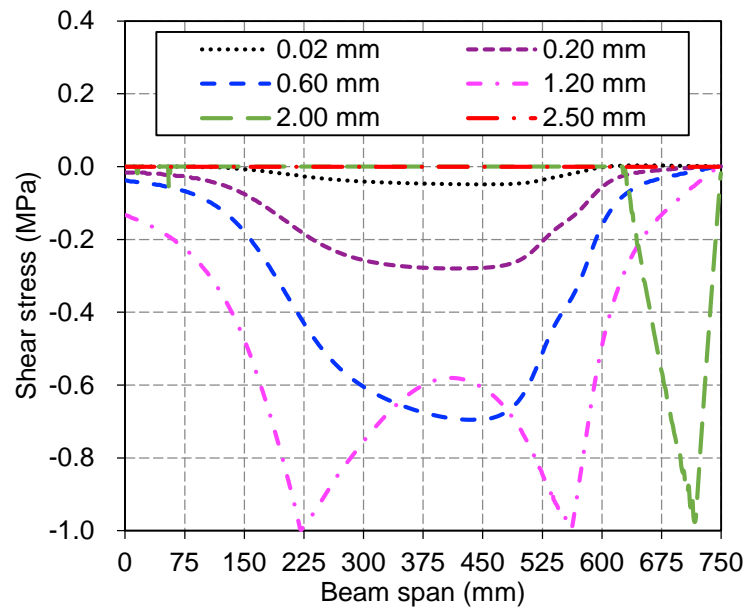
(b) Concrete-to-concrete interfaces with 1.0 MPa tensile strength of new concrete
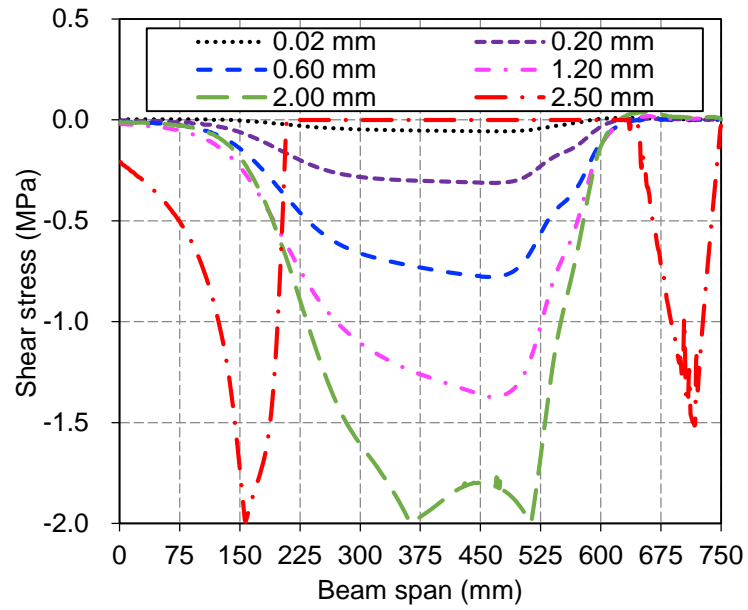
(c) Concrete-to-concrete interfaces with 3.0 MPa tensile strength of new concrete

Figure 7.14 Interfacial shear stress distributions along beam span with various interfacial property
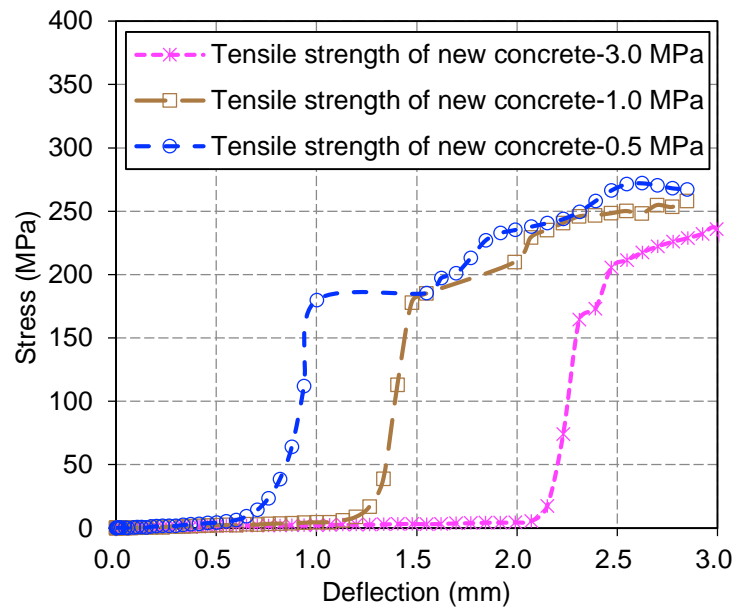
(a) Stress-deflection curves
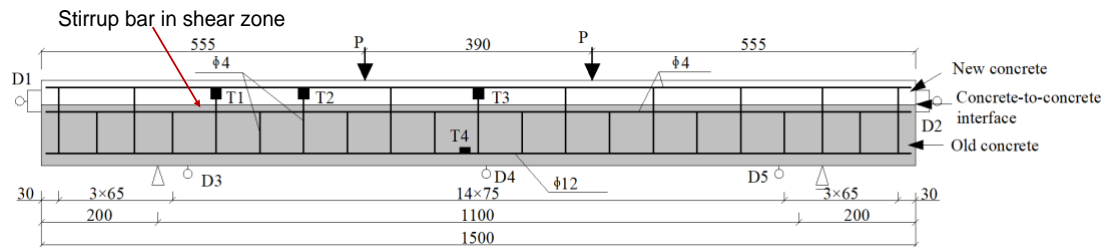
(b) Location of stirrup bar in the shear zone

Figure 7.15 Stirrup bar stress-deflection curves with various interface property
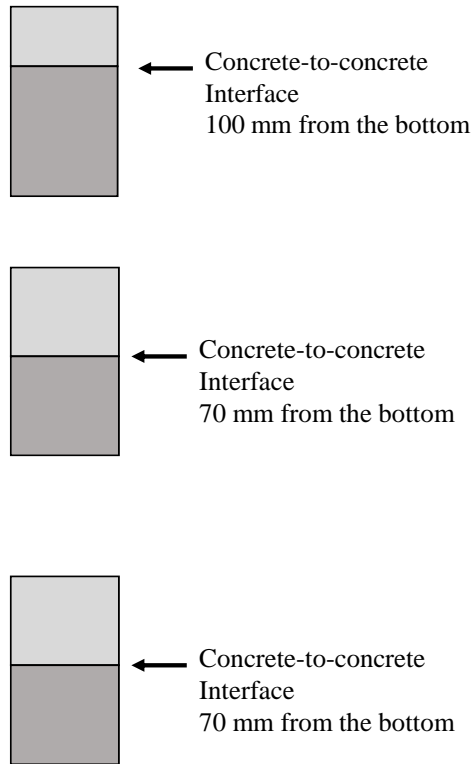
(a) Layouts of the cross-sections for the three beams
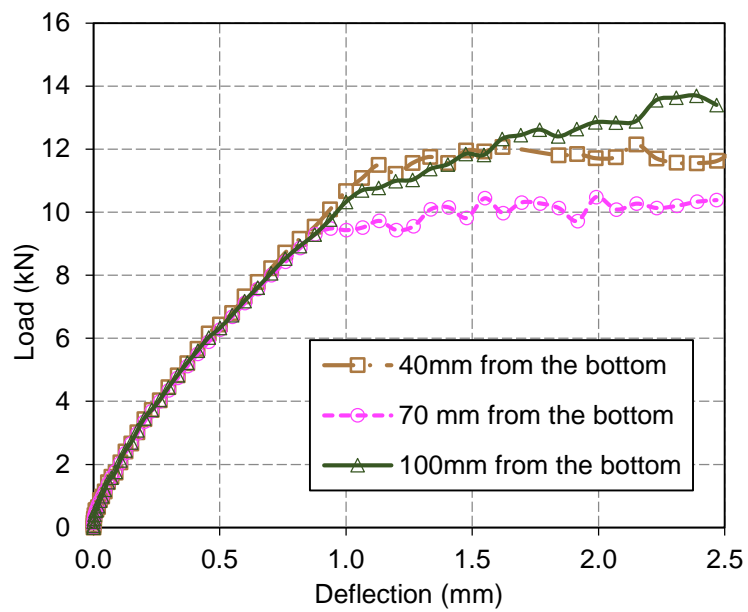
(b) The corresponding load-deflection curves

Figure 7.16 Predicted load-deflection curves for different cross-section layouts
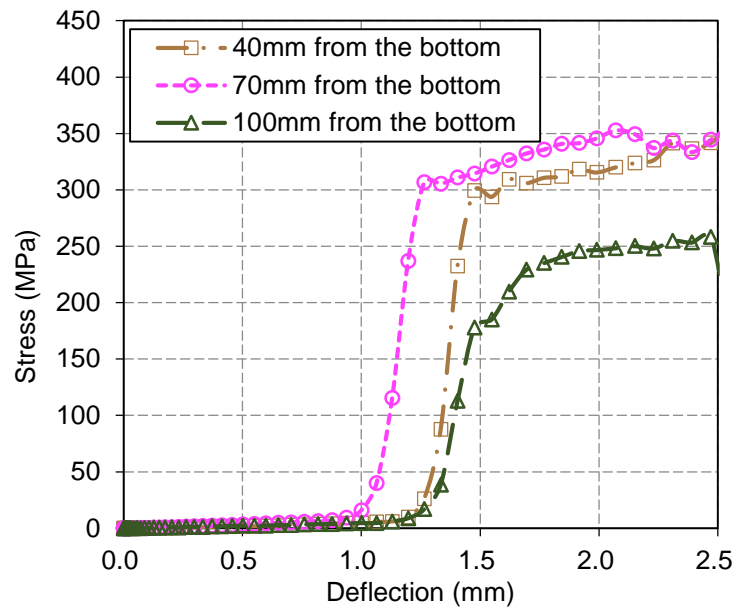
Figure 7.17 Stirrup bar stress-deflection curves with interface position
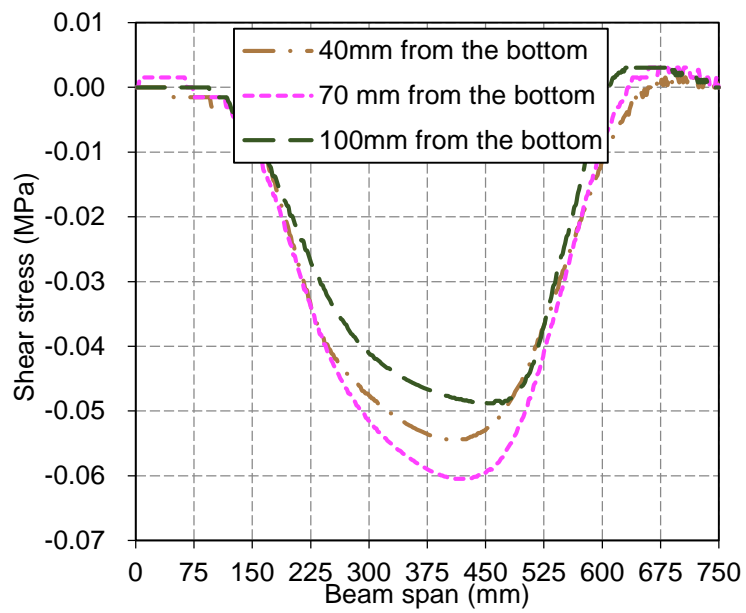
(a) 0.02 mm deflection
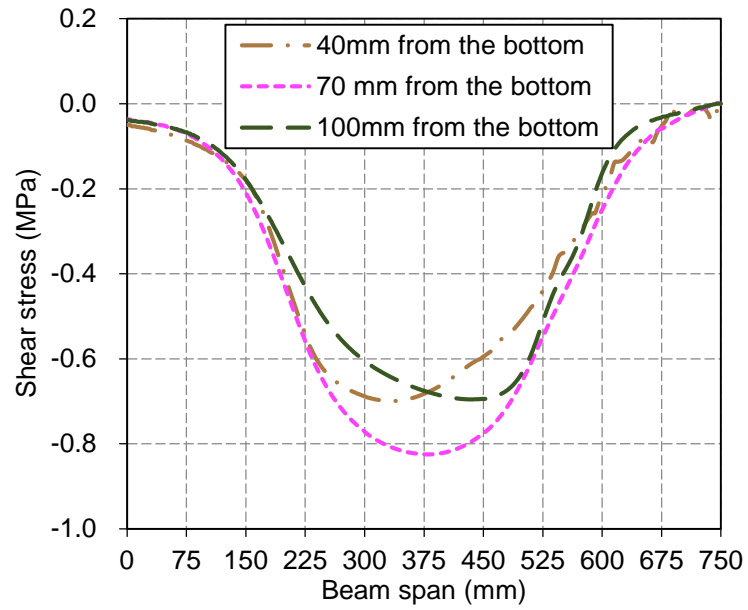
(b) 0.6 mm deflection
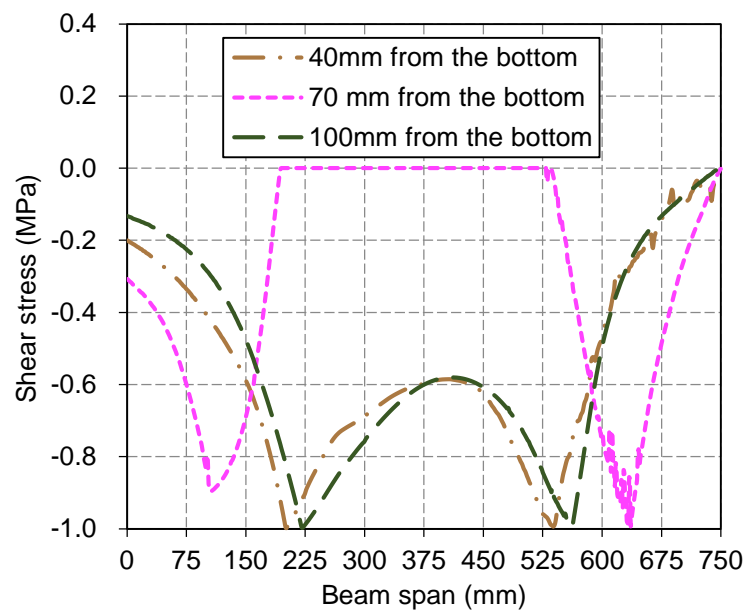
(c) 1.2 mm deflection

Figure 7.18 Interfacial shear stress along beam span with interface position

CHAPTER 8

CONCLUSIONS AND RECOMMENDATIONS FOR FUTURE RESEARCH

8.1 INTRODUCTION

Concrete-to-concrete interfaces are widely present in concrete structures, such as repaired and strengthened concrete structures and precast concrete structures. In general, the normal tensile and shear strengths of concrete-to-concrete interfaces are lower than those of the base concrete, while the compressive strength of the interface could be considered equal to that of the base concrete. Therefore, except under pure compressive actions, the concrete-to-concrete interfaces are likely to be the weak part of the structures that degrades and fails prior to the other parts under increasing load. The sufficient understanding and accurate prediction of the interfacial behaviour is critical to the analysis of concrete structures involving concrete-to-concrete interfaces.

The actual mechanical behaviour at the concrete-to-concrete interface involves the interaction between the local interfacial behaviour and the apparent global interfacial response. It is straightforward for tensile loading that the interfacial tensile stress distribution is uniform, whereas it is rather complicated for shear loading since the interfacial shear stress distribution is non-uniform. The interfacial behaviour is further complicated under combined shear and compressive actions. Therefore, a successful model for the interfacial shear behaviour is the key for the constitutive description of concrete-to-concrete interfaces.

Most of the existing models for the interfacial shear behaviour have been developed based on a fundamental assumption that the interfacial shear stress distribution is

uniform, which permits the direct but oversimplified link between the apparent global interfacial response and the local interfacial behaviour for concrete-to-concrete interfaces. Accordingly, interfacial shear tests of various types have been conducted to investigate the apparent global response of the concrete-to-concrete interface under shear-dominated loading conditions. The collective experimental data have generally indicated that the apparent global interfacial shear response follows a linear elastic behaviour terminated at a failure load, which can be translated into an equivalent local interfacial linear elastic shear behaviour with a maximum shear strength by simply dividing the global resistance by the interfacial area.

However, such models are inaccurate due to two major defects. First, the testing methods used for developing such interfacial models are incompatible with the fundamental assumption of uniform interfacial shear distribution. Second, the current models only describe the maximum shear strength while ignoring the damage evolution ability of the local interface. Consequently, the existing test methods are mostly inappropriate and the resulting models are inaccurate. In order to achieve accurate descriptions for the critical concrete-to-concrete interfacial behaviour, a deep understanding of the test method and a more sophisticated local bond-slip model are needed.

In this context, an experimental-theoretical-numerical study is presented in this thesis to advance the understanding and modelling of concrete-to-concrete interfaces. The existing test methods have been examined using finite element analysis; their advantages and disadvantages have been fully understood. Thereupon, a modified testing method is proposed for understanding the interfacial shear behaviour for concrete-to-concrete interfaces. Subsequently, a comprehensive experimental programme is conducted using the newly developed testing method to fully understand

287

the interfacial shear behaviour considering various factors impacting the interfacial behaviour. A local bond-slip model that is much more sophisticated than the previous maximum strength model is then developed based on the experimental data. Finally, this bond-slip model is implemented into a finite element framework, which is used to simulate the behaviour of concrete structures in which the concrete-to-concrete interfaces play a vital role. The main conclusions and recommendations for further research are summarized in this chapter.

8.2 ANALYSIS OF EXISTING TEST METHODS

Existing test methods for the interfacial shear behaviour of concrete-to-concrete interfaces include direct and slant shear test, of which the former applies nominally pure shear load and the latter applied combined compressive and shear load on the interface. While the interfacial stress state in the slant shear tests is closer to the practical scenarios, it is much more complicated than the interfacial behaviour under pure shear stress state, which has not yet been fully understand. Therefore, the slant shear tests are not considered in the scope of the current research aiming at understanding the interfacial shear behaviour of concrete-to-concrete interfaces.

The direct shear tests are categorized into the one-interface, L-shaped one-interface, and two-interface direct shear tests. A literature review and a comprehensive finite element (FE) analysis has been conducted to analyse these shear test methods, focusing on the interfacial failure mode, interfacial shear stress distribution, and the influences of the testing parameters on the interfacial behaviour. For the test methods without dowel reinforcement at the interface, the interfacial failure mode is brittle interfacial debonding occurred at the capacity of the interface; for those with dowel reinforcement at the interface, the failure model is stable interfacial debonding after reaching the

capacity of the interface. While the dowel reinforcement enables the stable interfacial debonding that is critical in understanding the interfacial damage evolution behaviour, the concrete-to-concrete interface and the dowel reinforcement are deeply entangled making inaccessible the isolated behaviour of the interface. Therefore, the FE analysis is focused on the test methods without dowel reinforcement.

The FE results indicate clearly that the interfacial shear stress distribution is non-uniform and the normal interfacial stress is inevitable for all test methods with various specimen configurations. The specimen designs leading to highly non-uniform interfacial shear stress distribution and normal tensile stress concentrations will induce interfacial brittle failure when the majority of the interface is little stressed. Therefore, such test methods are highly inaccurate for evaluating the maximum interfacial strength model based on the uniform interfacial stress distribution assumption. Nevertheless, the analysis indicates that by optimizing the specimen design, a generally uniform interfacial shear stress distribution with a moderate level of normal stress at the interface can be achieved for the L-shaped one-interface direct shear test specimen. This allows for the approximation of the local interfacial behaviour using the apparent global response leads to brittle failures.

However, such a specimen is still subject to a brittle interfacial debonding failure. A reinforcing method by replacing the dowel reinforcement crossing the interface by reinforcement that is parallel to while outside of the interface is therefore proposed to enable the stable interfacial deboning in the L-shaped one-interface specimen while avoiding the entanglement between the reinforcement and the concrete-to-concrete interface. In so doing, the brittle failure can be avoided; the interfacial softening behaviour can be isolated by testing two companion specimens, one with bonded interface and parallel reinforcement and the other with unbonded interface and parallel

reinforcement, and deducting the global resistance of the latter from the former.

The proposed test method has been validated through trial experiments. A generally uniform interfacial shear slip was observed for the optimized specimens, and a stable interfacial debonding process has been achieved. Moreover, the isolated interfacial shear relationship consisting of a linear elastic stage, a softening stage, and a residual stress stage has been obtained from the test data. Therefore, the proposed modified testing method is suitable for the investigation of the interfacial local bond-slip behaviour of concrete-to-concrete interfaces.

8.3 DEVELOPMENT OF A BOND-SLIP MODEL

A comprehensive experimental programme has been conducted to evaluate the interfacial bond-slip relationship at the concrete-to-concrete interface using the modified testing method. Four series of specimens have been prepared to investigate the influences of concrete strength, surface roughness, and applied compressive stress on the interfacial behaviour. The failure mode, load-displacement behaviour, slip distribution, and bond-slip relationship for the specimens have been examined.

All specimens were failed by separation at the concrete-to-concrete interface as a result of the stable interfacial debonding propagation. The shear load increased linearly to the maximum level, which was followed by a sudden drop of the load and an increase of the slip. Thereafter, gradual interfacial debonding took place until complete separation at the interface. The isolated apparent global shear response follows a typical tri-linear model that includes a linear elastic stage that terminates at the peak load, a subsequent softening stage that terminates at a residual load level, and a residual stress stage that the load diminishes continuously. Since the interfacial slip is generally uniform, the local bond-slip behaviour can be directly obtained from this global response.

The interfacial stiffness of the initial linear elastic stage and the maximum interfacial shear stress increase with the increase of the old and new concrete strengths, surface roughness, and the applied compressive stress. The residual stress level is dependent on the applied compressive stress but not the concrete strength nor the surface roughness. Specifically, for the interface without applied compressive stress, residual stress is minimal; for the interface with compressive stress, a considerable level of residual stress exists after the softening stage.

A shear bond-slip model for concrete-to-concrete interfaces has thus been developed based on the test data. The key parameters employed in the shear bond-slip model are the interfacial shear bond strength and interfacial fracture energy. Their values have been comprehensively analyzed and determined through regression analysis. The relatively simple bi-linear model is only suitable for the concrete-to-concrete interface without normal stress, while the tri-linear model is applicable to all interfaces. In the proposed shear bond-slip model, the concrete strength, surface roughness and applied compressive stress were the three key parameters that considerably influence the shear bond strength and interfacial fracture energy. The results indicate that the proposed shear bond-slip model for the concrete-to-concrete interfaces could provide an accurate representation of the test data. In general, the proposed shear bond-slip model can be used for the sophisticated analyses of the structures containing concrete-to-concrete interfaces.

8.4 NUMERICAL SIMULATION OF CONCRETE STRUCTURES CONTAINING CONCRETE-TO-CONCRETE INTERFACES

The flexural behaviour of composite concrete beams depends on the composite action between the parts connected by the concrete-to-concrete interface. Therefore, accurate prediction of the behaviour of composite concrete beams depends on the accurate

simulation of the concrete-to-concrete interfaces. An FE framework has been established to simulate composite concrete beams, which incorporates the constitutive modelling of concrete, steel reinforcement, concrete-to-concrete interface, and concrete-to-steel interface. Therefore, it can be used to simulate composite concrete beams of various configurations.

The framework is then used to simulate composite concrete beams with rectangular-section and T-section, which have been tested and reported in the literature. The results indicate that when the concrete-to-concrete interface is not simulated, the flexural stiffness and capacity of the composite beams are overpredicted, while when the interface is properly considered, the predictions of the flexural behaviour and failure mode of these beams were in close agreement with the experimental data.

In addition, one parametric study was conducted using the framework to investigate the influences of the mechanical properties of the interface and the cross-section layout on the flexural behaviour of composite concrete beams. The results show that increasing the interfacial strength enhances the composite action between the concrete parts hence delaying the stiffness reduction of the composite beam. However, increasing the interfacial strength beyond a limit does not further enhance the flexural stiffness and capacities due to the diagonal cracks. The results for the different cross-section layouts indicate that with identical interfacial capacities, the beam with an interface located away from the centre has higher capacity than the beam with an interface located at the centre since the interface in the latter is subjected to higher shear load than that in the former.

8.5 RECOMMENDATIONS FOR FUTURE RESEARCH

In this thesis, a modified testing method for the interfacial shear behaviour of concrete-

to-concrete interfaces was proposed. By employing this test method, a shear bond-slip model for the concrete-to-concrete interface was developed, and the structural performance of concrete structures with concrete-to-concrete interfaces was analysed through numerical studies. However, further investigation is still required for certain issues.

Although the proposed test method induces only moderate normal stress levels at the interface, the shear behaviour is still affected. A more appropriate test method for the investigation of the shear behaviour of concrete-to-concrete interfaces remains to be developed.

The parallel reinforcing bar was introduced in the proposed testing method to avoid the brittle failure of the interface, thereby enabling the measurement of the softening behaviour of the interface. However, the experimental observation indicates that a sudden process of a considerable drop of load and jump of slip still exists after reaching the peak load for the proposed test method. Accordingly, an improved test method enabling a more stable post-peak softening behaviour can reveal more accurately the softening behaviour of the interface. Moreover, the apparatus used in the tests for applying interfacial compressive stress blocks the view of the DIC system, making it unable to measure the interfacial slip for specimens with interfacial compression. Therefore, in future studies, a more suitable test setup may be devised to allow for measuring the slip while applying interfacial compression.

Although a comprehensive experimental programme has been launched to investigate the effects of concrete strength, surface roughness and normal stress on the shear bond-slip relationship of concrete-to-concrete interfaces, the number of specimens was still rather limited. As a result, the parameters of the proposed bond-slip model are limited

293

to a certain range. For example, only normal strength concrete was considered. In the future, more tests as well as more numerical analyses can be conducted to achieve a more comprehensive database for the calibration of the bond-slip model.

The proposed bond-slip model is assumed to have a triangular shape instead of a trapezoidal shape in the peak stress region, which is therefore suitable for interfaces with a brittle interfacial behaviour characteristic; such interfaces are generated through direct casting. However, if the concrete-to-concrete interface is formed by bonding two precast concrete components using ductile structural adhesive, the developed model may be unsuitable for simulating the relatively more ductile interfacial behaviour. Moreover, the bond-slip model contains a constant residual stress segment with an assumed ultimate slip of 0.3 mm, which simulates the interfacial frictional behaviour after debonding. The assumed 0.3 mm ultimate slip is used to avoid a spurious infinite fracture energy but could be inaccurate in certain scenarios.

Finally, in the present FE analyses, compressive stresses normal to the interface were not considered in determining the values of the key parameters of the proposed bond-slip model (hence the bi-linear model was used), but the predictions were still accurate since the compressive stress level in these specimens is not considerable. When interfacial compressive stresses are considerable, the values of the key parameters of the proposed bond-slip model are expected to become much different (a tri-linear model is then needed because of the residual stress). Moreover, as the compressive stress level varies during the loading process, the resulting tri-linear bond-slip model should change accordingly due to the varying values of the key parameters. This can be achieved readily with the proposed equations, but implementing such a variable bond-slip model into the FE analysis is not currently feasible because of the need for complex user-defined subroutines. Therefore, for FE analyses, a user-defined cohesive element with

properties dependent on the normal compressive stress level should be developed in the future to achieve more robust interfacial modelling capabilities.